AeroCity:

Next generation high speed transportation

Group S02

TU Delft

AeroCity:

Next generation high speed transportation

Final Report

July 2, 2019

Group members		
Guus	Bloem	4554124
Simon	Daenens	4552520
Luis	Gambetta	4472772
Emre	Goekalan	4460073
Tuur	Knevels	4533461
Tessa	Mennink	4547462
Marloes	Nanninga	4547179
Giuseppe	Onorato	4547098
Gregory	Sanders	4559738
Wouter	Spek	4488148

Supervisors

A. Gangoli Rao
D. Peeters
P. Shrestha
M. van Sluis
E. van Rees

Version 1.0: Final Report

TU Delft

Executive Overview

The Project

The current transportation networks face a lot of challenges regarding pollution, noise and costs. The limits of current transportation systems are being pushed and with the increasing number of people travelling regularly, it is clear that new transportation systems must be created to comply with the customers' needs. Expansion and innovation of transportation infrastructure is needed and future transportation should become more sustainable while also being faster, cheaper, safer, and more reliable.

Examples of existing high-speed transportation systems are the TGV and Maglev. These systems can reach speeds over 300 km/h. However, their infrastructure comes with a ridiculous price tag (6.6 billion euros [1] for 100 km of track). The costs for infrastructure increase exponentially with the maximum speed of these vehicles as the required tolerances become tighter. This makes the break-even point very hard to reach and hence, high-speed transportation systems are very unattractive for investors. The challenge is thus to design a new high-speed transportation system. One that matches speeds of current alternatives while at the same time reducing infrastructural costs. The proposed solution: AeroCity.

What is AeroCity?

AeroCity is the next chapter in High-Speed Transportation. It is a high speed and zero emission vehicle for 116 passengers with low infrastructure costs. While Maglev and Hyperloop want to create lift magnetically to avoid friction, the AeroCity is an airfoil shaped vehicle, that generates its lift by using the Wing-in-Ground effect (WIG). Due to the WIG effect, AeroCity can fly approximately 5 cm above the track at a cruise speed of 305 km/h. Therefore, the necessity for an expensive magnetic levitation system (Maglev), a vacuum tube (Hyperloop) or train tracks with tight tolerances is excluded. For this reason, the construction and maintenance costs of AeroCity's infrastructure are significantly lower.

The objective of this DSE was to design the power & propulsion system, controls, structure and operational management of the Aerocity vehicle and implement it to a transportation system designed for the route between Utrecht and Berlin.

At the start of the project a mission need statement (MNS) and a project objective statement (POS) were decided upon. These are formulated as follows:

Mission need statement

Design a sustainable, cost-effective AeroCity vehicle and network for a route from Utrecht to Berlin that will improve current high-speed transport.

Project objective statement

Presenting a feasible innovative design for commercial high speed transport, by 10 students in 10 weeks.

Requirements

The requirements for this project were established after a thorough analysis of the project objective. The requirements considered during the design of AeroCity can be divided into user requirements, functional requirements and non-functional requirements. The most significant and driving functional requirements are presented below.

- FR-PWR-01: The vehicle shall be electrically driven.
- FR-PWR-02: The CO2 emissions shall be less than 25 % of TGV/ICE.
- FR-SaC-03: The stability of the vehicle shall be ensured autonomously.
- FR-JT-01: The total journey time shall be at maximum 2 hours and 15 minutes.
- FR-NO-01: Noise levels during normal operations shall not exceed 120 dB.
- NFR-S-08: The net energy consumption per passenger per km shall be 25 % less than TGV/ICE.
- NFR-C-01: The cost of the infrastructure and the vehicle combined shall be less than 50 % of TGV/ICE.

These requirements were used to verify the final design of AeroCity. At the end of the design phase, it was checked whether or not each requirement was met. An elaborate discussion on the requirement compliance matrix and a feasibility analysis is described in chapter 24.

Market Analysis and Route

A market analysis is done at the start of every new design project. The feasibility and market gab in current transportation has to be proven by analysing current transportation modes and competitors as well as possible future competition. For this report, a market analysis has been done specifically for the Utrecht-Berlin route. This is the route that was identified to be the most suited for AeroCity within Europe. This conclusion was drawn by looking at a map of the existing railway network in Europe as well as a population density map. Utrecht and Berlin were identified as two highly-populated regions without a connection that has low travel time. From the market analysis done previously, it was concluded that the addition of a stop in Duisburg and Hannover would be beneficial for the overall transport value of AeroCity. The reason for this is that the connection with Hannover and the Rhine-Ruhr Gebiet will increase the number of people that can be reached while keeping the additional travel time low and within acceptable boundaries. After looking into this possible route, the next step was to look into the current competitors on this route and their advantages and disadvantages. It was analysed how AeroCity could add value and fill the gap of a lacking high-speed medium range transportation option on this route. Finally, the market size was estimated by looking into the current number of travellers between Utrecht and Berlin. A conservative estimate was made on the number of travellers that would transfer to AeroCity when this concept would become reality. Additionally, when implementing a new, direct, high-speed route, the number of people travelling along this route increases [2]. The estimated number of passengers per year was 2 million, which is the number used for the initial planning of the operations of AeroCity.

Infrastructure

The infrastructure is arguably the most important part of the AeroCity network. Since the vehicle is made such that the infrastructure cost are at the minimal. Therefore is the main selling point of AeroCity system and its cost is what makes or breaks the project. AeroCity might be similar to aircraft in terms of design and performance, but without the appropriate infrastructure, it cannot fly. The requirements state that the infrastructure cost should be no more than 50 % of that of high-speed railway (HSR) and Maglev.

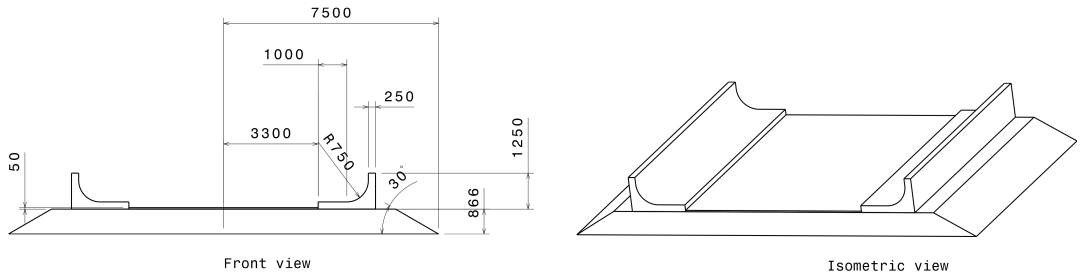

Figure 1: Cross-section of the track. Dimensions in millimetres.

The track itself is the main cost driver for the infrastructure. As depicted in Figure 1, the track is made up of the subgrade, which provides stabilisation and a smooth and uniform bed for laying the track. This subgrade is covered by concrete tracks, similar to a bobsled track. This component of the track provides passive vertical and lateral stability for the vehicle. This is also the part where the wheels make contact with the track during takeoff and landing. Lastly, the subgrade in between the two concrete components serves as a drainage for excess rainwater. This part will be covered by an anti-root fabric in order to prevent root penetration by plants. In the design and construction of the track, thermal expansion of the used materials is taken into account and the necessary measures have been considered. Besides a conventional ground track, AeroCity will also make use of viaducts and tunnels. This considerably increases the difficulty and cost of installation, but this is necessary for urban regions and river or road crossings.

The largest differences for a viaduct are the pillars necessary to support the entire structure and the subgrade used in the ground track that is exchanged for concrete. The supporting pillars, in turn, require additional support in their foundation, which further increases the installation cost. Furthermore, as the subgrade is replaced by concrete, an additional drainage system must be installed to get rid of rainwater in the middle of the track. Lastly, for the parts of the track where a viaduct needs to be installed, a single track will be used for traffic in both directions.

Even though the locations in which a tunnel needs to be constructed are very rare, they should be thoroughly considered in the design of the route. The main things to consider for tunnelling are serviceable and emergency pathways next to the track, the tunnel width, height and depth. Similar to viaducts, for the parts of the route where the vehicle passes through a tunnel, only a single track is used for traffic in both directions.

The first main advantage of the infrastructure compared to that of high-speed rail (HSR) is the lower maintenance required for the track, as there is no physical contact between AeroCity and its track. The second main advantage is the lower construction cost because only the subgrade is necessary to diffuse the exerted loads on the track, whereas for HSR multiple layers of ballast are required. When compared to Hyperloop, AeroCity has the advantage that its infrastructure is far more simple than that of Hyperloop due to the fact that there is no vacuum required. This implies that the design risk and cost is much lower for AeroCity.

The route between Utrecht and Berlin is analysed very carefully. The exact route, including viaducts and tunnels, has been mapped, using the minimum turn radius (1.6 km) and the available land along the route. It was found that a total of approximately 30 km of viaducts and 45 km of tunnels will be needed along the trajectory. The total distance of the track was estimated to be 651 km.

In terms of infrastructure, the final thing to be considered is the station placement. For this route, a total of 4 stations are needed: one in Utrecht, Duisburg, Hannover and Berlin. In Utrecht, the Lunetten Train station will be used. For the Rhine-Ruhr Gebiet, Duisburg is the chosen location for an AeroCity station. In Hannover, the AeroCity station will be constructed underneath the already existing Bismarckstrasse train station. Last but not least, in Berlin, the station will be located at Westkreuz, conveniently located between the city centre of Berlin and Hannover, less than 15 min away from Berlin Hauptbahnhof.

Final Design

The final design presented in this report addresses aerodynamics, propulsion, power, structure and stability & control. A schematic of this design is presented in Figure 5.

In terms of aerodynamics, the most important aspects are listed below. The aerodynamic design is optimised for the highest energy efficiency, while complying with time, cost, safety and comfort constraints. The vehicle has a canard configuration, where the main wing has a span of 8 m, a chord length of 20 m and a NACA 68115 airfoil shape. Attached to the main wing are the sideskirts, which increase the effective aspect ratio of the wing by containing the tip vortices. During take-off and cruise, they have a ground clearance of 5 cm. The maximum thickness of the sideskirts is 30 cm.

The canard has a span of 8 m, a chord length of 2.5 m and its leading edge is located 3.25 m in front of the leading edge of the main wing. It features the same airfoil as the main wing.

Furthermore, two ailerons, with a span of 1.4 m, a chord of 0.35 m and a NACA 0015 airfoil are placed inside the engine ducts. These control surfaces are used for roll control but can be used to assist in pitch control too. Two rudders with the same shape are placed right behind the ailerons and provide yaw control with the assistance of the differential thrust. Seven m behind the wing's leading edge, a rectangular spoiler of 8 m width and 1.5 m chord is placed. This spoiler is used during the braking phase to increase the drag. The most important aerodynamic parameters are tabulated in Table 1. Values are given for both takeoff and cruise speed, for maximum takeoff weight, 50 % payload and operational empty weight, respectively.

Another subsystem that was designed is the propulsion system. In the sizing process of this subsystem, various iterations have been done before reaching the final design. The propulsion system that AeroCity will use is a podded fan, from which the final design parameters are shown in Table 2.

Table 3: Electric vs. kinetic power

$P_{kinetic\_cruise}$	1.174 MW	
$\eta_{propeller}$	80%	[3]
P_{Shaft}	1.467 MW	
$\eta_{motor*MC}$	93% * 98.9%	[4]
$\eta_{DC-link}$	2x 98.5%	[5]
η_{cable_losses}	~99%	
$\eta_{batteries}$	~98%	
$P_{subsystems\_avg}$	~5 kW	
$P_{nominal\_cruise}$	1.70 MW	

Table 4: Source power budget estimations

Subsystem	$P_{nominal\_cruise}$	P_{budget}
Fans	1.695 MW	2.587 MW
Wheels	0 kW	±176 kW
Communication	1 kW	2 kW
Control	2 kW	10 W
Cooling	43 kW	60 kW
Climate control	3 kW	6 kW
Costumer comfort	1 kW	5 kW
Total subsystems	50 kW (excl. propulsion)	83 kW

The electric motors that drive the fans were sized, mainly based on the shaft power required for propulsion, but also taking into account the rotational rate, mass, size, efficiency, redundancy and technical readiness level. In the end, it was chosen to use two fans.

Table 1: Total vehicle lift and drag coefficient and their components. All the coefficients are normalised to the wing surface area and to the free-stream velocity. Standard sea-level atmospheric conditions are assumed.

	W = 360 kN		W = 300 kN		W = 240 kN	
	Take-off	Cruise	Take-off	Cruise	Take-off	Cruise
v $[m/s]$	55.5	84.8	55.5	84.8	55.5	84.8
α_w $[deg]$	4.75	2.73	3.80	2.52	3.12	2.30
α_c $[deg]$	5.0	-0.8	7.0	-0.8	7.0	-1.25
C_{L_w} [-]	1.05	0.51	0.83	0.43	0.63	0.35
C_{L_c} [-]	1.12	0.00	1.33	-0.01	1.33	-0.10
C_L [−]	1.19	0.51	0.99	0.43	0.80	0.34
C_{D_w} [-]	0.0287	0.0180	0.0231	0.0172	0.0197	0.0164
C_{D_c} [-]	1.75E-3	8.8E-4	2.13E-3	8.8E-4	2.13E-3	1E-3
$C_{D_{zero_{ail\&rudd}}}$ [-]	3.8E-4	2.0E-4	3.8E-4	8.8E-4	3.8E-4	8.8E-4
$C_{D_{enginesducts}}$ [-]	8.4E-4	6.4E-4	8.4E-4	6.4E-4	8.4E-4	6.4E-4
$C_{D_{enginespylon}}$ [-]	1.6E-4					
$C_{D_{extraskirts}}$ [-]	1.9E-4					
C_D [−]	0.0320	0.0201	0.0263	0.0193	0.0229	0.0186
L/D [−]	37.9	25.5	36.9	22.4	34.2	18.4

Table 2: An overview of the final fan design parameters.

$\#engines$	2	−
$V_{e_{cruise}}$	127.2	m/s
PR_{fan}	1.062	−
D_{fan}	1.42	m
RPM	3,475	$1/min$
$\dot{m}_{total}$	330.18	kg/s

The main power for all subsystems, and the propulsion system in particular, is stored inside the swappable battery. This battery is located in the front part of the main wing.

Firstly, in order to size the battery, the nominal power was calculated. For this, a value of 1.7 MW followed from the required kinetic power during cruise and is elaborated upon in Table 3. Furthermore, a power budget breakdown is given in Table 4.

The battery was sized by using the total energy consumption of 3.8 MWh. Combined with applied safety and degradation factors, the total battery capacity is 4.8 MWh. The battery consists of 32,000 cells in total. The system is divided in 10 battery systems, which are stand-alone units. One system contains 10 battery packs, which each contain 10 modules. One module is made up of 20 stacks, connected in series. One stack contains 16 cells, which are connected in parallel. This battery architecture is shown in Figure 2.

After the sizing of the batteries, the heat generated by each subsystem was examined. The total heat generated by all subsystems is 210.88 kW. This is the value that the cooling system will be designed for.

Another part of the design was the design of the structure. The structure was designed for the lowest weight, but it should be able to withstand all critical loads. The maximum loading in each direction was determined and various failure modes were evaluated.

As this design is still conceptual, conservative safety factors were applied. The results from research and calculations have proven that aluminium would be the most suitable material. In the sideskirts, the load-carrying structure is made of load-carrying beams, where the skin almost carries no loads. The load-carrying structure in the main wing is similar to a wingbox, where the load-carrying skin is reinforced by stringers. The main wing is connected to the load-carrying structure of the sideskirts in such a way that the wing can be moved with respect to the sideskirts in order to change angle of attack.

Another part of the structure that was designed is the landing gear.
As the vehicle accelerates on the ground for a significant part of

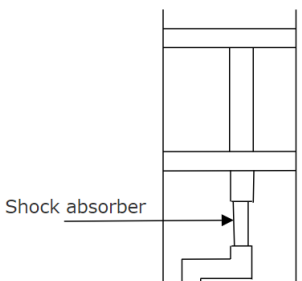

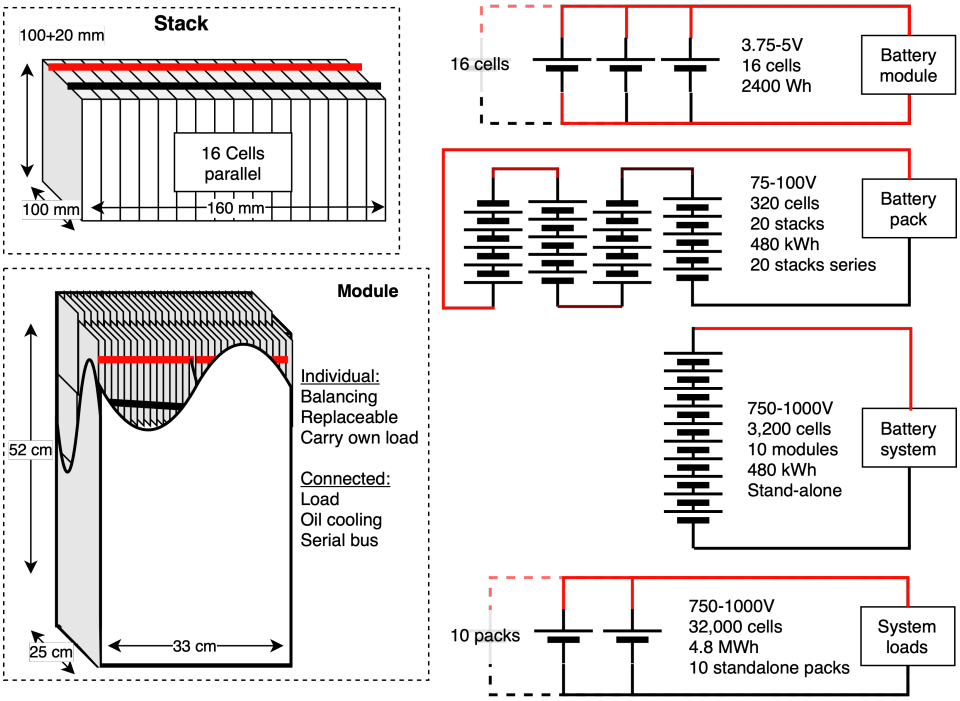

Figure 2: Battery architecture

the trajectory, the wheels and landing gear are quite important for successful operations. The ground phases considered in the landing gear design are taxi, take-off and landing. With these phases in mind, the number of wheels, the tires, the shock absorbers and the braking system were designed. The final design includes 8 wheels with electric motors which are connected to the sideskirts via shock absorbers. The whole landing gear system is located in the retractable sideskirts. Furthermore, the wheels stick out 2 cm underneath the sideskirt to ensure safety in emergency cases and to ensure proper landing in normal operations. For the braking, a spoiler, reverse thrust and disc brakes are used. The layout of the landing gear is presented in Figure 3.

Stability & control is an important design aspect that is crucial for passenger comfort. Without it, the AeroCity simply cannot fly. The vehicle will ensure stability and control with an autonomous system, for which the main aspects are described in this report.

In terms of pitch stability, the vehicle is passively stabilised since the C_{M_α} is negative in the relevant extreme flight conditions. This means that it will automatically come back to the original equilibrium condition without external inputs. Pitch controllability is ensured by a combination of the main wing and the canard.

Roll stability and control is rather challenging to achieve, due to the small aspect ratio and the payload distribution. In order to allow for controllability, horizontal control surfaces and a ballast are used for trimming the vehicle about the roll axis.

Yaw controllability is provided in an active way, by combining the use of rudders and differential thrust.

Vertical stability and control is ensured by the extreme wing-in-ground effect, while lateral stability and control is passive and relies on the shape of the track. For longitudinal stability and control, the thrust level is adjusted throughout the flight.

All of the above-mentioned control modes are controlled by an autonomous system, which is depicted in Figure 4

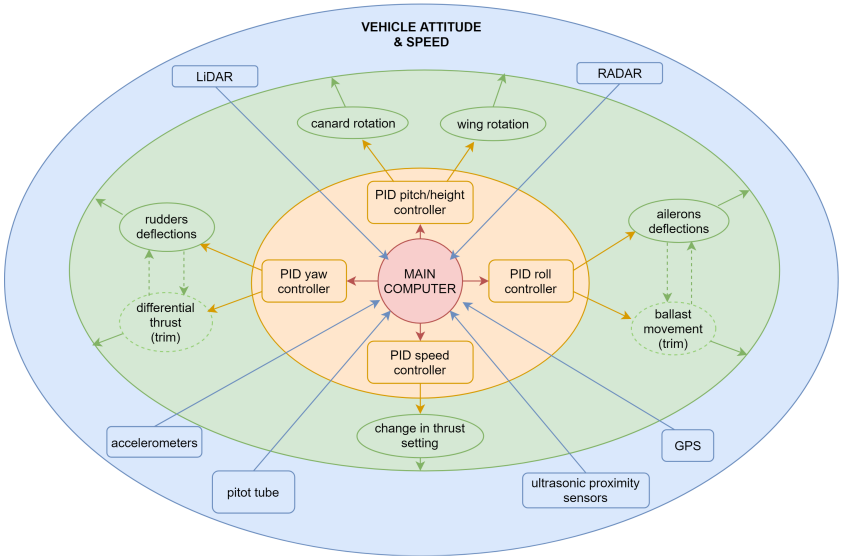

Figure 4: Attitude & speed control of the AeroCity vehicle.

Performance

The performance of the vehicle is a result of all the subsystems working together. The performance is looked at for all three operational phases: acceleration, cruise and deceleration. Acceleration is limited to 0.1 g to ensure passenger comfort. This acceleration is possible up to a speed of 46 m/s. After this velocity is reached, the power output of the fans and wheels cannot deliver the same acceleration due to an increasing drag, which is why the acceleration up to the desired cruise speed will decrease. During cruise, at a design cruise velocity of 84.8 m/s, the thrust force equals 13,830 kN. This results in a kinetic propulsive power of 1.18 MW, which is lower compared to the 1.95 MW required during take-off. For the deceleration phase, the ground clearance will be increased in order to increase the drag until the landing velocity of 55.5 m/s is reached. Then, the height will decrease and at touchdown all braking systems can be deployed in order to reach a braking acceleration of 0.1 g.

To acceleration from zero to cruise speed takes 2:05 min and has a ground distance of 1,691 m. While the deceleration phase takes 2:13 min and has a ground distance of 1,646 m.

The total energy consumption for the direct route between Utrecht and Berlin is 3825 kWh, with a travel time of 2:10 h. For the route with both stops, the energy consumption is 3688 kWh and the total travel time is 2:13 h + 10 min for stops in Duisburg and Hannover.

Operations

The operations on this route for AeroCity have been described in this report. This entails all that concerns the nominal operations, such as the phases during operations, maintenance, ground support and emergency procedures, but also the reliability and safety.

Most importantly, the timetable. From the market analysis followed an estimation of 5500 daily customers. With a vehicle capacity of 116 passengers, a total of 48 rides per day will depart (24 from each side). These will initially depart at time intervals of 42.5 minutes, equally spaced during the operating hours from 5AM to 10pm. After determining the demand this way, the time intervals will be adjusted to accommodate for rush hours.

Cost

The aspect that is the most important to stakeholders is cost. It determines whether or not the project can be successful, both in development and operations. The largest investment cost for AeroCity is the one associated with the infrastructure. In Table 5, the costs per kilometre for on-ground track, viaducts and tunnelling are displayed. In Table 6, an estimation of the total investment cost breakdown, excluding station costs, is given. For the Utrecht - Berlin route, the total investment cost is estimated at 16.45 €B, excluding the cost of stations.

Table 5: Capital Investment for the Infrastructure for a double track Utrecht to Berlin (Excluding station costs)

Direct Costs	**Cost [€]**
On Ground track (576 km)	€5.39B
Track on Viaduct (30 km)	€0.62B
Track in Tunnel (45 km)	€3.01B
Total Direct Costs	**€9.02B**
Indirect Costs (% of Total Direct Cost)	**Cost [€]**
Land Acquisistion (10%)	€0.90B
Engineering Charges (15%)	€1.35B
Cables and Ducts (3%)	€0.27B
Contracter Price (3%)	€0.27B
Total Indirect Costs	**€2.80B**
Total Basic estimate	**€11.82B**
Unpredicted costs (10%)	€1.18B
Expected deviation (5%)	€0.59B
Total Investment Cost excl. taxes	**€13.60B**
Taxes (21%)	€2.85B
Total Investment Cost incl. taxes	**€16.45B**

Table 6: Further breakdown of direct costs

On-ground Track	**Cost [€/km]**
Groundworks	€1M
Foundation Piles	€0.10M
Concrete Track	€0.61M
Steel Reinforcements	€0.56M
Manhours	€2M
Antiroot	€4k
Add. Cost (lighting, cables)	€10k
Total On-ground Track	**€9.36M**
Extra Cost Viaducts	**€11.32M**
Extra Cost Tunnelling	**€57.54M**

The ticket price for an AeroCity ride is composed of different cost components. A complete breakdown of the ticket price can be seen in Table 7. It can be seen that most of the cost goes back into the company and only a small percentage is profit. Infrastructure will not be paid directly by AeroCity, but, similar to the ProRail model used in The Netherlands, AeroCity will pay a yearly fee to use the track. A comparison to the costs of trains can be found in section 18.5.

Table 7: AeroCity fare breakdown

Components	**Cost** [€]	**Percentage** [%]
Vehicle	8.66	23.82
Infrastructure	15.31	42.11
Energy	1.85	5.10
Staff	5.62	15.44
Profit	4.92	13.53
Base Fare	36.36	100
Tax (21%)	7.64	21
Total	**44.00**	121

Sustainability

The sustainability strategy is explained chapter 19, but the most important conclusions are explained below.

The noise emissions were estimated using Heidmannn [6]. It was found that the engine fans will create a noise that is half as loud as that of a train, when standing one metre away from the track. Furthermore, a web tool was used to calculate the effect of the track wall on the noise propagation.

The CO_2 emissions were calculated using a weighted average between the average CO_2 per kWh in the Netherlands and Germany. This value was subsequently translated to a value for the amount of CO_2 per passenger per kilometre, which was found to be 28.4 $g\ CO_2/pax/km$ with an occupancy rate of 80%. In comparison to other modes of transport, AeroCity performs worse than trains, but better than cars, busses or aircraft. This comparison can be seen in detail in subsection 19.4.1. The total specific energy consumption per equivalent seat kilometre is 0.047 $kWh/Es/km$, which is 32 % lower than a high-speed train.

One last important aspect contributing to the sustainability of AeroCity are the materials used for construction of the track. In order to reduce carbon emissions during the construction of the track and stations, concrete produced in a carbon-neutral way will be used, as described in [7].

Compliance

In the end, a sustainable, visually stunning vehicle, that offers a smooth ride on low cost infrastructure and the best passenger experience, was created. Even though a feasible design has been created, not all predefined requirements were met.

The first requirement that was not met was FR-PWR-02: The CO_2 emissions shall be less than 25 % of TGV/ICE. The design value for this requirement was set at 2.4 grams per passenger per kilometre. The final value for AeroCity was found to be 28.4 g. This value is calculated at the current rate of CO_2 per produced kWh of electricity. However, when AeroCity is expected to make its first ride in 2027, electricity will likely be produced in a greener way, thus reducing the amount of CO_2 per kWh of energy produced.

Finally, requirement NFR-C-02: The break even time for the infrastructure shall not exceed 30 years, should be discussed. As the infrastructure of AeroCity will be subsidised by the government and AeroCity pays a yearly fee in

order to use the track, it is not possible to properly validate whether or not this requirement can be met.

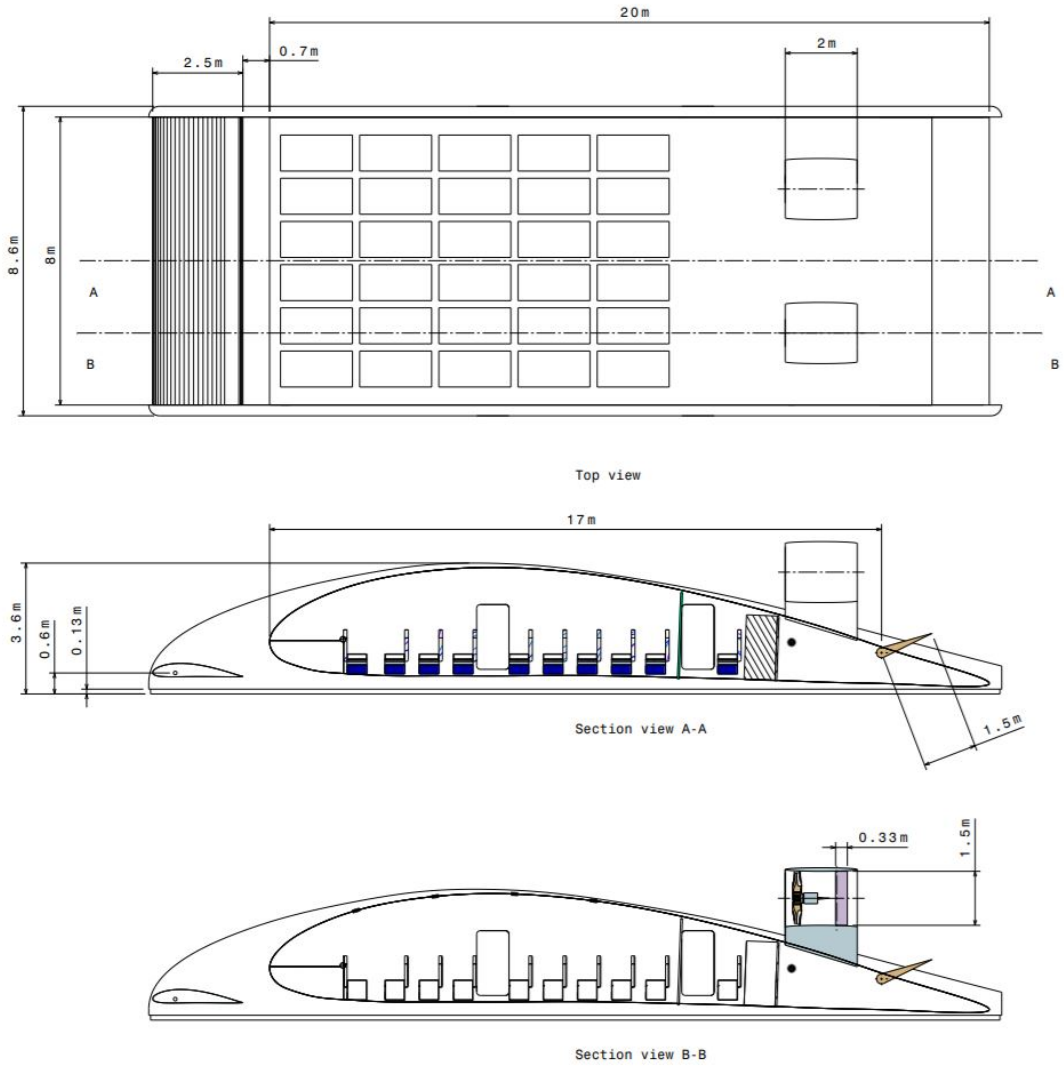

Figure 5: Final Design

Changelog

Version 1: Final Report

- 25/06/2018 - First draft

Contents

Nomenclature

List of Dimensional Symbols

α	Vehicle angle of attack	$[deg]$
α_c	Canard angle of attack	$[deg]$
α_w	Wing angle of attack	$[deg]$
$\dot{M}$	Massflow	$[kg/s]$
ρ	Density	$[kg/m^3]$
σ	Stress	$[N/m^2]$
θ	Banking angle	$[deg]$
A	Cross sectional area	$[m^2]$
a	Speed of sound	$[m/s]$
$C_{L_{\alpha_c}}$	Canard lift coefficient derivative with respect to the canard angle of attack	$[1/deg]$
$C_{L_{\alpha_w}}$	Wing lift coefficient derivative with respect to the wing angle of attack	$[1/deg]$
C_{L_α}	Vehicle lift coefficient derivative with respect to the vehicle angle of attack	$[1/deg]$
$C_{M_{\alpha_{wing}}}$	Derivative of the wing moment coefficient with respect to the wing angle of attack	$[1/deg]$
C_{M_α}	Derivative of the vehicle moment coefficient with respect to the wing angle of attack	$[1/deg]$
C_{M_α}	Vehicle moment coefficient derivative with respect to the vehicle angle of attack	$[1/deg]$
D	Diameter	$[m]$
E	Strength	$[Pa\ (N/m^2)]$
EI	Flexural Rigidity	$[Nm^2]$
F	Force	$[N]$
g	gravitational constant at sea level	$[m/s^2]$
I_{xx}	Moment of inertia around the x-axis	$[mm^4]$
I_{xy}	Product moment of inertia	$[mm^4]$
I_{yy}	Moment of inertia around the y-axis	$[mm^4]$
k	Spring stiffness	$[N/m]$
M	Bending moment	$[Nm]$
m	Mass	$[kg]$
n	Rotations per second	$[1/s]$
P	Applied load	$[N]$
P	Power	$[W\ (J/s)]$
p	Pressure	$[Pa\ (N/m^2)]$
$p_{0,x}$	Total Pressure at station x	$[Pa\ (N/m^2)]$
R	Radius	$[m]$
R	Turning Radius	$[m]$
S	Vehicle reference surface area	$[m^2]$
S_c	Canard reference surface area	$[m^2]$
S_w	Wing reference surface area	$[m^2]$
T	Temperature	$[K]$
T	Thrust	$[N]$
$T_{0,x}$	Total temperature at station x	$[K]$
v	Deflection	$[m]$
v_0	Velocity at station 0,in front of the motor	$[m/s]$
V_∞	Free stream velocity	$[m/s^2]$
v_∞	Free Flow Velocity	$[m/s]$
v_e	Exit Velocity	$[m/s]$
v_{rotmax}	Maximum Rotational Velocity	$[m/s]$
v_{tip}	Tip Velocity	$[m/s]$
x_{ac_c}	Canard aerodynamic centre longitudinal position	$[m]$
x_{ac_w}	Wing aerodynamic centre longitudinal position	$[m]$
x_{cg}	Canard moment coefficient	$[m]$
x_{cg}	Vehicle centre of gravity longitudinal position	$[m]$
x_{cp_c}	Canard centre of pressure longitudinal position	$[m]$
x_{cp_w}	Wing centre of pressure longitudinal position	$[m]$
x_{gg}	Vehicle centre of gravity longitudinal position	$[m]$

List of Non dimensional Symbols

$\bar{x}_{cg}$	Vehicle centre of gravity longitudinal position normalised to the vehicle length
$\bar{x}_{cp_c}$	Longitudinal position of the canard centre of pressure normalised to the canard chord length
$\bar{x}_{cp_w}$	Longitudinal position of the wing centre of pressure normalised to the wing chord length
$\bar{x}_{cp}$	Longitudinal position of the vehicle centre of pressure normalised to the vehicle length
$\bar{x}_{np_\alpha}$	Position of the neutral point with respect to the vehicle angle of attack normalised to the vehicle length
$\bar{x}_{np_{h/c}}$	Position of the neutral point with respect to the wing side skirts ground clearance to chord ratio, normalised to the vehicle length
η	Efficiency
η_{prop}	Propulsive efficiency
$\frac{d\epsilon}{d\alpha_w}$	Derivative of the upwash angle with respect to $alpha_w$
AR_{eff_c}	Canard effective aspect ratio
AR_{eff_w}	Wing effective aspect ratio
C_{D_c}	Canard moment coefficient
C_{D_w}	Wing moment coefficient
$C_{L_{c_{MAX}}}$	Maximum canard lift coefficient
C_{L_c}	Canard lift coefficient
C_{L_w}	Wing lift coefficient
C_{M_c}	Canard moment coefficient
C_{M_w}	Wing moment coefficient
C_M	Vehicle moment coefficient
C_N	Normal force coefficient
C_p	Power coefficient
C_p	Pressure coefficient
C_t	Thrust coefficient
g	Unit of acceleration, equal to 9.81 m/s^2 [−]
HS	Vehicle height stability coefficient
J	Advance Ratio
L/D	Lift over Drag Ratio
SM_α	Stability margin related to the vehicle angle of attack
$SM_{h/c}$	Stability margin related to the side skirt ground clearance
x_{ac_c}	Canard aerodynamic centre longitudinal position normalised to the canard chord length
x_{ac_w}	Canard aerodynamic centre longitudinal position normalised to the wing chord length

List of Abbreviations

AF	Activity Factor
C	Cost
$c.g.$	Centre of Gravity
$C\&DH$	Communication and data Handling
$CBTC$	Commmunications based train control
CFD	Computational Fuid Dynamics
CPU	Central Processing Unit
CRP	Contra-rotating propeller
DC	Direct Current
DSE	Design Synthesis Exercise
HSR	High Speed Railway
ICE	Intercity Express
IS	Infrastructure
JT	Journey Time
$LIDAR$	Laser Imaging Detection And Ranging
LSM	Linear Stator Motor
MT	Maintenance
$NACA$	National Advisory Committee for Aeronautics
NLR	Nederlands Lucht- en Ruimtevaartcentrum
NO	Noise Emissions
NS	Nederlandse Spoorwegen
O	Other
OWC	Operational Weather Conditions
PC	Pasenger Comfort

PR	Pressure Ratio
PRF	Performance
PWR	Power
R	Regulations
RADAR	RAdio Detection And Ranging
RANS	Reynolds Averaged Navier Stokes
RPM	Rotations per minute
RPS	Rotations per second
RSS	Rotor Stator Spacing factor
S	Sustainability
S&C	Stability and Control
SaC	Stability and Control
SaR	Safety and Reliability
SFT	Safety
SPE	Speed
SRV	Swirl Recovery Vane
SSD	Solid State Drive
SWOT	Strengths, Weaknesses, Opportunities and Threats
TBM	Tunnel Boring Machine
TGV	Train Grand Vitesse
TRL	Technical Readiness Level
USR	User Requirement
WIG	Wing In Ground

List of Figures

List of Tables

I

Project & Concept Description

In the first part of this report, the project is introduced and the work that was conducted until the midterm report is summarised and presented in order to make the reader aware what the detailed design that is presented in Part III is based on. This is followed in the second part of the report by the market analysis and the operations of the system and the system requirements in order to give the reader a more detailed understanding on the need for the system and its operation, based on the requirements that were set. The subsequent part discusses the detailed design of AeroCity and is followed in Part IV by a detailed analysis of the final design. In the last part of this report, a conclusion is drawn and recommendations for future work on this project are given.

1 Introduction

The need for transportation systems that are faster and more efficient than existing ones has been around for as long as people have been travelling. This need continues to exist in a world where there is an increasing number of people wanting to travel. For most of the past century, the fastest way to travel for long and medium distances has been by aircraft. The development of high-speed trains has challenged the aircraft on medium distance routes, especially in terms of convenience and comfort. However, high-speed trains have come with their own set of issues, the cost of the required infrastructure being the main one. This high cost originates from the low tolerances on the track that are required for a train to travel at 300 km/h. This same issue is present with Maglev trains and the very optimistic, yet very well funded Hyperloop concept.

The high infrastructure cost for these systems makes them difficult to deploy as large upfront investment is required, with little or no expectation to ever break even within a reasonable time frame. Hence, investment is lacking and deployment is slow in a time where the transportation demand is increasing and it is ever more important to reduce carbon emissions.

Aircraft on the other hand still create large amounts of carbon dioxide, which continues to heat up Earth's atmosphere. If no serious measures are taken to reduce these emissions, ecosystems will start to collapse and extreme weather events will soon be the norm. This outcome has to be avoided and one of the key ways to avoid this climate catastrophe is by reducing the number of short and medium distance flights by offering a faster, more efficient and more convenient way to get from one place to another.

This creates a need for a new alternative transportation mode. One that, unlike a conventional aircraft, does not create carbon emissions and on the other hand is not as expensive to deploy as a high-speed train. In order to offer low prices, maintenance should also be kept to a minimum and hence track interference should be limited.

From the desire to create a new transportation system that can accomplish these things, the idea for AeroCity was born. A flying wing that utilises the wing in ground effect (WIG) to lift itself a few centimetres above the ground and that is guided by a track, similar to that of a train. This track, however, does not require the same levels of tolerance that a regular high-speed train requires since there is no physical contact between the vehicle and the track. This gives AeroCity a crucial advantage over high-speed trains because it eliminates much of the cost associated with track construction. Another advantage due to the lack of physical contact between the vehicle and the track is that the load that the track needs to support is not concentrated at the wheels, but is evenly distributed along the entire width of the vehicle, which also simplifies the civil works required to build the track.

Due to the relatively large amount of lift that the WIG effect offers, battery weight, which is a major concern for electric aircraft, is not an issue with AeroCity and thus a long range, while transporting 116 people at a time, can be achieved. The use of electric propulsion makes AeroCity emission-free since the electricity to power it will come from renewable sources. In order to travel further distances, the battery pack was designed to be easily swappable at an AeroCity station. By travelling at a cruise speed of 305 km/h, large metropolitan areas will become more connected. Furthermore, travel times will be reduced since AeroCity will have a similar level of convenience as a train and does not require its passengers to travel to distant airports many hours in advance.

To design and present a commercially viable AeroCity system that can go into operation by 2027 was the goal of this project. This was to be achieved by ten aerospace engineering students in ten weeks time.

Over the past ten weeks, a final design was created and is presented in this report. During the first week of the project, a project plan was created and the purpose and scope of the project were defined. After this, the conceptual design phase began and many different design concepts were explored in order to fulfil the requirements that were set by the project plan. Lastly, the detailed design phase began, during which the final concept that was chosen was worked out in detail.

2 Final Concept

In this chapter, the trade-off performed in the midterm report as well as the final concept is summarised. The trade-off was initially done for three different concepts, each with their own unique subsystems. From these three concepts, one was excluded after the first trade-off and a second trade-off was performed on the other two concepts, after interchanging some of the subsystems. This is described in section 2.1. The final concept that followed from this second trade-off is shown in section 2.2

2.1. Trade-off

After preliminary brainstorming on a lot of different feasible and infeasible design options, three concepts were established. These concepts were different in the following subsystems: power, propulsion and stability and control. The first concept, concept 1, consisted of batteries for power storage, embedded fans for propulsion and uses a canard for stability and control. The second concept, concept 2, relies on the track to provide power, uses open fans for propulsion and a moving ballast for stability and control. The third concept, concept 3 is powered by hydrogen, has podded fans for propulsion and uses elevons for stability and control. These three concepts are summarised in Table 2.3.

Table 2.1: Overview of the three preliminary concepts

	Concept 1	**Concept 2**	**Concept 3**
Power	Batteries	Track	Hydrogen
Propulsion	Embedded fans	Open fans	Podded fans
Stability and control	Canard	Moving ballast	Elevons

For the landing gear, two options were established: a conventional landing gear with wheels, and a take-off and landing cart, which would launch the vehicle in the air at take-off and catch the vehicle during landing. For the required change in angle of attack from take-off to cruise, or from cruise to landing, a change in height and a change in angle of attack were considered.

The track of AeroCity was designed to be a bobsled track, to allow for passive stability. There were no feasible other options to consider for the trade-off that came even a bit close to this design, therefore this track was chosen to be the track for this AeroCity design.

After the three preliminary concepts were established, the trade-off criteria were set up. The main criteria considered in the trade-off, in order of importance, are risk, weight, sustainability, flight range, cost and maintainability. After the trade-off was performed on the three concepts, the two winning concepts were improved and another trade-off was performed, for which the same criteria were considered.

The first trade-off criterion, risk, is the one that was deemed most important and was given a weight of 25%. In the trade-off, the risk was divided into design risk, operational risk and external risk and was assessed according to this division for each concept. The second most important parameter considered in the trade-off was the overall vehicle weight, which should be as low as possible. The decision weight for this criterion was 20%. Sustainability was considered of equal importance as the vehicle weight in the trade-off. It has been given a decision weight of 20%. The aspects of sustainability taken into account during the trade-off were noise, pollution, required energy and test time of each proposed concept. The next criterion on which the design decision was based was the flight range. All concepts that entered the trade-off required a certain minimum range, but some were able to perform better than others. This criterion has been given a weight of 15%. The cost, which is divided into vehicle cost, infrastructure cost and operational cost, is another trade-off parameter, given a decision weight of 13%. Finally, the criterion with the lowest importance is maintainability. However, this does not mean that this should be neglected. The weight given to this criterion in the trade-off was 7 %.

The first trade-off is shown in Table 2.2. A detailed analysis on the trade-off is provided in [8].

After this trade-off, the worst option for the power and propulsion was excluded, since these are strictly linked together and together have a total weight of 40%. For the power, the hydrogen was excluded. The reason for excluding hydrogen is that the efficiency of hydrogen fuel cells with current technology is limited. The technology is not as advanced for hydrogen as it is for either batteries or electrical power from the track. Furthermore, development in short-term future is not expected to reach a sufficient level as needed for AeroCity. Then for the propulsion, embedded fans were excluded since they are a lot more complex to design than open or podded fans, whereas there

Table 2.2: Trade-off summary table for the three concepts. Red indicates the scores for concept 1, yellow indicates the scores for concept 2 and indigo indicates the scores for concept 3

Trade-off criteria	Weight	Rating	Element criterium	Weight [%]	Rating
Total grade	**Concept 1**	5.37			
	Concept 2	5.21			
	Concept 3	5.47			
Risk	25		**Design risks**	40	
	Concept 1	5.22		**Concept 1**	4.45
	Concept 2	5.3		**Concept 2**	5.9
	Concept 3	5.24		**Concept 3**	4.5
			Operational risks	40	
				Concept 1	5.1
				Concept 2	5.35
				Concept 3	5.1
			External risks	20	
				Concept 1	7
				Concept 2	4
				Concept 3	7
Weight	20				
	Concept 1	4.65			
	Concept 2	4.65			
	Concept 3	4.65			
Flight range	10				
	Concept 1	8			
	Concept 2	10			
	Concept 3	8			
Sustainability	15				
	Concept 1	5.3			
	Concept 2	5.35			
	Concept 3	5.3			
Cost	18		**Cost of infrastructure**	80	
	Concept 1	5.2		**Concept 1**	6
	Concept 2	2.9		**Concept 2**	2
	Concept 3	5.22		**Concept 3**	6.5
			Cost of vehicle	10	
				Concept 1	4
				Concept 2	6
				Concept 3	4.55
			Operation cost	10	
				Concept 1	5
				Concept 2	7
				Concept 3	3
Maintainability	12				
	Concept 1	5.05			
	Concept 2	5.25			
	Concept 3	4.75			

are also no real advantages when compared to these other options. Therefore, open and podded fans entered the second trade-off.

A second trade-off was performed after the first trade-off. Other subsystems that were already excluded for this trade-off were the elevons option for stability and control, since the c.g. location could not be placed to meet stability requirements. Furthermore, all designs use the aforementioned bobsled track. Also, a combination of the change in height and a change in angle of attack of the main body to increase the lift coefficient is used. Lastly, the landing gear is chosen to be a conventional landing gear system, since a cart would be very complex to design and emergency cases would be hard to design for. This results in the following two concepts for the second trade-off:

Table 2.3: Overview of the two iterated concepts for the second trade-off

	Concept 1	**Concept 2**
Power	Batteries	Track
Propulsion	Podded fans	Open fans
Stability and control	Canard	Moving ballast

A second trade-off was performed on these concepts, using the same criteria. This trade-off is shown in Table 2.4:

Table 2.4: Final trade-off summary. Red represents revised concept 1 and yellow represents revised concept 2

Trade-off criteria	Weight	Rating	Element criterium	Weight [%]	Rating
Total grade	**Concept 1**	6.07			
	Concept 2	5.41			
Risk	25		**Design risks**	40	
	Concept 1	6.32		**Concept 1**	6.25
	Concept 2	5.96		**Concept 2**	6.1
			Operational risks	40	
				Concept 1	6.3
				Concept 2	5.55
			External risks	20	
				Concept 1	6.5
				Concept 2	6.5
Weight	20				
	Concept 1	4.65			
	Concept 2	4.65			
Flight range	10				
	Concept 1	8			
	Concept 2	10			
Sustainability	15				
	Concept 1	5.3			
	Concept 2	5.55			
Cost	18		**Cost of infrastructure**	80	
	Concept 1	5.84		**Concept 1**	7
	Concept 2	2.9		**Concept 2**	2
			Cost of vehicle	10	
				Concept 1	5.35
				Concept 2	6
			Operation cost	10	
				Concept 1	5
				Concept 2	7
Maintainability	12				
	Concept 1	6.45			
	Concept 2	5.25			

As can be seen in Table 2.4, concept 1 has come out on top, which included the batteries, podded fans and a canard. Hence for the power subsystem, the batteries have been chosen. The main reason for this is that the infrastructure costs remain low when using batteries, and the infrastructure is a highly important benefit that AeroCity has over other high speed transportation systems. Furthermore, maintainability will be simpler since the batteries can be swapped out and in at stations, and can be worked on in an open space. For the propulsion, the podded fans came out on top. Open fans and podded fans are very much the same propulsion mechanism, however, the podded fans were chosen due to the noise advantage it has. The noise of podded fans is a lot more quit than an open fan, thus was the chosen propulsion system. For the stability and control, the canard has been chosen since it provides more safety during operational phases. The canard can also be used as a 'bumper' in case of emergency, whereas the ballast has more possibilities to fail as the required ballast would be large and the mechanisms to move the ballast may not meet the demands of the vehicle.

2.2. Final concept

The AeroCity, as described in this technical report, is an autonomous, flying wing that uses the wing-in-ground effect in order to take away friction drag as this is a limiting factor for the performance of currently existing ground transport modes. This vehicle is equipped with a canard surface for stability and control, which is located 3.25 m in front of the main wing. The canard is connected to the main wing by the sideskirts that cover the entire length of the vehicle. The propulsion system consists of two podded fans, driven by electric motors. All systems, including the propulsion system, are powered with batteries which are located in a swappable structure in the most forward part of the main wing. AeroCity is capable of transporting 116 passengers and will do so on a route between Utrecht and Berlin, with stops in Duisburg and Hannover. The cruise speed is 305 km/h and the direct travel time between Utrecht and Berlin is 2:15 h.

II

System Requirements

As soon as the project and the concept have been defined and described, the following step is to analyse where AeroCity can best fit for an initial beginning phase. This then means that a market analysis must be done, the operational load cases must be investigated, and requirements must be set as to better define the direction that the project will go. With these three tasks done, AeroCity will be guided in the right direction and the work that is later done in Part III will be applied in a practical sense.

3 Market Analysis

In this chapter, the market analysis is described. The market analysis is one of the crucial components to make AeroCity economically feasible. Firstly, section 3.1 explains why the Utrecht Berlin route is the perfect route to kick-start the AeroCity concept. Secondly, a competitor analysis is done in section 3.2. This is done by looking into current available transportation options for the Utrecht - Berlin route. Thirdly, from the competitor analysis, the market for high-speed transportation between Utrecht and Berlin is estimated in section 3.3. Section 3.3 also explains how much market share AeroCity is aiming to gain. From this analysis, the yearly amount of passengers that would travel with AeroCity will be determined.

3.1. Utrecht - Berlin route

Currently, there is a market gap for sustainable high-speed ground transportation for routes between 300 and 700 km since both aircraft as well as high-speed trains take approximately 4-6 hours to cover these distances. The goal of AeroCity is to fill this market gap by providing a high speed network that transfers passengers within 1.5-2.5 hours over these distances, without requiring very high infrastructural costs. A suitable route to kick-off the AeroCity concept was chosen mainly by looking into existing high-speed train infrastructure connecting big cities in Europe. Figure 3.1a shows the existing high-speed rail (HSR) network in Europe in 2017. Combined with the population density information given in Figure 3.1b, it became apparent that there is an opportunity to construct an AeroCity connection, either from Amsterdam to Berlin or from Utrecht to Berlin. These cities are situated in highly-populated regions and do not have an existing high-speed ground connection yet, as opposed to other feasible routes like Amsterdam-Brussels-Paris, Brussels-London, Madrid-Barcelona, etc. In the end, it was chosen that a connection from Utrecht would be the better option because Utrecht is located in the centre of the Netherlands and this would make AeroCity more accessible and convenient for more passengers. The combination of the two aforementioned market opportunities was the reason to choose the Utrecht - Berlin route to accelerate the AeroCity project.

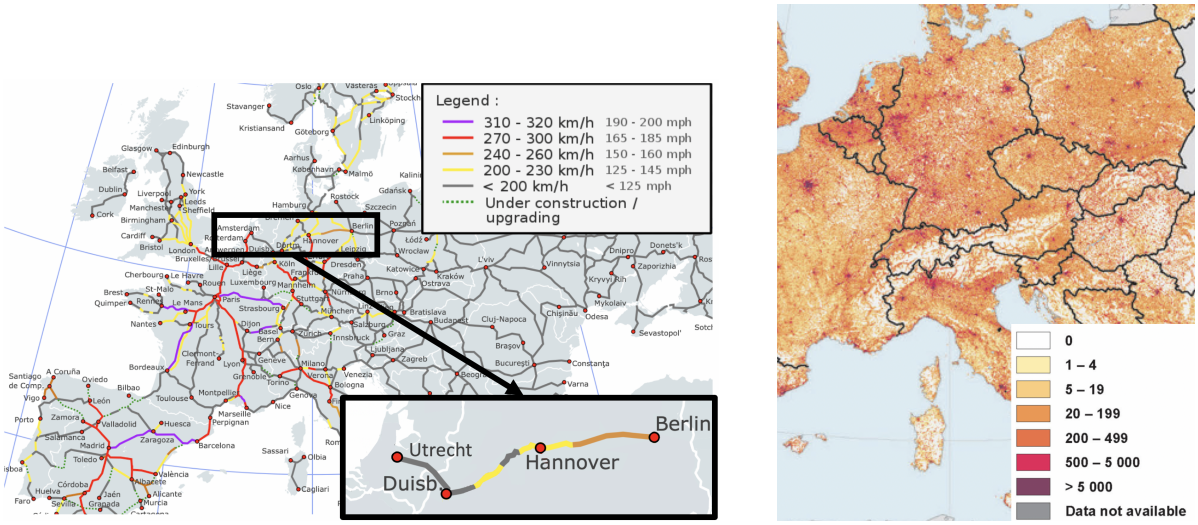

(a) High-Speed Rail Network in Europe [9]

(b) Population density map of Europe [10]

Figure 3.1: High-Speed Rail Network in Europe and Population Density Map

3.2. Current Competitors

Currently, there are four different options to travel from Utrecht to Berlin and back. This section compares the different travel modes, seen in Table 3.1.

Travel mode	Travel time	Average ticket price	Options per day
Aircraft (KLM, TUIFLY)	4h30m	€195	11
Train (NS, DB)	6h15m	€100	7
Bus (Flixbus)	8h20m	€40	40
Car	6h30m	€275	/

Table 3.1: Current travel options for the Utrecht - Berlin connection.

3.2.1. Intercity train and ICE

Seven times a day NS and Deutsche Bahn operate a conventional intercity train between Amsterdam and Berlin. With a travel time of 6 hours and 16 minutes between Utrecht and Berlin (including one transfer in Amersfoort) this is the fastest train connection. The prices are relatively cheap, starting at 39 euros for a one-way ticket in second class. One way tickets in first class start at 70 euros. However, these prices vary and depending on the booking time, the prices can go up to 130 euros. Therefore the average ticket price for a first class one-way ticket was considered to be around 100 euros [11].

There is also the possibility to take the ICE train from Utrecht to Berlin. Although the ICE train is a high-speed train and can exceed speeds over 300 km/h, it is not the fastest option for the Utrecht - Berlin route. The reason for this is because of the many stops it makes and therefore it can not reach high speeds. It takes approximately 7 hours and 15 minutes. Hence for the Utrecht - Berlin route, it is slower than the intercity train operated by NS and Deutsche Bahn. Additionally, ticket prices are higher. The cost for a one-way ticket can vary from 103 to 170 euros and can go easily up to 250 euros for the first-class [12] [13]. Because travel time takes longer than intercity train, it is excluded from the competitor analysis.

3.2.2. Aircraft

Travelling to Berlin can also be done by aircraft. From Schiphol and from Brussels Airport there are on average 17 direct flights to Berlin every day, which take around 1 hour and 30 minutes. However, this travel time does not include boarding time and time needed for security clearance. Normally it is advised to arrive 2 hours in advance at the airport before the departure. Additionally, travelling to and from the airport takes time as well. From Utrecht it takes approximately 30 minutes to go to Schiphol by train. And from Utrecht to Brussels it takes 2 hours and 30 minutes. Another disadvantage of travelling by aircraft is that the airport in Berlin is relatively far away from the city centre. The prices of the tickets vary considerably. A one-way ticket starts from 40 euros (if booked in advance) and can go up to 350 euros. 195 euros was considered to be the average price for an one-way ticket. And for taking extra luggage, an extra fee needs to be paid [13].

3.2.3. Flixbus

The cheapest option to go to Berlin is to travel with Flixbus. FlixBus is a German intercity bus provider, operating in 16 countries, mostly in Western Europe. Each day, Flixbus operates 4 buses from Utrecht to Berlin. Another 34 buses depart from close to Utrecht (Eindhoven, Rotterdam, etc) to Berlin each day. The price for a one-way ticket is relatively low, around 40 euros. But the travel time can easily exceed 11 hours and there is a transfer in Hanover or in Hamburg for most connections [13].

3.2.4. Car

Lastly, there is the option to go by car from Utrecht to Berlin. This is a 640 kilometres drive and the journey lasts approximately 6 hours and 20 minutes not accounting for any traffic jams or any other potential delays. Driving by car can also be one of the more expensive options as it costs around 275 euros for the 640 km route. This is considering that the cost for driving 1 km with an medium sedan 42 euro cents, according to [14]).

3.3. Market Size

The market for AeroCity was sized based on the current amount of travellers between Utrecht and Berlin, from section 3.2. It is estimated that currently there are 5 million passengers travelling between Utrecht and Berlin. Of these 5 million passengers, around 38% travel by plane, 28% by train and 34% by car and bus. This is the current market volume and it is visualised in Figure 3.2a.

The current market value was calculated by multiplying the number of estimated travellers of a particular travel option with its average ticket price (found in section 3.2). The total market value is estimated to be 610 million euros per year. This is visualised in Figure 3.2b.

Aviation has 61% market share in terms of value. The train has a 23% market share and bus and car transport together have 16 % market share. Since AeroCity is targeting travellers who consider travel time and comfort as important factors, AeroCity is mainly competing with aircraft and train. Car and bus are not really considered as a competitor for AeroCity.

AeroCity's ambition is to take over 25 % of the current passengers from aviation and rail in the first 5 operational years. It is expected that as sustainable transportation is becoming more and more important for people, AeroCity's market share will grow over the years. This speculation is based on the added value (travel time of 2h15 min, sustainability and cheaper ticket prices). AeroCity will bring compared to current high-speed transportation modes. This is further explained in section 3.4. Therefore, AeroCity's long term ambition is to have a 60 % market share in terms of travellers and hence it will become the dominant player in high-speed transportation for the Utrecht - Berlin route.

As a result, it is estimated that AeroCity will transport yearly 2 million passengers and will capture around 50.4 % of the current market in terms of value [13].

(a) Current Market Volume

(b) Current Market Value

Figure 3.2: Current Market of the Utrecht - Berlin route

3.4. Product Validation by SWOT analysis

This section validates the AeroCity concept by the use of a SWOT (Strengths, Weaknesses, Opportunities and Threats) analysis. It analyses the potential of AeroCity and its chances to succeed. This is done by analysing AeroCity's strengths and weaknesses on the internal and external level. The SWOT analysis is shown in Table 3.2. It is intended to spot opportunities and threats such that in the end the AeroCity concept succeeds and satisfies the mission objective.

Table 3.2: Strengths, Weaknesses, Opportunities and Threats Analysis

	Pros	**Cons**
Organisational (internal factors)	**Strengths**	**Weaknesses**
	-Convenient transport -Fast Transport -Cheap infrastructure -Sustainable -Low maintenance cost -Autonomous -Less weather dependence	-Not "backward compatible" -New technology (risk) -Land acquisition (inefficient land use) -High tunnelling cost
Environmental (external factors)	**Opportunities**	**Threats**
	-Political strategies to rise sustainability awareness -Rising noise awareness -Decongestion of cities -Expanding the network of The Netherlands	-Other future competitors (Hyperloop,...) -Unified infrastructure needed -Dependent on government (taxpayers) -Societal resistance to change

3.4.1. Strengths of the AeroCity concept

AeroCity's biggest selling point is travel speed (305 km/h) whilst at the same time reducing the initial capital required to build the infrastructure (See section 18.2. As at this moment, HSR is very capital intensive due to its high infrastructural cost. This is where AeroCity comes into play. AeroCity matches the speeds and the convenience of current HSR whilst at the same time reducing infrastructural costs and the break-even time. The maintenance cost of the track will be lower as well since AeroCity is flying above the track and therefore does not have any contact with the track. As a result, AeroCity is also less weather dependent, making it more reliable than trains. (For example, a common problem for trains is the forming of ice during winter on the infrastructure overhead line which decreases the flow of electricity to the train and damages the pantograph. [15]) Comparing AeroCity with aircraft, AeroCity is a much more convenient way of travelling because the time for boarding and security clearance is lower. Furthermore, the AeroCity stations are located closer to the city centre. Additionally, AeroCity is much more sustainable since it is electrically powered. Since a lower initial investment is required and thereby the break-even time is reached earlier compared to HSR, ticket prices can be cheaper [13].

3.4.2. Weaknesses of the AeroCity concept

AeroCity is not "backwards compatible". This means that AeroCity can't use parts of existing intercity railway infrastructure (compared to HSR). For AeroCity a whole new infrastructure is required. AeroCity is less space-efficient as it is more than twice as wide when compared to HSR and therefore more land acquisition is needed. Also, since the required tunnel diameter for AeroCity is twice the tunnelling cost will be 4 times more expensive than tunnels for HSR, as further explained in subsection 18.2.4. Therefore AeroCity is only economically beneficial for relatively flat areas where the need for tunnels is limited. For example, AeroCity's infrastructure would not be economically beneficial in mountainous areas as for example the Pyrenees [13]. Since AeroCity is a rather new technology, this concept has a higher risk to fail than e.g. improving current systems. As a result, the development costs will be higher compared to improving already existing systems.

3.4.3. Opportunities of the AeroCity concept

Some of the external factors which can help to bring AeroCity to market are explained in this subsection. As sustainability awareness is growing and more and more people consider sustainability as an important aspect, AeroCity has a greater chance to become successful. AeroCity has significantly fewer noise emissions than its competitors (explained in section 19.3). AeroCity runs on renewable energy and does not produce any harmful local emissions. This is another reason to choose AeroCity as currently one of the major concerns around transport in communities is the loud noises that are produced by the passing vehicles. Additionally, AeroCity will bring social and economic benefits to the country e.g. it will decongest the current traffic, etc [13].

3.4.4. Threats of the AeroCity concept

There are several external threats which could make it hard for AeroCity to come to market. One of the major threats is the politics involved in such a big project. As the construction of the infrastructure is highly dependent on time-intensive administration performed by the government (land acquisition, permits, legal, etc). This could greatly slow down the construction process for the AeroCity system. Also, the public has, in general, a high resistance to change. AeroCity will take some time to get accepted by the people. Consequentially, politicians in favour of AeroCity could be voted out, greatly reducing support and potential of AeroCity [13].

4 Load cases during operation

4.1. Normal operation

In this section, the loading diagrams for AeroCity in stationary, take-off and landing, cruise and turning condition are shown. From these loading diagrams, the maximum forces and bending moments can be seen as these are the input for the calculations for the structure of AeroCity.

4.1.1. Stationary phase

For stationary phase, the loading diagrams are given for both front and side view. The front view being the view at the yz-plane, when the bending moment considered acts around the x-axis. The side view is the view from the xz-plane where the bending moment acts around the y-axis. The coordinate system used throughout this report is shown in Figure 12.1. While generating these diagrams, the vehicle was modelled as a beam. In front view, the weight was assumed to act as an evenly distributed load, supported by the wheels. In the side view, the weight is distributed along the length of the vehicle in a way such that each subsystem acts as a point load in its centre of gravity. This yields the loading diagrams as displayed in Figure 4.1 and Figure 4.2.

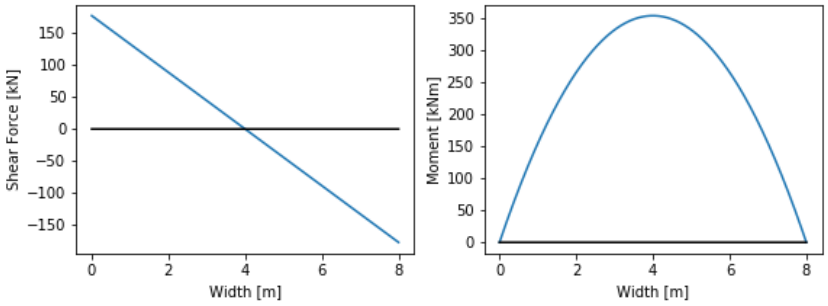

Figure 4.1: Loading diagram: Stationary - front view

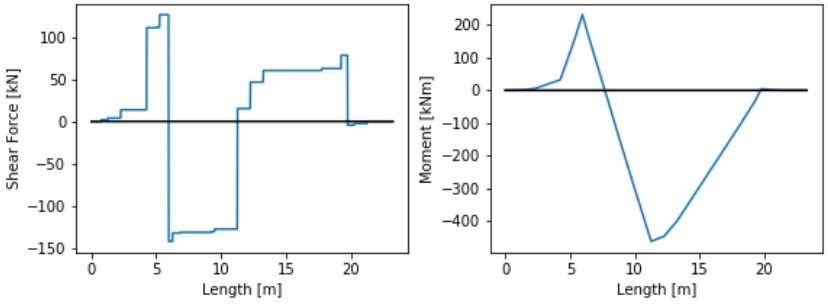

Figure 4.2: Loading diagram: Stationary - side view

The loading diagrams for cruise flight are made with the same weight distribution, but in this case, the thrust, drag and lift are added. The lift is assumed to act in the centre of pressure, which coincides with the centre of gravity. It is chosen to model the lift as a point load, as this will result in the most critical loading condition. The loading diagrams for normal force, shear force and bending moment are shown in Figure 4.3. The loading diagrams of the vehicle from the front view are omitted because this load case is less critical than in stationary phase due to the lift force relieving part of the bending moment and shear force.

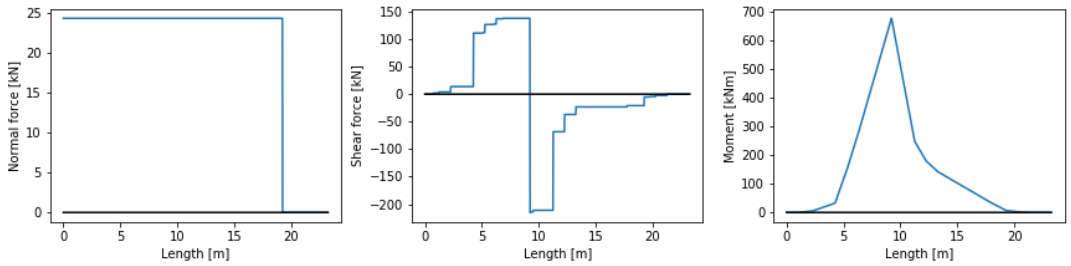

Figure 4.3: Loading diagram: Cruise - side view

For take-off and landing, the loading diagrams are identical. The difference with cruise is that during take-off and landing, the canard produces lift, hence a bending moment and an increase in shear force are created in the side skirts in front of the main wing. The corresponding loading diagram can be found in Figure 4.4.

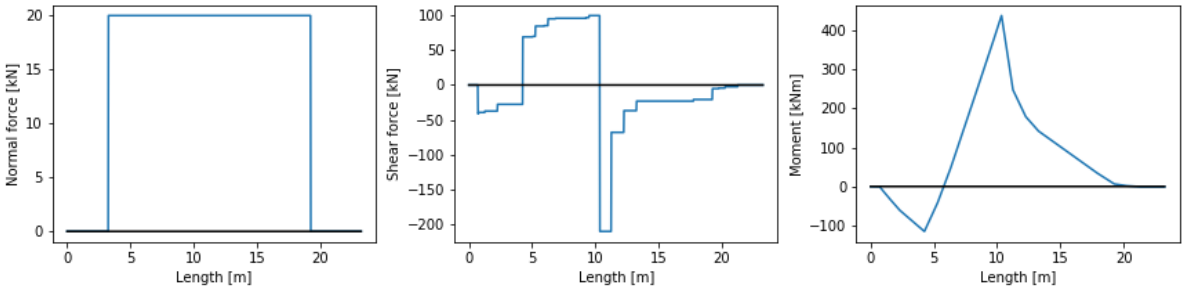

Figure 4.4: Loading diagram: take-off & Landing - side view

The final loading diagram that was considered is the one for turning flight. This diagram is constructed for maximum bank angle at cruise speed with the weight modelled as a point load on the symmetry axis in order to simulate the most critical scenario. This loading diagram can be found in Figure 4.5.

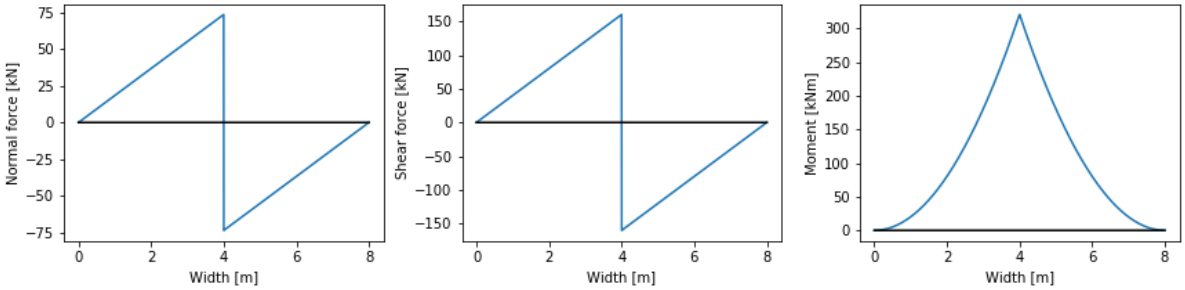

Figure 4.5: Loading diagram: Turning - front view

4.2. External inputs

External inputs for the vehicle can be divided into two cases. Aerodynamic inputs like wind and thermals, and impact forces. The most important aerodynamic force to consider is crosswind, because it is a limiting factor for high-speed ground transport. The vehicle should be able to counter these forces to ensure normal operation. The full aerodynamic design must be validated to operate safely in these conditions. Wind gusts will also have an effect on the operations. The control system should be stable enough to cope with these inputs.

For impact with things on the track, passenger' safety must be ensured. This means that crucial systems must be safe or redundant. The structure in front should be able to cope with impacts in a way that the passenger compartment is not compromised. Other system must also be designed such that they will do minimal harm to the passengers.

5 System requirements

5.1. User requirements (USR)

Performance (PRF)

- USR-PRF-01: Zero emission: the vehicle shall be electrically driven.
- USR-PRF-02: Safe and comfortable travel in the track within the legislation.
- USR-PRF-03: Safe stopping and departure within legislation, comfort level comparable to that of a car, accelerations 0.1 g or below, emergency conditions excluded.
- USR-PRF-04: Reduction of transport system overall cost compared to existing systems, the designed track should reduce the infrastructure cost compared to TGV/ICE by 50%.
- USR-PRF-05: The AeroCity should be available for operation by 2027.
- USR-PRF-06: The structural design has to comply with the airworthiness regulations, CS25.
- USR-PRF-07: Design of infrastructure must be based on the Utrecht to Berlin route.
- USR-PRF-08: The journey time between Utrecht to Berlin should be less than 2:15 hrs.
- USR-PRF-09: The track should require minimum maintenance.
- USR-PRF-11 The speed of the vehicle should be at least 300 kmph.
- USR-PRF-12 The total CO_2 emission from AeroCity shall be 25% less than ICE/TGV.

Safety and reliability (SaR)

- USR-SaR-01: The design should incorporate both the infrastructure at ground level as well as all engineering structures required for high-speed operations.
- USR-SaR-02: The signalling system should be designed with redundancy.
- USR-SaR-03: The AeroCity control systems should have redundancy.
- USR-SaR-04: The tracks should be designed such that the passengers can safely be evacuated in case of emergency.
- USR-SaR-05: The aerodynamic forces at crosswind should be looked at and the crosswind stability must be established up to a crosswind of 100 kmph.
- USR-SaR-06: The vehicle should be autonomous with a possibility of the need-based remote pilot.

Sustainability (S)

- USR-S-01: The track should be as sustainable as possible.
- USR-S-02: The construction of the vehicle should also be made with sustainability taken into account.
- USR-S-03: The life cycle analysis has to be performed on the proposed project.
- USR-S-04: Lower noise levels than a train.
- USR-S-05: The net energy consumption per passenger per km should be 25% less than ICE/TGV.

Cost (C)

- USR-C-01: The cost of the infrastructure and the vehicle should be less than 50% of that of existing high-speed trains (ICE/TGV).
- USR-C-02: The break-even time for the infrastructure should not exceed 30 years.

Passenger comfort (PC)

- USR-PC-01: Seats and pitch are like first class ICE; design seats layouts.
- USR-PC-02: Ticket prices are 50% of first class ICE.
- USR-PC-03: Check-in time less than 5 minutes.
- USR-PC-04: Consider acceleration/deceleration comfort with or without seat belts.
- USR-PC-05: Consider on-board toilets or off-board compared to station-platform facilities and taking next AeroCity.
- USR-PC-06: Consider passenger comfort compared to weight speed range, number of seats, number of doors.

Other (O)

- USR-O-01: The designed AeroCity should be compared with other TGV/ICE to compare infrastructure cost, safety, CO_2 emission, energy consumption, noise emission, passenger capacity, etc.

- USR-O-02: The final design must be also be compared to Hyperloop and a deetailed technical report on the advantages and disadvantages of AeroCity w.r.t. Hyperloop should be made.

5.2. Functional requirements (FR)

Power (PWR)

- FR-PWR-01: The vehicle shall be electrically driven.
- FR-PWR-02: The CO2 emissions shall be less than 25 % of TGV/ICE.

Speed (SPE)

- FR-SPE-01: The vehicle shall have a cruise speed of 305 km/h
- FR-SPE-02: The vehicle shall have a takeoff speed of 200 km/s.
- FR-SPE-03: The maximum taxiing speeds in the station shall be less than 35 km/h

Stability and control (SaC)

- FR-SaC-01: The vehicle shall be able to operate in extreme crosswind conditions of up to 75 km/h
- FR-SaC-02: The vehicle shall be able to operate with nominal crosswind conditions of up to 65 km/h
- FR-SaC-03: The stability of the vehicle shall be ensured autonomously.

Infrastructure (IS)

- FR-IS-01: The infrastructure shall be able to withstand snow
- FR-IS-02: The infrastructure will be able to drain up to 10 cm of rain per hour
- FR-IS-03: There will be a maximum altitude gradient of up to 4 %
- FR-IS-04: The station shall be accessible by other methods of public transportation
- FR-IS-05: The track surrounding the station (± 2km) shall be free of ice

Journey time (JT)

- FR-JT-01: The total journey time shall be at maximum 2 hours and 15 minutes.
- FR-JT-02: Boarding time will be on average less than 5 minutes.

Maintenance (MT)

- FR-MT-01: There will be one maintenance session per week that will last up to four hours
- FR-MT-02: There will be one overhaul maintenance session every five years

Noise Emissions (NO)

Noise emissions shall be as low as regular trains.

- FR-NO-01: Noise levels during normal operations shall not exceed 120 dB.

Operational weather conditions (OWC)

- FR-OWC-01: During normal operations, rainfall shall not exceed 25 cm per hour.

Safety (SFT)

- FR-SFT-01: Deceleration shall not exceed 1.5 m/s^2

5.3. Non-functional requirements: (NFR)

[nosep] The non-functional requirements are divided into the following categories.

Sustainability (S)

- NFR-S-01: The track shall be constructed using sustainable methods.
- NFR-S-02: The track shall be constructed using sustainable materials.
- NFR-S-03: The station shall be constructed using sustainable methods.
- NFR-S-04: The station shall be constructed using sustainable materials.
- NFR-S-05: The vehicle shall be constructed using sustainable methods.
- NFR-S-06: The vehicle shall be constructed using sustainable materials.
- NFR-S-07: The full life-cycle of the whole system shall be sustainable.
- NFR-S-08: The net energy consumption per passenger per km shall be 25 % less than TGV/ICE

Cost (C)

- NFR-C-01: The cost of the infrastructure and the vehicle combined shall be less than 50 % of TGV/ICE.
- NFR-C-02: The break even time for the infrastructure shall not exceed 30 years.
- NFR-C-03: The designed track shall be less than 50 % of TGV/ICE.
- NFR-C-04: The ticket prices are 50% of first class ICE tickets.

Regulations (R)

- NFR-R-01: The structural design shall comply with the airworthiness regulations, CS25.

Safety and reliability (SaR)

- NFR-SaR-01: The vehicle shall be designed with emergencies in mind.
  - There shall be an emergency break system
  - There shall be a cabin emergency lighting system
  - There shall be the correct number of emergency exits as to comply with the CS25 regulations.
- NFR-SaR-02: The track shall have emergency escape paths
- NFR-SaR-03: The vehicle shall have redundancy of the control systems.
- NFR-SaR-04: The track shall have redundancy of the signalling system

III

System Design

Now that the system has been introduced and the market gap and its basic operations were outlined. In this part, the detailed design of the system is presented. This is done by going through the design of all the different subsystems and presenting the design process and the final results for each. This part contains most of the technical details of the design and represents most of the technical design work that was conducted for this project. This is followed in the next part by a performance analysis of the final design. Lastly, the report is then concluded in Part V.

6 Infrastructure

When looking at the concept of AeroCity, one of the most important parts is the infrastructure. Infrastructure is one of the key elements that give AeroCity an advantage when comparing to high-speed rail. Infrastructure is an integral part of AeroCity as it gives the vehicle a medium to travel. In this chapter, the major aspects of the infrastructure plan for AeroCity will be discussed. Firstly, the detailed design of the track will be analysed in section 6.1. This involves the layout, the cross-section and the drainage. Secondly, a comparison to high-speed rail and hyperloop will be done in section 6.2, to show how AeroCity is better and where costs can be saved. After this, the route will be discussed in section 6.3. Lastly, the location of the station in Utrecht and Berlin, as well as the stops in between will be discussed in section 6.4.

6.1. Track

Depending on geographic obstacles, different track types will need to be used. In this subsection, these three track types will be discussed.

6.1.1. Ground Track

For most of the route between Utrecht and Berlin, geographical obstacles such as hills, rivers, and urban areas, are minor. Therefore, for most of the route, the track can be built on ground without the need for any viaducts or tunnels. However, viaducts and tunnels will be described in subsection 6.1.2 and 6.1.3, respectively. Additionally, the way the pressure is distributed is described later in this section and the track turning radius is described in subsection 6.1.4.

Track Layout

The cross-section and the layout of the track is displayed in Figure 6.1

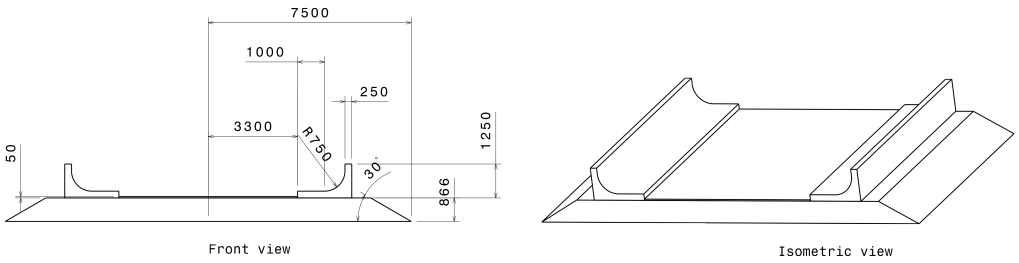

Figure 6.1: Cross-section of the track. Dimensions in millimetres.

In Figure 6.1, the lowest part is the foundation for the track. The subgrade is the layer above the ground, this provides a smooth and uniform bed for laying the track and it also provides soil stabilisation. Additionally, it bears the load transmitted by the wheels during both taking-off and landing, to the ground. Last but not least the subgrade is used to facilitate drainage. At cruise speed, the height of the track is required to be constant in order to guarantee comfort for the passenger. Therefore the subgrade is also used to level out the ground contours of the land. This is done by either providing additional earthwork over the existing ground or by excavating the existing ground.

On top of the subgrade, the bobsled concrete tracks are installed. The bobsled shaped track provides some passive vertical and lateral stability for the vehicle. When the vehicle is increasing in height more air can escape from the sides which implies a reduction in aerodynamic lift and AeroCity will then automatically decrease in height. The bobsled shaped track will also function as a lateral guidance system. When the vehicle is banking on the bobsled sides of the track, the vehicle will automatically return to the middle due to the angled lift vector. During the take-off and the landing phase, the concrete track will function as more of a regular track to transfer the loads exerted by the wheels into the subgrade. As the pressure during this phase on the track is higher than during cruise, the foundation below the track will need some extra reinforcements in the form of ballast.

After a recurring distance of five meters, a concrete bar will be placed between the two sides of the track to fix the distance between the sides. The rest of the middle of the track will be filled with subgrade earth material and will be covered with an anti-root fabric. This anti-root fabric will resist root penetration by plants but will be permeable allowing rainwater to flow through for drainage.

One final aspect to consider when looking into the track is the materials thermal expansion. To prevent any accidents or incidents the thermal expansion coefficient should be taken into account when constructing the concrete prefab. If this is not done, there runs the risk that gaps may occur between the prefab sections, or it can even be possible that the prefab sections expand into each other thus further spacing the track when the concrete returns to its normal state on a day with nominal weather conditions. Issues can arise during the trajectory of the route, as the spacing can eventually become so great between the prefab sections that debris can fall into this place and can cause a disruption into operations by ruining the path of the vehicle.

The best solution for this, besides taking the thermal expansion coefficient into account when creating the prefab sections, is to add an expansion joint in between the prefab sections. This can prevent any defects during the length of the track. When considering the width of the track the concrete bar that is installed in between the two sides shall be able to control and limit the expansion and contraction. This shall eliminate any issues considering the vehicle fitting on the track.

It has been determined that for the ground portion of the track there will be a double track meaning that there will be two tracks allowing AeroCity vehicles to travel in both directions.

Pressure Distribution

One of the most important items that the track must do, is distribute the pressure so that the ground does not take a significant load, potentially crumbling the ground. Traditionally, a track for a rail has multiple layers, this is due to the fact that the weight of the train, also known as rolling stock, has a large weight and this weight is concentrated on the wheels as point loads. This means that there is a large amount of pressure on the rails and this weight must be distributed before it hits the ground (subsoil). The pressure distribution can be seen in Figure 6.2.

As seen in Figure 6.2, the pressure directly on the rail coming from the train is approximately 1000 MPa. Therefore, there must be multiple layers for the track in order to reduce this pressure to a final pressure of 0.01 MPa on the subsoil. When comparing trains to AeroCity, the pressure on the track is much lower during cruise as there are no point loads. This is due to the aircraft flying above the ground thus having a greatly distributed pressure over the track. The pressure above the track can be calculated using Equation 6.1. According to Nouwens [17], it is known that the maximum C_p is roughly around 1.0 during cruise. Additionally, a cruise speed of 84.8 m/s and a surface area of 160 m^2 is assumed for the calculation. It can then be calculated that the pressure above the track is roughly 0.67 MPa. This means that by simply having the track and subgrade above the subsoil, this is sufficient to reduce the pressure to 0.01 MPa at the subsoil level.

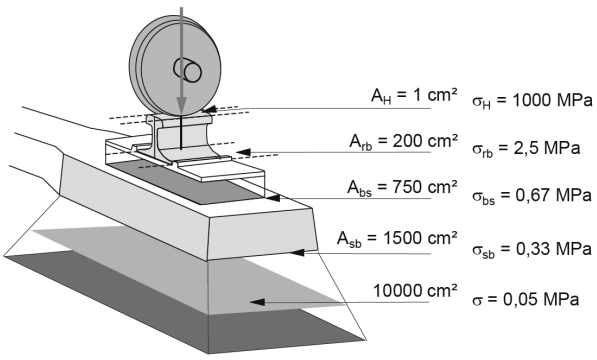

Figure 6.2: Railway pressure distribution [16]

$$C_p = \frac{p - p_\infty}{\frac{1}{2}\rho_\infty V_\infty^2 S} \tag{6.1}$$

6.1.2. Above Ground Track (Viaduct)

Occasionally along the route of AeroCity, there will be sections where a flat track will not be acceptable. These sections primarily will involve any river crossings or highway crossings. In these cases, it is not feasible to cross directly over the ground. Therefore, in these scenarios, an alternative will be needed to successfully continue the track. The most viable option for these scenarios is a viaduct. A viaduct will be able to cross over any obstacle easily, while still maintaining an almost constant elevation at both the beginning and the end. This is ideal as it is preferred to keep the elevation of the AeroCity track relatively flat with small slope gradients to account for the elevation changes along the route.

The viaduct is composed of two different elements. The first element is almost entirely the same as the one used for the ground track, however, this element will be entirely composed of concrete. This track will additionally no longer have any subgrade. The second part will be the necessary pillars that support the track while it is above the

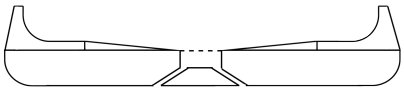

Figure 6.3: Viaduct Cross section

ground. These pillars will be of varying length depending on the difference between the elevation of the track and the elevation of the ground. Additionally, these pillars will have a foundation that is underneath the ground. The size of this foundation will be large as they are needed to support the track which is under pressure.

One additional difference between the ground track and the viaduct is the drainage system. As the track is now entirely made from concrete, rainwater cannot simply flow from the central part of the track into the ground. Therefore there must be an alternative to ensure that rainwater does not accumulate on the track and potentially causing a disruption of the operations. To solve this issue a ditch has been placed inside the middle of the cross-section of the track. This ditch will have additional piping every 5 meters to free the water and release it into the free space below. This ditch will be covered with a drain cover to protect it from being filled with any large objects. This can be seen in Figure 6.3. It has also been noted that the ditch will have minimal impact on the ground effect of the vehicle as it is travelling at high speeds and the ditch is not of great width.

Additionally, it has been considered whether to construct the pillars and the track from either concrete or a strong metal. The advantages of the metal are that the metal is stronger while being lighter. This means that the pillars themselves and the foundation do not have to be as large to support themselves. However, concrete may also be used and can be built with rebar, this can make the concrete stronger while adding minimal extra weight. Concrete was decided to be used as this can keep the costs low and will not add much complexity. Additionally, it has been determined that the viaduct portion of the track will be of a single lane.

6.1.3. Underground Track (Tunnelling)

In certain parts of AeroCity, there will be places where the traditional ground track or a viaduct will not be feasible. In these locations, the last alternative to continue the track would be to construct a tunnel. These locations, however, are very rare and will mainly be occurring during operation in densely populated areas, such as the Rhine-Ruhr-Gebiet area and Hannover. In these locations, it has been determined that the simplest, and most cost-effective solution would be to build underground.

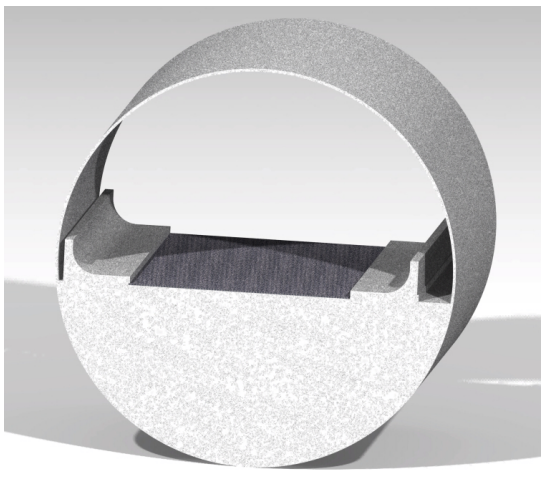

Figure 6.4: Tunnel render

One of the important things to consider is the width of the tunnel. This is of course dependent on the width of the track and the size of AeroCity. As the vehicle must still be able to fit and shall be able to turn with the aid of a bank angle of the track. The bank angle needed for the vehicle will then be lower than its maximum due to these constraints. Additionally, there must be service pathways and emergency pathways next to the track. These pathways should be between 0.75 and 1.5 m wide depending on the final length of the tunnel [18]. Additionally, It has then been determined that the outer diameter of the tunnel will be 12 m. Additionally, it is determined that the thickness of the tunnel should be 80 mm [19]. A rough render of the tunnel can be seen in Figure 6.4.

One of the things that have to be taken into consideration when constructing the tunnel, is just how deep the tunnel

must be built underneath the city. The depth of the tunnel is dependent on the diameter of the tunnel, this can be between 1.5 to 3 time the diameter of the tunnel [20]. This number is also dependent on the soil conditions and any further jurisdictional authority. Based on the width of the tunnel, the depth will be approximately 18 to 36 m.

The other item that has to be taken into consideration when planning the construction of a tunnel, is the rate at which the tunnel can be built. There are three different ways in which a tunnel can be built, however, due to the depth of the tunnel, only two methods can be used. These are the methods of conventional tunnelling and by the use of a tunnel boring machine (TBM). However, the TBM is able to operate at a rate that is faster than that of the conventional methods, reaching between 15 and up to 50 meters a day, with the potential of reaching up to 150 m a day in the future [21] [22]. Additionally, it has been determined that when going through tunnels the track will be single lane.

6.1.4. Track Turning Radius

When analysing the trajectory of the route between Utrecht and Berlin, via the Rhine-Ruhr Gebiet area and Hannover, it can clearly be seen that turns will be required multiple times along the route. Therefore, it is important to determine what the turn radius can be along the route because if a turn is smaller than this turn radius the vehicle will be limited in speed thus the travel time would increase. It is then of utmost importance to determine the minimum turn radius for AeroCity.

To determine the minimum turn radius of the track, it is important to first determine at which bank angle AeroCity can travel at, while maintaining a load factor of 1.1. This can be calculated using Equation 6.2. Once the bank angle has been determined, the turn radius can be determined using the dynamic equation for centripetal acceleration. This is given by Equation 6.3. It is then determined that the minimum turn radius required for the AeroCity track is 1.6 km.

$$\theta = cos\left(\frac{1}{n}\right) \tag{6.2}$$

$$R = \frac{V^2}{n \cdot g \cdot sin(\theta)} \tag{6.3}$$

6.2. Advantages over HSR and Hyperloop

AeroCity has multiple advantages when comparing to HSR and Hyperloop. There are discussed below respectively.

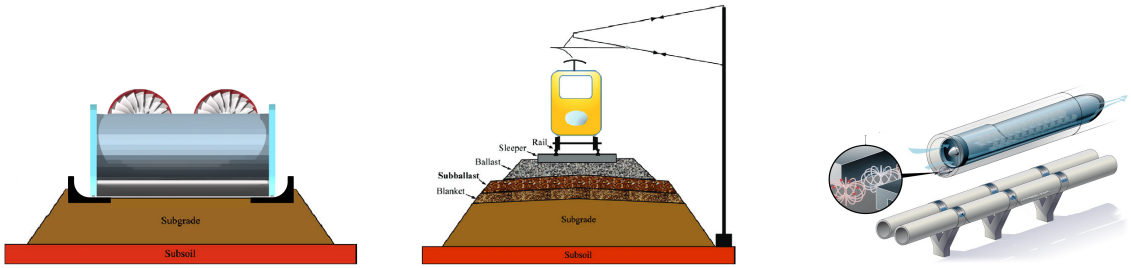

(a) AeroCity infrastructure (b) High-speed rail infrastructure [23] (c) Hyperloop infrastructure [24]

Figure 6.5: Infrastructure comparison

6.2.1. Advantages over HSR

The main advantage of AeroCity's track compared to High-speed Rail (HSR) is that the tolerances are significantly looser as it is flying, and the aerodynamic pressure is uniformly distributed over the track due to the wing-in-ground-effect (WIG). Therefore AeroCity's concrete track can be placed directly on the subgrade. For AeroCity, multiple layers of ballast are not required to diffuse the high dynamic loads from the wheels into the ground as is the case for HSR. Additionally, as there is no physical contact between the AeroCity vehicle and the track during cruise, the maintenance required is significantly lower when compared to HSR. The difference between the track layout of HSR and AeroCity can be seen in Figure 6.5.

6.2.2. Advantages over Hyperloop

Comparing Hyperloop to AeroCity, the infrastructure for Hyperloop is much more complex. This is because AeroCity is using the air instead of fighting against it and the tolerances for AeroCity are looser and the infrastructure is simpler. The tolerances for Hyperloop are significantly tighter, mainly due to the vacuum tubes, magnetic propulsion, and

other elements that are in the track. In order to accomplish this, Hyperloop will use an airtight tube system made from steel connected to vacuum pumps. This will imply more design risks for Hyperloop's infrastructure, e.g. the steel vacuum tubes will experience thermal expansion above ground. On the other hand, building and maintaining vacuum tubes capable of withstanding pressure fluctuations at tight tolerances is difficult and will escalate the infrastructure cost. Accommodating emergency exits for this system makes the infrastructure even more complex. The maintenance for hyperloop is also significantly more labour intensive than for AeroCity as problems such as searching for air leaks can be very difficult and time-intensive. Lastly, steel tubes can be a bigger issue in terms of landscape pollution. AeroCity does not have these drawbacks and can still carry a substantial amount of passengers at high speeds.

6.3. Route

Figure 6.6: Utrecht - Berlin Route

One of the important aspects of AeroCity is routing. For this specific project, it has been decided to do an analysis for a route between Utrecht and Berlin. It has been decided that the route will go through Rhine-Ruhr-Gebiet area and Hannover. This was decided because it would help AeroCity to expand in the future as it would provide potential connections to other cities. Hannover and Rhine-Ruhr-Gebiet are two great areas since they are conveniently located in between Utrecht and Berlin. Hannover is the capital of the Lower Saxony province and counts 586,000 inhabitants. The Rhein-Ruhr-Gebiet is largest urban area in Germany with a population of over 5 million people (2018) [25].

When considering route planning there are a few important aspects to consider, firstly the most important aspect to consider is where to place the stations along the route. This should be done to minimise the total distance. As this aspect is an important and detailed part, it is described in section 6.4. The following item to consider is just how many times a viaduct or a tunnel will be needed. Additionally, it must be mentioned how the turn radius affects the route trajectory.

Table 6.1: Distances between stops

Routing	**Distance** $[km]$
Utrecht - Rhine-Ruhr	186
Rhine-Ruhr - Hannover	196
Hannover - Berlin	269
Total	**651**

The number of viaducts and tunnels needed is dependent on the trajectory. Viaducts and tunnels can be avoided by changing the placement of the route. However, this can only be done up to a certain extent because if one changes the placement too much the added distance can increase by a significant amount. Therefore in certain situations, it is unavoidable to place a viaduct or a tunnel. The two main situations where a tunnel or a viaduct cannot be avoided is during river or road crossings. Therefore it is important to estimate just how many rivers and highway crossings there will be on the trajectory between Utrecht and Berlin, including the deviations to the Rhine-Ruhr-Gebiet area and Hannover. When performing a simple analysis it has been estimated that there will be approximately 10 river crossings along the planned trajectory. The following step is to estimate what length is needed for the viaduct to cross over the river or highway. As the rivers along the trajectory are not very wide, it has been assumed that each viaduct will have a length of 1 km. This will account for the additional terrain that may be needed to keep the track at the same elevation at both the beginning and the end of the viaduct. When considering highway crossings it has been estimated that there will be approximately 40 highway crossings along the planned trajectory. As highways are not as wide as rivers, and not much additional land is needed to maintain the same elevation or a small grade, it is assumed that most highway crossings will have a viaduct length of 500 meters. This makes a total of approximately 30 km of viaducts.

As mentioned in subsection 6.1.3, tunnelling is a long lasting, expensive, and difficult process. Therefore it is ideal to limit tunnelling to the locations where the alternatives would not be feasible. These locations would be when going through the densely populated areas of both the Rhine-Ruhr-Gebiet as well as when crossing through Hannover. It has been estimated that in total approximately 45 km of tunnelling will be needed along the whole trajectory.

The final element to take into account when planning the route is the minimum turn radius. This has been estimated to be 1.6 km in subsection 6.1.4. This, however, is quite a small radius when compared to alternatives such as high-speed rail (HSR). When performing a direct comparison to HSR, for the same speeds as AeroCity, a minimum turn radius of approximately 5 km is needed [26]. This means that AeroCity can be more flexible with its routing as smaller turns are allowed.

6.4. Station Placement

The location of the stations in Utrecht, Rhine-Ruhr-Gebiet, Hannover and Berlin were chosen on different criteria. Good connectivity with established public transportation is considered to be important for passengers. The location of the stations is also chosen in order to avoid the need to cross the residential and industrial areas to decrease the need for tunnels and viaducts but also to decrease land acquisition costs. This section explains the location of the different stations. In Table 6.2 one can see how far each station is from the city centre.

6.4.1. Utrecht

For Utrecht, the Lunetten Train Station was chosen for the Utrecht Berlin route. The Lunetten train station is conveniently located in the direction of the Rhine-Ruhr-Gebiet in the south of Utrecht. Therefore the need to cross residential areas in Utrecht is reduced and no tunnels or viaducts in Utrecht are needed which decreases the infrastructure cost significantly. This station is easily accessible, it only takes 5 minutes by sprinter to get from Utrecht Central station to Utrecht Lunetten station. Utrecht Lunetten station is also easily accessible from the city centre by bus and tram as can be seen in Figure A.2. Additionally, around this station, there is enough area to expand the already established sprinter station. The combination of all these reasons mentioned above made the choice of the Lunetten Train station easy.

6.4.2. Rhine-Ruhr-Gebiet

When searching for a station located in the Rhine-Ruhr-Gebiet, there are a few elements to take into consideration. The first element that must be taken into consideration is the accessibility of the AeroCity vehicle in and around the city. The next element that must be taken into consideration is the connectivity to the city centre as well as the nearby larger cities. The major cities in the Rhine-Ruhr-Gebiet area are Cologne, Dortmund, Dusseldorf, Duisburg, and Essen. Therefore to be better connected within the region, it is best to be placed in one of these cities. When analysing the route from Utrecht and towards Hannover it is ideal to place the station in one of the northern cities. This would eliminate Cologne and Dusseldorf as possible options.

When considering the accessibility of the AeroCity vehicle, the three remaining cities have no significant advantage over each other. This means that the main criterion to take into consideration is the connectivity to the other large cities in the region. This leaves Duisburg as the best location to place an AeroCity station. Duisburg in relation to the other larger cities in the area can be seen in Figure A.3. Duisburg is less than 15 minutes to Dusseldorf, half an hour to Dortmund, and is only 10 minutes to Essen. This was compared to placing a station in Dortmund, where a connection to Dusseldorf would be close to an hour.

However, as this location is close to existing dense housing and industry, there will be a considerable amount of tunnelling or viaducts needed. This choice was made as it is considered the simplest option, considering that in large part it is not likely that the land can be acquired from existing landowners within the city. The way that tunnels and viaducts will be made for AeroCity will be described in subsection 6.1.3 and subsection 6.1.2, respectively.

6.4.3. Hannover

From a proper urban area analysis of Hannover, it was decided that the location of the AeroCity station will be built next to the already existing Bismarckstrasse train station, see Figure A.4. This location is great because it is close to the city centre while there is room for the construction of the track coming from the south and going to the east. Building the AeroCity station next to Bismarckstrasse train station makes it so that travelling with AeroCity is very convenient because of its central location and its great connectivity with other stations in Hannover. Travelling from Bismarckstrasse to Hannover Hauptbahnhof only takes 4 minutes by train. Also, other stations in Hannover are easily accessible from this station. As the location is relatively close to the centre and it is surrounded by residency and industry some tunnels or viaducts will be needed. However, considerably fewer tunnels or viaducts are needed comparing to if the location was chosen to be next to the Hannover Hauptbahnhof Station.

6.4.4. Berlin

When looking into where to place a station in Berlin, various options were considered. When considering passengers' convenience, it is ideal to place the station as close to the city centre as possible. This is to allow for ultimate connectivity to all other parts of the city so passengers can have a minimal travel time to get to the station. It was then thought to have the station placed close, or next to Berlin Hauptbahnhof. This would have provide a central location, allowing for minimal travel time for most passengers. However, when looking into this option it was decided that this location may have proven to be unfeasible. The reasons for this location being unfeasible was due to the high costs associated with building in the city centre, and the high costs associated with running a track through the city. It was thought that a tunnel may be constructed to get to the central station, however, tunnel costs through such a dense city may prove to be high.

As this option has been shown to be unfeasible, an alternative was searched for. When looking for an alternative it was thought that a station could be placed as close to the city as possible, and as close to existing public transport infrastructure as possible. This would be to significantly reduce travel time into and around the city. When looking into possible options, it was determined that a station for AeroCity can be built at Westkreuz. This location is conveniently located between the city centre of Berlin and Hannover, thus making it a convenient location to have a station. Additionally, Westkreuz is less than 15 minutes away from Berlin Hauptbahnhof. A detailed version of the Berlin public transport map can be seen in Figure A.5. As can be seen, this option allows for good connectivity within Berlin, without being in the city centre. This then saves cost and time, as construction, land acquisition, and tunnelling will not have to be done in the dense city of Berlin.

Table 6.2: Distance and Time to Central Station

Location	**Distance to Central Station** [km]	**Time to Central Station** [min]
Utrecht	3.8	5
Duisberg	0	0
- to Dortmund	52	35
- to Dusseldorf	25	12
- to Essen	18	12
Hannover	3.2	4
Berlin	7.7	13

7 Aerodynamics

This chapter presents the aerodynamics of the AeroCity vehicle. It begins with an introduction to the vehicle shapes and the flight envelope described in section 7.1. It continues with an overview of the work of Nouwens [17] in section 7.2, and it ends with the presentation of the relevant aerodynamic parameters in section 7.3.

7.1. Vehicle Shape & Flight Envelope

The AeroCity vehicle presents an original canard aircraft configuration, optimised to obtain the highest energy efficiency while also complying with time, cost, safety and comfort constraints. A drawing of the vehicle concept is presented in Figure 7.1.

Its main wing surface (from now onward referred as "wing") has a span of 8 m and a chord length of 20 m. It features a NACA 68115 airfoil shape, which possesses the flat bottom characteristic necessary to avoid the diffuser effect. It has no sweep, no dihedral, and no twist. The pivoting point for changes in the angle of attack is located at the half chord point and it lies at about 1 m from the bottom of the sideskirt. Two sideskirts terminate the wing tips and

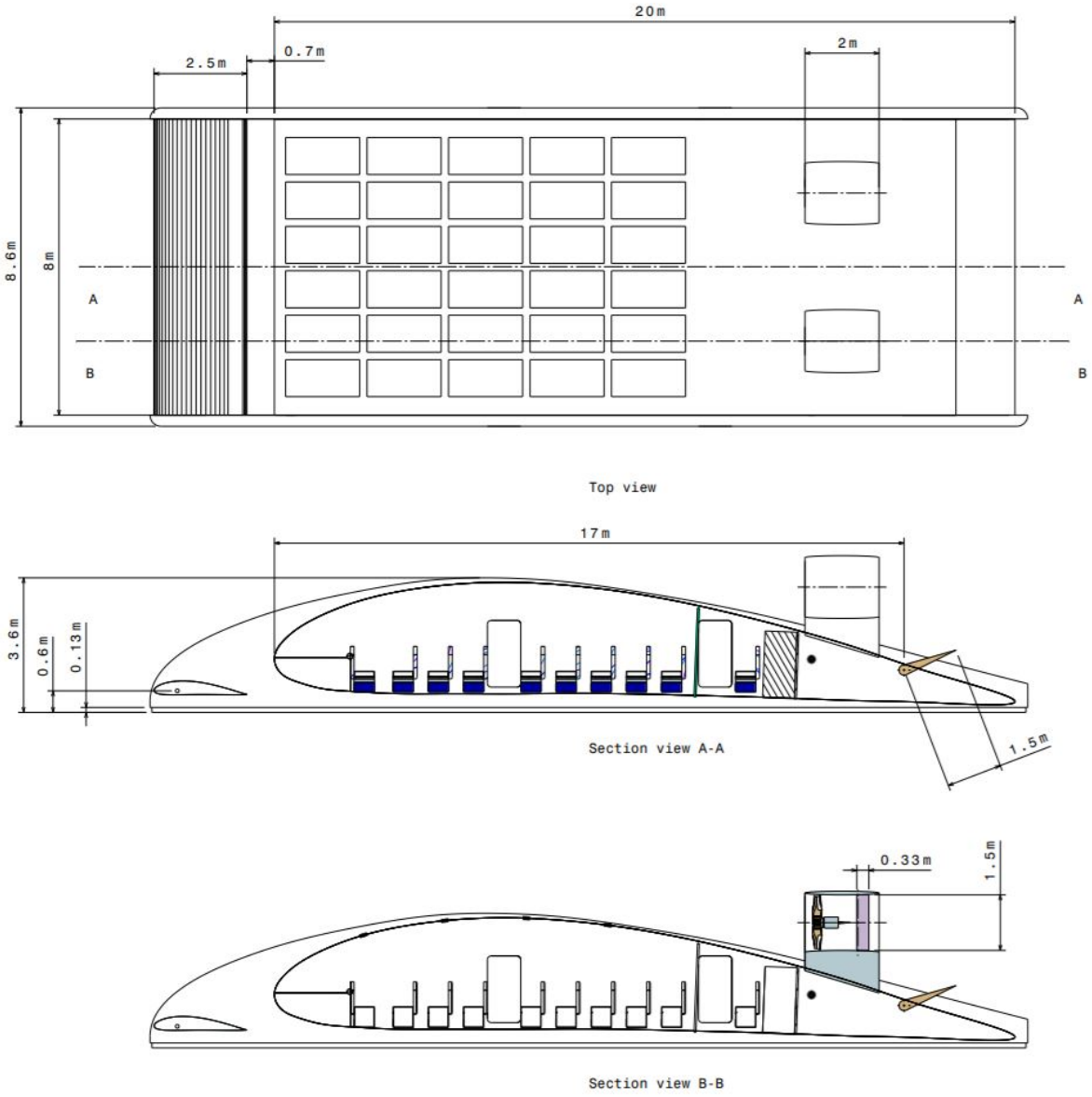

Figure 7.1: Drawing of the AeroCity vehicle.

extend downward to achieve a ground clearance of 5 cm. Their maximum thickness is 30 cm and, as suggested by both Nouwens [17] and Van Sluis [27], they are made of an asymmetrical airfoil shape, with a curved outer edge and a straight inner edge. The wing is the main lifting surface of the vehicle.

Its second wing surface (from now onward referred to as "canard") has a span of 8 m and a chord length of 2.5 m. Its leading edge is located 3.25 m in front of the wing's leading edge. It also features a NACA 68115 airfoil shape for the reason mentioned above. It has no sweep, no dihedral, and no twist. The half point of the chord is fixed at about 0.6 m from the bottom end of the sideskirt, and it is the pivoting point for changes in the angle of attack. On its sides, it is terminated, like the wing, by sideskirts with the same ground clearance, size and shape described above. The canard, of the fully movable type, is used for control and trim during the whole flight envelope and to provide extra lift during the take-off and cruise phases.

Two ailerons, with a span of 1.5 m and a chord of 0.35 m, are placed inside the engines ducts, 1 m behind the fan motors. They feature a NACA 0015 airfoil shape. They are primarily used for roll control with the assistance of a ballast system and could be used to assist in pitch control too.

Two rudders, of the same ailerons' shape, are placed right behind the ailerons. They provide yaw control with the assistance of the differential thrust.

The sideskirts leading edge has been given an half-airfoil shape, as Nouwens [17] suggested.

A rectangular spoiler, with 8 m span and 1.5 m chord, is located 17 m behind the wing's leading edge. When deployed, it has the drag coefficient of a flat plate, approximately equal to 1.17 [28], where the reference area used in the drag equation is the frontal area. It was designed for use only during the on-ground braking phase.

The cruise speed is set at 84.8 m/s and the take-off/landing speed is fixed at 55.5 m/s (see chapter 16).

7.2. Relevant Literature

Nouwens has presented the aerodynamic performance and the stability analysis of the Aerocity[1] vehicle in his master thesis[17]. Nouwens did not perform a design process, but rather a sensitivity study on three parameters, namely the aspect ratio, the body angle (angle of attack in AeroCity) and the endplate elevation (sideskirts ground clearance in AeroCity). His investigation was performed by creating a three dimensional model of the Aerocity vehicle and by solving the flow using the CFD code ENSOLV. ENSOLV, being a 3D Navier Stokes solver, made it possible to implement moving boundary condition on the ground, model the viscosity (a crucial aspect for extreme WIG vehicle) and access the complete flow domain. His sensitivity study covered a design space that comprehends aspect ratio from 0.2 to 0.4, body angle from 3° to 5° and endplate elevations from 0 m to 0.5 m. Worth mentioning is that the study was performed considering a wing chord of 20 m, a cruise speed of 100 m/s and a standard sea-level atmospheric condition resulting in a Mach number of 0.3 and a Reynolds number of $1.38 \cdot 10^8$. Moreover, it is relevant to consider that the change in body angle was obtained by rotating the airfoil around the halfway point of the chord, which was located at approximately 1 m from the ground. Lastly, it is essential to notice that the endplates were considered to be always parallel to the ground.

7.3. Aerodynamic Parameters

This section is divided into three parts. These three parts present, respectively, the aerodynamic parameters of the wing (subsection 7.3.1), of the canard (subsection 7.3.2) and finally of the overall vehicle (subsection 7.3.4). This division reflects the design approach taken for the aerodynamic analysis.

7.3.1. Wing aerodynamic parameters

This subsection presents the aerodynamic parameters of the wing in the relevant range of the designed mission flight envelope. The C_{L_w}, the C_{D_w} and the C_{M_w} are the result of second order polynomial regressions, expressed respectively in Equation 7.1 Equation 7.2 and Equation 7.3, of the three data points retrieved from the Nouwens master thesis [17]. Moreover, employing JavaFoil, it was possible to obtain the angle of attack for which the wing produces zero lift, as this angle is independent of the effective aspect ratio. This angle was found to be equal to 1°.

$$C_{L_w} = -0.033 \cdot \alpha^2 + 0.518 \cdot \alpha - 0.666 \tag{7.1}$$

$$C_{D_w} = 0.00055 \cdot \alpha^2 + 0.00115 \cdot \alpha + 0.0108 \tag{7.2}$$

[1] When referring to the previous Aerocity concepts the lower case letter "c" is used.

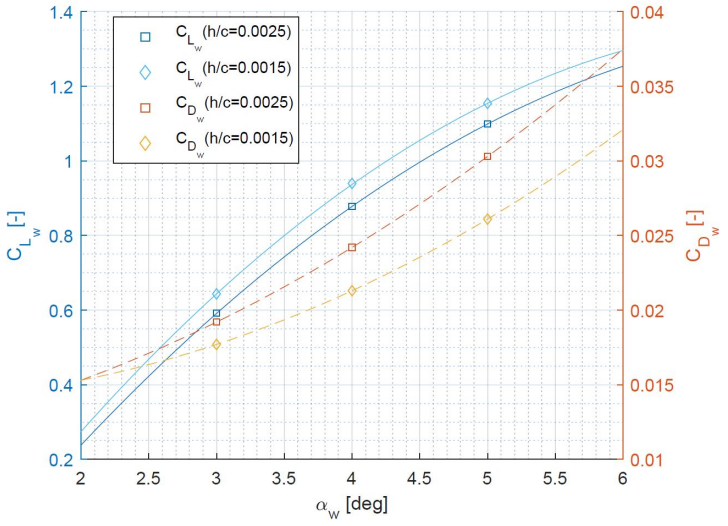

Figure 7.2: Lift coefficient and drag coefficient of the wing. The markers indicated data that comes directly from the Nouwens master thesis [17], the regressions are 2nd order polynomials.

$$C_{M_w} = 0.0175 \cdot \alpha^2 - 0.1725 \cdot \alpha + 0.316 \tag{7.3}$$

The x_{Cp_w}/c and the x_{AC_w}/c have been computed by means of Equation 7.4 and Equation 7.5 respectively. In Equation 7.4 the parameter l is the distance of the half point of the mean aerodynamic chord from the bottom of the sideskirt and the moment coefficient C_M is calculated around a reference point located 5 m from the nose on the bottom of the sideskirt.

$$x_{cp_w}/c = 0.25 - \frac{C_{M_w}}{C_{L_w}} + \frac{C_{D_w}}{C_{L_w}} \cdot \frac{l}{c} \tag{7.4}$$

$$x_{ac_w}/c = x_{cp_w}/c - \frac{C_{M_{\alpha_{wing}}}}{C_{L_{\alpha_{wing}}}} \tag{7.5}$$

In Equation 7.5 a simplification was made, as it was assumed that the contribution of the drag on the pitching moment is negligible.

The wing lift coefficient and frag coefficient are presented in Figure 7.2

The wing centre of pressure and aerodynamic centre are presented in Figure 7.3

7.3.2. Canard aerodynamic parameters

This subsection presents the aerodynamic parameters of the canard in the relevant range of the designed mission flight envelope. The C_{L_c}, the C_{Dc}, the x_{Cpc}/c and the x_{ACc}/c have been computed by means of the JavaFoil software using, as input for the aspect ratio, the effective aspect ratio of the canard.

Because both the wing surfaces employ sideskirts as the primary mechanism to reduce the downwash, the effective aspect ratio of the wing was investigated to obtain sufficient insight in the sideskirts' phenomenon and ultimately estimate the canard's effective aspect ratio. The hypothesis was made that the capability of the sideskirts in containing the magnitude of the tip vortices could be higher than the one of an increase in the wing geometric aspect ratio. The sideskirts remain parallel and close to the ground with increasing angle of attack and should, therefore, be more effective in containing the vortices in comparison with the effect of an increase in the wing geometric aspect ratio.

Firstly, the aerodynamic data of the wing reported in the work of Nouwens [17] were compared to the ones obtained with JavaFoils simulations. JavaFoil can extrapolate the aerodynamic parameters for simple finite wings in ground effect, but it cannot simulate the effect of the sideskirts, and therefore, as mentioned above, it requires the effective aspect ratio to be calculated separately and then given as input. After setting the exact geometry and boundary

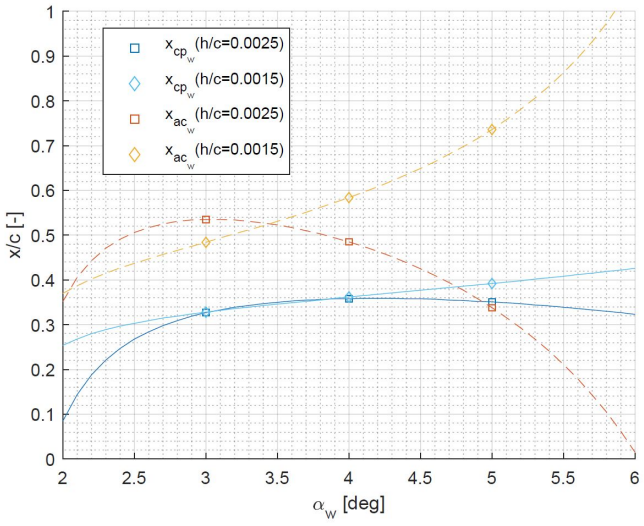

Figure 7.3: Centre of pressure and aerodynamic centre of the wing. The markers indicate the values that result from Equation 7.4 and Equation 7.5 using as input Nouwens' data. The continuous and the dashed lines respectively indicate the values that result from Equation 7.4 and Equation 7.5 using as input the values obtained from the regressions on C_{L_w}, C_{D_w} and C_{M_w}.

conditions, the effective aspect ratio remains the only unknown in an equation in which the lift coefficient given by the software has to be equal to the one given by Nouwens. Different aspect ratios were, therefore, iteratively fed to Javafoil until convergence of the aforementioned coefficient was reached. The aspect ratio for which convergence was reached was deemed to be the effective aspect ratio of the wing in that specific configuration (angle of attack, wing height from ground and sideskirts ground clearance). The process was applied in multiple configurations to cover the relevant aerodynamic design space of the wing. An approximately linear relation was noticed between the effective aspect ratio and the angle of attack as given in Equation 7.6 and Equation 7.7.

$$AR_{eff_w}\Big|_{\frac{h}{c}=0.0025} = 1.17 \cdot \alpha_w - 0.66 \tag{7.6}$$

$$AR_{eff_w}\Big|_{\frac{h}{c}=0.0015} = 1.42 \cdot \alpha_w - 0.66 \tag{7.7}$$

It is essential to mention that Equation 7.6 and Equation 7.7 are intended to approximate the effective aspect ratio with sufficient accuracy only for angles of attack corresponding to lift coefficients in the range from 0.6 to 1.1 as this is the range of lift coefficient obtained from the Nouwens data and relevant to the vehicle design space. It is interesting to notice that at zero-lift angle of attack (approximately 1°), the effective aspect ratio almost matches the geometric aspect ratio. This finding led to the choice of estimating the effective aspect ratio of the canard with a similar equation, in which the slope of 1.17 is retained, and the constant -0.66 is replaced by the value for which the effective aspect ratio of the canard matches its geometric aspect ratio at its zero-lift angle of attack (that JavaFoil shows to be -0.7°). Equation 7.8 and Equation 7.9 present the above mentioned equation.

$$AR_{eff_c}\Big|_{\frac{h}{c}=0.0025} = 1.17 \cdot \alpha_c + 4.02 \tag{7.8}$$

$$AR_{eff_c}\Big|_{\frac{h}{c}=0.0015} = 1.42 \cdot \alpha_c + 4.02 \tag{7.9}$$

For Equation 7.8 and Equation 7.9 the same limitation of Equation 7.6 and Equation 7.7 apply. For angles of attack corresponding to lift coefficients outside the above-mentioned range, the equations were still applied but the lower reliability of the results must be enphasizedF. For angles of attack corresponding to negative lift coefficients, the geometric aspect ratio was used as a conservative approach. Worth noting is that for angles of attack corresponding to the lift coefficient values close to zero, the effect of the aspect ratio is reduced, and consequently, the approximation errors in the calculation of the effective aspect ratio are limited.

The canard lift and drag coefficients are presented in Figure 7.4

The canard centre of pressure and aerodynamic centre are presented Figure 7.5

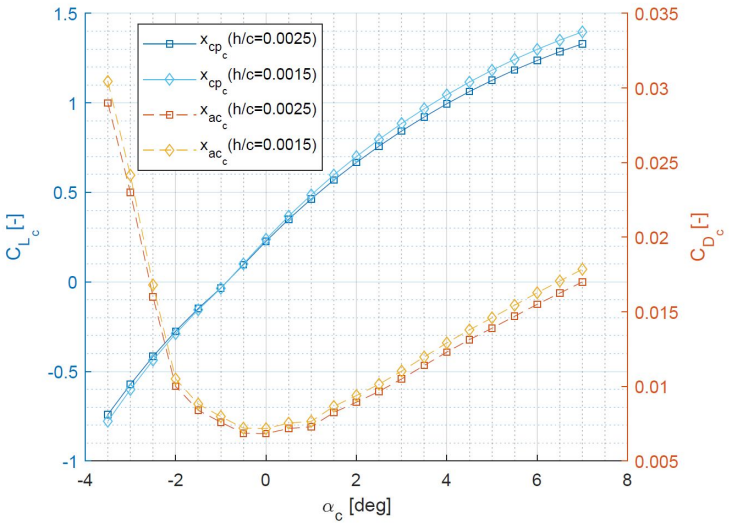

Figure 7.4: Lift coefficient and drag coefficient of the canard obtained using JavaFoil.

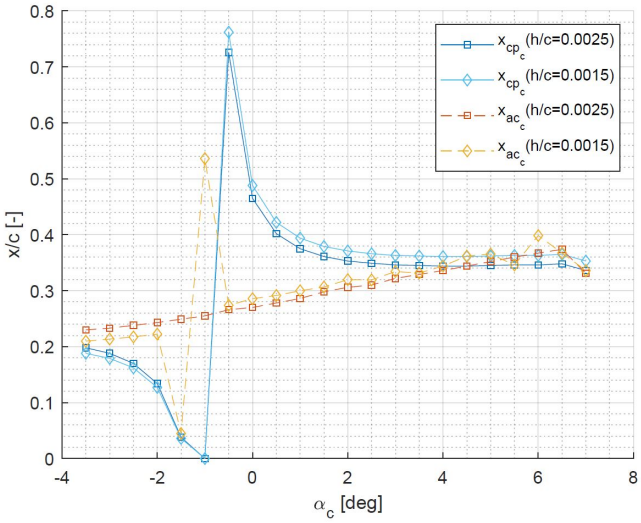

Figure 7.5: Centre of pressure and aerodynamic centre of the canard obtained using JavaFoil.

7.3.3. Ailerons and rudders aerodynamic parameters

This subsection presents the aerodynamic parameters of the ailerons and the rudders in the relevant range of the designed mission flight envelope. As these two control surfaces feature the same geometry, they present the same C_L vs α, C_D vs α x_{cp} vs α $x_{ac} vs \alpha$ curves. The effect of the duct on the ailerons and rudders was modelled by assigning an infinite aspect ratio to these control surfaces. For lift and drag calculations the air velocity at the engine exit (about 1 m after the fan) has been used. The aerodynamic values have been computed utilising the JavaFoil software and are presented in Figure 7.6 and Figure 7.7.

7.3.4. Vehicle aerodynamic parameters

This subsection addresses the effects resulting from the combination and interactions of the canard and the wing. Moreover, it presents the estimation of the drag caused by the engine structure and the extra sideskirts and finally combines the total lift and drag coefficients in the relevant flight conditions.

Three effects have to be considered: the downwash generated by canard and experienced by the wing, the upwash generated by the wing and experienced by the canard and the turbulent flow generated by the canard and experienced by the wing.

For the downwash and the upwash effects, superposition of the wing flow field and the canard flow field was utilised. The JavaFoil software was deemed to be able to simulate the aforementioned with the accuracy needed for the design stage.

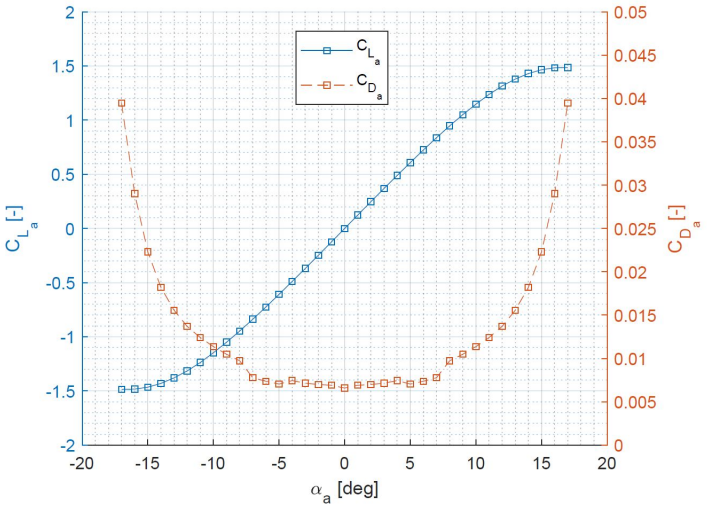

Figure 7.6: Lift coefficient and drag coefficient of the ailerons and the rudders obtained using JavaFoil.

The downwash generated by the canard was found to have a negligible effect on the wing, even in the most critical aerodynamic situation (at $C_{L_{c_{MAX}}}$). The reason for this relies on the limited magnitude of the canard downwash, due to the extreme ground effect condition, and the significant distance between the quarter chord locations of the two lifting surfaces. It follows that the vehicle angle of attack α is equal to the wing angle of attack α_w.

The upwash generated by the wing was instead found to have a considerable effect on the canard in both cruise and take-off/landing conditions. The induced angle experienced by the canard ranges between 2.5° at cruise condition with the lightest vehicle configuration (absence of payload) to 4° in take-off/landing condition with maximum take-off weight (maximum payload). This effect was considered during the design of the rotation mechanism of the canard, to ensure the possibility to set the canard to all the necessary angles of attack required for controlling and trimming the vehicle. Important to consider is that the lift coefficient generated at a specific angle of attack in "upwashed" flow is not equal to the one created at the same angle of attack in undisturbed flow condition. In the second case, the lift coefficient would be higher as the canard trailing edge would be closer to the ground and consequently the outflow area would be reduced, the flow under the canard decelerated and the high pressure better maintained. This means that the effect of the upwash on the lift coefficient of the canard would be overestimated when the induced upwash angle is algebraically added to the undisturbed flow angle of attack.

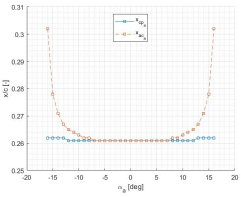

Figure 7.7: Centre of pressure and aerodynamic centre of the ailerons and the rudders obtained using JavaFoil.

Finally, the effect of the turbulent flow generated by the canard on the wing aerodynamics was addressed. The canard was entirely located at a height from the ground such that the turbulent flow impacts only the pressure side of the wing. As demonstrated by Nouwens [17], in this region the air flow is virtually stagnant ($Cp \approx 1$), especially when the wing is at a high angle of attack. Therefore the turbulent flow does not deal significant damage to the wing aerodynamic performace. Worth noting is that the canard produces the highest amount of turbulent flow when it is at a high angle of attack, and this situation occurs during take-off and landing, exactly when the wing too is at a high angle of attack. For this reason, the effect of this turbulence was considered to be minimal and was neglected.

The drag generated by the engines' ducts was estimated by assuming the drag coefficient to be the one of the NACA 0010-93 airfoil with 0.025 leading edge radius-to-chord ratio ($C_D = 0.0058$, from JavaFoil). The reference area was estimated to be the area of the duct (17.6 m^2). The air velocity inside the duct was estimated to be on average 85

m/s at take-off and 106 m/s at cruise. The air velocity outside the duct was assumed to be equal to the free-stream velocity (V_∞). The drag generated by the engines' pylon was estimated by assuming the drag coefficient to be the one of the NACA 0015-23 airfoil with 0.05 leading edge radius-to-chord ratio (C_D = 0.0066, from JavaFoil). The reference area was estimated to be the area of the strut (4.0 m^2). The air velocity around the duct was assumed to be equal to the free-stream velocity (V_∞).

These two NACA 4-digits modified airfoils, feature a leading edge radius-to-chord ratio, have been chosen for their particularly low zero-lift drag characteristics.

One last aspect to be addressed was the increase in skin friction drag due to the forward extension of the sideskirts. In his master thesis, Nouwens [17] reports the friction coefficient on the body of Aerocity. It can be seen that the average skin friction coefficient on the sideskirt surface is on average 0.0025. The extra sideskirts have a reference area of about 12 m^2.

Table 7.1 presents the total lift and drag coefficients of the vehicle for the relevant flight speeds, the take-off and the cruise ones, and for three different weight configurations:

- maximum payload, with a 1.05 safety factor to account for some variability in payload composition;
- zero payload, to simulate operations of vehicle relocation;
- medium payload, to establish a trend between the aerodynamic parameters and the total vehicle weight.

The table also includes the individual contributions to the lift and drag coefficients from the individual aerodynamic elements, normalised to the wing surface area.

Table 7.1: Total vehicle lift and drag coefficient and their components. All the coefficients are normalised to the wing surface area and to the free-stream velocity. Standard sea-level atmospheric conditions are assumed.

	W = 360 kN		W = 300 kN		W = 240 kN	
	Take-off	Cruise	Take-off	Cruise	Take-off	Cruise
v [m/s]	55.5	84.8	55.5	84.8	55.5	84.8
α_w [deg]	4.75	2.73	3.80	2.52	3.12	2.30
α_c [deg]	5.0	-0.8	7.0	-0.8	7.0	-1.25
C_{L_w} [-]	1.05	0.51	0.83	0.43	0.63	0.35
C_{L_c} [-]	1.12	0.00	1.33	-0.01	1.33	-0.10
C_L [−]	1.19	0.51	0.99	0.43	0.80	0.34
C_{D_w} [-]	0.0287	0.0180	0.0231	0.0172	0.0197	0.0164
C_{D_c} [-]	1.75E-3	8.8E-4	2.13E-3	8.8E-4	2.13E-3	1E-3
$C_{D_{zero_{ail\&rudd}}}$ [-]	3.8E-4	2.0E-4	3.8E-4	8.8E-4	3.8E-4	8.8E-4
$C_{D_{enginesducts}}$ [-]	8.4E-4	6.4E-4	8.4E-4	6.4E-4	8.4E-4	6.4E-4
$C_{D_{enginespylon}}$ [-]	1.6E-4					
$C_{D_{extraskirts}}$ [-]	1.9E-4					
C_D [−]	0.0320	0.0201	0.0263	0.0193	0.0229	0.0186
L/D [−]	37.9	25.5	36.9	22.4	34.2	18.4

8 Propulsion

In this chapter, the design of the propulsion system is discussed in detail. A number of decisions about the propulsion system were already made and described in previous reports and will briefly be summarised.

8.1. Design constraints of the propulsion system and preliminary design choices

During the preliminary design phase, a number of propulsion systems were considered and compared. For the preliminary design, it was decided that the propulsion system should consist of a number of electrically driven ducted propellers. This choice was made after performing a qualitative trade-off between open propellers, embedded and ducted propellers. This trade-off considered the emitted noise, efficiency, safety and maintainability of the different concepts and the ducted propeller design performed the best out of all of them.

In order to go further, a number of design constraints were identified. These are the following:

- Rotor tip velocity shall not exceed 0.8 Mach due to noise and performance
- The propulsion system shall be able to provide sufficient thrust to overcome the drag during cruise and acceleration.
- The propellers placed side by side shall not exceed the width of the vehicle
- The propeller area should be maximised in order to improve efficiency according to Roskam [29]
- The engine placement shall not substantially increase the height of the vehicle in order to prevent expensive tunnelling costs
- The flow around the vehicle shall not be negatively affected by the engine placement

8.2. Location of the propulsion system

Based on the constraints on the placement of the engines, it was clear that the ideal placement would be towards the rear of the vehicle. Due to the shape of the vehicle, the aft section is significantly lower and thus placing the engines here would not increase the height of the vehicle much and would keep tunneling costs low. Furthermore, it does not create turbulent flow over the rest of the airfoil as would be the case if the engine would be placed in front of the vehicle.

The exact aft mounting location was adjusted with respect to the structural components in order to minimise the weight of the vehicle. Finally, after having decided the location of the engines, the number and size have to be determined. This will be treated in section 8.3.

8.3. Motor number trade-off

In order to determine the preferred number of motors a trade-off is performed, in this trade-off the options of having either one, two, three or four motors will be compared. This is based on the following criteria:

- **Efficiency:** As can be derived from Roskam [30], a propeller is generally more efficient if a large amount of air is accelerated a little bit. Therefore, a larger propeller diameter would be preferred. As the space on the vehicle is limited, the largest propeller diameter would be achieved by a single propeller whereas only a smaller diameter would be possible if the thrust were to be distributed over four different propellers. Therefore the highest score has been given to one motor and the lowest to four motors.
- **Redundancy:** More motors are preferred because if a motor were to fail, other motors would still be able to provide a part of the thrust. Therefore, the highest score has been given to four motors and the lowest to one motor.
- **Thrust placement:** As mentioned before, fewer motors result in larger propellers. Meaning that if the thrust is modelled as a point force acting through the centre of the propeller, the thrust will be placed further above the centre of gravity, resulting in a pitch down moment. This affects the trim condition of the vehicle and would preferably be minimised as much as possible. Therefore, smaller propellers and thus more motors are preferred and have been given a higher score than one motor.
- **Development risk**: As there currently already exist electric motors for the aviation industry that would be able to provide the required power in a scenario where the power is distributed over three or four propellers each of these have been given the highest score [4]. If only one or two motors were to be selected, currently existing motors would have to be scaled up accordingly, which introduces development risk. Hence, the options for one or two motors have been given a lower score.

- **Interference:** Since the motors would be placed next to each other, some interference would occur between the wake of several propellers. Although the propellers are meant to be ducted and this effect is therefore significantly reduced, it is still present and therefore the highest score has been given to one motor and the lowest to four motors.
- **Drag:** As each propeller would require a duct, which would introduce additional drag, fewer propellers are preferred over more. Therefore, the highest score has been given to one motor and the lowest to four motors.
- **Maintainability:** Because a smaller and lighter motor is obviously easier and cheaper to replace or repair than a large, heavier and more expensive motor, multiple motors are preferred from a maintainability perspective. Therefore, the highest score has been given to four motors and the lowest to one motor.

As for the decision weight, each criterion has been given a percentage such that the total sum would equal 100. Initially, the efficiency and redundancy of the system were considered to be the most important but the efficiency was still considered to be slightly more important than the redundancy therefore they have been assigned a weight of 22 and 17 respectively. Both the thrust placement and the development risk were considered to be directly relevant to the design but not as important as the efficiency and redundancy and were therefore assigned a weight of 15. The interference, drag and maintainability were given a weight of 13,10 and 8 respectively as they are still relevant to the design but their impact is considered to be lower than that of the other criteria. The maintainability has been given the lowest score as this is considered to be minimal for electric motors without a gearbox.

Table 8.1: A trade-off on the preferred number of propellers/engines.

Criteria	Weight	One motor	Two motors	Three motors	Four motors
Efficiency	22	4	3	2	1
Redundancy	17	1	2	3	4
Thrust placement	15	1	2	3	4
Development risk	15	1	2	4	4
Interference	13	4	3	2	1
Drag	10	4	3	2	1
Maintainability	8	1	2	3	4
Total	100	235	245	270	265

From this trade-off, it can be seen that three motors would be the preferred solution. The option of having four motors, however, scores really close and should therefore also be considered. The decision between either of these options will depend further on the propeller design.

8.4. Initial propeller sizing

The sizing of the propeller largely depends on the chosen configuration. The configuration mainly depends on the number of propellers selected which has been treated in section 8.3. Secondly, the comparison between a traditional and a contra-rotating propeller is given in subsection 8.4.1.

8.4.1. Comparison between a traditional and contra rotating propeller

As one aims for an optimal propeller efficiency it is desired to look past the performance of conventional open propeller design. One of the ways in which the propeller efficiency could possibly be increased is by introducing contra-rotating propellers. In summary, these could provide an increase in propeller efficiency of $6-8\%$ due to swirl recovery but at the cost of added weight, mechanical complexity and noise emissions.

Previous work

Traditional propellers are already well understood and several design methodologies and approaches, as seen in Roskam and Raymer [30, 31], have been developed over the course of aviation history, as well as standardised propellers and corresponding propeller performance maps such as the Hamilton Standard [3].

Contra-rotating propellers (CRPs) on the other hand are less well understood and less commonly used. In essence a CRP exists out of two propellers which are mounted on the same axis but rotate in different directions, the concept was first patented in 1909 by Frederick W. Lanchester [32] but only saw practical applications during the second world war when more powerful engines were tried to be fitted in existing aircraft that could only accommodate propellers of a certain size. The addition of the CRP would thefn increase the disk loading $[W/m^2]$. After the second world war, the development of CRPs and traditional propellers has halted as more resources were directed towards the development and optimisation of jet engines. In recent years more interest has developed towards CRPs as the development of electric aircraft has also increased. There are however only a few currently available aircraft that

make use of CRPs and most of them are Ukrainian or Russian military freight aircraft such as the AN70 and the TU95 [33, 34], both of which operate on a vastly different scale and flight regime than the AeroCity would.

Advantages and disadvantages of CRPs

The main advantages of CRPs over traditional propellers are that a large part of the swirl behind the first propeller can be recovered by the second propeller, that the torque of the two propellers would counteract each other and that a higher shaft power can be converted to thrust per propeller area. The disadvantages, however, are the added mechanical complexity and/or friction losses on the shafts, the added noise emissions and the added weight of the overall system.

The swirl recovery works such that the second propeller is optimised for the flow behind the first propeller, which has an added rotational component with respect to the free stream velocity in front of the first propeller. This also results in a smaller rotational component of the flow behind the second propeller than that behind the first propeller and that the kinetic energy of the flow is also manifested in straight flow rather than a rotating flow.

As for the torque, both propellers have a similar rotational rate and size and provide a similar amount of thrust. Consequently, the torque acting on the supporting structure would be equivalent but opposite for either propeller and the torsional loads on the structure would be minimised. This effect has been validated by several studies such as (Deng) and (Mieloszyky et. al) [35–37].

As presented in a previous DSE study [38], a highly optimised contra-rotating propfan could theoretically reach a disk loading of up to 600 kW/m^2 but practical physical limitations would most probably reduce this to 400-500 kw/m^2. However, it should also be stated that this is mainly applicable for extremely high powered applications, something which might not be relevant to this design.

As a contra-rotating system would involve two rotors spinning in opposite directions, it is obvious that this would involve a more complex system than a traditional propeller. Since the two rotors would be turning at a comparable rotational rate, the difference between the two shafts - one passing through the other - would be twice as high, for which the bearings would also need to be designed. Moreover, there is also the complexity of getting the axles to rotate in opposite directions. This could either be achieved by a specially designed gearbox or by two different electric motors operating in different directions. A gearbox would obviously introduce more friction losses, wear and maintenance, whereas the latter option would require an axle passing through another electric motor, for which a part of the axle should also be designed to be non-magnetic as the second motor would otherwise introduce an opposing torque to the same axle.

Lastly, there is the additional disadvantage of added weight and noise. The added weight is a logical result from a more intricate mechanical system. As for the noise, several studies such as Kingan [39] and the 2011 HUULC DSE [38] stated that a CRP would increase noise emissions by up to 30dB in axial direction and 10dB in radial direction [40].

Applicability

After considering both the advantages and the disadvantages of CRPs, the design constraints mentioned in section 8.1 and external advice the decision was made to not use contra-rotating propellers as the advantages were not critical points of this design and the disadvantages are. Moreover, the variables and design complexity of such a system would exceed what was realistic to perform within the given time frame and resources of the DSE. Especially when considering the estimation of the aerodynamic interactions between the two propellers.

Instead, the decision has been made to use a traditional ducted propeller or fan with the addition of swirl recovery vanes (SRVs) as this is sufficient enough for the set requirements and can be analysed more in-depth with the given resources.

8.4.2. First iteration on the propeller sizing

As the decision has been made to use traditional propellers or fans, the number of engines is also changed to either 2 or 4 in order to have no resulting roll moment on the vehicle. From the trade-off performed in Table 8.1 it can be seen that 4 motors would be preferred over 2. The first iteration on the propeller sizing is therefore based on 4 propellers.

Firstly, the thrust and output power per propulsion unit have to be calculated as per Equation 8.1 and 8.2. Secondly, the shaft power can be determined through Equation 8.3 by using an assumed propulsive efficiency of 80%. The

shaft power is rounded up to 375 kW as this can be related more easily to existing electric motors and to take a safety factor into account such that the vehicle can provide more thrust when needed in case of delays or headwind.

$$\frac{T}{engine} = \frac{Thrust}{NO_{engines}} \quad (8.1) \qquad P_{out} = \frac{T}{engine} * V_0 \quad (8.2) \qquad P_{shaft} = \frac{P_{out}}{\eta_{prop}} \quad (8.3)$$

Thirdly, the maximum tip velocity, V_{tipmax}, can be defined in Equation 8.4. It is taken at 80% of the speed of sound in order to minimise sound and shock waves over the blades. Roskam actually states that 72% would be preferred for traditional low noise propellers but with the addition of a duct, the noise is already dampened and some extra margin can be taken [30]. Another reason for the increase of 72% to 80% of the speed of sound is that the overall performance will increase. From the maximum tip velocity the maximum rotational velocity, V_{rotmax} can be calculated via Equation 8.5.

$$V_{tipmax} = 0.8 * a_0 \quad (8.4) \qquad V_{rotmax} = \sqrt{V_{tip}^2 - V_0^2} \quad (8.5)$$

As can be seen in Equation 8.6, the maximum propeller diameter, D_{max}, also depends on the rotational rate expressed in RPS (rotations per second). This value depends on the selected motor and a value of 1900/60 = 31.6 $1/s$ is chosen. This value comes from the Magnix 250 electric motor which is a currently available state of the art electric motor for aviation purposes [4]. This results in a maximum propeller diameter of 2.87 m. However, it has to be taken into account that the 4 propellers should be able to fit next to each other within the boundaries of the vehicle ($8m$). Therefore, the propeller diameter has been lowered to 1.5 m in order to ensure that all 4 propellers and ducts would fit within the given constraints.

$$D_{max} = 2 \cdot R_{max} = 2 \cdot \frac{V_{rotmax}}{2 \cdot \pi \cdot n} \quad (8.6)$$

Lastly, the previously determined values for the diameter, rotational rate, cruise velocity and shaft power can be combined in Equation 8.7 and 8.8 to determine the advance ratio, J, and the power coefficient, C_p of the propeller.

$$J = \frac{V_0}{n \cdot D} \quad (8.7) \qquad C_p = \frac{P_{shaft}}{\rho \cdot n^3 \cdot D^5} \quad (8.8)$$

Now, the calculated values for the advance ratio and the power coefficient can be used in combination with a propeller performance map [3] to determine the propeller efficiency and subsequently the thrust coefficient, C_t, as per Equation 8.9. Finally, the found C_t values can be used to find the provided thrust per engine as per Equation 8.10.

$$C_t = \frac{\eta_{prop} \cdot C_p}{J} \quad (8.9) \qquad C_t = \frac{T}{\rho \cdot n^2 \cdot D^4} \quad (8.10)$$

Several performance maps for propellers of varying activity factors and integrated lift coefficients are available in the Hamilton standard for propeller sizing [3]. These are available for both three and four-bladed propellers but as presented in Gangoli [41], a four-bladed propeller is generally 3% more efficient than a three-bladed propeller. Therefore, only a four-bladed propeller has been analysed for different activity factors, AF, ranging between 100 and 220, similarly different charts were available for different integrated lift coefficients, CL_{int}, ranging between 0.3 and 0.7. The propeller efficiency and thrust coefficient have been looked up for each of these variations as can be seen in Table 8.2. For all variations, the thrust has also been calculated and as can be seen, none of the variations would be able to provide sufficient thrust. Therefore, a second iteration was needed which will be presented in subsection 8.4.3.

8.4.3. Second iteration on the propeller sizing

Table 8.2: Overview of the propeller efficiency and thrust coefficient for different propeller blade geometries [3].

AF	100			140			180			220		
CL_{int}	0.3	0.5	0.7	0.3	0.5	0.7	0.3	0.5	0.7	0.3	0.5	0.7
η_{prop}	0.77	0.81	0.83	0.81	0.84	0.84	0.83	0.84	0.83	0.83	0.83	0.81
C_t	0.22	0.232	0.237	0.232	0.24	0.24	0.237	0.24	0.237	0.237	0.237	0.232
T	1362	1436	1467	1436	1436	1486	1467	1486	1467	1467	1467	1436

As the initial propeller sizing resulted in a design that was unable to provide sufficient thrust, a second iteration is necessary. The main flaw in the initial iteration was that the propeller diameter had to be reduced in order to fit all four propellers within the boundaries of the vehicle. It has therefore been investigated whether or not a design with two propellers would provide a more feasible solution.

Similar calculations as in subsection 8.4.2 can be performed for this new iteration. With only two propellers, each should be able to provide a thrust of 7000 N and the shaft power of each motor would equal 750 kW whilst still operating at an RPM of 1900. The subsequent results of Equation 8.1 through 8.8 can be seen in Table 8.3. The results of performing the same method as discussed in subsection 8.4.2 can be found in Table 8.4.

Table 8.3: An overview of the intermediate results of the second iteration on the propeller sizing.

$\frac{T}{engine}$	7000	N
V_{tipmax}	272	m/s
V_{rotmax}	258.6	m/s
R_{max}	1.302	m
D_{max}	2.6	m
J	1.02	–
C_p	0.1633	–

Table 8.4: Overview of the propeller efficiency and thrust coefficient for different propeller blade geometries [3].

AF	100			140			180			220		
CL_{int}	0.3	0.5	0.7	0.3	0.5	0.7	0.3	0.5	0.7	0.3	0.5	0.7
η_{prop}	0.8	0.84	0.84	0.84	0.84	0.81	0.81	0.82	0.75	0.83	0.80	0.60
C_t	0.128	0.134	0.134	0.134	0.134	0.129	0.134	0.131	0.12	0.132	0.128	0.096
T [N]	7155	7490	7490	7490	7490	7210	7490	7322	6707	7378	7155	5366

After performing the above-mentioned calculations, a more in-depth analysis of the propeller and duct design would be needed. Especially considering the effect that different AFs and CL_{int}s would have on the propeller blades and the additional drag of the duct around the propeller. However, after consulting the groups mentor, DR. A. Gangoli Rao, the group was advised to perform another iteration in which a fan would be investigated instead of a propeller as, for the thrust that a propeller can provide, the duct would be far too large and cause too much drag. Therefore a third iteration on the propeller/fan sizing was performed in section 8.5.

8.5. Third iteration on the fan sizing

As this iteration occurred in the later stage of the project, the decision has been made to calculate the desired fan pressure ratio (PR_{fan}) and other parameters as a function of propulsive efficiency such that it could be tailored to be compliant with other subsystems without needing an iteration on those as well. This is done through a python script with an iterative loop that varies the desired propulsive efficiency, η_{prop}, between 0.6 and 1 such that the fan parameters can be analysed for different efficiencies.

Table 8.5: An overview of the constants used in the final fan design.

$NO_{engines}$	2	–
$Thrust$	14000	N
a_0	340.3	m/s
V_0	84.8	m/s
k_a	1.4	–
T_0	288	K

P_0	101,325	Pa
ρ_0	1.225	$kg/m3$
η_{fan}	0.9	–
η_{inlet}	0.95	–
η_{nozzle}	0.95	–
Cp_{air}	1000	$kJ/kg/K$

Firstly, a number of constants and set parameters that were used throughout the calculations is presented in Table 8.5. From these constants the mach number, M_0, and the inlet conditions of the fan, $T_{0,2}$ and $P_{0,2}$, are calculate through Equation 8.11, 8.13, and Equation 8.12.

$$T_{0,2} = T_{0,0} = T_0 \cdot \left(1 + \frac{k_a - 1}{2} \cdot M_0^2\right) \tag{8.11}$$

$$M_0 = \frac{V_0}{a_0} \tag{8.13}$$

$$p_{0,2} = p_0 \cdot \left(1 + \eta_{inlet} \cdot \frac{k_a - 1}{2} \cdot M_0^2\right)^{\frac{k_a}{k_a - 1}} \tag{8.12}$$

$$v_e = \left(\frac{2}{\eta_{prop}} - 1\right) \cdot v_0 \tag{8.14}$$

Secondly, the required exit velocity can be calculated for each desired propulsive efficiency via Equation 8.14 which can then be used to find the specific thrust (thrust per unit mass flow), $T_{specific}$, and the total mass flow for the thrust that is required. The total mass flow can then be used to find the total fan area, $A_{required}$, and the area per fan, A_{fan}, which can also be related to the fan diameter, D_{fan}, as presented in Equation 8.15 through 8.19. As the Mach number is sufficiently low to assume a non-choked condition at the exit of the nozzle, Equation 8.20 can be used to determine the temperature difference between the stage right after the fan and the stage at the exit of the nozzle/duct.

$$T_{specific} = \frac{T}{\dot{m}} = (v_e - v_0) \tag{8.15}$$

$$\dot{m}_{total} = \frac{T}{T_{specific}} \tag{8.16}$$

$$A_{requried} = \frac{\dot{m}_{total}}{\rho \cdot v_0} \tag{8.17}$$

$$A_{fan} = \frac{A_{required}}{NO_{engines}} \tag{8.18}$$

$$D_{fan} = 2 \cdot R_{fan} = 2 \cdot \sqrt{\frac{A_{fan}}{\pi}} \tag{8.19}$$

$$\Delta T_{nozzle} = \frac{V_e^2}{2 \cdot Cp_{air}} \tag{8.20}$$

In order to determine the required pressure ratio for the assumed propulsive efficiency, a second loop has been written in the python script to calculate the temperature and pressure right after the fan, $T_{0,21}$ and $P_{0,21}$, in terms of the pressure ratio, fan efficiency and inlet conditions, this was done by using Equation 8.21 and 8.22. For each of these pressure ratios, the resulting temperature difference in the nozzle is then calculated by virtue of Equation 8.23. Eventually, the pressure ratio for which the temperature difference is closest to the required temperature difference (see Equation 8.20) is selected.

$$T_{0,21} = T_{0,2} \cdot \left(1 + \frac{1}{\eta_{fan}} \cdot \left(PR_{fan}\right)^{\frac{k_a - 1}{k_a}} - 1\right) \tag{8.21}$$

$$p_{0,21} = PR_{fan} \cdot p_{0,2} \tag{8.22}$$

$$\Delta T_{nozzle} = T_{0,21} \cdot \eta_{nozzle} \cdot \left(1 - \frac{p_0}{p_{0,21}}\right)^{\frac{k_a - 1}{k_a}} \tag{8.23}$$

$$n_{max} = 60 \cdot \frac{V_{rotmax}}{2 \cdot \pi \cdot R_{fan}} \tag{8.24}$$

Finally, the cruise velocity and fan radius can be used in combination with a maximum tip velocity to determine the maximum rotational rate of the propeller. This can be done by using Equation 8.4, 8.5 and 8.24. The results for the pressure ratio, exit velocity, fan diameter, maximum RPM and mass flow with respect to the propulsive efficiency can be seen in Figure 8.1 and 8.2. Figure 8.2 also shows the duct surface in terms of the fan diameter as the actual drag of the duct also depends on the geometry of the airfoil as well as the flow interaction between the normal airflow and accelerated airflow through the fan and duct.

It is therefore considered that an estimation of the total drag of the duct falls outside of the scope of this project. Instead, a relation between the duct surface area and the fan diameter is given as generally the drag scales linearly with the surface area. The calculated surface area results from the circumference of the fan diameter multiplied by 1.1 and a chord/duct length of 0.5 times the diameter of the fan.

As can be seen in Figure 8.1 and 8.2 all parameters change considerably for a different propulsive efficiency. Because this iteration occurred at a late stage in the design process, it was chosen to minimise the effect it would have on other subsystems. Moreover, as losses are guaranteed to occur, care has to be taken to not overestimate a feasible propulsive efficiency. Therefore, a propulsive efficiency of 80% has been chosen, an overview of the resulting parameters can be found in Table 8.6.

Table 8.6: An overview of the final fan design parameters.

$NO_{engines}$	2	–
$V_{e_{cruise}}$	127.2	m/s
PR_{fan}	1.062	–
D_{fan}	1.42	m
RPM	3475	$1/min$
$\dot{m}_{total}$	330.18	kg/s

8.6. Motor selection

Finally, the electric motors driving the fans need to be sized, this is mainly based on the shaft power required for the propulsion but also takes into account the required rotational rate, mass, size, efficiency, redundancy and the technical readiness level.

An investigation into currently available state of the art electric motors for aviation led to two different companies, Yasa and Magnix [4, 42]. Each of these currently provides electric motors that are readily available and would be

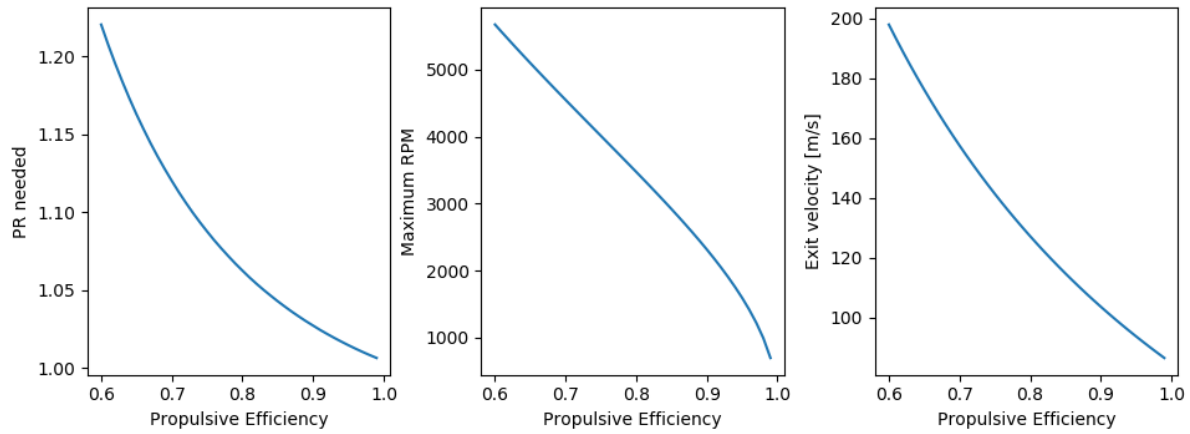

Figure 8.1: Pressure ratio, Maximum RPM and Exit velocity with respect to Propulsive efficiency.

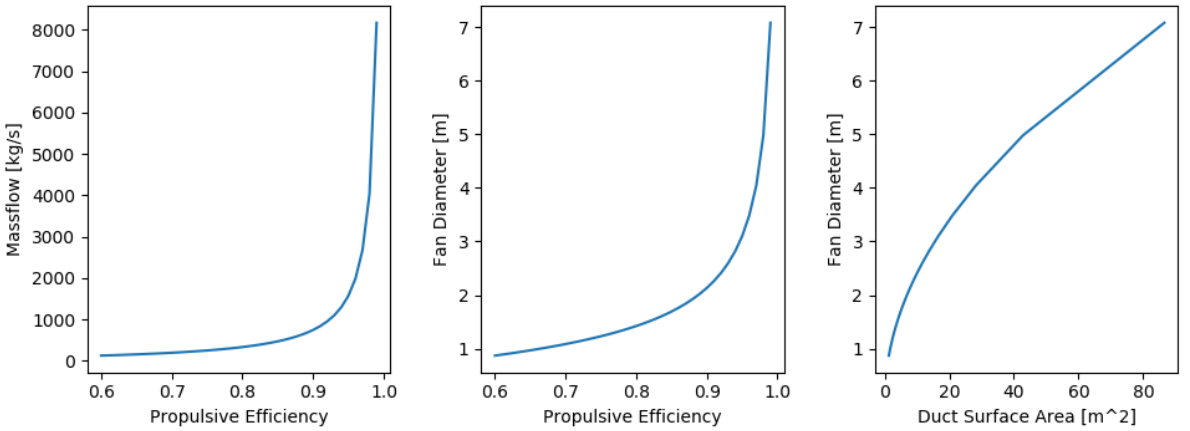

Figure 8.2: Massflow and Fan diameter with respect to propulsive efficiency and Duct surface area with respect to Fan diameter.

able to provide the required power within the size and mass budget. The technical specification of each of their listed products can be found in Table 8.7. It is important to note that the physical dimensions of either of the Magnix motors are estimates based on reference figures on their website [4], and that following from those dimensions both the volume and the power density are an approximation.

As for the actual selection of the electric motor, most attention is given to the specific power in continuous performance. Based on this parameter both the Magnix 500 and the YASA P400 R are comparable, but because the values and information on the Magnix 250 and Magnix 500 seem to be more consistent, an extrapolation on the Magnix 250/500 design was selected as a base for further sizing and power calculations.

It is also important to note that the Magnix 500 is, in essence, a combination of 2 Magnix 250s stacked together. Therefore, the assumption has been made that this idea can be extrapolated to meet the power requirements of the AeroCity. Unfortunately, the rotational rate of the current Magnix motors is not equal to what is required for this design. This problem can, however, be solved with a highly efficient gearbox or a future design tailored to meet the AeroCity's requirements. More detail on the number of motors required and the power usage will be given in chapter 9 and a visualisation of either electric motors is given in Figure 8.3.

Table 8.7: An overview of the listed specifications of various electric motors [4, 42].

Brand		Yasa				Magnix			
Product		YASA 750		YASA P400 R		Magnix 250		Magnix 500	
Cooling		Integrated							
DC link Voltage	$[V]$	-				540			
DC link Voltage range	$[V]$	-				450-750			
Axial length	$[mm]$	98		80.4		≈300-400		≈ 600-800	
Diameter	$[mm]$	368		305		≈400-500		≈ 400-500	
Volume	$[ltr]$	10.42		5.87		≈38-79		≈76-157	
Mass	$[kg]$	37		24		72		135	
η_{motor}		>0.95		0.96		>0.93		>0.93	
Operation point		cont.	peak	cont.	peak	cont.	peak	cont.	peak
Torque	$[Nm]$	400	790	200	370	1407	-	2814	-
Power	$[kW]$	70	200	20-100	160	280	-	560	-
RPM	$[1/min]$	-	3250	-	8000	1900	3000	1900	3000
Specific power	$[kW/kg]$	1.891	5.405	0.83-4.16	6.6	3.8	-	4.148	-
Power density	$[kW/ltr]$	6.71	19.19	3.4-17	27.25	≈7.4-3.54	-	≈7.4-3.6	-

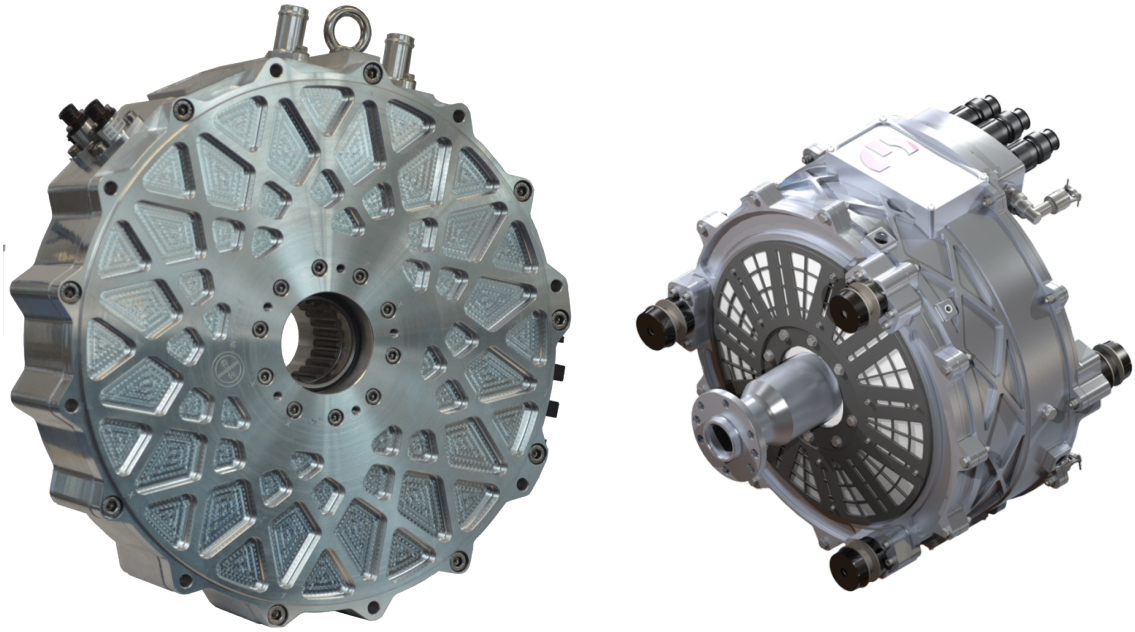

(a) The YASA 750R electric motor [42].

(b) The Magnix Magni 250 electric motor [4].

Figure 8.3: A visualisation of the reference motors used.

9 Electric Power System

An infographic of the full power system is visualised in Figure 9.1. The main power will be transferred between the swappable battery and the electric fans, but other subsystems also require a power budget. Each subsystem will be connected to a system bus to have knowledge on the full system and some subsystems will have individual busses if higher accuracy or speed is required. Each of the systems as well as the relays in the power stage will be controlled by the main computer as described in chapter 15.

9.1. Use of Batteries

The system uses a battery that can be swapped when empty. A battery has been chosen to limit track interaction and provide electric power throughout the mission without emissions. The batteries can be swapped such that the vehicle itself can depart immediately and will not need the time to charge. Another big advantage is to be able to charge the batteries when the energy grid is at its lowest demand. This reduces energy costs and helps with the power transition. Electric energy demand during peak hours is likely to increase and to be linked to a increased price in the time that AeroCity will be operational.

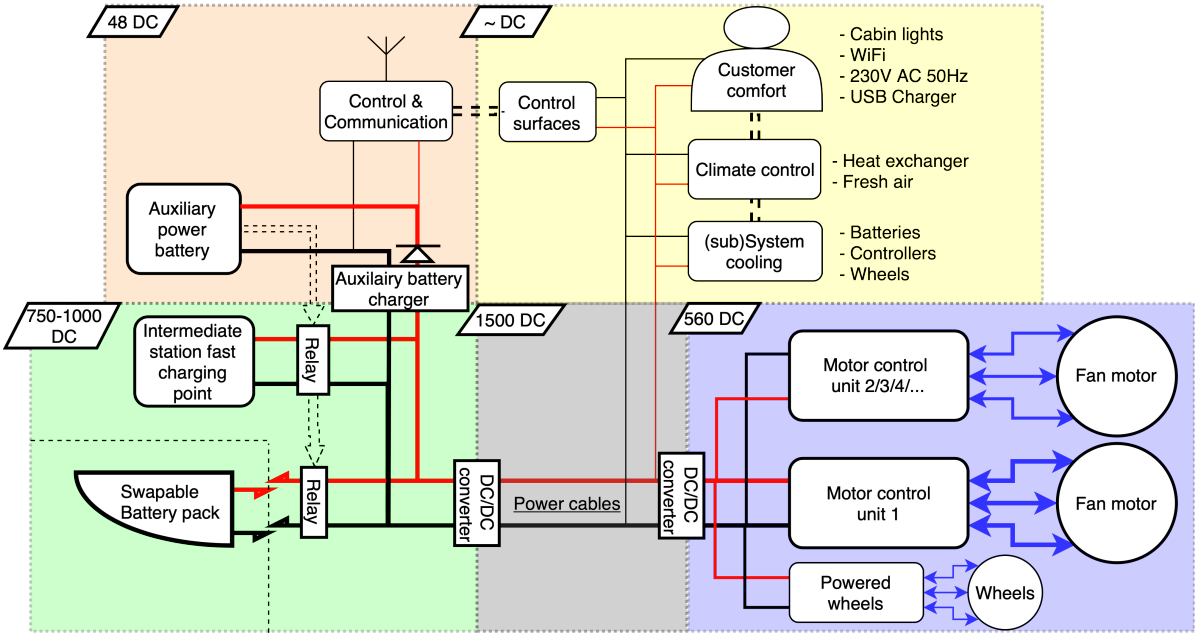

Figure 9.1: Power system

9.2. Power Requirements

The propulsive thrust power of the vehicle is 1.174 MW during cruise. This is calculated using the total C_D of cruise configuration as shown in Table 7.1. The electric power this requires is calculated in Table 9.1. This combined with the subsystems results in the nominal power of the total vehicle of 1.70MW.

9.3. Energy Requirements

The total energy consumption of the vehicle is calculated as discussed in chapter 16 under the stated assumptions. The total energy consumed per trip is 3.68 MWh. This is because the vehicle does not stop and thus does not quick charge during a stop. The battery size is chosen to be 130 % of the calculated energy consumption. Resulting in a total battery capacity of 4.8 MWh. This contains buffers for design uncertainties, operational buffers and battery degradation. Further analysis has to be performed on the state of charge of the battery necessary to have enough power available.

Table 9.1: Electric vs. kinetic power

$P_{kinetic\_cruise}$	1.174 MW	
$\eta_{propeller}$	80%	[3]
P_{Shaft}	1.467 MW	
$\eta_{motor*MC}$	93% * 98.9%	[4]
$\eta_{DC-link}$	2x 98.5%	[5]
η_{cable_losses}	~99%	
$\eta_{batteries}$	~98%	
$P_{subsystems\_avg}$	~50 kW	
$P_{nominal\_cruise}$	1.75 MW	

Table 9.2: Source power budget estimations

Subsystem	$P_{nominal\_cruise}$	P_{budget}
Fans	1.695 MW	2.587 MW
Wheels	0 kW	±176 kW
Communication	1 kW	2 kW
Control	2 kW	10 W
Cooling	43 kW	60 kW
Climate control	3 kW	6 kW
Costumer comfort	1 kW	5 kW
Total subsystems	50 kW (excl. propulsion)	83 kW

9.4. Auxiliary Power

A low voltage system will be used to power the vehicle's control system and communication. This system will be able to open and close the power stages and give inputs for each subsystem. All electric emergency and communication systems will be connected to this system and the battery will be kept at full charge at all times. This system will be able to land the vehicle in case of full battery failure. This event is very unlikely since it will only happen if all 10 packs are damaged or the battery pack detaches. The charge is kept by connecting the auxilairy battery with a flyback converter to the power stage. This will eliminate the possibility of a direct connection to the high voltage power stage.

9.5. Fan Motors

The motor design is based on a design of low weight redundant motor for avionic application [4]. The motors are modular blocks of 280 kW with double redundancy resulting in a total shaft power of 2.24 MW. This means, to cope with the cruise shaft power, 6 motors are needed. The final system with 2 fans, as discussed in section 8.4, will have a total of 8 double redundant electric motors. The 2 added motors for acceleration will run idle to let the other motors run on the highest efficiency [43]. Each motor, requires 2 motor controllers, thus resulting in a total of 16 separate motor controllers.

9.6. Wheel Motors

Wheels will be used for taxiing, this is further elaborated in subsection 11.1.1. After taxiing, the fans will take over to produce the thrust. The 8 wheels (number of wheels and wheel sizing is elaborated upon in section 11.2) will each be able to produce 4.4 kN of thrust for operations below 5 m/s, which result in a 22 kW power output per wheel. With a wheel diameter of 0.64 m, the required torque per wheel is 1.4 kNm. Another requirement is that the wheel should be pre-span during all nominal ground operations and that the wheels continue to operate nominally in the case of emergencies. This translates in $\omega_{nominal}$ = 174 rad/s and $\omega_{max\_emergency}$ = 266 rad/s. The motors should be designed or chosen to fit this set requirements. This will most likely result in a motor with a gearbox since the required torque is very high. The operating voltage of the motor controller should be able to regenerate during the deceleration phase and has to be connected to the 1500V bus or have a unidirectional DC-link. The wheels will also contribute to a higher overall acceleration power on the ground as the fans alone will not be able to keep accelerating at 0.1g at high velocities. This is further elaborated upon in chapter 16.

9.7. Subsystems

The most relevant power subsystems are the electric motors for the fans and wheels as they will consume most of the energy. The next big system will be the cooling system of the batteries, air conditioning, motors and other electric systems.

9.8. Battery Architecture

The battery system is designed to be modular and redundant. This is done considering the maintenance required on batteries. The system will consist of 10 standalone battery packs. The full battery consists of 32,000 cells. From a system point of view, the battery is divided into 200 series of 160 cells in parallel. The battery system itself is divided into 10 battery packs, consisting of 10 modules with 20 stacks of 16 cells in parallel each. Each pack will be boosted from 750-1000V, to 1500V in order to reduce cable losses. Each motor will have its own buck converter to step down to the correct voltage. Further analysis will tell if and which converter must be unidirectional for things as regenerative braking. The maximum power as stated by the cell manufacturer combined with the nominal power used during cruise operation. The cell mass of the battery will be 8,520 kg, with an estimated 1,400 kg of added structural and cable mass totalling in 9,920 kg for the full swappable battery.

9.8.1. Chosen Battery Cell

The chosen battery cell for the system is a lithium metal battery cell based on data provided by Licerion and Leyden-Jar [44, 45]. Both of these companies claim to be able to produce batteries with an energy density of 1000-1200 Wh/l and specific energy of 450-500 Wh/kg. To take future development into account an inference has been made and an energy density and specific energy of 1500 Wh/l and 600 Wh/kg have been chosen.

The motivation behind this selection is that innovation has to be taken into account and given the recent uprise in research and development with respect to batteries this is deemed a reasonable consideration. As Baes et al. [46] stated, the global battery market is expected to increase at a rapid pace over the course of the coming years as more focus and resources are being directed towards the development of sustainable energy systems, zero or low-emission transportation, grid balancing and short term energy storage for wind, solar and tidal energy.

Secondly, the claims provided by both Licerion and Leyden-Jar have to be looked at critically as well. However, both of them provide a small amount of information on what sets their development apart from currently available commercial solution. The most common problem with current lithium-ion and lithium-metal batteries, and also the reason as to why battery weight and volume is still an issue, is that the anode is often made from graphite or lithium instead of silicon, causing it to be a lot thicker and heavier [45]. The reason why graphite would be used instead of silicon is due to the fact that silicon has the tendency to swell up when lithiated causing the battery to be mechanically unstable. Another option is to use lithium as an anode material, but when there is a direct contact between the lithium material and the electrolyte, degradation or poisoning occurs in the anode. Therefore, extra anode material has to be added to compensate for the loss in performance from the poisoning of the anode. The way that both of these companies, Licerion and Leyden-Jar, manage to provide such higher prospects is by reducing the size of the anode. To prevent the degradation or poisoning of the anode Licerion's concept makes use of a ceramic layer in between the anode and the rest of the cell. Leyden-Jar's concept, however, makes use of a silicon anode, which is grown directly on the copper substrate in a porous structure. This porous structure guarantees that the silicon will not swell during lithiation. Finally, an overview of the assumed electric characteristics of the battery cells can be seen in Table 9.3.

Table 9.3: An overview of the battery characteristics

	Power system	**Battery pack**	**Module block**	**Stack**	**Cell**
NO_{cells}	32,000	3,200	320	16	1
$E_{full-new}$	4.8 MWh	480 kWh	48 kWh	2.4 kWh	150 Wh
P_{cruise}	1.695 MW	169.5 kW	16.95 kW	848 W	53
$P_{acceleration}$	2.721 MW	272 kW	27.2 kW	1.36 kW	85 W
V_{cruise}	750-1000 V	750-1000 V	75-100 V	75-100 V	3.75-5 V
A_{cruise}	1,695-2,260 A	170-226 A	170-226A	170-226 A	10.6-14.1 A
$A_{acceleration(\sim 900V}$	3023 A	302 A	302A	302 A	18.9 A
$A_{max\_continuous}$	9600 A	960 A	960 A	960 A	60 A

9.8.2. Module

Modules are made up of 20 stacks in series, where a stack contains 16 cells in parallel. The modules are modular boxes that have an internal oil cooling circuit and cell balancing system. The balancing can be either passive or active, which will be decided on in more detailed design. Each module is connected to the following module in series, central oil cooling system and serial bus. They could be replaced in case of failure.

9.8.3. Battery Pack

One pack consists of 10 modules in series getting the voltage to the desired height. Each pack is standalone in terms of balancing and power output. The total required power can easily be reached even when missing a full pack. This is done to mitigate the risk of battery failure during operation. Although not desired, one battery pack is allowed to differ in voltage compared to other packs, because this will be corrected by the DC-links.

9.8.4. Battery Substructure

As mentioned before, the battery system is meant to be completely interchangeable and as modular as possible. Subsequently, the substructure in which the different battery boxes and modules reside should be completely self-supportive. A visualisation of the design of the modules and how the cells are placed in them can be seen in Figure 9.3a. The design of one battery box (10 modules) is presented in Figure 9.3b and similarly the configuration of five battery boxes together can be found in Figure 9.3c. Finally, a representation of how the 10 battery boxes would fit in the complete package that is mounted to the vehicle can be seen in Figure 9.3d.

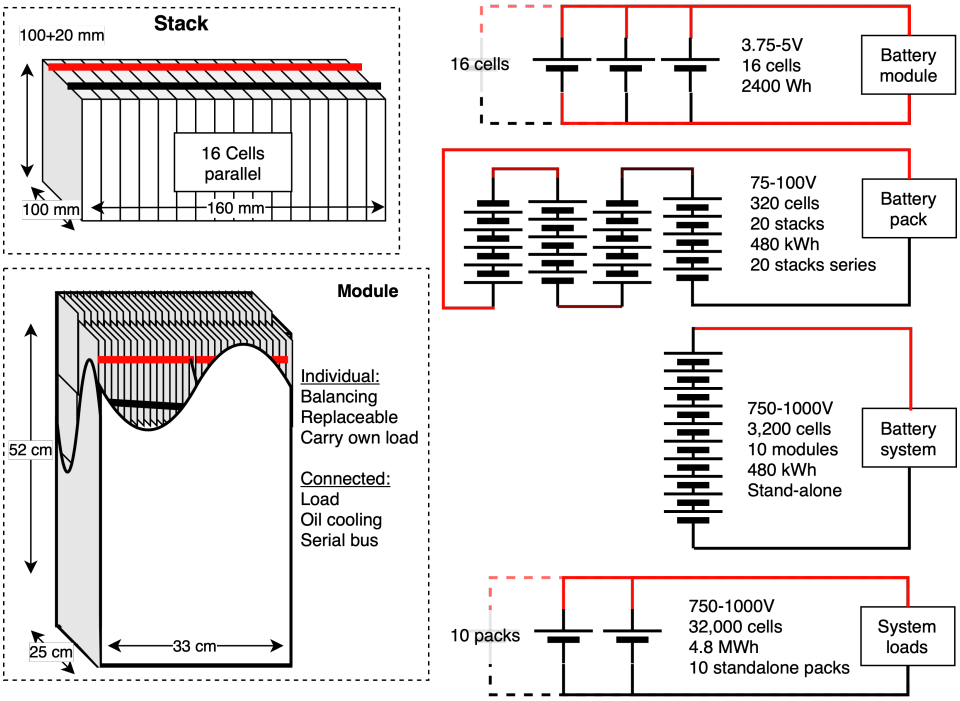

Figure 9.2: Battery architecture

9.9. Cooling

The electric system needs cooling to operate at its optimum level. The required cooling power can be estimated by using the total electric efficiency, combined with the heat produced by the passengers and the heat absorbed from solar radiation. An overview of the heat generated by every component is given in Table 9.4.

Table 9.4: Generated heat

Subsystem	$P_{nominal\_cruise}$	Scale	$Q_{generated}$	
Fan motors & MC	1.467 MW	8 %	117.7kW	[4]
Batteries	1.695 MW	2 %	33.9kW	
Wheel motors	8*22 kW	8 %	0/14.08kW	
Passengers	120 W/pax	116 pax	13.9kW	[47]
Solar radiation	~200 W/m^2	160 m^2	32kW	20% absorption full sun
Total	-	-	210.88 kW	

9.9.1. Electronic Losses

The efficiency of electric systems is dependent on the internal resistance. The efficiency losses result in a heat production that is equivalent to 1-η. The produced heat of the subsystem must be dissipated by a heat sink, active cooling or a combination of both.

9.9.2. Passengers

Passengers dissipate heat by evaporation and radiation. The amount of heat produced by the two different factors is a function of the room temperature. But the total sum of the two is fairly constant. This results in 120 W/pax of added heat power in the cabin space. This must be cooled using the air conditioning unit, which is connected to the general cooling system.

9.9.3. Solar Radiation

The average solar irradiation received on the earth surface equals 1000 W/m^2 [48], however, considering that this project is designed for the route between Utrecht and Berlin, the average irradiation that the vehicle receives will be lower. Also, only a factor of the received radiation is actually absorbed by the structure as a large part can be reflected by choosing an appropriate coating or livery of the vehicle. Therefore a total loss factor of 80% is assumed. The heat that will eventually be absorbed by the structure shall also be cooled by the integrated cooling system.

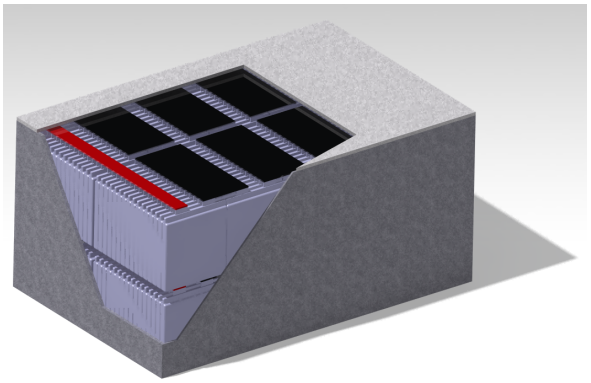

(a) A representation of the placement of the individual battery cells and stacks in one module.

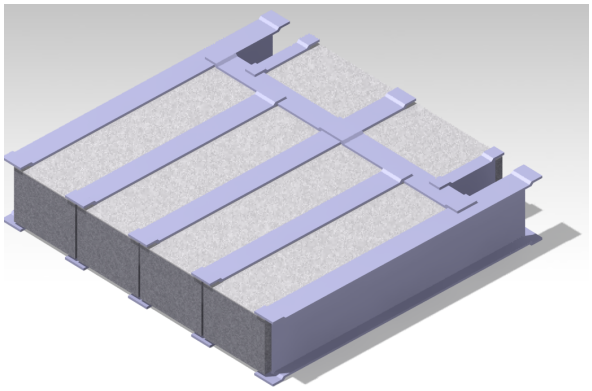

(b) A representation of one battery box, composed of 10 modules and a substructure.

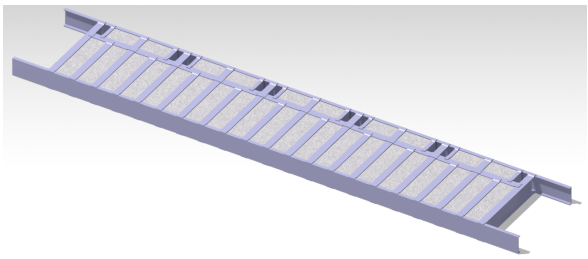

(c) A representation of 5 battery boxes joined together. Two of these packages will be placed on top of each other.

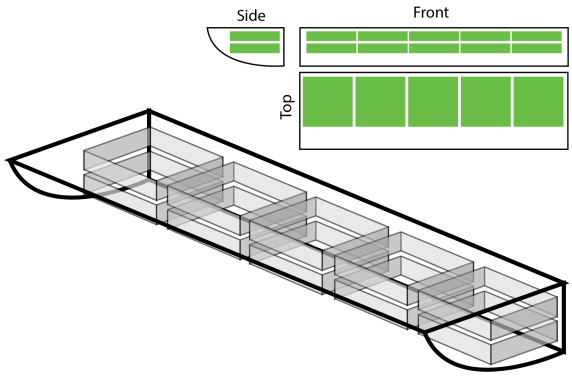

(d) A visualisation of how each of the ten battery boxes would be place within the enclosure of the entire battery package.

Figure 9.3: An overview of the structure and placement of the battery cells, stacks, modules and boxes.

9.9.4. Heat Dissipation

For the actual heat dissipation of the system, four primary cooling systems are being used. The first one will be an air conditioning system for the passenger cabin, the second an oil-based cooling system for the batteries, thirdly, a water-based cooling system for the electric motors and motor controllers and lastly an air-cooled radiator. The first three are used to dissipate the heat generated by the mentioned subsystems to the coolant - either air, oil or water - and the last is used to dissipate the heat captured in the coolants to an airflow passing through a radiator. Based on the power used of each subsystem and their respective efficiencies, Equation 9.1 and Equation 9.2 have been used to generate Figure 9.4, which represents the required massflow of the coolant and the required surface area between the coolant and the heat source for both acceleration and cruise in terms of temperature difference.

$$\dot{m}_{coolant} = \frac{P_{heat}}{Cp_{coolant} \cdot \rho_{coolant} \cdot \Delta T} \tag{9.1}$$

$$S_{contact} = \frac{P_{heat}}{h_{coolant} \cdot \Delta T} \tag{9.2}$$

It is important to note as well that the massflow and surface areas presented are per battery module and per motor+fan. Thus, for the battery cooling Figure 9.4 presents the oil massflow and contact area needed per enclosed box of 320 cells. In total there are 100 of these modules present in the vehicle. As for the motor cooling, these values are per propulsion unit and are each composed of 4 electric motors and 8 motor controllers. For the radiator, all battery modules and both propulsion units have been taken into account.

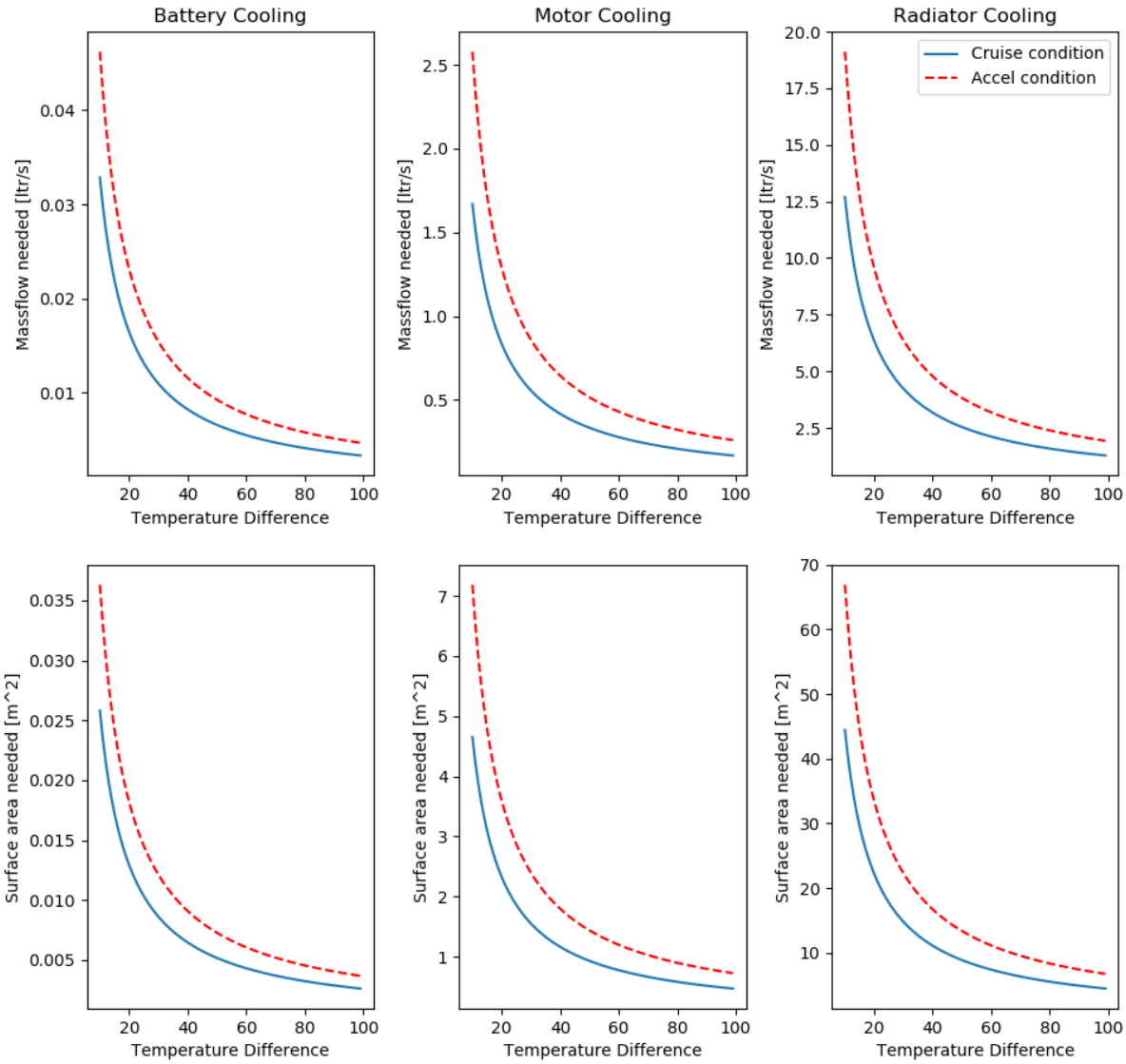

Figure 9.4: An overview of the coolant massflow and surface area required.

10 Structure

In this chapter, the materials considered for the structure of the AeroCity vehicle are discussed. After this, the different structural failures modes of the system are explained. For several components of the section, the most critical failure mode is discussed in detail. Lastly, the layout of the structure is discussed.

10.1. Selection of Materials

In this section, the different materials considered for the structures of the vehicle are discussed.

Nowadays, steel is used for applications that require high strength and fatigue resistance [49]. Steel is cheaper than aluminium and is also easy to fabricate [50]. However, steel has a high density and therefore adds weight to the structure. Also, a particular component can be difficult to fabricate using steel. Nowadays, steel is only used for smaller parts in aircraft.

Titanium alloys have high specific properties; such as a good fatigue strength/tensile strength ratio with a distinct fatigue limit [50]. Furthermore, it has good resistance to corrosion and discrete corrosion fatigue characteristics [50]. However, titanium has a high density, which makes it unsuitable to use often in structures due to the weight requirements. Furthermore, the fabrication cost of titanium is approximately seven times the cost of the fabrication of aluminium and steel. [50]. Thereby, the cost of the structure would increase significantly.

Composites have a low density and are therefore very weight efficient. Typically, the strength of carbon fiber reinforced polymer is three times that of an aluminium alloy. Also, it is estimated that replacing 40 percent of the aluminium alloys in a structure will reduce the total weight by 12 percent [50]. However, it is a brittle material, which means that it does not yield plastically in regions of high-stress concentrations [50]. The main reason for the limited use of composites in aircraft design is due to the high manufacturing costs [50]. Also, for the vehicle considered in this design, the loads are of the same order of magnitude in all directions. Composites are especially beneficial when loaded in one direction. In this case, a quasi-isotropic composite would be needed, which would significantly reduce the benefits of using composites. Nonetheless, for AeroCity, a high strength carbon fibre/epoxy composite with quasi-isotropic laminate could be used.

Pure aluminium has relatively low strength and is extremely flexible. However, if the aluminium is alloyed with other materials, its properties significantly improve. Aluminium alloys are commonly used in aerospace structures since they have a good ratio between the strength and the density of the material. Moreover, they have a relatively low manufacturing cost.

A summary of the comparison between the materials mentioned above is made in terms of ultimate strength (σ_{ult}), density (ρ) and cost. This can be found in Table 10.1.

Table 10.1: Comparison between different materials

Material	σ_{ult}	**Density**	**Cost** $[euro/kg]$
Steel (AM-350)	1262	7822	4.4
Aluminium (7075-T6)	552	2801	6.6
Titanium (Ti-6AI-4V)	958	4438	22
Quasi-Isotropic composite	603	1550	32

Eventually, it was decided to use aluminium for the the main structure. The inner structure of the sideskirt will also be made of aluminium, and the outer skin will be made of carbon fibre. An aluminium structure is chosen due to the low cost of aluminium compared to composites, and the low density compared to steel and titanium. The characteristics of the chosen aluminium are shown in Table 10.2.

Table 10.2: Density, yield and shear strengths of aluminium 7075-T6

Yield strength Aluminium [51]	483	MPa
Shear strength Aluminium [51]	331	GPa
Density Aluminium (ρ_{al}) [51]	2800	$\frac{kg}{m^3}$

10.2. Structural Analysis

In this section, several failure modes will be discussed. The methodology of calculating the critical stress/load will also be explained.

10.2.1. Normal Stresses

The normal stresses in a structural element are calculated using Equation 10.1. Normal stress can be applied in tension and in compression. The compression strength of materials is generally lower than the strength they provide in tension. In the structure of the AeroCity vehicle the normal stresses are never the critical failure mode and are therefore not discussed in further detail.

$$\sigma = \frac{F}{A} \tag{10.1}$$

10.2.2. Deflections

The deflection failure mode is expected to be critical if a large force acts on a long unsupported beam. To determine the deflection of a beam the elastic curve of the beam needs to be determined. The bending formula can be determined by calculating the moment along the beam. By integrating the bending formula, the deflection can be calculated by applying Equation 10.2.

$$\begin{aligned} EI\frac{dv^2}{dx^2} &= M = -Px \\ EI\frac{dv}{dx} &= -\frac{1}{2}Px^2 + C1 \\ EIv &= -\frac{1}{3}Px^3 + C1x + C2 \end{aligned} \tag{10.2}$$

To be able to determine the deflection at a specific point, boundary conditions must be set for each specific case. With these boundary conditions, the formula for the deflection at each particular point can be established. Certain limits can be set for the deflection; using these constraints, the needed moment of inertia can be determined. Therefore, the beam can be sized in such a way that the requirements are met. Furthermore, a safety factor of 1.5 will be applied on the load (P).

10.2.3. Bending

Bending occurs when a beam is loaded in the direction perpendicular to its thickness. To be able to calculate bending stresses the internal bending moment needs to be determined. The analysis of the internal moments was performed in chapter 4. An equation that relates the stress distribution inside a beam to the internal resultant bending moment acting on the beam's cross section is the Flexure formula, given in Equation 10.3 [52]. In this case, the assumption is made that the material behaves in a linear-elastic manner. Equation 10.3 can be significantly simplified if the cross-section is symmetrical or if there is only a moment in one direction acting on the structure. The simplifications mentioned earlier are often applied during the design of the AeroCity.

$$\sigma_z = \frac{\left(M_x I_{yy} - M_y I_{xy}\right)y + \left(M_y I_{xx} - M_x I_{xy}\right)x}{I_{xx} I_{yy} - I_{xy}^2} \tag{10.3}$$

10.2.4. Torsion

The torsional stresses are not expected to result in critical failure loading for the main body and the sideskirts. This was expected based on the shear and moment diagrams created. Therefore, torsion is not further analysed in this report.

10.2.5. Shear

Shear stress is likely to be the structural failure mode if the highest loads on the structure act in the plane perpendicular to the plane with the largest dimension of the structure. For the AeroCity vehicle, the most critical shear loading is experienced in the beams connecting the main wing to the sideskirts. When calculating the shear, at first the point loads on the structure are analysed. Based on these point loads, a shear force diagram is created. From this diagram, the maximum shear forces can be retrieved, which are then used to calculate a combination of the moment of inertia and thickness. The equation used to calculate the required combination of the moment of inertia and thickness makes use of the shear strength of the material. The other parameters used in Equation 10.5 are the moment of inertia (I), the thickness (t) and Q. Q can be defined as a product of the area from the neutral axis and the area itself, as can be seen in Equation 10.4.

$$Q = y' A' \tag{10.4}$$

$$\tau = \frac{VQ}{It} \tag{10.5}$$

10.2.6. Buckling

Buckling is a form of structural failure in which there exists an unstable equilibrium [53]. Buckling is often a critical failure mode in case of long and slender beams or plates, that are relatively thin with respect to the other dimensions.

There are multiple kinds of buckling. Firstly, Euler buckling was analysed. During this analysis, it was assumed that the beam is torsionally stable and the deformations which occur are elastic. Formulas for the critical load at which buckling may occur are dependent on the kind of support and boundary conditions. In the AeroCity vehicle, two types of supports can be found in the structure: a Fixed-Fixed support and a Fixed-Free support, with Equation 10.6 and Equation 10.7, respectively.

$$P_{cr} = \frac{\pi^2 E I_{xx}}{\left(\frac{L}{2}\right)^2} \tag{10.6}$$

$$P_{cr} = \frac{\pi^2 E I_{xx}}{(2L)^2} \tag{10.7}$$

In this case, the calculations are mainly made with a more general equation, Equation 10.8. Here, only the parameter C changes if the support changes. The values for a Fixed-Fixed support and a Fixed-Free support are 4 and 0.25 respectively.

$$P_{cr} = \frac{\pi^2 E I_{xx}}{(2L)^2} \tag{10.8}$$

For buckling of thin plates, the equations have to be altered slightly due to the introduction of buckling in two directions. The general equation for a thin plate becomes Equation 10.9. In this equation, b is the side of the plate that is being compressed. These thin plates are frequently found in the AeroCity structures, as the skin of the main wing is assumed to be a (reinforced) thin plate. In this equation, C is a parameter dependent on the boundary conditions but also on the aspect ratio of the plate. Furthermore, for aspect ratios greater than 3, the parameter C can be assumed to be constant. For a SSFF plate C = 0.92 and for a CCFF plate C = 3.72. An SSFF plate is a plate that has simple supports on two sides and is free, or unsupported on the other two sides. The sides that are simply supported are the loaded sides. The CCFF plate has two clamped supports and 2 free supports. Here, the sides that are clamped support are loaded. For all other cases, the parameter C can be extrapolated from Figure 10.1.

$$\sigma_{cr} = C \frac{\pi^2 E}{12(1-\nu^2)} \left(\frac{t}{b}\right)^2 \tag{10.9}$$

Besides Euler buckling, the critical loads for local buckling and crippling needed to be analysed. Crippling is a structural failure mode that is caused by instability below the global buckling load [53]. This failure mode frequently appears in stiffeners. The analysis of this structural failure mode is semi-empirical, which means that it includes several approximations and assumptions. The crippling load and stress are called P_{cc} and σ_{cc}, the Euler buckling load and stress are called P_{cr} and σ_{cr}. The value of σ_{cc} can be calculated using Equation 10.10. In this case, the corners are excluded when calculating the area A_i. To calculate the buckling load Equation 10.11 is used. For this case, the considered area (A) includes the area of the corners. This is done to account for the higher loads carried by the corners. Now, $\sigma_{cc}^{(i)}$ can be calculated using Equation 10.12 [53]. For aluminium alloys $\alpha = 0.8$ and $n = 0.6$. If $\sigma_{cc}^{(i)}$ is greater than the yield stress of the material, the yield stress will be used in further calculations. This means that the structure will first yield instead of cripple.

$$\sigma_{cc} = \frac{\sum \sigma_{cc}^{(i)} A_i}{\sum A_i} \tag{10.10}$$

$$P_{cc} = \sigma_{cc} A \tag{10.11}$$

$$\frac{\sigma_{cc}^{(i)}}{\sigma_y} = \alpha \left[\frac{C}{\sigma_y} \cdot \frac{pi^2 E}{12(1-\nu^2)} \left(\frac{t}{b}\right)^2 \right]^{1-n} \tag{10.12}$$

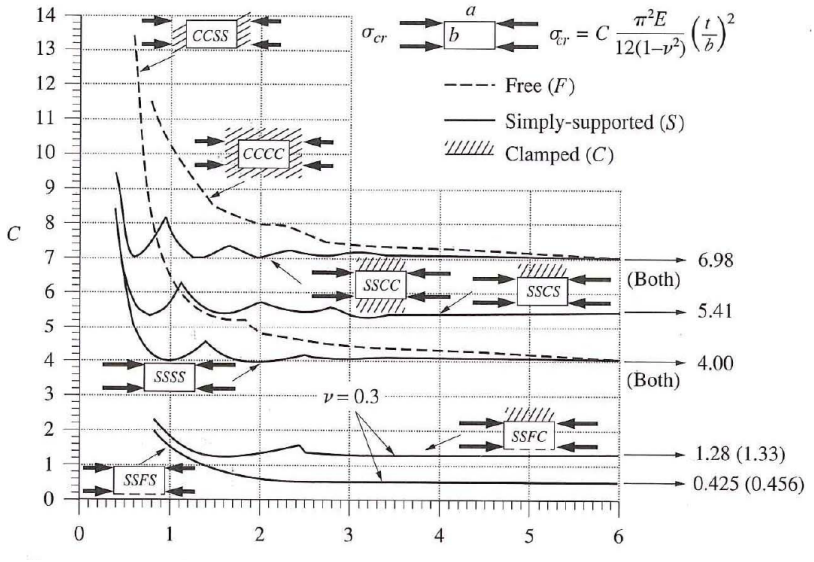

Figure 10.1: Parameter C [−]used for buckling calculations

Figure 10.2: Structura of main wing [mm]

Using the equations mentioned before, the buckling stress and crippling stress of both plates and stringers can be calculated. However, if the plates are stiffened by the stringers, the critical buckling stress of the complete structure can be determined. In reality, first, the skin will start to buckle at the critical buckling load of the skin. The stiffeners will continue to carry the applied load, and the skin, that is reinforced by the stiffeners, will also continue to carry the load. The reinforced area of the skin is defined as $2w_e$. Eventually, when internal crippling stress of the complete structure, including skin as well as stiffeners, is reached, the plate will fail. In case of failure, the stress in the region $2w_e$ is equal to the stress in the stiffeners. Determining the size of the region $2w_e$ is difficult but an estimate can be made using Equation 10.13 [53]. Here, $C = 4.0$ for SSSS supported plates and $C = 6.98$ for CCSS supported plates.

$$2w_e = t\sqrt{\frac{C\pi^2}{12(1-\nu^2)}}\sqrt{\frac{E}{(\sigma_c)_{stiff}}} \tag{10.13}$$

Using the equations mentioned above, the resistance against buckling of a stiffened panel can be computed.

10.3. Main wing

In this section the critical failure modes of the main wing are discussed. The main wing is defined as the body of the AeroCity in which the passengers, the main part of the battery pack and propulsion system are located. It was decided to reinforce the skin of the main body to save passenger space to use the available space to its full potential. A drawing of the main structural elements present in the main wing can be seen in Figure 10.2.

To perform structural analysis on the main wing of AeroCity, the structure was simplified as can be seen in Figure 10.3. The moment of inertia of the non-idealised structure is calculated using the vehicle model made in Catia. The difference in the moment of inertia of between the idealised and the non-idealised structure is less than 10 %, and therefore it is assumed that the simplification is valid for this stage of the design. Furthermore, the simplifications

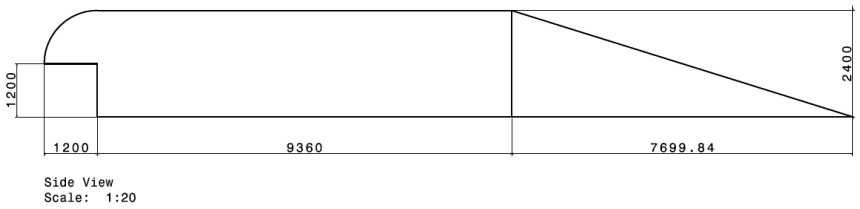

Figure 10.3: Structural idealisation of main wing [mm]

result in a lower moment of inertia for the idealised structure than the moment of inertia for the non-idealised structure. This means that the structure will be slightly over-designed and this introduces an extra safety margin.

The first failure mode analysed for the main body is bending. In the first approximations on the required bending stiffness, the moments generated in different flight phases are compared to the moment of inertia provided by the shape of the main body. This is a preliminary calculation to estimate the required thickness of the skin. In these calculations, the body is considered to be a beam. The body is analysed in two different directions. The first direction is looking at the AeroCity vehicle from the front. The body is segmented in parts with a depth of 1 cm. The moment of inertia of the small segment is compared to the moment acting on the body at that specific point, and this is used to determine if the body provides the required bending resistance. The second direction considered is the AeroCity vehicle seen from the side. In this plane, the moment of inertia is assumed to be constant over the depth, and the structure is analysed once with the highest loading case. It is assumed that the thickness throughout the structure of the vehicle is constant.

For these calculations, a Python program was written to analyse the loads per section and to discover the most critical cases. First, the height (the z-coordinate) is calculated for each combination of x- and y-coordinates. Next, the moment of inertia around the y-axis is calculated. It is assumed that the moment of inertia about the z-axis is negligible compared to the other bending moments; therefore it is not analysed in further detail. The moment of inertia about the x-axis is constant since the skin thickness is assumed to be constant for now. This will be elaborated upon later on. The stress due to the bending around the y-axis is calculated by using the equations mentioned in subsection 10.2.3. The calculated stresses are then multiplied by a safety factor of 1.5. The thickness of the skin is iterated until the stress found is lower than yield stress in all different loading cases. This will ensure that the designed structure is stiff enough to cope with the bending loads. In Figure 10.4b the internal stresses due to bending for the idealised structure with a skin thickness of 1 mm can be seen. As the internal stresses during all flight phases are below the yield strength of aluminium, a skin thickness of 1 mm would be sufficient to withstand the bending moment around the y-axis. The skin thickness is not decreased any further to ensure proper and easy manufacturing.

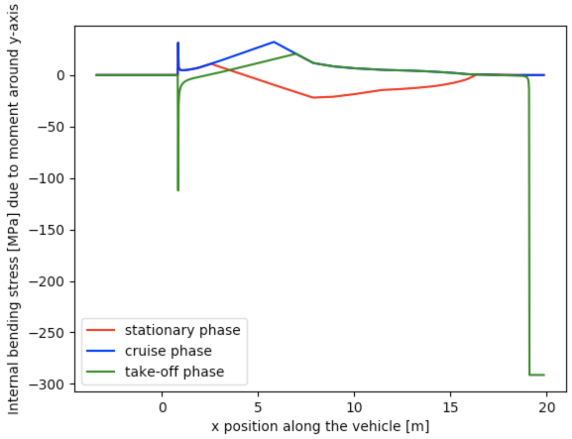

(a) Bending moment around the y-axis in different flight phases, for a skin thickness of 1 mm.

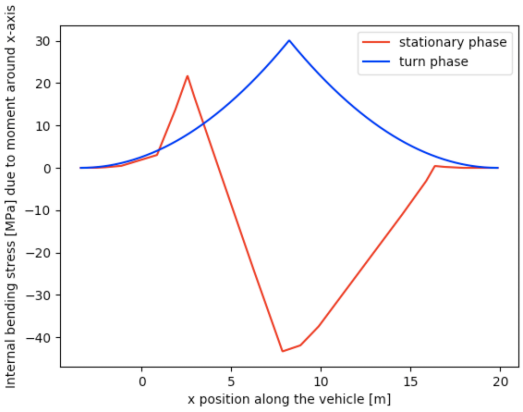

(b) Bending moment around the x-axis in different flight phases, for a skin thickness of 1 mm.

Figure 10.4: Figure representing the bending moments in x- and y-direction.

For analysing the bending about the x-axis only the stationary phase and the cruise phase are analysed as only in these phases a significant bending moment around the x-axis is applied. In Figure 10.4b, the internal stresses due to the bending around the x-axis can be seen. The skin thickness is assumed to be 1 mm here as well, and as can be seen in the graph, the stresses in the structure are well below the yield strength of aluminium and therefore no reinforcement or thicker skin is required.

In conclusion, it can be seen that the structure of the main body can resist bending even with a skin thickness of 1 mm. This is therefore used as a thickness of the skin of the main body.

Now that the main body has been sized for bending, other failure modes need to be analysed. A critical failure mode is buckling. For buckling, the normal stresses working on the skin of the main body are analysed. The thrust and drag forces applied on the structure are the highest normal loads the structure encounters. A program is written in Python that checks if the skin itself is stiff enough to prevent buckling. If the skin is not stiff enough, stiffeners are added until the stiffened skin does not buckle when the maximum normal load is applied. In Figure 10.5a, it can be seen that two stringers should be sufficient. Moreover, redundancy and safety margins need to be taken into account. Also, it must be noted that the plates are only analysed for bending and buckling; this means failure modes that are not considered could potentially be critical ones. Therefore, a number of 8 stringers is chosen. This number is chosen based on reference vehicles and to add some safety margins. The dimensions of the stringers used here can be seen in Figure 10.5b. The spacing between the stringers is 1 m.

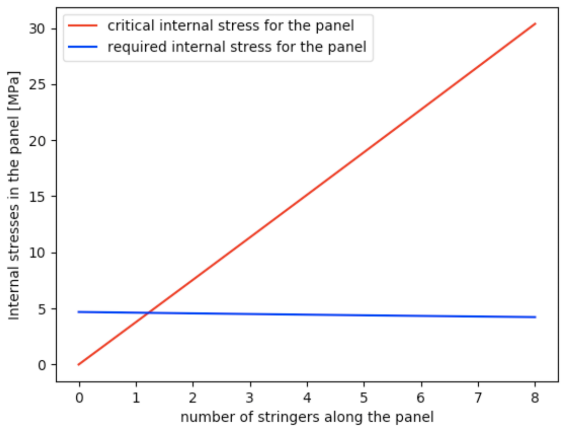

(a) Graph showing the amount of stringers needed to prevent the plates of the main body from buckling

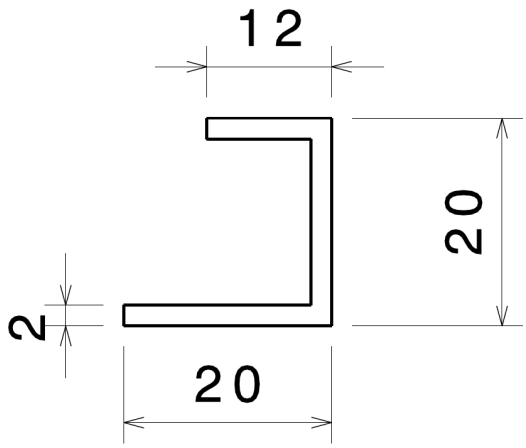

(b) Dimension of the stringer of the main body [mm]. The lower horizontal side of the stringer is going to be attached to the plate.

Figure 10.5: Stringer number and dimensions

To conclude; the skin of the main body will be 1 mm thick and have 8 stringers with a spacing of 1 m.

10.3.1. Moving structure for the main wing

To achieve take-off and landing requirements, the lift coefficient of the overall vehicle should be changed, as discussed in chapter 12. In order to change this lift coefficient whilst still keeping the vehicle stable, the angle of attack of the main wing is altered. The main wing of the AeroCity vehicle is rotating about half-chord. The rotation point is thus at 10 m from the leading edge of the main wing. This rotation point is chosen for aerodynamic reasons, and to prevent the wing from hitting the ground. The main wing is rotating with respect to the sideskirts, which means that the connection between the sideskirts and the main wing consist of movable parts only.

The rotation of the main wing with respect to the sideskirts is achieved by placing two beams throughout the depth of the main wing. The beams will be around 8.3 m in length, running from the middle of one sideskirt to the middle of the other sideskirt. The first beam is placed at 2 m from the leading edge of the main wing, in front of the passengers' seats. The second beam is placed at 14.5 m, just behind the passenger compartment. As the second beam is located further away from the centre of gravity it will carry less load. It is estmitated that the first beam will carry double the amount of load compared to the second beam. If the first beam and second beam would move vertically over the same length, but in different direction, the resulting rotation point would be at 8 m from the

leading edge. In order to still have the resulting rotation point at 10 m the first beam has to have a larger change in vertical position compared to the second beam. The change in the angle of attack that needs to be achieved is 2.45 degrees, from 2.3 degrees to 4.75 degrees. The first beam has to move about 0.35 m vertically. This is achieved by a screw jack that will rotate the beams up or down.

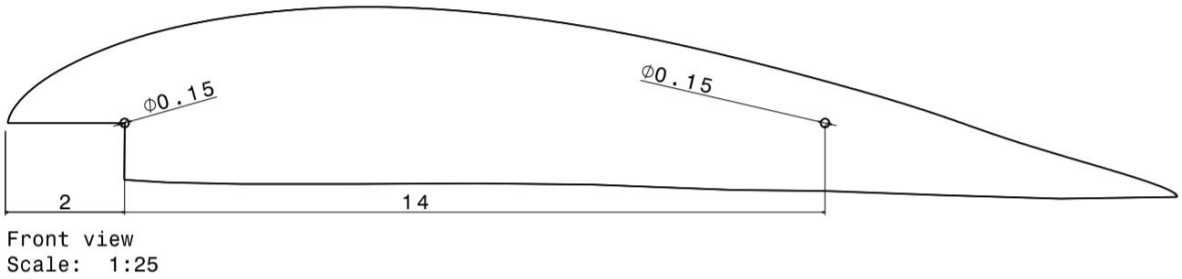

Figure 10.6: Placement of the beams that move the main wing with respect to the sideskirts in mm

The beams that need to connect the main wing to the sideskirts are the only connection between the two elements. This connection is thus of great importance. Therefore, multiple calculations were performed. Firstly, the beams were designed to withstand the bending loads. Looking at the AeroCity vehicle from the side, the structure can be assumed to be a beam with point loads acting on it as shown in Figure 10.7. The top view of the load carrying structure is shown in Figure 10.8. From Figure 10.7, the loads acting on each beam can be calculated by assuming the vehicle to be in equilibrium and then summing the forces and moments.

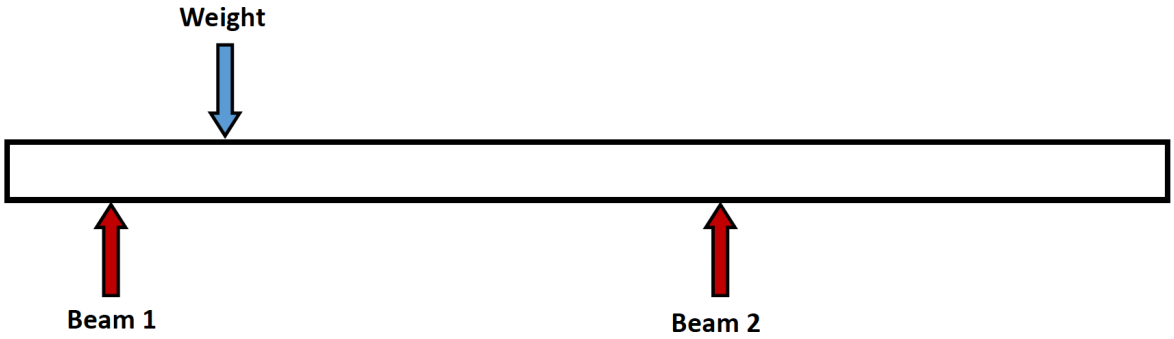

Figure 10.7: Side view of a simplification of the system that moves the main wing with respect to the sideskirts

Once the loads on each beam are found, the structural analysis of the beam itself can be performed. This can be seen in Figure 10.9. From this loading, it can be seen that the shear force in the beam is constant in magnitude but switches sign in the middle. The maximum bending moment will occur in the middle of the beam. The normal forces working on the beams will be negligible, therefore, the normal forces will not be considered in further detail. A more detailed analysis will be performed on the bending and shear of the beam. It was expected that shear would be the failure mode. The calculations confirm that shear will the critical failure mode of the beam, therefore, the beams are designed on this criteria. From the calculations it follows that the beams will be 15 cm in diameter with a thickness of 3 mm. This results in an internal shear stress of 185 MPa.

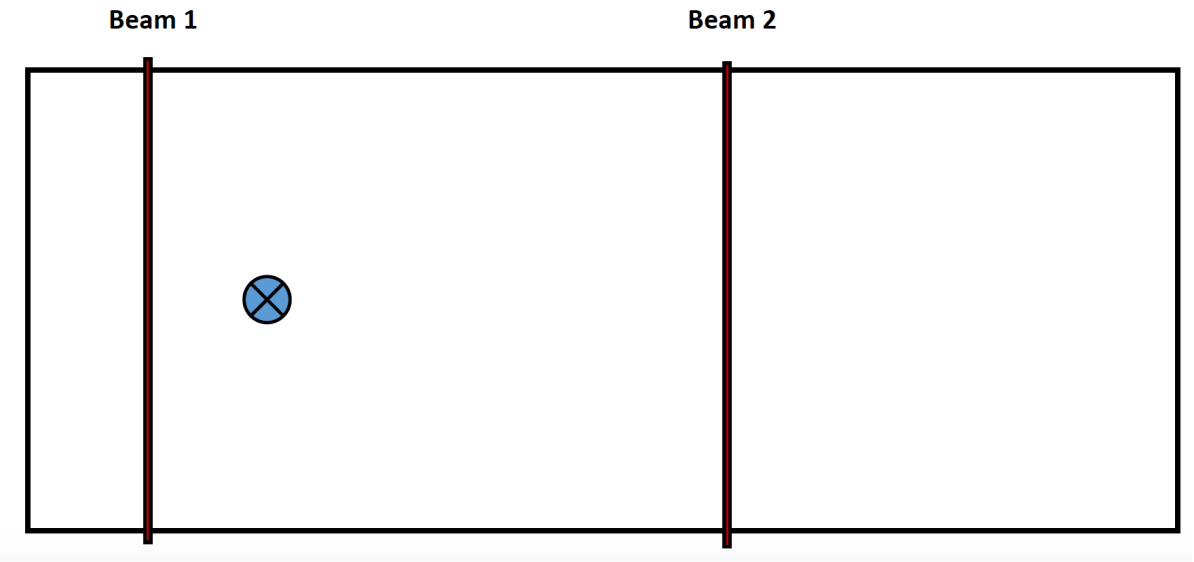

Figure 10.8: Top view of a simplification of the system that moves the main wing with respect to the sideskirts

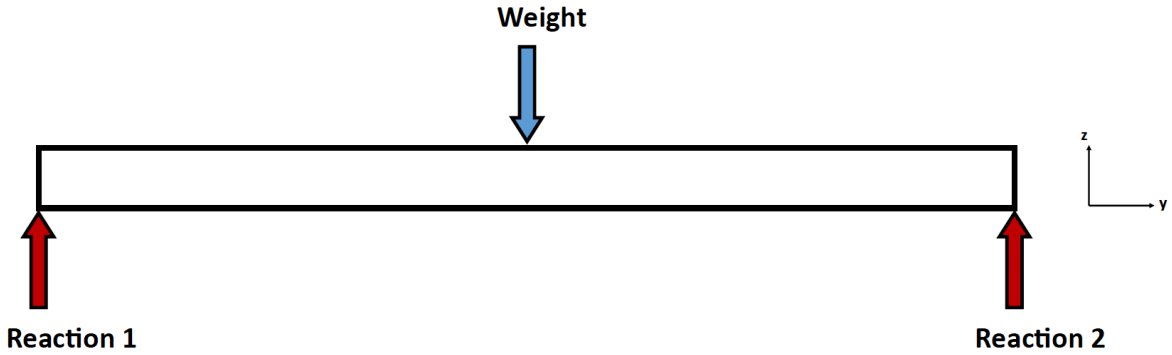

Figure 10.9: Simplification of beam 1 of the system that moves the main wing with respect to the sideskirts

10.4. Sideskirt

In this section, the structure of the sideskirts will be discussed in more detail. First of all, the front parts of the sideskirts will be described. After this, the critical failure mode of the other components will be discussed. Also, some optimisations of the structure will be discussed. A sketch of the initial structural layout of the sideskirt is given in Figure 10.10.

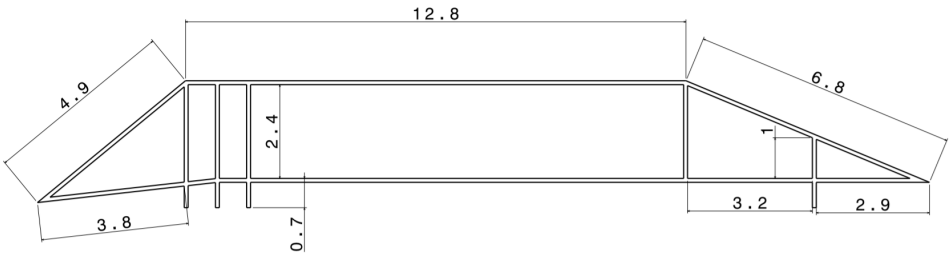

Figure 10.10: Sketch of simplified structure of the side skirt, dimensions given in metres

The leading edge of the canard will be located 3.3 m in front of the main wing. The force on the canard will be created by the lift produced and by the presence of ballast in the canard; the lift force produced is significantly larger. Therefore, the deflection of the front part of the structure is expected to be the critical failure mode for the

front of the canard and will be discussed in more detail. The method discussed in subsection 10.2.2 will be applied. Furthermore, optimisation of the weight will be performed.

To start with, the calculations are based on an aluminium beam with a square cross-section. It is assumed that this beam carries all the load applied on the canard.

To determine the deflection of the beam the elastic curve of the beam is determined. The loads on the canard will be largest during take-off and landing since the canard will produce lift during those phases. The weight of the canard structure will cause bending relief, however, this is not yet taken into account. Therefore, the structure will be slightly over-designed. The lift generated by the canard is modelled as a point load at the end of the structure, this load presented as F_1. It is estimated that the canard will create approximately 50 kN of lift. The lift is placed under an angle of 39.4 °. The load that will work perpendicular on the beam will be 31.7 kN. To account for an increase in loading a safety-factor of 1.5 is applied. The free body diagram of this problem is shown in Figure 10.11. It is assumed that this beam is fixed at one side and free on the other side. Therefore the following boundary conditions apply: $V = 0$ at x=L and $\frac{dv}{dx} = 0$ at x = L

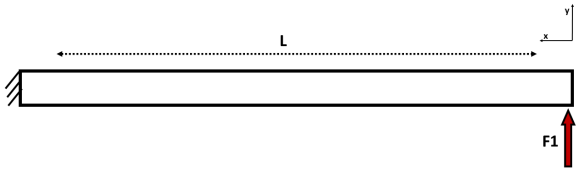

Figure 10.11: Free Body Diagram of the forces on the main beam

Applying the above-mentioned boundary conditions, the deflection of the beam can be calculated by applying Equation 10.14.

$$v_1(x) = \frac{F}{6EI}\left(-x^3 + 3(L^2)x - 2L^3\right) \tag{10.14}$$

It was decided that the maximum deflection of the supporting structure should be 0.10 m to reduce the aerodynamic inferences. It was found that the solid square beam will have a height of 15 cm and will have a weight of 312 kg, in order to meet the deflection requirement.

To comply with the weight requirements, several optimisations are performed. First of all, it is assumed that the main beam will be supported by two vertical beams. This is shown in Figure 10.12. It is assumed that this structure will carry the complete load of the canard. Furthermore, it is assumed that the triangular structure is fixed at points A and B, as shown in Figure 10.12. Also, beam number four is not taken into account during the calculation of the maximum deflection. Therefore, the supporting beams, beam one and two, will be over-designed. By introducing supporting beams the length considered for deflection will be decreased from approximately 5 m to 2.3 m.

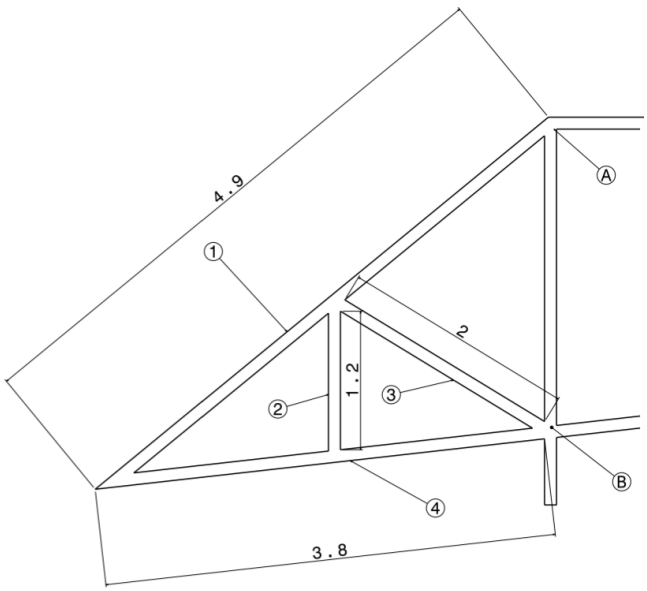

Figure 10.12: Sketch of the canard supporting structure. The structure is assumed to be fixed at point A and point B. Beams 1 and 2 are supporting beams.

The supporting beams are modelled as springs and placed in the middle of the main beam. Beam number three will support beam one in normal operation. In case

of failure of beam three, beam two will limit the deflection of the structure.

To determine the size of the beam the required stiffness needs to be determined. The deflection at the tip of the leading edge created by the supporting beam was determined by applying Equation 10.15.

$$v_{spring_{end}} = -v_{1_{max}} + 0.10 \tag{10.15}$$

Once the desired deflection at the end of the beam, caused by the supporting beam, is found, the required force can be computed with Equation 10.16. After this, the deflection in the middle of the beam due to the spring force and the weight of the beam is determined. via Equation 10.17.

$$P = \frac{v_{spring_{end}}}{\frac{(0.5L)^3}{3EI} + \frac{(0.5L)^2}{2EI} 0.5L} \tag{10.16}$$

$$\delta_{spring} = v_{1_{mid}} - \frac{P(0.5L)^3}{3EI} \tag{10.17}$$

From this, the stiffness of the supporting beam was determined using:

$$k_{beam} = \frac{P}{\delta_{spring}} \tag{10.18}$$

$$A_{suport} = \frac{k_{beam} L_a}{E} \tag{10.19}$$

$$m_{support} = \rho_{al} L_a A_{support} \tag{10.20}$$

An iterative process was performed to determine the optimal combination between the weight of the main beam and the supporting beam. To account for the internal stresses, the deflection of the main beam without the support needed to be less than 0.5 metres. The cross-sectional area of the supporting beam should be 4 mm^2 to provide the minimal required stiffness.

To optimise the weight of the supporting structure, the cross-sectional shape is optimised. The cross-sections considered are shown in Figure 10.13.

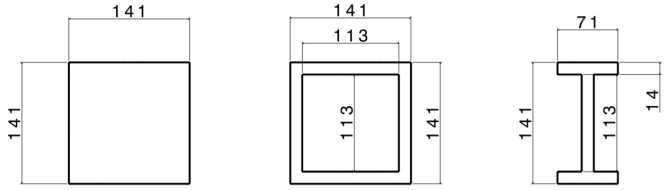

Figure 10.13: Sketch of different cross sectional areas, dimensions give in are given in centimetres

It is assumed that the height of the beam remains constant for all the cross sections considered. For the sizing of the cross section the ratios shown in Equation 10.21, Equation 10.22 and Equation 10.23 In which b is the width of the I beam, H the total height of the cross-section and a the thickness along the I beam.

$$b = \frac{H}{2} \tag{10.21}$$

$$a = H * 0.01 \tag{10.22}$$

$$h = H - 2a \tag{10.23}$$

The moment of inertia of the I beam cross section is calculated using Equation 10.24. The moment of inertia of the solid square can be calculated using Equation 10.25. Lastly, the moment of inertia of the hollow square can be calculated using Equation 10.26.

$$I_{xx} = 2\left(\frac{b^3}{12} + ab\left(\frac{H}{2} - \frac{a}{2}\right)^2\right) + \frac{(H-2a)^3 a}{12} \tag{10.24}$$

$$I_{xx} = \frac{H^4}{12} \tag{10.25}$$

$$I_{xx} = \frac{H^4}{12} - \frac{h^4}{12} \tag{10.26}$$

As mentioned before, the maximum deflection of the main beam should be limited to 0.5 m. Taking this, and the reduced length of 2.3 m into account, the required moment of inertia was found to be 1278 cm^4. As can be seen in Figure 10.14, the I-beam cross section has the lowest weight for the required moment of inertia to comply with the requirement of the maximum deflection of the beam. Therefore, the I-beam is chosen as the shape for the cross-sectional area.

The critical failure mode of the beams in the middle section of the structure, will be buckling. Therefore, the method explained in subsection 10.2.6 will be used to size the beams. To reduce the effective length of the middle beam, vertical beams are placed. In this way, the needed moment of inertia could be reduced and, therefore, the weight of the structure can be reduced. By applying equation Equation 10.6, a moment of inertia of $6.310^{-7}\,m^4$ is found. As shown in Figure 10.14, an I beam is most optimal in terms of weight. Therefore, the same ratios as mentioned earlier are assumed for the I beam. The final height of the beam will be 6.0 cm. It is assumed that all beams, except from beam 1, will have an I shaped cross sectional area and a height of 6 cm. The final dimensions of the beam are shown in Figure 10.15.

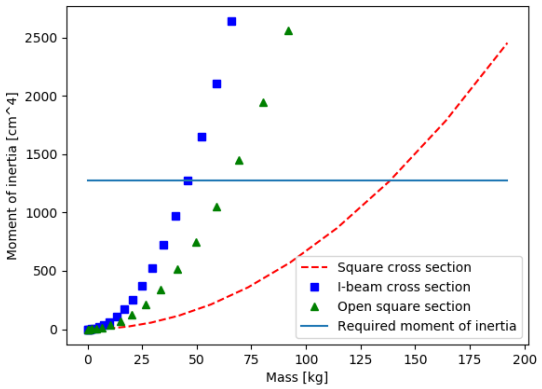

Figure 10.14: Graph showing comparison between different cross sectional areas

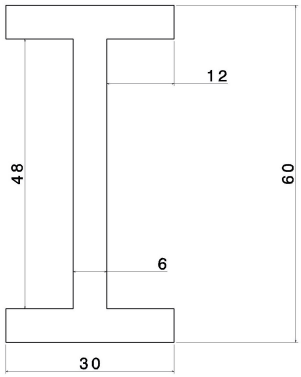

Figure 10.15: Sketch of I beam in the structure of the sideskirts, dimensions given in mm

A sketch of the final structure with the optimisations is shown in Figure 10.16.

The final results of the optimisations are shown in Table 10.3.

Table 10.3: Summary of optimisation

	Component $[kg]$	**Maximum length** $[m]$	**Cross sectional area** $[cm^2]$	**Mass**	**Needed Moment of Inertia** $[m^4]$	**Failure mode**
Non optimised shape	8,11	11	0.1458	45.3	$1.57*10^{-6}$	Buckling
	1	4.9	2.59	356	$8.9*10^{-5}$	Deflection
Optimised shape	8,11	5.9	0.064	20.1	$4.52*10^{-7}$	Buckling
	1	2.3	0.36	49	$8.6*10^{-6}$	Deflection

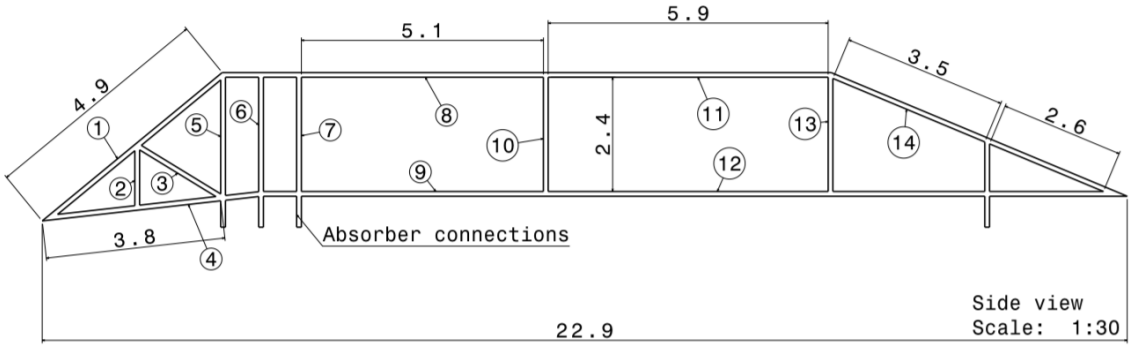

Figure 10.16: Sketch of the inner structure of the sideskirt, dimensions are given in metres

From this, it is concluded that two supporting beams will be used for redundancy and weight reduction, in the front of the structure. Furthermore, the complete structure of the sideskirt will consist of I shaped beams.

11 Ground operations

In this chapter, the ground operations of the AeroCity vehicle are described. Firstly, in section 11.1, the ground procedures are described, which consist of taxi, take-off and landing. Secondly, the landing gear is described in section 11.2, including the general layout, configuration, and placement. Thirdly, in section 11.3, the design of the shock absorbers for the landing procedure is described. Lastly, the braking system is elaborated upon in section 11.4.

11.1. Ground procedures

In this section, the general ground procedures and operations are described. Firstly, the taxiing of the vehicle on the ground is described in subsection 11.1.1. Secondly, the take-off procedure is described in subsection 11.1.2. Lastly, the landing procedure is described in subsection 11.1.3.

11.1.1. Taxi

AeroCity should be able to taxi in the station, to slowly approach and leave the station and move over small distances. For this, wheel propulsion is used. As stated in the requirements, acceleration and deceleration of the vehicle shall be max $0.1g$. To move a 36,000 kg vehicle with an acceleration of $0.1g$, a thrust force of 35.3 kN is needed ($F = m \cdot a$). Then, the required power to accelerate the vehicle up to a velocity of 5 m/s is then 177 kW ($P = F \cdot V$). When this is divided over all 8 wheels (a description about the number of wheels is given in subsection 11.2.1), the required power per wheel motor becomes 22 kW. In each wheel, an electric motor will be placed, together with a gearbox, which means that in total there will be 8 wheel motors. These motors together allow the vehicle to move from standstill up to 5 m/s. At speeds higher then 5 m/s, the fans will produce the main thrust. An elaborate description of the wheel requirements and power required to accelerate the vehicle is given in section 9.6.

11.1.2. Take-off procedure

When exiting the station, the vehicle will use powered wheels to accelerate. After the vehicle has left the station, the fan will be activated to keep a constant acceleration of 0.1 g. The power and accelerations will be discussed in chapter 16. Both the main wing and the canard will have their maximum angle of attack as described in subsection 12.1.1. This configuration will allow take-off at 200 km/h. After take-off, both aerodynamic bodies will decrease their angle of attack to keep the same lift at increasing speed towards cruise speed.

11.1.3. Landing procedure

During landing, the vehicle will lose speed through increasing drag. While still in the air, AeroCity will not be able to use spoilers without interfering with the lift. To increase the drag, AeroCity will change its shape to the high angle of attack shape of take-off. This will increase ground clearance of the entire vehicle to 45 cm, which will increase the vortexes and thereby the drag. The deceleration starts by stopping forward thrust. More detailed aerodynamic analysis will investigate the effects of the fans stopping, regenerating or moving freely. When approaching the landing velocity of 200 km/h, the ground clearance reduces and the vehicle will land with minimal vertical velocity.

After touchdown, several braking mechanisms will be activated. The combined braking power will result in a total deceleration of 0.1 g. This will be discussed in more detail in section 11.4 and chapter 16.

11.2. Landing gear

In this section, the landing gear design of AeroCity is discussed. Firstly, the general layout, configuration and placement of the landing gear are elaborated upon. Secondly, different options for the tires are discussed and the tire is selected.

11.2.1. General layout and placement

For the general layout of the vehicle, the landing gear had to be designed. For the design of the AeroCity vehicle, the landing gear was chosen to use wheels. An elaborate discussion on the different landing gear concepts is given in the midterm report of this AeroCity design [8].

With the selected wheels as landing system, a design was made for the layout and placement. For the layout, the wheel landing system consists of eight wheels, with shock absorbers for each wheel which will have to absorb the landing impact of the vehicle (in normal conditions as well as in extreme (emergency) conditions). These shock absorbers are attached to the wheels, to make sure that the vehicle will land as comfortably as possible.

A design choice that had to be made was whether a retractable or non-retractable system would be used. For the AeroCity design, a non-retractable system is chosen. A non-retractable system was preferred because there would be no need to design a retract system for the wheels, which makes the design of the landing gear a lot less complex. However, the sideskirts of the AeroCity are only five centimetres above the ground. This means that the

non-retractable landing gear has to stick out underneath the sideskirts, to prevent the sideskirts from bumping into the ground.

Moreover, the wheels should not touch the ground during small crosswinds or other destabilising movements, thus it was decided that the wheels would stick only 2 cm out underneath the sideskirts. To go from cruise condition to landing condition in normal operations, the impact has to be controlled to not hit the ground with the sideskirts. To reduce the impact, the thrust will slowly be reduced, leading to a controlled downwards movement. When this procedure is used, the impact velocity of the vehicle will be minimal, thus leading to a low impact, making a landing with a margin of only 2 cm possible.

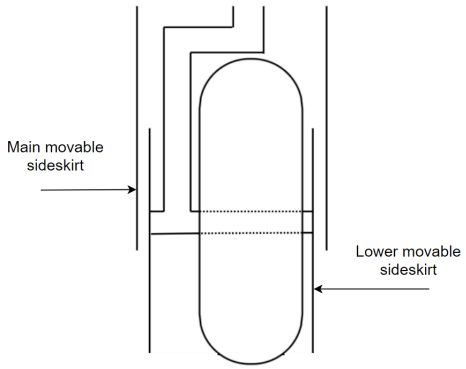

Figure 11.1: Front view cross-sectional overview of the movable sideskirts

Moreover, due to the damping, the vehicle will go down more than 5 cm, as described in section 11.3. Therefore, the sideskirts have to be made movable in order to not touch the ground. This means that the sideskirt is split up in a lower part and a main part. The lower part of the sideskirt will move inside the main part of the sideskirt during landing, to account for the required damping. This means that the lower sideskirt will not bump into the ground, which is necessary to not damage the vehicle. A sketch of the movable sideskirts is shown in Figure 11.1.

For the placement of the wheels, it was assumed that the static load would be the highest load case for the tires. For the placement, a calculation was performed based on the centre of gravity range. The centre of gravity varies due to passenger loading, so a centre of gravity range of 5.7-6.3 (centre of gravity when fully loaded +- 5%) meters is accounted for. The most extreme cases are then calculated for the front and the rear landing gear, according to [29]. The maximum static load on the main gear can be determined using Equation 11.2.

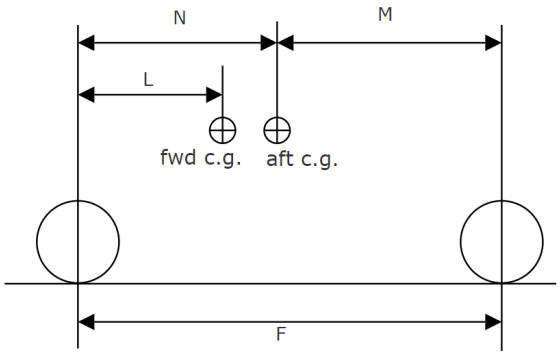

Figure 11.2: Schematic overview of distances used for calculations [49]

$$P_{front_{max}} = \frac{w(f-l)}{f}) \tag{11.1}$$

$$P_m = \frac{w(f-m)}{2f * n_s} \tag{11.2}$$

The iteration led to a result which included 8 wheels in total, where 6 wheels are placed in front, with the centre of the middle wheel at 2.7 meters from the leading edge (3 wheels in each sideskirt) and 2 wheels at 16.5 meters (1 wheel in each sideskirt). For this configuration, the maximum load on each wheel is 5,869 kg (58 kN). A sketch of the layout of the wheel placement is shown in Figure 11.3.

11.2.2. Tire selection

Now that the number of wheels and their placement have been designed, the tires have to be selected accordingly. For preliminary design, it is justifiable that the shock absorber design will be adapted to the energy the tire can absorb at maximum deflection. In that case, the choice of the tire can be based on the maximum static load on the wheel [29]. For designing the tire, multiple aspects need to be taken into consideration. The ones considered in this design are listed below [54].

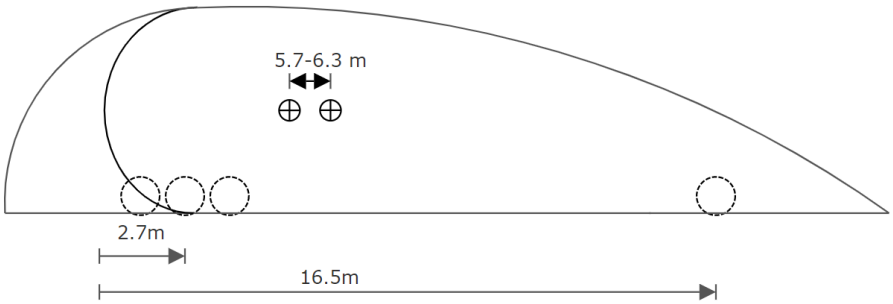

Figure 11.3: Wheel layout

1. Maximum dimension of the inflated tire
2. A growth allowance due to service
3. The effect of centrifugal forces at high speed rolling

Taking into account these aspects, it was found that the tire design should allow for a 4% growth of the diameter and a 10% growth of the maximum diameter. The tires will be placed inside the side skirts, which have a width of 30 centimetres. To also account for some room for the brakes and the structure connected to the wheels, the maximum tire width was determined to be 22 cm.

From [55], several tires, which could apply to this AeroCity design, were selected . The main tire characteristic that has been looked at, eliminating most of the existing tires, is the velocity. Namely, the tires will be designed such that they can also handle emergency manoeuvres. This means that they should be able to act as a bumper underneath the sideskirts such that the vehicle does not crash on the ground. Therefore, the cruise speed multiplied by a safety factor of 1.2 [54] is accounted for. This leads to a minimum speed of 368 km/h. Furthermore, the maximum width of the tires is only allowed to be 22 cm, since wider tires do not fit in the sideskirts. This already greatly reduces the tire possibilities, which leads to the following options, shown in Table 11.1:

Table 11.1: Optional tires

Tire type	**Speed** $[km/h]$	**Maximum width** $[cm]$	**Maximum diameter** $[cm]$	**Maximum loading** $[kg]$
18x5.7	402	14.5	45.6	4082
20x4.4	410	10	49.4	2950
22x7.7	443	19.5	55.8	4782
24x7.7	402	19.5	61	3720
25.5x8.0	402	20.3	64.8	7348

In Table 11.1 the maximum width, maximum diameter and maximum loading are compared. As can be seen, all tires fit inside the sideskirt and can withstand the maximum speed in case of emergency. To decide which tire should be picked, the maximum loading has to be accounted for. As shown in subsection 11.2.1, the maximum loading on each wheel is 5869 kg. This means that the only suitable option left is the last one in Table 11.1. Hence, tire type 25.5x8.0 is chosen for the design of the landing gear and further calculations take into account this tire type. The outer diameter of this tire is 64.8 cm, whereas the maximum width of the tire is 20.3 cm. This tire consists of layers of rubber-coated nylon chord, which are placed diagonally. This placement allows for strength in both axial as well as lateral direction. From this tire selection, it follows that for the forward wheel placement, the most forward wheel of the three wheels is placed at 1.9 meters from the leading edge of the main body and the most aft wheel of the three wheels is placed at 3.5 meters from the leading edge of the main body. This takes into account that there is sufficient spacing between the wheels.

11.3. Shock absorbers

The landing gear must absorb the shock created during landing and must even out irregularities when the vehicle does not fly. The oleo-pneumatic is the most common type of shock absorber used in current landing gear configuration. Furthermore, it has the highest efficiency weight ratio as shown in Figure 11.4. Therefore, this option is chosen for this design.

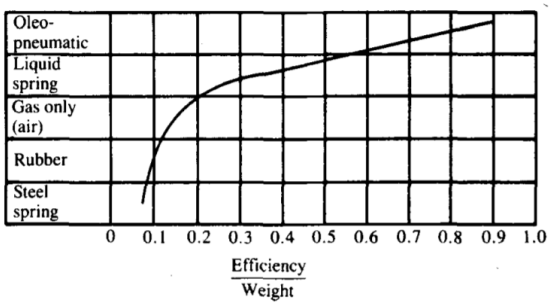

Figure 11.4: The effiency weight ratio is shown for different types of shock absorbers [56]

The maximum amount of energy that needs to be absorbed by the landing system can be determined using Equation 11.3. The kinetic energy of the landing gear can be expressed as shown in equation Equation 11.4.

$$E_t = 0.5 W_L \frac{w_t^2}{g} \tag{11.3}$$

$$E_t = n_s P_m N_g (\eta_t s_t + \eta_s s_s) \tag{11.4}$$

For the design of the main landing gear, it is assumed that all the kinetic energy produced during touch down is absorbed by the main landing gear. This means that the mean landing gear is slightly overdesigned.

It is assumed that $P_m = \frac{W_L}{n_s}$, in which W_L is defined as the total weight of the vehicle and n_s is defined as the number of struts. To calculate the length of the shock absorber the landing gear load factor N_g is assumed to be $N_g = 1.5$ due to requirements set by FAR25 [29]. The aforementioned oleo-pneumatic shock absorber is used for this. Therefore, the efficiency of the strut was found to be $\eta_s = 0.80$. Furthermore, the maximum sink speed was found to be $w_t = 4 fps$. This was calculated using the maximum acceleration of $9.81 \frac{m}{s^2}$ and the distance to ground of $5cm$. Furthermore, a safety factor of 1.5 is applied for the sink speed. Also, the allowable tire deflection can be determined using the properties of the chosen tire using Equation 11.5. Furthermore, the tire deflection efficiency was stated to be $\eta_t = 0.47$ [29]. The loaded radius of the tire is 11 inch and $D_0 = 64.8cm$. Combining Equation 11.3 and Equation 11.4, the stroke length can be calculated with equation Equation 11.6.

$$s_t = D_0 - 2(loaded radius) \tag{11.5}$$

$$S_s = \frac{\frac{0.5 \frac{W_L}{g} (w_t)^2}{n_s P_m N_g} - \eta_t s_t}{\eta_s} \tag{11.6}$$

Moreover, in [29] it is suggested to add some length to the calculated strut length. This is shown in Equation 11.7. The total length of the oleo including the stroke distance can be approximated by Equation 11.8 [57]. Using the maximum static main gear load (P_m) the required radius of the strut can be calculated applying Equation 11.9 [29]. Furthermore, the cross-sectional area of the piston can be estimated by Equation 11.10.

$$s_{s_{design}} = s_s + \frac{1}{12} \tag{11.7}$$

$$L_{pist} = s_{design} + 2.75 \sqrt{\frac{A_{piston}}{\pi}} \tag{11.8}$$

$$d_s = 0.041 + 0.0025 \sqrt{P_m} \tag{11.9}$$

$$A_{piston} = \frac{P_m}{1500} \tag{11.10}$$

The external diameter of the oleo can be approximated by Equation 11.11 [49]. To determine the extension in the stroke while in the extended position, it is assumed that the air volume at the compressed position is 10% of the total displacement [57]. Using this, the volume at compressed position (V_3) can be calculated using Equation 11.12.

$$D_{oleo_{ext}} = 1.3 d_s \tag{11.11}$$

$$V_3 = 0.10(s_{s_{design}} A_{piston}) \tag{11.12}$$

Furthermore, it is assumed that the pressure ratio between the extended piston and the piston in static position is $\frac{2.1}{1}$ [57]. Also, the pressure ratio between the compression state and the static state is equal to $\frac{1.9}{1}$ [57]. A static pressure of 1500 psi is assumed, this is equal to 103 Bar. Using the compression factor between the compressed state and static state, it was found that the $P_{strut_{max}} = 4500 psi$. Then the air pressure at full extension (P_1) can be calculated using Equation 11.13.

$$P_1 = \frac{4500 V_3}{V_3 + D} \tag{11.13}$$

$$V_2 = \frac{P_1 V_1}{P_2} \tag{11.14}$$

Using the values calculated above, the stroke extension from static to extended position can be calculated applying Equation 11.15.

$$S_{extended} = s_{s_{design}} - \frac{(V_2 - V_3)}{A_{piston}} \tag{11.15}$$

A sketch of the shock absorber showing the different positions of the absorber is given in Figure 11.5 [49]. The results of the above mentioned formulas are summarised Table 11.2. The calculations for the landing gear structure are mainly based on direct stresses and literature research. It was decided to use torque links for the forces introduced in the horizontal direction.

Table 11.2: Summary of final sizing shock absorber

Stroke length $[m]$	**Length piston** $[m]$	**Stroke extension** $[m]$	**Internal diameter** $[m]$	**External diameter** $[m]$
0.12	0.09	0.10	0.09	0.11

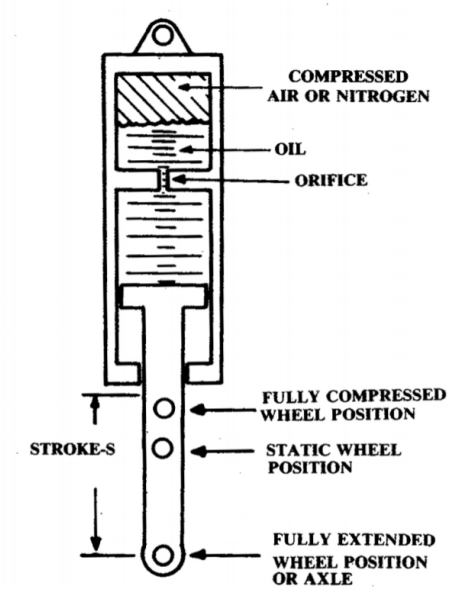

Figure 11.5: Schematic overview of the oleo shock absorber showing the different positions of the piston [49]

It is assumed that the upper beam carries all the load from the beam. To simplify the calculations of the loads on the landing gear, it is assumed that the tire does not deflect and thereby the normal force and the friction force are carried by shock absorbers and the torque links.

It is expected that the critical failure mode will be load in compression, therefore the normal loads on the torque

links need to be calculated. The maximum normal force on the wheel equals 58 kN. The friction force is calculated assuming a friction coefficient of $\mu = 0.8$ [57], the friction force can be determined applying Equation 11.16.

It is assumed that the torque link carries all the horizontal load caused by the friction of the wheels. Furthermore, it is assumed that the torque links are made of aluminium. By applying Equation 11.17, the minimum area of the beam can be found.

$$F_{friction} = \mu F_{normal} \tag{11.16}$$

$$\sigma = \frac{F}{A} \tag{11.17}$$

It was found that torque links with a radius of 10mm would be sufficient to carry the direct stress caused by the friction load. From existing landing gear [57], it was estimated that the length of the torque links is approximately 10 cm. This value will be used during the design. A sketch of the complete landing gear system is shown in Figure 11.2.

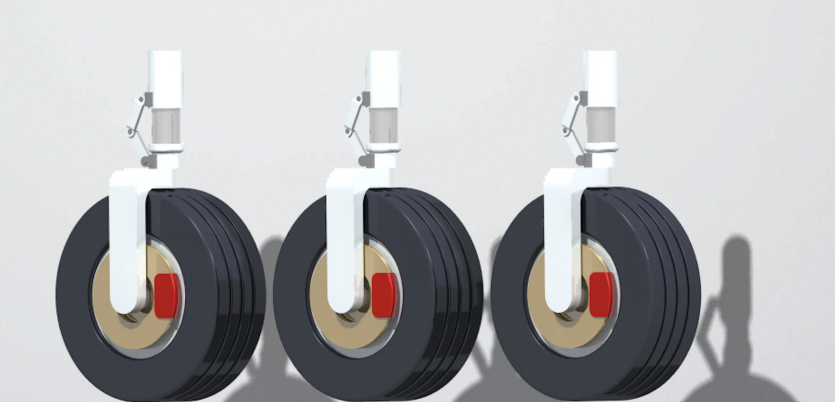

Figure 11.6: Lay-out of front landing gear

11.4. Braking system

To come to a standstill at stations, a braking system has to be designed. This braking system consists of an airborne braking system and a ground braking system. A performance analysis of the braking system is given in chapter 16.

For braking while in air, the engines will be turned off. Since the drag is not enough to decelerate the vehicle with 0.1g, an additional air brake could be used. However, since the aerodynamic consequences of this air brake cannot be estimated and the sideskirts fly at a height of only 5 cm above the ground, this option is rejected. Nonetheless, the vehicle should still create enough drag to decelerate with 0.1g. Therefore, the vehicle will increase the angle of attack to increase the drag. Consequently, the vehicle will fly higher to approximately 45 cm due to the increase in the lift coefficient. With decreasing velocity, the lift decreases and the vehicle lowers eventually until the vehicle lands on the ground.

Once the vehicle lands on the ground at around 200 km/h, the ground braking system should start to work. The first ground brake that becomes active is a spoiler. This spoiler is placed on top of the vehicle and spans the entire width of the vehicle. The spoiler can be used without any problematic aerodynamic interference since the vehicle is already on the ground. The spoiler, which consists of a rectangular plate of 8 m by 1.5 m, can be fully deflected once the vehicle has landed. This is a very efficient way of braking since simply the drag of the vehicle is drastically increased by increasing the frontal area. No additional power is needed for this braking system, apart from actuators which have to deflect the spoiler.

Next to the spoiler, which does not create enough drag to continue a $0.1g$ deceleration, a combination of regenerative braking, reverse propulsion and disc braking is used, to make sure enough power and force can be generated to decelerate the vehicle with $0.1g$ after landing.

For the regenerative braking, use is made of the wheel propulsion system to decelerate the vehicle. The maximum wheel propulsion power, for which the wheel motors are designed, is used for this. These wheel motors are designed to be largely inside the wheels, in order to provide the required power to the wheels and to allow for regenerative braking. Moreover, by using regenerative braking, an anti-lock braking system (ABS) is integrated into the system, preventing the wheels from locking during braking [58].

Furthermore, reverse thrust is used to decelerate the vehicle from landing to standstill. Since the required power to perform the reversed thrust is lower than the required power to propel the vehicle at cruise, the engines can provide this with no additional designing. The thrust power available for reverse thrust is elaborated upon in chapter 8.

Once the vehicle has decelerated to a speed of 100 km/h, disc braking will be used to bring the vehicle to stand still. A disc brake consists of a brake disc (rotor), a caliper and brake pads. Under normal conditions, the deceleration that the disc brakes have to provide is less than 0.1g due to the reverse thrust and regenerative braking of the motors. However, in case of emergency, the brakes have to be able to decelerate with 0.1g. Thus, the discs are designed for a deceleration of $0.1g$. Moreover, the whole brake system has to fit inside the sideskirt.

The material for the discs was chosen to be carbon, for its high thermal conductivity, high specific heat and constant high specific strength with increasing temperature. Additionally, carbon requires low maintenance, has a low density and has a long service life (up to 5-6 times longer than steel) [59]. To calculate the size of the discs, the weight of the discs had to be calculated first, for which Equation 11.18 was used [57]:

$$KE = M \cdot \theta \cdot specificheat \cdot 1400 \tag{11.18}$$

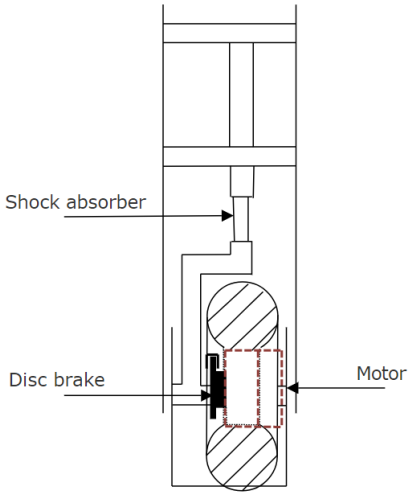

Figure 11.7: Schematic overview of the landing gear system, including brakes (in black), shock absorbers and motor (in red dashed line)

Where KE is the kinetic energy of the vehicle at 100 km/h ($KE = \frac{1}{2}mV^2$) because only from 100 km/h the disc brakes start working. Furthermore, θ is the allowable temperature rise of 500 °C, according to [57]. Then, the specific heat of carbon, which is $0.71 J/gK$, is used to determine the total disc weight to be 27.95 kg. This total weight is distributed over all 8 wheels since they all contribute to the braking of the vehicle. Thus, the weight of the discs for each wheel is equal to 3.5 kg. With a density of $3.51 \cdot 10^3 kg/m^3$, this means that the total required volume for the brakes is $7.96 \cdot 10^3 cm^3$.

Since the disk brakes should not interfere with the tires, the disc brakes are designed to be smaller than the rim diameter. This means that the discs have a diameter which is smaller than 35.5 cm. Thus, a radius of 17.5 cm or smaller is possible. Since the caliper should also fit between the wheel and disc, a maximum radius is determined to be 15 cm. Dividing the total disc required volume over all eight wheels, this leads to a disc width of 1.4 cm for each wheel.

A sketch of the entire landing gear is shown in Figure 11.7. This sketch includes the shock absorbers, disc braking and motor (including gearbox, indicated with a red dashed line). Furthermore, the wheels are sticking 2 cm out underneath the movable sideskirts.

11.5. Wheel pre-spinning

In order to properly land on the ground, the wheels have to be pre-spun. This has to be done to make sure the impact of the landing is as low as possible as well as to reduce the wear of the tires. Pre-spinning of the wheels is performed with the same electric motors that drive the wheel at ground operations.

The wheels cannot be pre-spun in case of emergency since the vehicle lands too quickly under this condition. Thus, the pre-spinning of the wheels is designed for normal operations. This means that the wheels have to be pre-spun with a velocity of 200 km/h. Implementing the radius of the tire and using Equation 11.19, the angular velocity of the wheels can be calculated:

$$\omega = \frac{V}{R} \tag{11.19}$$

Thus, the angular velocity of the wheels has to be 171.5 rad/s.

12 Stability & control

In this chapter, the stability and control (S&C) of the AeroCity vehicle is presented. The chapter is divided into six sections in which the stability and control about the vehicle's six degrees of freedom is addressed. The reference systems for the stability derivatives is the standard one used for aircraft and it is illustrated in Figure 12.1. The reference system for the lift coefficients and for the longitudinal positions of the vehicle's element is also the one employed in aircraft design and it is illustrated in Figure 12.2.

A block diagram of the control system is presented in Figure 12.3

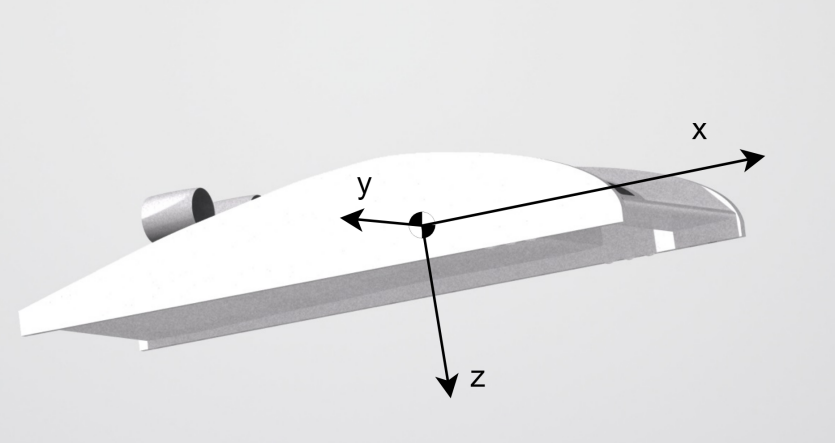

Figure 12.1: Axis system used for stability derivatives. The system is centred in the centre of gravity, the x-axis for roll, y-axis for pitch, z-axis for yaw.

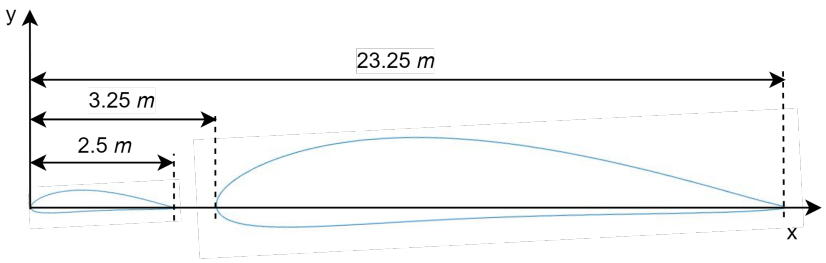

Figure 12.2: Axis system used for lift coefficients and elements' longitudinal positions.

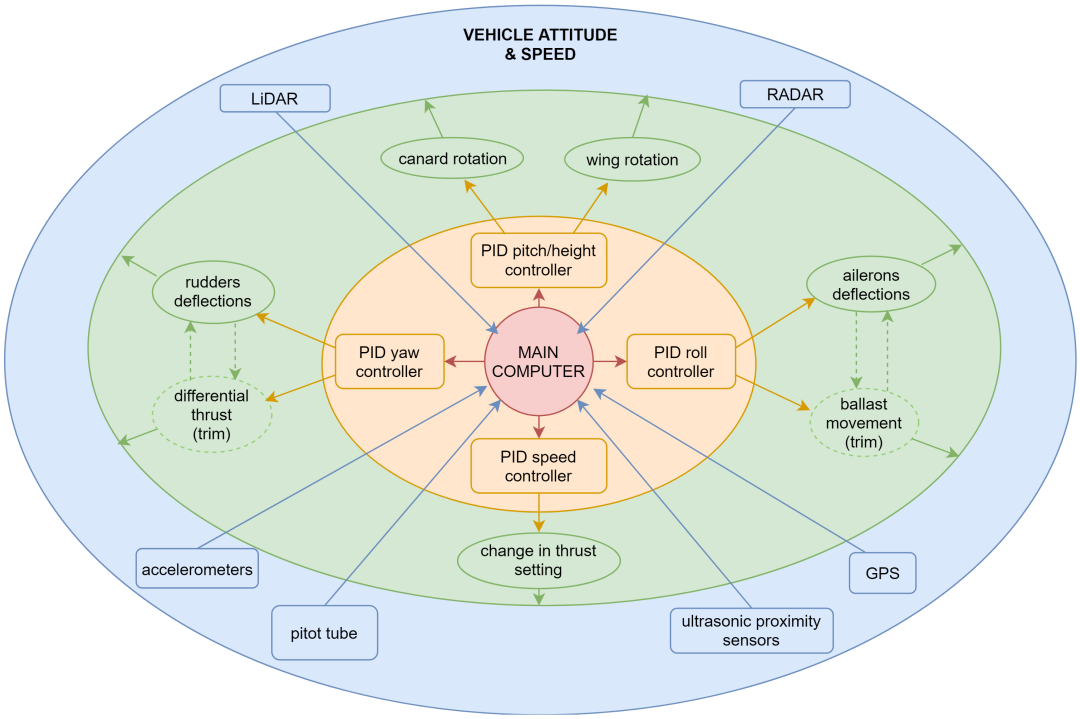

Figure 12.3: Attitude & speed control of the AeroCity vehicle.

12.1. S&C in Pitch

This section is divided into three subsections. In the first two subsections (subsection 12.1.1 and subsection 12.1.2) the static pitch stability and the pitch controllability are discussed. In the third and last subsection, the results are combined, and the allowed longitudinal location range of the centre of gravity is presented.

12.1.1. Pitch static stability

The vehicle possesses static pitch stability when a small perturbation in angle-of-attack generates a pitching moment that counteracts that perturbation. The static pitch stability is formalised in Equation 12.1.

$$\frac{dC_M}{d\alpha} = C_{M_\alpha} < 0 \tag{12.1}$$

C_{M_α} is defined by

$$C_{M_\alpha} = -C_{L_\alpha} \cdot SM_\alpha \tag{12.2}$$

For what concerns the pitch static stability, the contribution of the engines' thrust has been neglected, as it does not vary with small disturbances in the angle of attack. Moreover, the contribution of the ailerons is neglected both because of their small size and because their location behind the fan makes the direction of the flow impacting on them insensitive to disturbances in the angle of attack.

Equation 12.3 shows how C_{L_α} has been obtained. As Equation 12.3 shows, C_{L_α} has been normalised with respect to the total surface area, $S = S_w + S_c = 180\ m^2$.

$$C_{L_\alpha} = \frac{C_{L_{\alpha_w}} \cdot S_w + C_{L_{\alpha_c}} \cdot S_c}{S_w + S_c} \tag{12.3}$$

The stability margin for static pitch stability, SM_α, is defined in Equation 12.4, where $\bar{x}_{np_\alpha}$ and $\bar{x}_{cg}$ have been normalised with respect to the total vehicle length of $c_v = 23.25\ m$.

$$SM_\alpha = \bar{x}_{np_\alpha} - \bar{x}_{cg} \tag{12.4}$$

The position of the neutral point x_{np_α} can be calculated by Equation 12.5. Many of the parameters used in Equation 12.5, namely $C_{L_{\alpha_c}}$, x_{ac_c}, $C_{L_{\alpha_w}}$ and x_{ac_w}, vary with the flight condition and, therefore, the position of the neutral point has been calculated in different points of the flight envelope.

$$x_{np_\alpha} = \frac{C_{L_{\alpha_c}} \cdot (1 + \frac{d\epsilon}{d\alpha_w}) \cdot S_c \cdot x_{ac_{\alpha_c}} + C_{L_{\alpha_w}} \cdot S_w \cdot x_{ac_{\alpha_w}}}{C_{L_{\alpha_c}} \cdot (1 + \frac{d\epsilon}{d\alpha_w}) \cdot S_c + C_{L_{\alpha_w}} \cdot S_w} \tag{12.5}$$

In Equation 12.5 $\frac{d\epsilon}{d\alpha_w}$ is the derivative of the upwash angle with respect to the angle of attack α_w.

In Table 12.1 the C_{M_α} is reported to be negative in the relevant extreme flight conditions. Therefore, in the case of short disturbances in the pitch angle, the vehicle is passively stabilised, and it will automatically come back to the original equilibrium condition.

12.1.2. Pitch controllability

The vehicle possesses pitch controllability when it can be trimmed through the entire flight envelope. Assuming the drag and the thrust vector passing through the centre of gravity, the vehicle is considered trimmed when the overall centre of pressure coincides with the centre of gravity and concurrently vertical equilibrium is present. These two conditions are formalised in Equation 12.6 and Equation 12.7.

$$x_{cg} = x_{cp} = \frac{C_{L_c} \cdot S_c \cdot x_{cp_c} + C_{L_w} \cdot S_w \cdot x_{cp_w}}{C_{L_c} \cdot S_c + C_{L_w} \cdot S_w} \tag{12.6}$$

$$C_{L_w} \cdot S_w + C_{L_c} \cdot S_c = \frac{W}{\frac{1}{2}\rho V^2} \tag{12.7}$$

In case of semi-permanent disturbances (for example a longitudinal shift in the centre of gravity) the control system, composed of ultrasonic proximity sensors, accelerometers, a PID control unit and actuators, is tasked with maintaining the desired pitch angle (equal to 0° in nominal conditions). The accelerometers, placed on the wing, on the canard, and on the sideskirts, are necessary because of the high accuracy and speed in measuring relative changes. The ultrasonic proximity sensors, placed on the bottom side of the sideskirts in the front and in the back of the vehicle, are desired because of the high accuracy in measuring absolute distance values. By carefully integrating the two devices, their benefits are combined. The PID controller reads the differences between the set values and the measured values and applies an accurate and responsive correction. The actuators for the canard consists of two electromechanical motors placed at the canard-sideskirts connections. The actuators for the wing consists of four electromechanical motors placed at the wing-sideskirts connections.

12.1.3. Centre of gravity longitudinal position range

The canard has a positive effect on the stability when it is used to produce positive lift. This is a crucial contribution in the take-off/landing phase, where the wing tends by itself to become unstable (see Figure 7.3). Moreover, it is necessary to provide pitch control and to trim the vehicle. It has been sized and positioned such that it can provide significant additional lift at take-off and landing, improving concurrently the otherwise critical vehicle stability. During the cruise phase, it is mainly used for trimming and control, as a high wing lift coefficient is preferred for aerodynamic efficiency.

Table 12.1 presents the centre of gravity position and the neutral points locations for the relevant flight speeds, the take-off and the cruise ones, and for three different weight configurations:

- maximum payload, with a 1.05 safety factor to account for some variability in payload composition;
- zero payload, to simulate operations of vehicle relocation;
- medium payload, to establish a trend between the aerodynamic parameters and the total vehicle weight.

The table also includes the individual contributions to the stability and the equilibrium from the individual aerodynamic elements, normalised to their respective surface areas and lengths. The process to obtain satisfying results has been highly iterative, as the parameters in Equation 12.5 and Equation 12.6 are dependent on each other.

12.2. S&C in Vertical Direction

This section is divided into two subsections. In the first subsection (subsection 12.2.1) the static vertical stability is discussed. In the second subsection (subsection 12.2.2) the vertical control is presented.

Table 12.1: Centre of gravity and neutral points longitudinal positions, stability coefficients and parameters relevant for their calculation. Standard sea-level atmospheric conditions are assumed.

	W = 360 kN		W = 300 kN		W = 240 kN	
	V = 55.5 m/s	V = 84.8 m/s	V = 55.5 m/s	V = 84.8 m/s	V = 55.5 m/s	V = 84.8 m/s
α_w $[deg]$	4.75	2.73	3.80	2.52	3.12	2.30
α_c $[deg]$	5.0	-0.8	7.0	-0.8	7.0	-1.25
C_{L_w} $[-]$	1.05	0.51	0.83	0.43	0.63	0.35
C_{L_c} $[-]$	1.12	0.00	1.33	-0.01	1.33	-0.10
x_{cp_w} $[m]$	10.35	9.33	10.39	8.67	9.93	7.67
x_{cp_c} $[m]$	0.70	0.75	0.70	0.75	0.70	0.1
$C_{L_{\alpha_w}}$ $[1/rad]$	12.7	17.6	15.5	17.8	16.6	23.5
$C_{L_{\alpha_c}}$ $[1/rad]$	6.0	14.1	5.0	14.1	5.0	13.8
C_{L_α} $[1/rad]$	12.0	17.2	14.3	17.4	15.3	22.4
$x_{ac_{\alpha_w}}$ $[m]$	11.35	13.85	13.29	13.43	13.95	12.67
$x_{ac_{\alpha_c}}$ $[m]$	0.70	0.68	0.70	0.66	0.70	0.63
$\frac{d\epsilon}{d\alpha_w}$ $[-]$	0.5	0.5	0.5	0.5	0.5	0.5
x_{cg} $[m]$	9.21	9.21	8.79	8.79	8.00	8.00
x_{np_α} $[m]$	10.40	12.12	12.57	11.78	13.88	11.48
SM_{α_w} $[-]$	0.0516	0.126	0.163	0.129	0.253	0.150
C_{M_α} $[-]$	-0.619	-2.167	-2.331	-2.245	-3.871	-3.36
$C_{L_{h/c_w}}$ $[-]$	-54	-52	-53	-51	-53	-50
$C_{L_{h/c_c}}$ $[-]$	-55	0	-67	0	-67	12
$C_{L_{h/c}}$ $[-]$	-54	-46	-65	-45	-55	-46
$\bar{x}_{ac_{h/c_w}}$	0.82	0.40	0.40	0.73	0.40	0.89
$\bar{x}_{ac_{h/c_c}}$	0.57	N/A	0.57	N/A	0.57	-1.60
$x_{np_{h/c}}$	17.60	11.25	9.91	17.85	9.91	21.82
$SM_{h/c}$ $[-]$	0.361	0.088	0.048	0.390	0.082	0.594
$C_{M_{h/c}}$ $[-]$	-19.48	-4.03	-3.13	-17.54	-4.52	-27.34
HS $[-]$	-432	-78	-84	-181	-73	-228

12.2.1. Vertical static stability

An aircraft possesses vertical static stability, also called height static stability, when a small perturbation in height would cause a change in lift coefficient that counteracts that perturbation. The longitudinal stability can be formalised by Equation 12.8

$$HS = \left.\frac{\partial C_L}{\partial (h/c)}\right|_{C_M=0} < 0 \tag{12.8}$$

After approximating a discrete change in the lift and in the pitching moment by Equation 12.9 and Equation 12.10 respectively, the two equation are combined to obtain Equation 12.11.

$$\Delta C_L = C_{L_\alpha} \Delta\alpha + C_{L_{h/c}} \Delta h/c \tag{12.9}$$

$$\Delta C_M = C_{M_\alpha} \Delta\alpha + C_{M_{h/c}} \Delta h/c \tag{12.10}$$

$$\Delta C_L = \left(C_{L_{h/c}} - C_{L_\alpha} \frac{C_{M_{h/c}}}{C_{L_\alpha}}\right) \Delta h/c + \frac{C_{L_\alpha}}{C_{M_\alpha}} \Delta C_M \tag{12.11}$$

Keeping in mind the condition that C_M remains zero, Equation 12.8 simplify to Equation 12.12:

$$HS = C_{L_{h/c}} - C_{L_\alpha} \frac{C_{m_{h/c}}}{C_{m_\alpha}} \tag{12.12}$$

In order to analyse the height stability of the AeroCity vehicle, the wing and the canard are considered as one aerodynamic body. The stability derivatives involved in Equation 12.12 are thus obtained by combining the stability derivatives of these two wing surfaces in the relevant flight and weight conditions. C_{L_α} and C_{M_α} have already been obtained in subsection 12.1.1 .

Equation 12.13 shows how $C_{L_{h/c}}$ has been obtained. $C_{L_{h/c}}$, like C_{L_α}, has been normalised with respect to the total surface area of $S = 180\ m^2$.

$$C_{L_{h/c}} = \frac{C_{L_{h_w}} \cdot S_w + C_{L_{h_c}} \cdot S_c}{S_w + S_c} \tag{12.13}$$

Equation 12.14 show how C_{M_h} has been obtained.

$$C_{M_h} = C_{L_{h/c}} \cdot SM_{h/c} \tag{12.14}$$

The stability margin for static height stability, $SM_{h/c}$, is defined in Equation 12.15 where, in accordance to what had been done for the static pith stability in subsection 12.1.1, $\bar{x}_{np_h}$ and $\bar{x}_{cg}$ have been normalised with respect to the total vehicle length of $c_v = 23.25\ m$.

$$SM_{h/c} = \bar{x}_{np_h} - \bar{x}_{cg} \tag{12.15}$$

Equation 12.16 show how $x_{np_{h/c}}$ has been obtained.

$$x_{np_{h/c}} = \frac{C_{L_{h/c_c}} \cdot S_c \cdot x_{ac_{h/c_c}} + C_{L_{h/c_w}} \cdot S_w \cdot x_{ac_{h/c_w}}}{C_{L_{h/c_c}} \cdot S_c + C_{L_{h/c_w}} \cdot S_w} \tag{12.16}$$

Equation 12.17 and Equation 12.18 show respectively how $x_{ac_{h/c_w}}$ and $x_{ac_{h/c_c}}$ have been obtained.

$$\bar{x}_{ac_{h/c_w}} = -\frac{C_{M_{h/c_w}}}{C_{L_{h/c_w}}} = -\frac{C_{L_w} \cdot \bar{x}_{cp_{h/c_w}}\big|_{\frac{h}{c}=0.0025} - C_{L_w} \cdot \bar{x}_{cp_{h/c_w}}\big|_{\frac{h}{c}=0.0015}}{C_{L_w}\big|_{\frac{h}{c}=0.0025} - C_{L_w}\big|_{\frac{h}{c}=0.0015}} \tag{12.17}$$

$$\bar{x}_{ac_{h/c_c}} = -\frac{C_{M_{h/c_c}}}{C_{L_{h/c_c}}} = -\frac{C_{L_c} \cdot \bar{x}_{cp_{h/c_c}}\big|_{\frac{h}{c}=0.0025} - C_{L_c} \cdot \bar{x}_{cp_{h/c_c}}\big|_{\frac{h}{c}=0.0015}}{C_{L_c}\big|_{\frac{h}{c}=0.0025} - C_{L_c}\big|_{\frac{h}{c}=0.0015}} \tag{12.18}$$

In Table 12.1 the HS is reported to be negative in the relevant extreme flight conditions. Therefore, in case of short disturbances in the sideskirts ground clearance (vehicle height from ground), the vehicle is passively stabilised, and it will automatically come back to the original equilibrium condition.

The analysis on the height stability reveals how the high pressure maintained under the vehicle's wing surfaces is dependent on the size of the ground clearance between the sideskirts and the ground. This effect is beneficial not only for vertical stability but for pitch static stability too. An increase in pitch angle would lead to a loss of lift in the forward part of the vehicle, while an increase in lift in the aft part of the vehicle.

Important to mention is that height stability cannot be achieved by shifting the centre of gravity longitudinal position. The last only affects the magnitude of the stability margin [17].

12.2.2. Vertical controllability

In the case of semi-permanent disturbances, for example during the $1.1g$ turns or during the acceleration/deceleration phase, the same control system used for pitch control is tasked with maintaining the desired distance from the ground. Moreover, a GPS system provides information on the vehicle location so that the main control computer can reduce the pitch/height controller response time.

12.3. S&C in Roll

The vehicle possesses static roll stability when a small perturbation in the bank angle generates a rolling moment that counteracts that perturbation.

The AeroCity vehicle static stability around the roll axis is directly connected to the height stability. When a disturbance around the roll axis is experienced, the vehicle tends to bank; one side of the wing, together with its respective sideskirt, gets closer to the ground, while the other one gets further away from it. Because of the principle explained in subsection 12.2.1, the side of the wing closer to the ground experiences an increase in lift, while the one further from the ground sees its lift decreased. The resulting lift distribution creates a correcting moment that brings the vehicle back to equilibrium. Therefore, in the case of short disturbances in the bank angle, the vehicle is passively stabilised, and it will automatically come back to the original equilibrium condition.

In case of semi-permanent disturbances (for example for a lateral shift in the centre of gravity due to changed payload disposition) the control system, composed of ultrasonic proximity sensors, accelerometers, a PID control unit and actuators, is tasked with restoring the desired bank angle (equal to 0° in nominal conditions). The accelerometers, the proximity sensors and the PID controller are combined as described in subsection 12.1.2 The actuators for the ailerons consists of two electromechanical motors per aileron placed at the aileron-engine duct connection. The actuator for the ballast consists of one electromechanical motor placed in the canard structure.

The two ailerons always deflected equally, therefore they generate the same amount of lift and drag. This means that when deflected, apart from the desired rolling moment, they introduce only a slight increase in the overall vehicle drag coefficient. The equilibrium and the stability around the yaw axis, the pitch axis and in the vertical direction is therefore not affected.

The ballast system, located in the canard, consists of a 200 kg that can move 3 m to the right and 3 m to the left of the vehicle symmetry plane. It is used to trim the vehicle during the flight phase to retain available for control the full range of the ailerons' deflection. Moreover, the ballast system can be used to correct the centre of gravity lateral position during the boarding phase.

In table Table 12.2, the maximum amount of rolling moment provided by the ailerons and the ballast in the relevant flight conditions is presented.

Table 12.2: Maximum rolling moment obtained by means of ailerons deflection. Standard sea-level atmospheric conditions are assumed.

	W = 360 kN		W = 300 kN		W = 240 kN	
	V = 55.5 m/s	V = 84.8 m/s	V = 55.5 m/s	V = 84.8 m/s	V = 55.5 m/s	V = 84.8 m/s
$M_{roll_{ail}}$ $[kN \cdot m]$	12.5	14.4	12.5	14.4	12.5	14.4
$M_{roll_{ball}}$ $[kN \cdot m]$	5.9					

The scales, located in the landing gear suspension, are used to indicate the payload weight distribution during boarding — more on that in section 17.6.

12.4. S&C in Yaw

The vehicle possesses static directional stability when a small perturbation in the sideslip angle generates a yawing moment that counteracts that perturbation.

The AeroCity track design requires the longitudinal axis of the vehicle and the one of the track to be continuously aligned. This means that in the presence of crosswinds, the vehicle needs to fly in sideslip. The sideskirts, the engine ducts and the engine pylons have been designed to offer to the crosswinds (or possible side gusts) an equal amount of exposed area (the track sides cover part of it) forward and aft of the centre of gravity location in order to reduce (or even completely remove) the induced yawing moment. The remaining yawing moment is then counteracted by means of differential thrust and with the assistance of the rudders. The rudders are especially crucial in case of complete loss of one of the two engines The centre of gravity location mentioned above is the one for maximum payload. When the payload is less than its maximum the centre of gravity moves forward (see Table 12.1) and consequently the yawing moment resulting from crosswind becomes larger. The engines will require to provide a higher amount of differential thrust; nevertheless, they don't need to be overpowered as in this low payload condition the drag is also lower.

In case of short disturbances on the yawing axis, the rudders will be the primary yaw control mechanism. For prolonged disturbances, the differential trust will be the preferred yaw control mechanism in order to retain available

for control the full range of the rudders deflection.

This form of yaw stability and control is evidently not passive. The artificial control system tasked with the control around the yaw axis, composed of ultrasonic proximity sensors, accelerometers, a PID control unit and actuators, is tasked in maintaining the desired sideslip angle. The accelerometers, the proximity sensors and the PID controller are combined as described in subsection 12.1.2, with the difference that the proximity sensors are located on the outer sides of the sideskirts, at a high corresponding to the flat vertical section of the track side walls. The actuators for the rudders consists of two electromechanical motors per rudder placed at the rudder-engine duct connection.

In table Table 12.2 the maximum amount of yawing moment generated by the rudders and by differential thrust in the relevant flight conditions is presented.

Table 12.3: Maximum yawing moment obtained by means of rudder deflection and by means of differential thrust. Standard sea-level atmospheric conditions are assumed.

	W = 360 kN		W = 300 kN		W = 240 kN	
	V = 55.5 m/s	V = 84.8 m/s	V = 55.5 m/s	V = 84.8 m/s	V = 55.5 m/s	V = 84.8 m/s
$M_{yaw_{rudder}}$ $[kN \cdot m]$	50.0	57.6	50.5	57.6	50.5	57.6
$M_{yaw_{thrust}}$ $[kN \cdot m]$	15.2	14.1	15.2	14.1	15.2	14.1

12.5. S&C in Lateral Direction

The vehicle possesses static lateral stability when a small perturbation in its lateral position generates lateral force that counteracts that perturbation.

The AeroCity vehicle static stability and control in lateral direction is provided by the track cross-sectional shape. The concept is similar to the one of the bobsled track. When the vehicle is pushed to the side of the track (for example in case of crosswinds), it encounters the curved edge of the track. Because of the principle explained in subsection 12.2.1, the vehicle will climb, but not touch, the curved slope until the horizontal component of the tilted lift vector becomes equal to the side force. In case of side gusts the same principle applies, but with the difference that in this case the process does not reach a prolonged equilibrium state: once the gust ends the vehicle comes back to its initial state. Worth noting is that while the vehicle is banked and the lift vector tilted, the vehicle requires a higher amount of lift; this will be obtained by increasing the wing and the canard angles of attack, as explained in subsection 12.2.2.

12.6. S&C in Longitudinal Direction

The vehicle is stable in longitudinal direction when an increase in longitudinal velocity is counteracted by a negative longitudinal acceleration. This naturally happens because an increase in velocity leads to an increase in drag, and if the engines' thrust did not change, the vehicle is slowed down to its equilibrium velocity condition. Control in the longitudinal direction is achieved by varying the engine thrust or the vehicle drag. The airspeed is obtained, like for aircraft, through pitot tubes, while the speed with respect to ground is obtained via GPS. High accuracy is not needed and once a reference speed is set a simple PID controller can maintain the set value sufficiently constant. Moreover, a LiDAR and RADAR systems are integrated in the control system to provide on-track object detection and therefore assist in the eventuality of emergency braking procedures. The LiDAR sensors can identify details of a few cm at more than 100 m and thus can, for example in case of people or animals, detect which direction they are facing and predict in which direction they are going to move. Nevertheless, LiDAR sensors are less reliable in snow, fog, rain or dusty air condition. The RADAR system works well in the above mentioned adverse weather conditions and has a greater sensing range than the LiDAR. Nevertheless it lacks accuracy and reliability when identifying the object type. By integrating in the control system both the RADAR and the LiDAR, their specialities are combined and their deficiencies are mitigated. The LiDAR sensors can be easily integrated in the forward section of the sideskirts. The RADAR system employs a phased array antenna which is embedded in the canard structure and therefore it does not interfere with the vehicle aerodynamics.

13 Traffic monitoring and control system

In order to assure a smooth operation of AeroCity, a traffic monitoring and control system is indispensable. This system should allow for control of the AeroCity network from a control facility, without the need of an on-board driver. The purpose of the monitoring system for AeroCity is twofold. Firstly, the traffic monitoring system shall keep track of the position and velocity of all vehicles and provide the necessary input to the control system. Furthermore, the monitoring system shall be able to detect debris on the track as well as evaluating the state of the track, such that maintenance can be done in time and the emergency procedure can be initiated when needed.

The system AeroCity will use for traffic monitoring will be a system similar to what modern train- and metro systems use, CBTC or Communications-based train control [60]. By means of the CBTC systems, the exact position of a train can be known more accurately than with conventional signalling systems, which contributes to the safety and reliability of the system. Another advantage of CBTC is the fact that location determination is independent of track circuits and thus easy to scale. This system comprising of sensors and communication links issues movement authority and control commands for each vehicle in the network. Due to limitations in demand for transport on the chosen route, the AeroCity will not operate with maximum frequency. Also, with a network consisting of only one route, Utrecht-Berlin, the monitoring system will be fairly simple. However, the accuracy as can be provided by a system such as CBTC becomes more and more necessary when the network is expanded, and the traffic density increases.

The monitoring system uses speed measurement and location determination sensors on board of the vehicle, sensors to check the state of the vital subsystems on board and sensors for debris detection and to check the state of the track along the route. These sensors will then communicate their data to a central computer, which processes the data. The computer will continuously output the actual vehicle position on the route, as well as the current state of the subsystems. This data can be read by the personnel responsible for controlling the fleet, who will then be able to dispatch vehicles and handle departure and arrival procedures in the stations, control the interchange points and act in the event of an emergency. Failure of the monitoring and control system of AeroCity should not have disastrous consequences, hence, a fail-safe mode will be incorporated in the system. The vehicle control system is equipped with a failure memory, which will activate the emergency brakes when a critical system fails. The system is also equipped with an over-speed control system, which will electronically limit the maximum speed of the AeroCity [61].

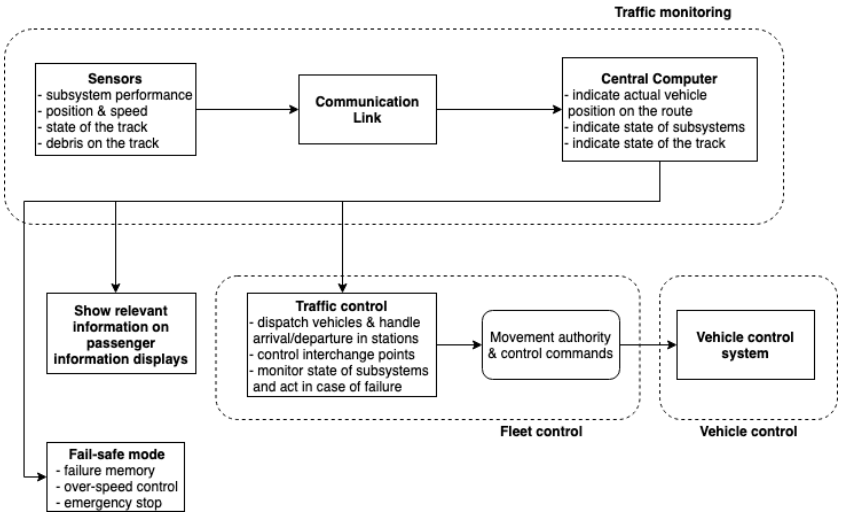

Figure 13.1: Traffic monitoring and control for AeroCity

The monitoring system of AeroCity will work closely together with the vehicle control system. The output information of the monitoring system is communicated to the vehicle control system, so that it knows what to do on a high level, such as when to accelerate or to decelerate. On a deeper level, the vehicle control system as described in chapter 12, will control all subsystems, such as the thrust level, the control surfaces for stability, the retraction and deployment of the landing gear, etc.

Finally, in order to add another aspect of safety, the stations and vehicles are equipped with cameras, emergency buttons and an intercom to communicate with the control room. This will give the station crew a better overview and allow them to intervene when necessary.

14 Passengers

14.1. Configuration and Layout

The main body is designed to carry 116 passengers. In figure 14.1 the layout of the main body is shown. The layout is based upon the layout of conventional aircraft and trains. There are 10 rows of 11 seats and a last row with 6 seats and 2 toilets.

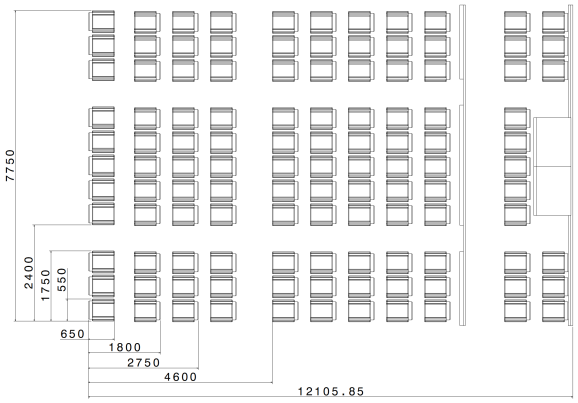

Figure 14.1: Seating plan of the main body with dimensions in mm

The seats are placed in a 3-5-3 configuration to comply with the CS-25 aircraft regulations. Rule CS 25.817 states that: 'no more than 3 seats abreast may be placed on each side of the aisle in one row' [62]. All aisles have a minimum width of the required 51 cm as stated by rule CS 25.815 [62]. Furthermore, the emergency exits present are 2 doors on each side of the vehicle of at least 61 cm width and 122 cm high, as can be seen in Figure 14.2. Furthermore in the front of the vehicle there will be a window of at least 51 cm by 91 cm that can function as emergency exits as well. This ensures that the AeroCity vehicle complies with the rules on emergency exists as stated by CS25.807 [62].

The chairs have the dimensions as shown in figure 14.3. The pocket underneath the chair is a piece of luggage of the maximum allowable size of carry-on luggage that passengers are allowed to carry on board of a plane. This is therefore also the amount of luggage passengers are allowed to carry on board of AeroCity. The dimensions of this luggage are 25x35x55 cm and can be stored underneath the seats. For this configuration of the vehicle there is no possibility to check in luggage. The toilets are sized in the same way as toilets of conventional aircraft.

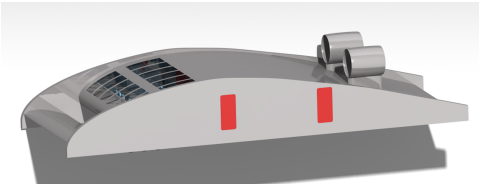

Figure 14.2: Placement of the doors

14.2. Passenger experience

When the passengers enter the vehicle they are free to pick a seat to their preference. The passengers can pick and choose from all seats that have a green light. Once seated, each passenger has the opportunity to put their carry-on luggage underneath the chair in front. In the seats, an USB outlet will be placed so all passengers are given the chance to charge their equipment during the journey. Next to this, a stable and free internet connection will be available to all passengers in the AeroCity vehicle and at the stations. The passengers area will be equipped with windows in the front and with lights in the floor as well as attached to the roof, to ensure it will not get too dark inside. The passengers compartment will be equipped with air conditioning as well, in order to keep the temperature at a comfortable level at all times. The passengers are free to walk during cruise and will be informed with light signals once the vehicle is in its take-off or landing phase. During these phases the passengers are asked to stay seated because shifts in the centre of gravity have a bigger influence during these phases. Also, the change in attitude of the vehicle may cause passengers to loose their balance and fall.

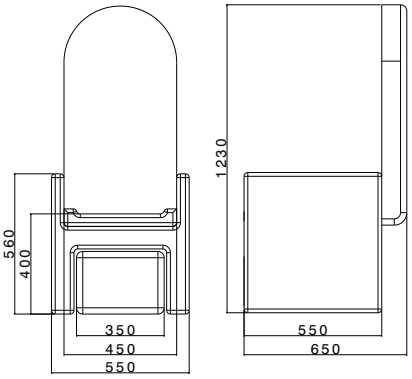

Figure 14.3: Chairs with dimensions in mm

15 System Interaction

15.1. Data handling

The data handling subsystem is the central computer in the AeroCity vehicle that is responsible for handling all data. The diagram in Figure 15.1 shows the command and data handling block diagram and how it communicates with the control facility. It shows the major components of the AeroCity computer system and how they interact with each other [63].

The main command and data handling (C&DH) components are connected in the box labelled as such. They are connected to all subsystems through the AeroCity data bus, which transfers data and instructions between the processor and the various subsystems. This, is then connected via the bus interface, which acts as a bridge between the systems and the computer, to the processor data bus. The processor data bus then transfers data between the other components. The CPU and co-processors perform all tasks and carry out instructions. The number of cores and the clock rate is dependent on the intensity and number of tasks to be performed. The CPU is equipped with a watchdog timer to detect faults in the CPU and subsequently forcing the system to reset. The memory consists of RAM (random access memory) and ROM (read-only memory), which are like short-term and long-term memory, respectively. The mass storage is a large scale read-only memory. In the on-board computer of the AeroCity, this will be in the form of an SSD. The SSD will store the general info and state of all subsystems for five days. It will also permanently store a failure memory, to be activated when data processing or another critical subsystem fails. The final component of the C&DH subsystem contains a number of I/O or input/output ports. These are used for communication between the bus and other devices. This C&DH module is connected to the subsystems; it handles the data for the subsystems and returns instructions. On the other hand, the subsystems and the C&DH module are in connection with the control facility through the communication link. Redundancy of this critical system is achieved by having an identical back-up computer that is able to perform the same tasks and can read the failure memory.

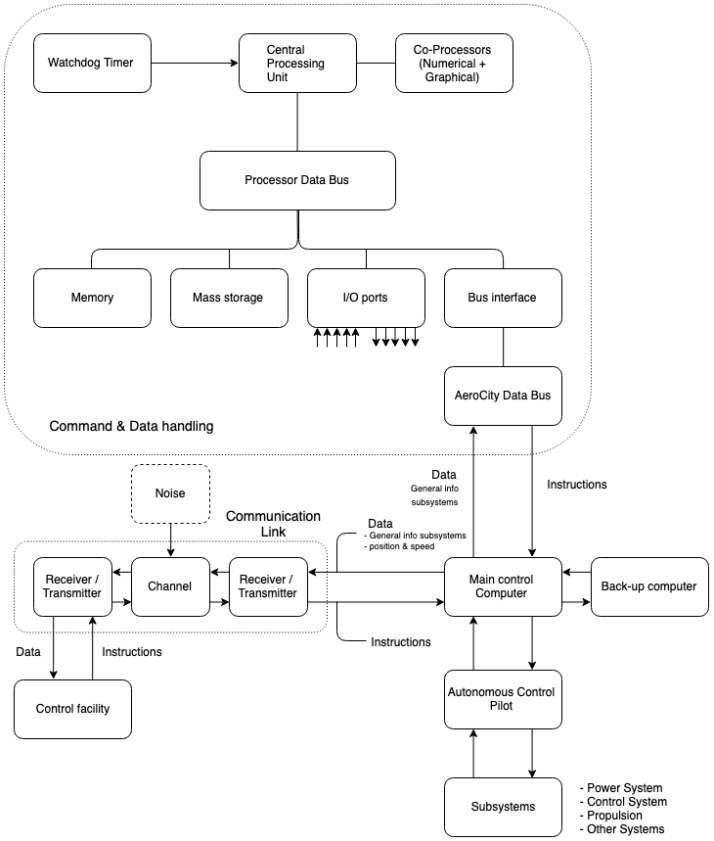

Figure 15.1: Data handling block diagram

15.2. Communication

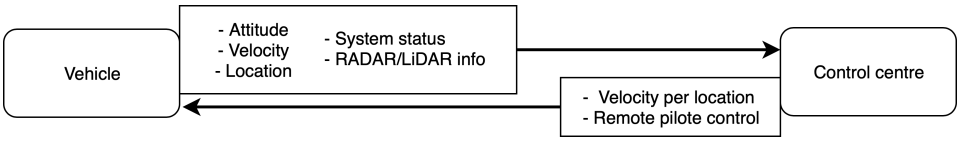

Figure 15.2: Interaction with control centre

The communication between the control centre and the vehicle is presented in Figure 15.2. The main input for the vehicle will be for an operational aspect, namely, the velocities for specified parts of the track and safety margins.

The vehicle will sent data of the system, attitude and location on a periodic basis. If the connection were to be lost for to long, the vehicle will start a deceleration. This is done, since the vehicle does not receive any recent information on the track and vehicles in front.

15.3. Total Weight division

The total weight of the vehicle consists of all the subsystems. For aerodynamic purposes, the location of the total centre of gravity must coincide with the resultant lift vector. This is discussed in subsection 12.1.3. For aforementioned reasons, during the design of the system as a whole, subsystems were limited in the positional options. For the payload, which includes passengers and their luggage, there is very limited space due to the configuration and layout, as shown in chapter 14. Therefore, the passenger c.g. location is set at 8.00 m, as shown in Table 15.1. Then, the c.g. location of the structure is determined by the structure layout and what materials are used for which section. The c.g. of the structure is very hard to change in order to have the c.g. location at 5.95m. Therefore, the structure c.g. will be at 7.32 m and does not change. Next, the batteries for the provision of the required power have to be placed at the front of the vehicle, since this is the only place where the batteries fit. The c.g. location of the batteries is therefore determined to be at 1.46 m from the leading edge.

Table 15.1: Weight division

	Mass $[kg]$	**C.G. location** $[m]$
Payload	11,600	8.00
Comfort	3,070	9.63
Power	12,770	1.46
Propulsion	1,340	15.73
Ground operation	320	6.15
Control	900	5.44
Electronics	300	11.33
Structure	5,700	7.32
Total	36,000	5.95

After the batteries, the landing gear system was designed according to the c.g. location for aerodynamic purposes, including a shift in c.g. The c.g. location for the landing gear that followed accordingly was at 6.15 m from the leading edge. Now that the subsystem c.g. locations were determined which could not really be changed due to the limitations, the rest of subsystem c.g. locations could be determined. For the comfort, which includes WiFi, air-conditioning, etc. The c.g. location was set as 9.63m from the leading edge. For the control, the c.g. location was set as 5.44 m from the leading edge. Then, for the electronics, the c.g. location was determined to be 11.33 m. At last, the propulsion system could be integrated, where it was decided to put the propellers at the rear of the vehicle, for aerodynamic reasons as well as c.g. reasons, since the c.g. had to be shifted a bit more to the back. Therefore, the c.g. location of the propulsion was set at 15.73 m from the leading edge. When all subsystems were integrated to the design of the vehicle as a whole, the total c.g. location came down to be at 5.95, which is what was needed for aerodynamic purposes.

15.4. Actuators

All moving surfaces will use actuators to move to a new state. In later design, the actuator systems will be defined in more detail per subsystem. To be as energy efficient as possible, all systems will be designed such that they only require power when a change in location is desired. The system must be electromechanically driven. Several systems can be designed to meet this requirements. A spindle, would be a suitable solution as the forces can be carried by the connection of the thread. The motor is just used to rotate the thread if desired.

15.4.1. Main wing movement

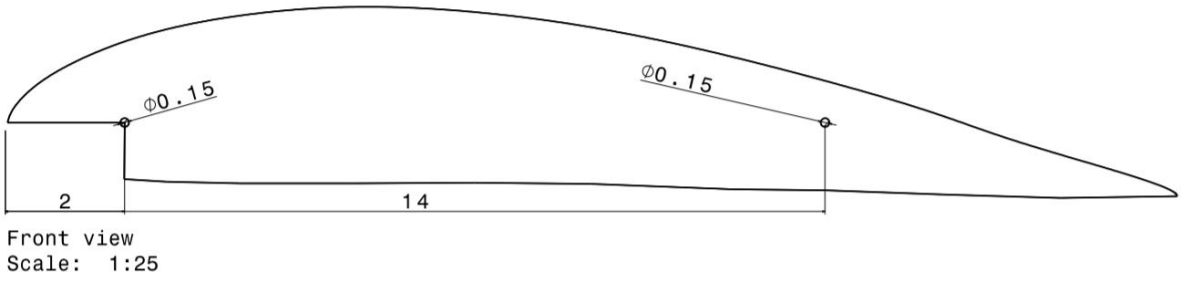

Figure 15.3: Main wing attachments

The main wing has to change its angle of attack which is a function of its velocity. At the same moment, for aerodynamic reasons, the ground clearance of the side skirts and canard should stay constant. This is accomplished by moving the main wing with respect to the the side skirts. Aerodynamics require the wing to move around 0.5 x/c and thus around 10 m from the leading edge of the main wing. The structure has 2 main vertical bulkheads

Table 15.2: Mass allocation on lateral position

Subsystem	**Part**	**Mass** $[kg]$	x_{cg} **from LE**$_{wing}$
Payload	Passengers	11,600	8
Comfort	Climate control	300	16
	Toilets	100	18
	Sanitary water tank	50	16
	Water	150	16
	Seats	2,470	8
Power system	Auxilairy	50	18
	Swappable structure	1,400	1
	Main wing battery	8,520	1
	DC converter	1,500	2
	Cooling (radiator/pumps)	1,000	3
	Cables	300	6.25
Propulsion (2 fans)	Inverter	220	14.5
	Cooling + circuit	20	14.5
	Cables	40	16
	Motor (/coils)	560	16
	Propeller	100	16
	Nacelle	400	16
Landing gear	Wheels	200	1.8; 2.7; 3.6; 16.5
	Motors	120	1.8; 2.7; 3.6; 16.5
Control	Canard actuator	200	-2
	Main wing actuator	300	8
	Ballast	200	-2.5
	Ailerons & Rudders	150	17
	Spoiler	50	17
Electronics	Telometry	100	6
	Computers	100	18
	Cables	100	10
Structure	Main wing	3,200	9
	Side skirts	1,300	9.5
	Canard + front skirts	1,000	-1
	Doors	200	8
Total system		36,000	5.95

through the main wing, at 2 and 14 m. These bulkheads are optimal to transfer the loads into the wing. Therefore the actuators will be placed at these locations. The wing structure will be attached to actuators in the side skirts. The electromechanical actuators will be a fail safe system that move the wing around an non physical pivoting point.

The wing has to rotate from 5 degrees during take-off, to 3 degrees in cruise conditions. The front system therefore has to move 28 cm, whereas the rear system has to move 14 cm. The actuators have to be able to withstand primarily vertical loads of the main wing and the introduced forces.

IV

Performance Analysis

Once the detailed design of both the infrastructure and the vehicle has been completed it is then important to see how the operation will perform. Initially a performance analysis is done to look into a general profile of the operation of the vehicle. Once this is done it is then necessary to look into the operations, to see what the initial operation of AeroCity will look like. With the operations done then the costs can be looked into, seeing how much the investment costs will be, and then seeing how much can be made with a yearly operation. After this the sustainability will be looked into, to ensure that AeroCity will provide a sustainable way of transport for the future. Once these items have been looked into, verification & validation is done to ensure the detailed design was done correctly, risk is looked into to see what can go wrong and how these items can be mitigated, a sensitivity analysis is done to see just how small deviations in the detailed design can affect the overall designs. Once all of this has been done, a production plan is completed, the initial requirements are looked into again to see how well the detailed design performed based on the initial needs. As soon as all of this is completed, a project design and development logic, as well as the project Gantt chart are done to give better guidance for future operations.

16 Performance analysis

The performance of the vehicle is a result of all the subsystems working together. The most important assumptions are discussed in this chapter. Other more detailed operational or subsystem aspect are discussed in previous chapters.

16.1. Calculation Assumptions

For calculations on the vehicle performance a python script was run with specified inputs. In Table 16.1 the most important values are presented. These mainly originate from Chapters 7 and 9. A very important assumption is that all efficiencies are constant during the full operation. The two most effected systems are the electric propulsion systems and aerobreathing fans, as they are a function of the speed and thrust. The given values are the design efficiencies for cruise condition. The calculations are done for a straight track without corners. Therefore, the outcomes for power used and energy required will be slightly optimistic with respect to true operation.

Table 16.1: Assumptions Performance Calculations

Assumptions	Symbol	Value	Unit
Mass	m	$36 \cdot 10^3$	kg
Vehicle Speed	$V_{take-off}$	200	km/h
	V_{cruise}	305	km/h
Total Lift Coefficient	$C_{L_{cruise}}$	0.499	-
	$C_{L_{TO\&landing}}$	1.17	-
Total drag Coefficient	$C_{D_{cruise}}$	0.015	-
	$C_{D_{TO\&landing}}$	0.0196	-
Efficiencies *(constant)*	$\eta_{batteries}$	98	%
	$\eta_{DC-switches}$	98.5*98.5	%
	$\eta_{cablelosses}$	99	%
	$\eta_{motor+MC}$	93*98.9	%
	η_{fans}	80	%
Power	$P_{max_{kinetic}}$	1.968	MW
avg.	$P_{subsystems}$	10	kW
netto avg.	$P_{deceleration}$	0.73	MW

16.2. Acceleration phase

Acceleration is limited to $0.1g$ to ensure comfort for the passengers. The rest of the phase is mainly dependent on the maximum power output of fans and wheels. This power is sufficient to ensure maximum acceleration until 46 m/s and slower acceleration at higher velocities. Although the wheels can only contribute when they have sufficient traction with the ground. In Figure 16.1 the acceleration power, forces and accelerations are presented with respect to the velocity.

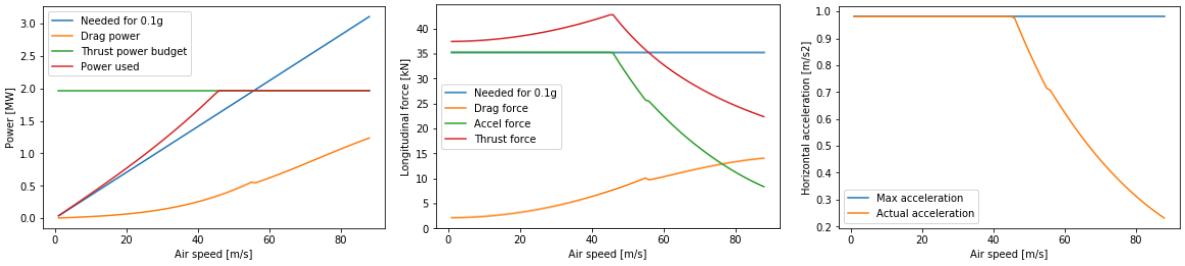

(a) Power (b) Forces (c) Acceleration

Figure 16.1: Acceleration phase

16.3. Cruise

During cruise, the vehicle's thrust must be equal to its drag. This equals to 13,830 N of thrust force at the design cruise velocity of 84.8 m/s. This results in a nominal kinetic propulsive power of 1.18 MW. The vehicle is considered to be in constant equilibrium for calculation purposes. This means that head wind, corners, control induced drag, etc. are not considered.

16.4. Deceleration phase

The deceleration phase is divided in an airborne and ground phase. During the airborne phase, the vehicle will increase its ground clearance in order to increase the drag. This height will slowly decrease when approaching the landing velocity of 55.5 m/s. After touchdown, all braking systems can be deployed. A combination of aerodynamic; regenerative wheel braking; wheel disk braking; and reverse thrust will produce a combined breaking force to brake with $0.1g$. The power as presented in Figure 16.2a is the kinetic power required to brake. This manoeuvres are described in more detail in chapter 11.

16.5. Full route

For the full route, four options are to be considered, direct; stop in Duisburg; stop in Hanover; make two stops. The total track distance is 651 km. The energy consumption and operational time are slightly increased if an extra

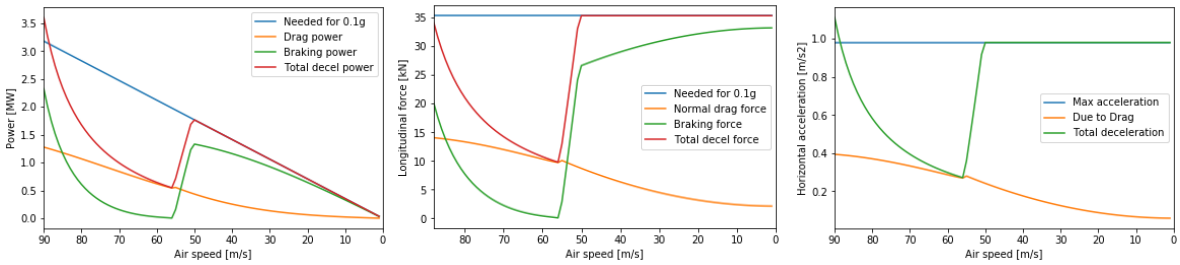

(a) Power (b) Forces (c) Deceleration

Figure 16.2: Deceleration / Braking phase

stop is made. The main extra time comes from (un)loading the passengers. The vehicle will stop for approximately 5 $minutes$ per station to unload and load the passengers. The energy consumption and added time are not considered in this calculation. A short charging boost at stations would counteract these consumption increases.

Table 16.2: Operational results (excluding (un)boarding time)

Phase		**Distance** $[m]$	**Time** $[h]$	$\mathbf{E}_{consumption}[kWh]$
Acceleration	Ground	1,691	0:00:57	81.4
	Air	4,912	0:01:07	
	Total	6,604	0:02:05	
Deceleration	Air	5,145	0:01:15	28.8
	Ground	1,646	0:00:57	
	Total	6,791	0:02:13	
Utrecht - Berlin (direct)		$651k$	2:9:36	3,672
One stop		$651k$	2:11:16 (+~5:00)	3,680
Two stops		$651k$	2:12:56 (+~10:00)	3,688

17 Operations

This chapter discusses the operations of the AeroCity system. First of all, a general timetable is outlined in section 17.1. Following this, all aspects needed for successfully operating AeroCity are covered. These include reliability, maintenance, safety, ground support, nominal operations, emergency situations and personnel required for operating AeroCity. Maintenance, which is divided into preventive and corrective maintenance, is covered in section 17.3. This is a crucial part of operations and should be done with care and on a regular basis. After this, section 17.4 discusses the safety of the operation of the vehicle as this is a very important factor to gain support for AeroCity. Then, the ground support operations are discussed in section 17.5. These entail all operations supporting the AeroCity from the ground. In section 17.6, the nominal operations of AeroCity are described and the swapping procedure of the battery will be treated in section 17.7. Then, section 17.8 discusses the operations and procedures during emergency situations.

17.1. Timetable and Frequency

As dictated by the user requirements, the total travel time between Utrecht and Berlin cannot exceed 2:15 h. In order to meet this requirement while still maintaining the advantage of the extra passengers provided by the Duisburg and Hannover stop, it is decided to have two different travel options on this route. Firstly, there is the direct option from Utrecht to Berlin in less than 2:15 h, without stopping. On the same track, there will also be a vehicle that travels along the same route, but this time stopping in Duisburg and Hannover. For this travel option, the total time between Utrecht and Berlin is slightly less than two and a half hours.

There are two factors that influence the frequency of vehicles following one another: the minimum headway needed for a vehicle to come to a standstill without hitting the preceding vehicle after it has suddenly stopped, and the number of daily passengers to be transported on this route. The former sets a constraint on the maximum vehicle frequency, while the latter is an indicator of the necessary frequency. The number of daily passengers, followed from the market analysis done in chapter 3, is shown to be approximately 2 million passengers per year. The maximum possible frequency has previously been calculated [8], but the numbers have been changed slightly since then. The maximum speed was decreased in order to increase the overall efficiency. With the updated values and using Equation 17.1, the minimum headway time was calculated to be 167 s and the maximum theoretical capacity of this route is 21 vehicles per hour.

$$T_{\text{min}} = T_{\text{reaction}} + \frac{v}{2a_b} + \frac{l_{\text{vehicle}}}{v} \text{[s]} \tag{17.1}$$

With an estimation of 5480 daily customers and a vehicle capacity of 116 passengers, the number of rides per day to accommodate all these people is 48. This includes both the rides from Utrecht to Berlin and from Berlin to Utrecht.

AeroCity's operating hours are between 5AM and 10PM. As Aerocity operates on a route where there is no high-speed and low travel time transport currently, no information on peak and off-peak hours are known yet. Thus, the design of the timetable will be a continuous process, as is done in the railway sector as well. In the beginning, vehicles shall be deployed at equal intervals of 42.5 min. Direct vehicles will alternate with non-direct vehicles, which stop in Duisburg and Hannover as well. This way, all demand can theoretically be fulfilled. However, there will most likely be times at which while one vehicle is full, whereas another one is almost empty. During this phase, but also continuously during the lifetime of AeroCity, the occupation rate of all vehicles shall be monitored and the timetable shall be adjusted accordingly. It is expected that after a certain period, peak and off-peak hours will form due to a shift from transportation for travel reasons to an increased amount of business-related travel on this route. One of the reasons for this phenomenon to occur is likely to be the drastic decrease in travel time between the large cities along this route.

17.2. Reliability

As with any transportation system the reliability of the system is key to its success. A distinction can be made between the reliability of the infrastructure and the reliability of the vehicle itself. Firstly the reliability of the infrastructure will be discussed in subsection 17.2.1 after which the reliability of the vehicle will be treated in subsection 17.2.2.

17.2.1. Reliability of the Infrastructure

As can be seen in other modes of transportation, the reliability of the infrastructure is rather important. For trains, the most obvious points where the infrastructure has to be very reliable are roadway crossings and switching points

between tracks. If these are not functional it can have disastrous results such as accidents or severe delays. For cars, the same can be said for traffic lights and road quality and for aircraft the logistics, ground communication and ground operations are also key to a successful operation.

As part of the design philosophy of the AeroCity concept is to have a cheap and simple track, most of the infrastructure reliability does not immediately translate to the track itself but more to the supporting operations near the stations and the communication between a control centre and the vehicle.

A first example would be the battery swapping and charging infrastructure. These have to be sufficiently reliable to always have at least one working battery swapping station and to provide sufficient charged batteries such that vehicle can depart. A way to guarantee this level of reliability is to again make the subsystem as simple as possible such that there are minimal points of possible failure. Furthermore, some redundancy has to be taken into account by having multiple swapping stations and a sufficiently large amount of stored batteries.

Secondly, as the vehicle is meant to be completely autonomous but also has to be able to be controlled via a control centre, communication between the vehicle and the control centre is key. A way to make this system reliable enough, from an infrastructure point of view, is to simply provide a sufficient amount of access points or antennas nearby the track such that even when one access point is not functioning, another one is nearby enough to function properly.

Lastly, as mentioned before, the track is meant to be as simple as possible. However, it should be able to withstand standard environmental impacts such as bad weather conditions, small deviations in ground level over time and hot conditions. Moreover, close to stations the track should be designed such that it can handle the pressure when the vehicle is still supported on its wheels. These points can be guaranteed by adequate civil works and possibly a slight overdesign of the track at critical points.

17.2.2. Reliability of the Vehicle

Apart from the reliability of the infrastructure, the reliability of the vehicle is at least as important. Within the vehicle, the most critical points of which the reliability is especially important are the power, the propulsion, the control and the structure subsystems. Each of these will be treated below.

Firstly, the power subsystem should be reliable enough to last a certain amount of charge-discharge cycles, to be easily swappable and to provide a continuous power throughout the operation. Additionally, the possible battery lifetime is guaranteed to be as high as possible by having an adequate battery balancing system and a low charge rate. The low charge rate is feasible as there are meant to be more batteries than vehicles such that the battery is used at a lower frequency than the vehicle. A way of guaranteeing that a sufficient and a continuous amount of power can be drawn from the batteries is by slightly over designing the battery capacity and making the subsystem as modular as possible. This is done to make sure that even when one element fails the other components can still provide enough power.

As for the propulsion subsystem, the reliability of the electric motors and motor controllers is guaranteed by having a very redundant system. As described in chapter 8, each motor unit - the motor driving one fan - exists of 4 smaller electric motors which are each controlled by two different motor controllers. If one element fails the others would still be able to compensate by operating slightly above the nominal performance. Similarly, the reliability of the control subsystem is guaranteed by redundancy. For this subsystem, this translates to having a redundant amount of sensors, computing nodes and secondary actuators.

Lastly, the reliability of the structure is guaranteed by taking enough safety factors into consideration, adding redundant elements and regular inspection to check for damage to the structure from either fatigue loads or external factors.

17.3. Maintenance

Both preventive and corrective maintenance shall be done for the track, the vehicle and the station. Preventive maintenance shall be scheduled on a regular basis and is performed in order to minimise the chance of system failures and the costs for corrective maintenance. Preventive maintenance includes daily high-level checks, but also more detailed inspections of subsystems and track on a regular basis. These inspections shall be described later on, when the design of the subsystem has been finalised and when AeroCity is ready for certification.

Corrective maintenance is done whenever necessary and includes daily operations such as cleaning, but also less frequent maintenance actions such as reparations or switching of degraded battery cells. Indicators are placed on subsystems in order to alert operators whenever a discrepancy is noticed and maintenance is required. Some corrective maintenance can be scheduled without resulting in unexpected delays. However, the need for corrective

actions could also be beyond the control of the operators and thus potentially result in delays or certain vehicles being inoperative for a given time period.

All subsystems and their integration are optimised for maintainability: the systems are integrated in such a way that they are easily accessible for mechanics and technicians.

Finally, the time available for maintenance also has to be taken into consideration. As AeroCity will only be operating between 5AM and 10PM there is plenty of time for small maintenance overnight. For larger maintenance, a vehicle would need to be taken out of operation for an extended amount of time. To not affect the general operation of the entire fleet, an extra vehicle can be then be operated as a temporal replacement or if needed the travel frequency could be reduced temporarily.

17.4. Safety

Passenger safety should be considered at all points throughout the design and operation of the AeroCity concept. This section will treat how this has been implemented in the design, special scenarios such as an emergency situation will be treated separately in a later section.

Starting on the front of the vehicle the first element is the canard. As in case of an impact, this would be the first point of impact extra redundancy has been taken into account in the design of the structural support of this element as explained in chapter 10. Secondly, in case of debris on the track, the canard could also function as a shielding, effectively protecting the front of the main body from possible impact.

The battery pack can be found in the front part of the main body since this part is meant to be a very safe part of the vehicle. Firstly, because it is such an important and possibly hazardous element, the surrounding structure and skin would be overdesigned such that this possible risk is mitigated. Secondly, the battery system is divided over a total of 100 different battery modules, each of which are separately enclosed in an oil-tight self-supporting structure. Thirdly, it is also one of the most maintained parts of the entire vehicle as it is replaced after every ride and can thus easily be inspected, maintained and if needed repaired or even completely replaced. Finally, as the entire weight of the battery package is carried by the surrounding structure in the main body, passenger safety is also guaranteed by this surrounding structure.

The motors can be found even further to the back of the vehicle. Their placement was mainly determined such that the influence on the aerodynamics of the body is as minimal as possible. It has, however, an added benefit that they are aft of the passenger cabin and are surrounded by the duct such that the chance of cabin intrusion of fan blades or bird strikes is minimised. Additionally, the location of the engines, above and aft with respect to the main body shields the fan blades from debris ingestion.

17.5. Ground Support

Ground support entails all actions supporting the normal operations of AeroCity. This includes swapping and recharging the batteries, operating the station, pre-flight checks and storage of the vehicles.

These are important aspects to consider during the design, as they are serious drivers for the operating costs. The possibility of swapping the batteries should be considered in station design and vehicle layout from the beginning of the design phase. This is included in the design of the power system by having modular batteries, where the different modules can be taken apart easily. The stations or storage facilities should be equipped with the necessary means to recharge the batteries and storage facilities should be able to accommodate the proper number of vehicles. Lastly, a manual for pre-flight inspection shall be put together for the technicians to use.

17.6. Nominal Operations

The nominal operations of AeroCity consist of a series of phases that need to be gone through, as well as some general operations to be performed in parallel such as traffic monitoring and control. The operational phases to be covered are:

- **Station access and security procedure**
  The daily operation of AeroCity starts with the opening of the stations. Customers can buy tickets in advance online or at the station, as long as supply lasts. The tickets are then used to open gates to the platforms, similar to the system used by NS. As AeroCity is a new concept, new regulations for security will be developed. These cannot be predicted yet, but will probably be similar to those for HSR, hence allowing for quick boarding as opposed to aircraft.
- **Boarding**
  As dictated by requirement $USR-PC-03$ in chapter 5, the boarding time shall be lower than 5 minutes. The

vehicle is equipped with two doors on each side, four in total, which can all be used for entering and exiting the vehicle. In order to ensure lateral control, not all passenger configurations are possible: for example, if the vehicle is filled with only 50 passengers and they would all sit on the right side, lateral control could not be achieved. For full payload, the maximum allowed lateral deviation of the c.g. position with respect to the symmetry line is 1.66 cm. Therefore, a system that measures the weight distribution through scales in the landing gear will tell the passengers where they can sit by means of indication lights on the seats. This system is also used to make sure that the longitudinal c.g. position is in the correct range.

- **Taxi**
  This is the phase where the vehicle enters and leaves the station, but also where the vehicle is transported to and from the storage facility. During this phase, the vehicle is propelled by the wheels at a maximum speed of 5 m/s and some systems may be inactive.
- **Flight phase: Takeoff-Cruise-Landing**
  The flight phase starts with takeoff, followed by a cruise phase at cruise speed, and finally landing before taxiing to the destination station. During flight, the vehicle is completely controlled from a distance, and no personnel is required inside the vehicle. The system used for control during this phase is described in chapter 12.
- **Storage**
  When the vehicles are inactive, during the night or while inoperable due to maintenance, they are stored in a hangar. Hangars are located near the stations in Utrecht and Berlin and will also be equipped with the necessary tools for maintenance and reparations.

Other operations in the category of nominal operations are traffic monitoring and control, the control of the vehicle, continuous evaluation of the timetable, ticket sales, operating the stations, etc. The first two are discussed in chapter 13 and chapter 12. 'Continuous evaluation of the timetable' means that delays must be kept track of and that the frequency of the vehicles should be adapted according to the demand at all times so that all vehicles are used in the most optimal way. There are more aspects to nominal operations such as ticket sales. However, it is chosen to not go too much in depth as this is beyond the technical scope of designing the AeroCity system and network.

17.7. Battery Swapping

One of the main aspects in which AeroCity aims to be competitive with other modes of transportation is by having a lower infrastructure cost, lower energy consumption and a future-proof sustainable design. This is partly achieved by having an on board battery package to provide the energy required for all on board systems. Because a battery package is being used, no on board emissions are generated, the track does not need to be electrified and less losses occur as less cabling is required. However, batteries do need to be charged and in order to maintain the battery health a slow charging process is preferred. As the charging procedure will likely take a longer period of time than the operating interval of the one vehicle, there are two options. The first option is have an excess of vehicles such that each individual vehicle remains at the station for a longer period of time. This has the benefit that the battery can be completely integrated in the design but has the downside that many extra vehicles are needed which will lead to a higher cost. The second option is to have a swappable battery package, this has the advantage that less vehicles are needed and only a redundant amount of battery packages which would be cheaper. However, the disadvantage is that the system needs to be swappable. One additional benefit of a swappable battery is the maintenance. As it is swapped after every trip it can also be easily maintained and inspected if needed.This is especially relevant for a battery system as degradation can also be measured easily. It is therefore chosen to use a swappable battery system.

As discussed previously in chapter 9, the batteries will be placed in front part of the main wing. A visualisation of this is presented in Figure 17.3. The battery swapping procedure is composed of three main parts: firstly there is the battery package itself which is shown in Figure 17.1, secondly, there is the cart that supports the battery which is shown in Figure 17.2a and lastly there is the hydraulic lift as shown in Figure 17.3.

As can be seen inFigure 17.1a and 17.1b, the battery package is shaped such that it can fit on the lower side of the main wing. 8 contact plates (4 positive and 4 negative) are placed on the top of the battery package such that contact can be made with the main body through spring loaded contact plates. The plates are divided over 4 different circuits to guarantee a form of redundancy. The battery package is kept in place by several metal rods that are inserted from the main body in the holes on the side of the battery package. Furthermore, the battery can be supported and kept in place on the cart by a similar system of pins on the cart that fit into the holes on the bottom of the package as can be seen in Figure 17.1b.

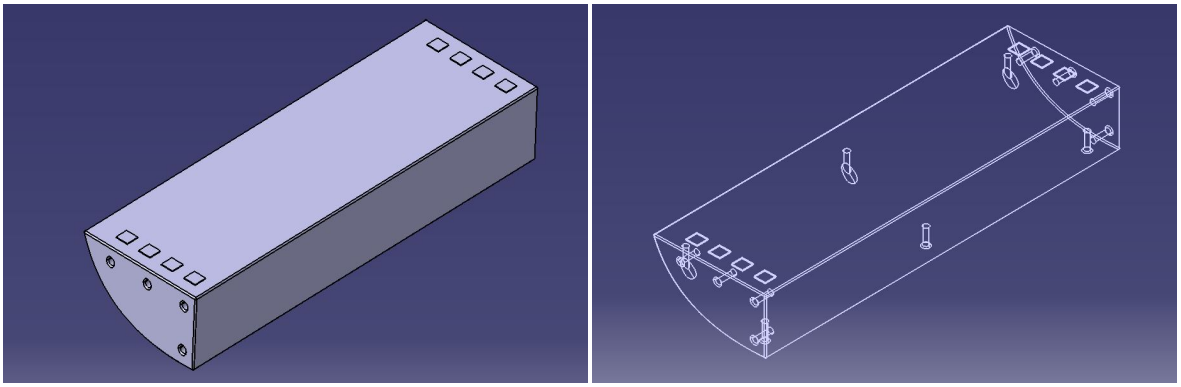

(a) A render of the battery package (b) A wire frame view of the battery package

Figure 17.1: A visualisation of the total battery package

Secondly, the battery cart can be seen in Figure 17.2a. This is designed such that it perfectly fits together with the battery package. The metal pins are positioned as such that they can keep the battery package fixed on the cart. Furthermore it has wheels such that it can transport the battery autonomously to the charging station. A complete assembly of the battery package and the cart can be seen in Figure 17.2b.

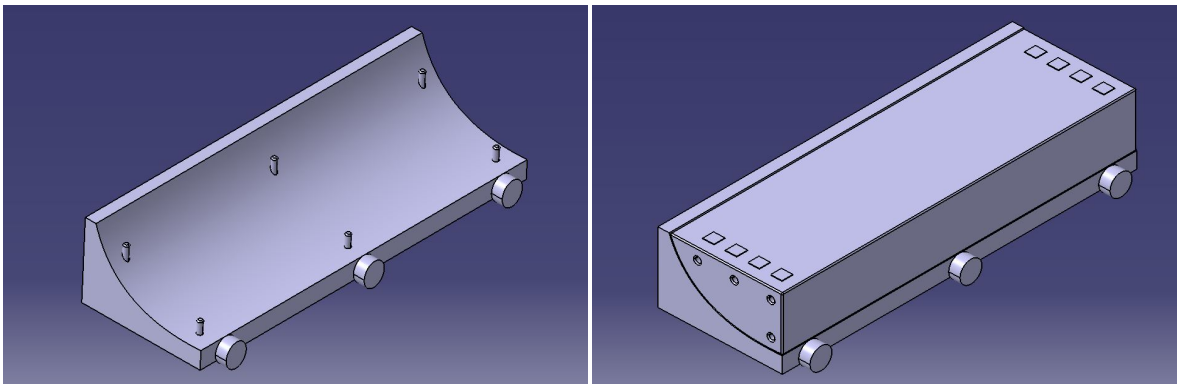

(a) A visualisation of the battery cart. (b) A visualisation of the battery cart and package.

Figure 17.2: A visualisation of the battery cart with and without the package.

Finally the procedure of how the battery would be swapped can be seen in Figure 17.3. During arrival the vehicle arrives with a depleted (yellow) battery, this can be seen on the top of the figure. After the passengers step out of the vehicle it first proceeds to the first swapping station and positions itself above the hydraulic lift with the cart. Secondly, the hydraulic lift with the cart rises, makes contact with the battery and supports it. Thirdly, not shown in this figure, the main body releases the metal rods that support the battery package and it is released. After this, the hydraulic lift moves down again together with the cart and the battery package to move out of the way of the vehicle. Next, the AeroCity vehicle moves forward via a conveyor band integrated in the swapping station and the hydraulic lift rises again such that the cart is raised up to the ground level such that the chart can autonomously drive of towards the charging station. After a battery has been charged, it moves back to a second swapping station, drives onto the hydraulic lift, moves down and is ready to be mounted underneath a departing vehicle. Again, an empty vehicle is positioned above the hydraulic lift, the lift rises, the battery package connects to the vehicle and the metal rods are inserted, the lift lowers again and the vehicle is ready to move to the passenger platform to prepare for departure.

The decision has been made to perform the battery swapping only at the end stations, Utrecht and Berlin, after the arriving passengers and before the departing passengers get in. In doing so, the battery swapping procedure does not happen during the travel time, allowing for a less rushed procedure. Moreover, either the vehicle or the hydraulic lift could be moved, but as the vehicle has to be turned around anyway this could be integrated with the conveyor belt system.

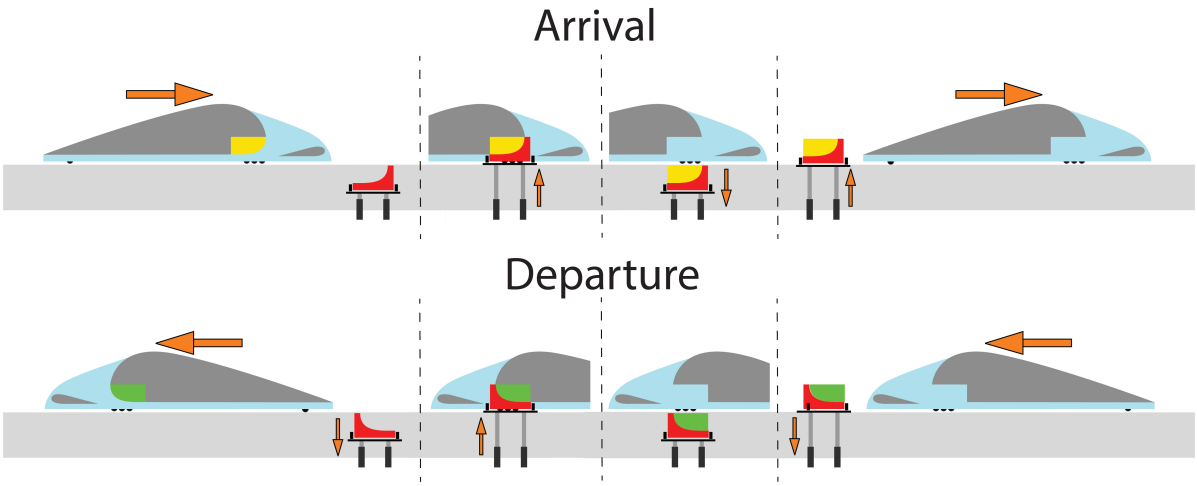

Figure 17.3: A visualisation of the battery swapping procedure

As for the actual charging station and infrastructure, this has not been worked out in detail as it falls outside of the scope of this project. It is however envisioned that a large reserve of battery packages would be present such that the batteries have sufficient time to charge at a safe rate. Furthermore, having an excess of battery packages also leads to a higher flexibility and possibly a secondary income stream. Firstly, they could be charged when the electricity prices would be very low and secondly it could potentially be used to stabilise the grid during hours of peak generation from wind or solar and to provide power back to the grid when needed.

17.8. Emergency

Passenger safety should be taken into account at all times, so in the event of an emergency, there must be a proper plan to ensure the passengers' safety. What exactly needs to be done depends on the severity of the problem, but the two main actions to be taken are an immediate standstill of the vehicle and a fast evacuation of all passengers.

As there is no driver inside the AeroCity, the vehicle has to rely on the sensors and control system inside the vehicle and the remote pilot to react quickly when a system failure is noted. When the central computer fails, the vehicle is brought to a standstill immediately by the failure memory in the back-up computer. After the vehicle is stopped, the passengers need to be evacuated if necessary and a rescue team is dispatched to the location of the vehicle. In case the compromised vehicle can cause a danger for other operating vehicles, these need to be warned and possibly delayed.

In an emergency scenario, the second priority, when all passengers are in safety, should be to resume operations as quickly as possible. A defect vehicle should be removed from the track as soon as possible in case it cannot complete its journey. In that case, the goal is to minimise the delay of other vehicles.

18 Cost

An aspect that is consistently most important to stakeholders, is cost. Costs determine whether or not a project can be successful, both in the development phase as well as in the operational phase. In this section, the development phase and the operational phase costs will be elaborated on. In the development phase, primarily the vehicle and the infrastructure costs will be explained and will be quantified. Following this, the operational exploitation costs will be discussed followed by the ticket cost for the consumer and the yearly operational balance will be quantified.

18.1. Vehicle Cost

To calculate the vehicle cost, a parametric method, developed by Jacob Markish [64], is used. For the AeroCity program, there are two primary cost categories: development cost and manufacturing cost. The former is mostly non-recurring, while the latter is mostly recurring.

The development cost is the non-recurring effort required to bring the AeroCity concept to production. It includes the preliminary design, detailed design, tooling, testing and certification. The non-recurring effort is broken into several processes (engineering, tool design, etc) for each part for AeroCity. These processes are characterised in terms of relative time and cost based on non-dimensional industry data for typical commercial aircraft. For simplicity, both the development model and the manufacturing model assumes that cost scales directly with the Operating Empty Weight (OEW), commonality effects notwithstanding. Given the scope of this research, it is a reasonable simplification. [64]

The method from Markish [64] assumes a direct relationship between weight and cost. Although, a minimum-weight design does not necessarily equal a minimum-cost design. However, within the scope of the project, this method gives a good first-order estimate for the cost. This method uses historical data that was collected on weight characteristics and cost fractions from a set of existing aircraft [29] [49], these aircraft are: MD-80, DC-10-30, 737-200, 747-100, and A300-B2. As stated earlier, the nature of manufacturing cost is recurring. This means that the cost is incurred repeatedly for each unit. Therefore it is subjected to a learning curve effect. This can be visualised in Figure 18.1.

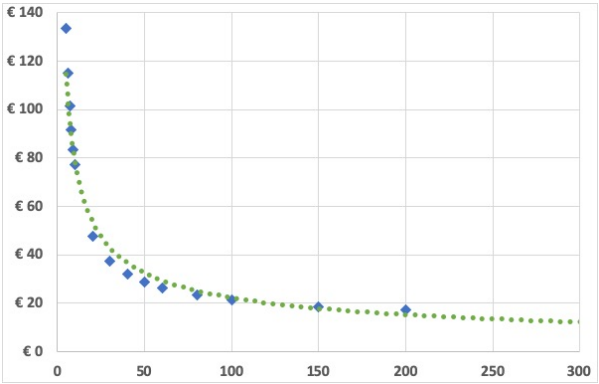

Figure 18.1: Cost Vehicle [Billion Euros] VS The amount vehicles to break-even

When analysing the data, a learning curve can be made to estimate the production and costs for AeroCity. Following this curve, an equation for the line can be estimated using excel, this is given in Equation 18.1. With this equation, the list price for an AeroCity vehicle can be estimated. The number of AeroCity vehicles to break even is set at 100, as at this price point the vehicle cost begins to converge. This then means that the cost of one AeroCity vehicle is set at 22 million euros.

Table 18.1: Learning Curve Slope [64]

	Labor	Materials	Other
Learning Curve Slope	85 %	95 %	95 %

$$y = 276.64 \cdot x^{-0.548} \tag{18.1}$$

18.2. Infrastructure

One of the most important aspects of AeroCity is the advantage it has compared to high-speed rail. One key area that AeroCity aims to be ahead of high-speed rail is in infrastructure. The goal of AeroCity has been to have significantly lower infrastructure costs compared to high-speed rail. In this section the associated costs with infrastructure have been investigated and will be explained. Firstly the topic of land acquisition will be discussed, followed by the topic of the track, then followed by necessary certification costs, followed by the estimated cost of the stations, then followed by the topic of any additional costs that have been shown to arise in previous infrastructure projects. A detailed version of the infrastructure cost breakdown can be seen in Appendix B. Following the table, it is important to note that the cost for the infrastructure is 50% of HSR infrastructure costs [1].

18.2.1. Land Acquisition

One of the larger parts when looking into infrastructure is land acquisition. Land acquisition is an important aspect of infrastructure, as there must be land that one can use to build on. As this is an important aspect, it is expected that land acquisition can take up a large part of the total infrastructure costs. This has been estimated to be between 5-10 % of infrastructure costs [65]. It is important to note that land acquisition costs will be necessary for not only above ground works, but to a certain extent underground work as well, such as tunnelling. Additionally, when looking into land acquisition costs it has been noted that the costs stated are also inclusive of any necessary feasibility studies, technical design plans, legal fees, administration fees, as well as permits [65].

Table 18.2: Further breakdown of direct costs

On-ground Track	**Cost [€/km]**
Groundworks	€1M
Foundation Piles	€0.10M
Concrete Track	€0.61M
Steel Reinforcements	€0.56M
Manhours	€2M
Antiroot	€4k
Add. Cost (lighting, cables)	€10k
Total On-ground Track	**€9.36M**
Extra Cost Viaducts	**€11.32M**
Extra Cost Tunnelling	**€57.54M**

When considering overground costs, it has been estimated that the costs, including planning, can range between €2.15 to €5.53 million per km. This information has been gathered from a number of studies that have looked into 45 high-speed rail projects across Europe [65]. This is assuming that between 5-10 % of infrastructure costs is the cost for land acquisition and planning as mentioned beforehand [65]. For AeroCity it is estimated that the land costs will be on the lower side, as most of the track will be running through rural areas (north of Germany), and will only occasionally be placed in densely populated areas (e.g. Utrecht, Rhine - Ruhr Gebiet).

Table 18.3: Capital Investment for the Infrastructure for a double track Utrecht to Berlin (Excluding station costs)

Direct Costs	**Cost [€]**
On Ground track (576 km)	€5.39B
Track on Viaduct (30 km)	€0.62B
Track in Tunnel (45 km)	€3.01B
Total Direct Costs	**€9.02B**
Indirect Costs	**Cost [€]**
Land Acquisistion (10%)	€0.90B
Engineering Charges (15%)	€1.35B
Cables and Ducts (3%)	€0.27B
Contractor Price (3%)	€0.27B
Total Indirect Costs	**€2.80B**
Total Basic estimate	**€11.82B**
Unpredicted costs (10%)	€1.18B
Expected deviation (5%)	€0.59B
Total Investment Cost excl. taxes	**€13.60B**
Taxes (21%)	€2.85B
Total Investment Cost incl. taxes	**€16.45B**

When considering underground land acquisition costs it is important to note that there may still be compensation fees to pay. These fees are generally not as high as if above ground land is purchased. These fees also vary between land plots as in the Netherlands the constructor will enter negotiations with the landowner to settle on a price. It is also important to note that this issue can change significantly between different countries, and it is dependent on the current law. When looking at other western countries such as Australia, it can be seen that any land 15 meters or lower beneath the surface level is no longer the property of the landowner [66]. However, the landowner can still file for compensation in the case that they feel their land value has degraded or if any issues arise as a result of the tunnelling [66].

18.2.2. On Ground track Cost

The track costs include all those costs related from terrain preparation to the installation of the concrete prefab rails. This cost depends highly on the characteristics of the terrain. Depending on geographic obstacles different track types will need to be used.

For the route between Utrecht and Berlin, the land is mostly flat. Therefore most of the time the track can be built on ground without the need for any tunnels or viaducts. When looking into the ground section of the track, it can be seen that the track can be split into multiple cost elements. These elements are explained and quantified in this section.

Groundwork and Foundation Costs

One of the first items to consider when constructing a track on the ground is how to deal with the earths soil. The first item to do before the laying of the track is to prepare the soil, this is called Earthwork. Earthwork is the process of reshuffling the soil and removing any water or clearing any soil impurities. The process of Earthworks also includes the addition of subgrade. Subgrade will ensure that the load of the track is spread and diffused, as well as ensuring that there is a constant flat surface for the track to be placed on.

The required cost for earthworks can be considered to be in the same range as for conventional trains. As explained in section 6.2, the tolerances for AeroCity are looser than HSR and because aerodynamic pressure is more equally distributed below the track no ballast is needed. Therefore only subgrade is needed to stabilise the track for AeroCity.

From this reasoning it is determined that the cost for the earthworks will be in the same range as for conventional trains. In Figure 18.2, the cost range for the earthworks for conventional trains and for high-speed trains is compared. The graph comes from a study from PWC done for the European Union [67]. The data was gathered from 208 rail infrastructure projects carried out in Europe over the 2000-2015 period. Following a study performed by the EU[67], a conservative estimate of 1 million Euros per kilometre is taken for the cost of earthworks.

Permanent Way

The costs for the permanent way, the physical track, is the cost for the concrete track itself. The cost for the permanent way is estimated to be around €3.22M per kilometre. This number includes the material cost for the track (concrete, steel reinforcement, anti-root) as well as the man-hours to install the track. Steel price is assumed to be €2 per kg [68]. Concrete is estimated to be €250 per m^3 [69]. In total 441k kilogram of steel and 2.8 km^3 of concrete is needed for 1 km of track. This means that the concrete and steel together will cost around €1.56M per kilometre of track. The cost for the anti-root cover is only a minor contribution to the overall track cost, it is €4k per kilometre, [70].

The man-hours cost is estimated to be €2M per kilometre. This number is based on [68]. The man-hours cost for Hyperloop is estimated to be €5M per kilometre. Since, the infrastructure for AeroCity requires fewer installation hours (e.g. no need to connect the steel tubes, ...) the €2M per kilometre considered to be realistic. Lastly, €10k per kilometre is taken into account for additional costs such as lighting, cables, etc [71].

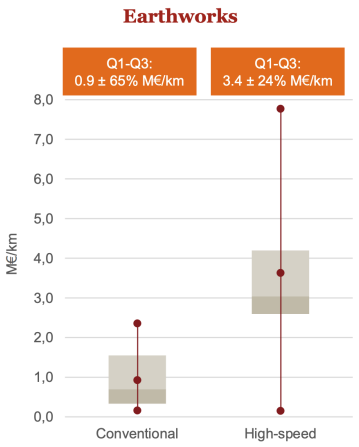

Figure 18.2: Earthwork cost estimates [67]

Certification Costs

The last item that has to be dealt with for the ground track, is the certification costs. Certification is important as without the proper certification from the applicable government, the track cannot be used legally. The certification confirms that the track is constructed properly, and that it is safe for the designed usage. As AeroCity is a new concept there is not much information to base a certification process on, this means that the certification process can take a larger amount of time than normal. However, this is not expected to impact the costs too much. It has been estimated that the certification costs are approximately 1 % of the total investment costs [68].

18.2.3. Additional Cost for Viaducts

During the trajectory of the route, there are various occasions where the track cannot simply be placed on the land. Therefore an alternative must be done to continue the track at an even elevation; the solution is to place a viaduct. The main reasons for this are due to river crossings and highway crossings, however other reasons for viaducts would be in the case of uneven, mountainous terrain. The largest issue with viaducts is that the costs are higher than for ground tracks. This is still the preferred option when needing to cross any obstacles.

When looking into the costs of constructing a viaduct it can be seen that the price can vary between 57 to 73 million Chinese Yuan (2014), which is equivalent to 7.9 and 10.1 million euros (2019) per km [72]. This is an estimate for a double-track viaduct, which is of a similar width of a single AeroCity track. These costs are considered low as the level of automation for constructing viaducts has increased significantly over the years. Automated machines are able to place the necessary track beams over the length of the bridge, this speeds up the process and saves on costs as these machines can be moved to other needed locations as soon as they have finished with a project.

18.2.4. Additional Cost for Tunnels

As the AeroCity vehicle will go through some densely populated areas tunnelling will be required. From literature [73], it was derived that tunnel costs are predominantly determined by the diameter. As the width of the AeroCity vehicle is currently determined to be 8.4 meters and is, therefore, more than double as wide as existing high-speed trains the tunnelling cost for AeroCity is more expensive. Additionally, tunnelling does not reduce the land acquisition cost as in the Netherlands and in Germany, it is required to own the land above the tunnel. However, the tunnelling cost per kilometre decreases with increasing its total length.

For the cost of the tunnels for AeroCity, it is assumed that the tunnel will be made from concrete and the tunnel diameter will be 12 meters, this is a conservative estimate to accommodate for cables, an emergency shaft etc. Also, the depth of the tunnel can be estimated to be between 1.5 and 3 times the diameter of the tunnel depending on the soil conditions and jurisdictional authority [20].

The British Tunnel Society investigated the cost of 21 tunnels, each with different lengths and diameters in the European Union. The correlation between the tunnel diameter and the cost can be seen in Figure 18.3a. The correlation between the tunnel length and cost can be seen in Figure 18.3b.

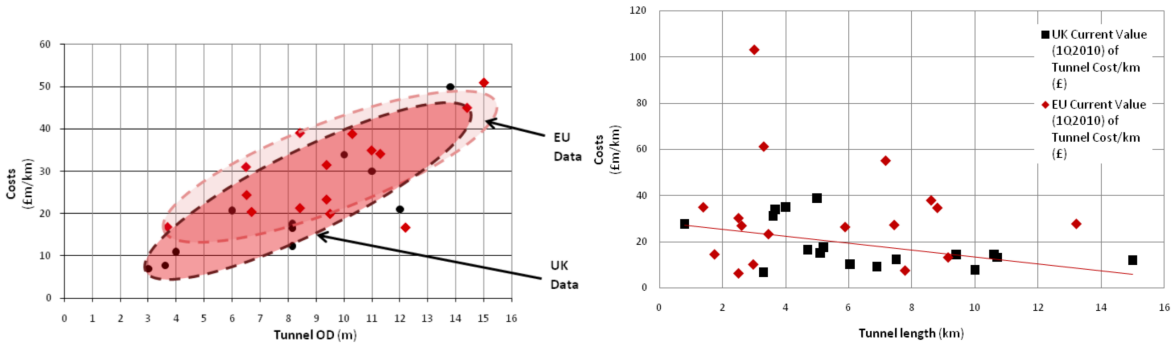

(a) The effect of outer tunnel diameter on unit cost. [74]

(b) The effect of tunnel length on unit cost. [74]

Figure 18.3: Tunnelling Cost in function of tunnel diameter and tunnel length.

According to Figure 18.3a, the cost for a tunnel with a diameter of 14 metres ranges from 35 to 50 million British Pounds (2010) per kilometre. From Figure 18.3b it can be seen that the average cost per kilometre of a 12 km tunnel is half of the one for a 6 km tunnel. As the average length of the tunnels for the Utrecht - Berlin route is expected to be on average around 12 km, the lower estimate of 35 million British Pounds (2010) per kilometre is taken. From this, it is estimated that the tunnelling cost for the AeroCity vehicle is estimated to be around 50 million Euros (2019) per kilometre. As tunnelling can increase the costs of infrastructure, a method to reduce or turnover the costs should be defined. One example to reduce, or create turnover would be to add utility lines inside the tunnel [68].

This additional utility space can be used for public or private electrical cables, telecommunication lines, water pipes, or even gas pipes. As these lines are currently already placed underground it can be beneficial to place these in an AeroCity tunnel as the utility companies can easily inspect these lines and perform maintenance. Additionally, this provides the potential for an extra source of income for AeroCity as the utility companies will have to pay for the possibility to place their lines in the tunnel [68].

Lastly, it needs to be stated that tunnelling is a rather slow process. Currently, Tunnel Boring Machines (TBM) are used to bore tunnels and these have a boring-rate of only 15 m/day [21]. However future development is expected to speed up this process, as, for example, The Boring Company from Elon Musk is aiming at 150 meters/day [22].

18.2.5. Stations

When looking into infrastructure costs, one of the largest single costs is the station. Stations are of importance as there must be a physical location at each stop where passengers can go to and board their vehicle. Additionally, stations can act as a place where light maintenance can be performed as well as where battery swapping can be performed. Stations act as a base and systems can be looked at in person at these physical locations. As stations are able to do all of these things and more, and as they are quite large locations allowing for a mass movement of people it is reasonable that station costs can rise to high amounts. The final estimated price of each station is shown in Table 18.4

For the route between Utrecht and Berlin four stations are needed for AeroCity. Additionally, each station will be different as at each location there are different variables that can affect the costs. The main difference between the stations is the fact that some stations will be placed underground due to densely populated areas above. These are the stations in both Duisburg and Hannover. It is estimated that these station costs can be 4 to 6 times higher than for ground level stations [75].

Looking into general station prices, it can be seen that there is a wide range of prices. However, it can be seen that stations can cost anywhere between 5.5 million euros [72] to around 400 million euros [76] based on the size of the station and any complications based on the location. Additionally, it is estimated that stations make up between 1 to 5 % of the total infrastructure costs [72]. It is important to note however that

Table 18.4: Station locations and their costs

Station	**Estimated Cost**[€M]
Utrecht Lunetten	80
Duisberg	320
Hannover	320
Berlin Westkreuz	80
Total	**800**

these values are based on projects done in China, where costs may not perfectly represent the costs in the Netherlands and Germany. However, using these values and looking at the total costs of the project and knowing the range of station costs, it can be estimated that the average single station cost for AeroCity will be approximately 80 million euros. This is assuming that approximately 1% of the total costs will be the station cost as the station for AeroCity is not large and will only have two tracks. Following this, it can be estimated that the underground station costs will be 320 million euros. These costs are comparable to current stations such as the stations in Breda, Utrecht, The Hague, and Antwerp [76] [77].

18.2.6. Comparison to Hyperloop

One of the important aspects of AeroCity, especially when in comparison to its competitors, such as Hyperloop, is the lower infrastructure costs. As AeroCity does not need any technology or tight tolerances, its costs can be considered lower even when considering the increased width of the track. The costs of Hyperloop's infrastructure can be seen in Table 18.5. This can be compared to the costs of AeroCity's infrastructure as shown in Table 18.2.

One of the largest differences when comparing Hyperloop to AeroCity is the fact that AeroCity does not make use of any vacuum pumps or tubing. As can be seen in Table 18.5 the costs for steel tubes and vacuum pumps can rise to almost 9 million euros per km. This is a significant amount of money and is a part of the costs that are not needed for AeroCity. Therefore significant cost savings are made regarding these items.

Table 18.5: Hyperloop estimated costs per kilometre [78]

Part	Costs
Concrete pillars	€ 200,000
Steel tubes	€ 8,631,254
Inductrack	€ 918,000
LSM propulsion	€ 12,900,900
Guidance	€ 200,000
Solar panels	€ 800,000
Aesthetic cover	€ 2,000,000
Vacuum pumps	€ 160,000
Additional and communication	€ 1,207,750
Man hours	€ 5,000,000
Total	€ 32,018,174

The next difference between Hyperloop and AeroCity is the fact that AeroCity does not make use of a linear stator motor (LSM). This, for Hyperloop, is one of the largest cost factors, costing 12.9 million euros per km. AeroCity will use a combination of electric propellers and batteries to both propel the vehicle and provide power to the propulsion system and vehicle respectively. Additionally, Hyperloop makes use of an inductrack system as a fail-safe for their propulsion system. This item is again not necessary as AeroCity is flying using electric propellers. This, in turn, results for cost savings for AeroCity when performing a direct comparison.

Lastly, an item that is needed for Hyperloop but not for AeroCity, is the usage of an aesthetic cover. As Hyperloop is an above ground tube, they have determined that they will have to spend 2 million euros per km to cover their steel tubes to make it aesthetically pleasing so they can indeed place it in the urban areas. AeroCity, however, has a track that is placed on the ground, therefore no aesthetic cover will be needed as it will not be blocking any views.

In total, this will bring cost savings of up to at least 24.8 million euros per km when performing a direct comparison to Hyperloop. Additional savings can also be had in terms of man-hours, as it has been estimated that the required man-hours will be less, as the infrastructure for AeroCity will take less work and less precision when compared to Hyperloop.

18.3. Exploitation Cost

Once the infrastructure has been built, the operation of HSR services involves two types of costs: those related to the exploitation and maintenance of the infrastructure itself, and those related to the provision of transport services using that infrastructure. Additionally, operational costs such as energy are expected to play a large role for AeroCity

When looking into the maintenance of the vehicle, the costs will not be too large of a factor as AeroCity has been designed with maintainability in mind. One of the best parts of the design of AeroCity is the design of the swappable batteries, this means that in the case of a power system issue a battery can be simply swapped and the vehicle can resume as normal. Additionally, the battery can be looked at entirely and not within the confined space of the vehicle. This provides ease of maintenance which in turn means faster repair times and lower costs. When considering one of the traditionally higher costs of maintenance, the infrastructure, it is seen that the maintenance will be significantly lower for AeroCity. The main reason for this is the fact that during a significant portion of the journey, AeroCity will never make direct contact with the track, instead, it is applying a distributed pressure as it flies above. This means that there is significantly less stress on the track and the track can last longer and the periods between inspection can be increased as no significant wear or tear will be produced as when comparing to current high-speed rail (HSR).

Additionally, when looking into the operations, a cost where AeroCity can save significantly when comparing to HSR is in terms of energy. It has been estimated that AeroCity will use half the energy of HSR, which is further explained in chapter 19. This means that the costs associated with energy will be significantly reduced thus saving on operational costs.

18.4. Ticket Cost

For AeroCity to be able to be self-sustainable it is important that there is a method to earn revenue. The most common form of earning revenue for transportation companies is through ticket sales. These tickets are sold to customers where they, in turn, reserve a spot on the vehicle and are transported from point a to point b. Therefore it is important to look into what a ticket fare is broken down into, as with the ticket breakdown it can be seen how much profit is made and how much of the ticket is used to pay for the operation of the service.

When looking into the ticket breakdown costs for the various transportation companies, it is assumed that the transportation method that most follows AeroCity is that of rail. This is mainly due to the fact that airlines pay higher fees and taxes such as landing fees and the varying passenger duty fees from varying countries. When looking into a fare breakdown from rail companies, it can be seen that only 2% of the cost is profit for a company. The remaining 98% is composed of vehicle costs, staffing, energy, infrastructure access, franchise support, and other costs such as maintenance, administration, contractors [79]. It is important to note that these numbers are representative of only one company, namely the Rail Delivery Group from the UK.

Table 18.6: AeroCity fare breakdown

Components	**Cost** [€]	**Percentage** [%]
Vehicle	8.66	23.82
Infrastructure	15.31	42.11
Energy	1.85	5.10
Staff	5.62	15.44
Profit	4.92	13.53
Base Fare	36.36	100
Tax (21%)	7.64	21
Total	**44.00**	121

For AeroCity, the ticket price will be composed differently as there are different cost drivers affecting the price of a ticket. A complete breakdown of the ticket can be seen in Table 18.6. It can be seen that most of the cost goes back into the company and only a small percentage is profit, similarly to the numbers from the Rail Delivery Group. It is important to note that the infrastructure will not be paid directly, instead a model similar to that of ProRail will be used. This means that the governments will subsidise a large portion of the cost and AeroCity will pay a yearly fee to use the track. Additionally, it was assumed that there will be an 80% load factor with AeroCity.

Furthermore, it is important to note that not all of the revenue for AeroCity will come directly from ticket sales. Another primary source of revenue for AeroCity will come from ancillary revenue, such as additional services on-board and other revenue will be the renting of retail space at the station, and the renting of advertising space at the station. Ancillary revenue and the renting of space is estimated to bring around 20% of the total revenue of AeroCity. This follows from an average ancillary revenue of 10% in the airline industry [80] and an estimated additional 10% source of revenue from the leasing of real estate at the stations. This additional source of revenue will help cover the costs required to operate AeroCity.

It is important to note that with this ticket fare, inclusive of taxes, the requirement USR-PC-02, has been met. This requirement states that the ticket price is at least 50% the price of a first-class seat on ICE. The price of a first-class seat on ICE for the distance between Utrecht and Berlin has been estimated to be an average of €178 [81]. As the ticket price for AeroCity is determined to be €44, the requirement has been met.

18.5. Operational Balance

When looking at the operational perspective of AeroCity, it is important to see what the yearly balance sheet will look like. This will give an impression of what the yearly costs are and where the yearly profit is coming from. Looking into a balance sheet it can be seen that the revenue will come in, the expenses will be taken out and the final profit will be shown at the end either in black for a positive profit, or in red for a loss. The balance sheet for AeroCity can be seen in Table 18.7.

When looking into the revenue sources it can be seen that the majority of the revenue, 80%, comes from ticket sales. The breakdown and the discussion of how a ticket price was made are discussed in section 18.4. When looking into the additional revenue sources, it is seen that an additional 10% of the revenue comes from ancillary revenue, and the final 10% comes from the leasing of retail and advertisement space in stations. Ancillary revenue will be made up of the sales of additional purchases both onboard and during the ticket buying process. These purchases will be things such as paying to select your seat ahead of time, paying to have a meal on-board, paying for the usage of faster WiFi on-board, and other smaller add-ons. The final additional source of revenue comes from leasing.

This will be the leasing of retail space at stations, letting larger companies set up their stores inside the station and potentially also letting pop-up stores take some space for a limited amount of time. Additionally, advertisement space will be sold, this will primarily be inside the station and will be placed in highly trafficked areas.

When looking into the costs, it can be seen that a majority of the costs for AeroCity is made up of vehicle and infrastructure costs. Infrastructure costs are assumed to largely be paid off with the assistance of the governments. This would mean that AeroCity will pay a yearly fee to use the infrastructure. This rate is based on the yearly fee that ProRail charges and a ratio of how much track AeroCity uses vs how much ProRail has. AeroCity has approximately 650 km of track compared to the 7000 km that ProRail has [82]. Additionally, ProRail charges up to 340 million euros per year as a usage fee [82], this would then mean that AeroCity would pay approximately 31.1 million euros per year as a usage fee. When considering the vehicle costs it has been determined in chapter 17 that a total of 12 vehicles will be needed for a successful operation of AeroCity. Additionally, it has been determined in section 18.1 that the list price of an AeroCity vehicle will be 22 million euros. Giving a break-even time of 15 years, the yearly cost for all the vehicles in AeroCity's fleet will be approximately 27.61 million euros.

Table 18.7: AeroCity Balance

	Yearly (€M)
Revenue Sources	
Ancillary	7.15
Leasing	7.15
Ticketing	57.19
Total Revenue	**71.49**
Costs	
Vehicle	17.61
Infrastructure Fee	31.11
Energy	3.77
Staff	9
Total Costs	**61.49**
Total Profit	**10.00**

The smaller costs that are involved in AeroCity are the energy costs and the staff costs. Energy costs total to 4.7 million euros per year. This is based on the amount of energy needed per ride, how many rides there are in a total year and an energy cost of 0.06 cents per kWh [83]. Additionally, for staff costs, it is assumed that a total of 15 million euros per year will be needed to pay all the staff of AeroCity. This is based on an average salary of €95,000 per employee and an assumption that approximately 10 employees will be needed per AeroCity vehicle.

When combining all the costs and the revenue it is then seen that the remaining balance is the profit for AeroCity. As seen in Table 18.7, AeroCity is a profitable operation with an estimated yearly profit of 10 million euros.

19 Sustainability

19.1. Contribution to Sustainability

AeroCity contributes to a sustainable future in many ways. It directly competes with more carbon-intensive transportation modes, it does not create any direct emissions and will be powered by renewable energy sources. It will draw people away from planes by offering a more convenient mode of travel, similar to that of a train, but will exceed the speed of the current high-speed rail at lower cost. This will reduce the overall carbon emissions since there will be fewer people travelling by plane.

Additionally, the design of AeroCity will be less than half as loud as a traditional train with the added benefit of having looser tolerances for track construction. This results in reduced cost for track construction compared to high-speed train lines. Increasing concerns regarding noise pollution mean that it will be more difficult to build new train lines to serve a growing urban population in the coming years as noise concerns, especially in residential areas, limit the possible locations for construction of train tracks [84] [85]. The reduced noise will make AeroCity a more sustainable transportation method compared to a train since it is better suited for increasingly densely populated areas due to its reduced noise[86].

19.2. Sustainable Development Strategy

This section is concerned with the sustainable development strategy for the AeroCity vehicle and the infrastructure. A more detailed version of the sustainable development strategy can be found in the midterm report [8].

During the design process of AeroCity, the main considerations for sustainability were the noise and the energy consumption and the resulting emissions. Further considerations were done during the design process with the choice of the batteries and the materials used for the construction of the vehicle, but most importantly the track as its construction will involve a large amount of concrete, which has a significant contribution to global annual carbon emissions due to the production process that is involved in creating cement, which is an essential component of concrete. [87].

The general approach here was to first define all aspects of sustainability in order to define the specific implications of design decisions. These aspects and the process of how to identify the specific implications of design decisions have been described already in the midterm report [8]. The next step is then performing the trade-off with these implications with sustainability in mind and adjusting the design if sustainability becomes a major concern. This was done for example with the choice of the propulsion system, where the counter-rotating propellers were an option that was considered, however, due to the additional noise that they cause, this option was discarded.

19.3. Noise Estimations

This section discusses the noise estimations that were done for the AeroCity vehicle. Understanding how much noise the vehicle will produce is important in order to determine whether or not the vehicle can pass through densely populated areas. Noise pollution is a major concern with aircraft and thus it is important for AeroCity to be below the regulatory limits.

It was determined that the main source of noise would come from the propulsion system. The aerodynamic body noise was not considered for this estimation since it is really difficult to estimate even with the most advanced methods and is beyond the scope of this project. There were some initial noise estimates done using other methods, however, it was decided to use the noise estimation method described by Heidmann [6].

Broadband Noise

This method differentiates between broadband noise, discrete-tone noise and combination tone noise. The latter can be omitted since the speed of the fan does not exceed the threshold value in order to make the contribution significant. The broadband noise is estimated using Equation 19.1 and Equation 19.2. Equation 19.1 gives the characteristic one-third octave band sound pressure level where ΔT is the change in temperature over the fan, $\dot{m}$ is the mass flow through it, M_{TR} is the relative tip velocity, RSS is the rotor-stator spacing and θ is the angle relative to the engine. The sound pressure level spectrum is given by Equation 19.2, where f is the frequency of the sound and f_b is the blade passing frequency. The calculated sound pressure level is the perceived sound in a one-meter radius from the engine.

$$L_c = 20\log_{10}(\Delta T) + 10\log_{10}(\dot{m}) + F_1(M_{TR}) + F_2(RSS) + F_3(\theta) \tag{19.1}$$

$$SPL(f) = L_c + F_4\left(\frac{f}{f_b}\right) \tag{19.2}$$

In order to calculate the broadband noise spectrum, the variables that are used Equation 19.1 have to be determined. The temperature difference ΔT before and after the fan can be determined using the isentropic relations and assuming an efficiency of 95%. Equation 19.3 and Equation 19.4 are the formulas used to calculate the temperature difference from the pressure ratio, that was found in chapter 8. This is assuming that T_1 is equal to the temperature of the air at sea level.

After determining the temperature difference, the mass flow across the fan had to be determined. This was already done in chapter 8 and was found to be 165 kg/s per engine. The relative inlet Mach number is the vector sum of the rotational velocity of the blade and the directional velocity of the vehicle. The velocities simply have to be expressed as Mach number by dividing the velocity by the speed of sound. The rotational Mach number of the blade can be calculated using Equation 19.5, where ω is the rotational velocity, r is the radius of the fan and a is the speed of sound at sea level. Furthermore, after determining the Mach number of the vehicle at cruise velocity, the relative inlet Mach number M_{TR} is determined by Equation 19.6:

$$T2 = T1\left(\frac{P2}{P1}\right)^{(\gamma-1)/\gamma}; \tag{19.3}$$

$$\eta = \frac{T_2 - T_1}{T_2' - T1} \tag{19.4}$$

$$M_{rot} = \frac{\omega r}{a} \tag{19.5}$$

$$M_{TR} = \sqrt{M^2 + M_{rot}^2}; \tag{19.6}$$

This relative inlet Mach number can then be used in combination with the empirical data provided by Heidmann [6]. With this data, the noise contribution due to the relative inlet Mach number is found.

The rotor-stator spacing (RSS) factor is calculated using Equation 19.7 and the variables c_1 and c_2 are explained in figure Figure 19.1. Based on this value, there is empirical data found in Heidmann [6] that determines the correction factor for the noise that is created due to the spacing of the rotor and the stator.

Lastly, the angle from which the noise is measured should be determined. The angle correction factor is also based on empirical data, found in Heidmann [6]. For this noise estimation, the most conservative values are taken, which means the noise is measured from a 40° angle relative to the front of the engine. This is the point where the engine will be the loudest.

With all these values determined, the value for L_c is found. This value is then plugged into Equation 19.2, the value for $F_4\left(\frac{f}{f_b}\right)$ also depends on empirical data. Equation 19.8 describes the formula which determines the value of $F_4\left(\frac{f}{f_b}\right)$. Now by plugging in various values for the frequency (f), the sound pressure level (SPL) for each frequency can be determined and the SPL spectrum can be plotted. This plot for the broadband SPL spectrum can be seen in Figure 19.2:

$$RSS = \frac{c_2}{c_1} \cdot 100 \tag{19.7}$$

$$L = 10\log_{10} e^{-\frac{1}{2}\left(\frac{\ln f/2.5 f_0}{\ln \sigma}\right)^2} \tag{19.8}$$

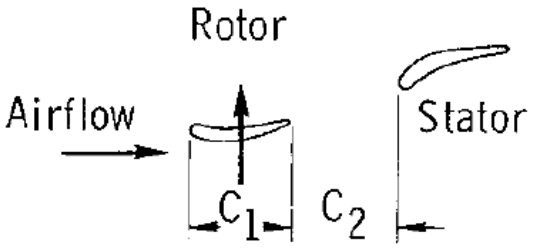

Figure 19.1: Rotor stator spacing geometry [6]

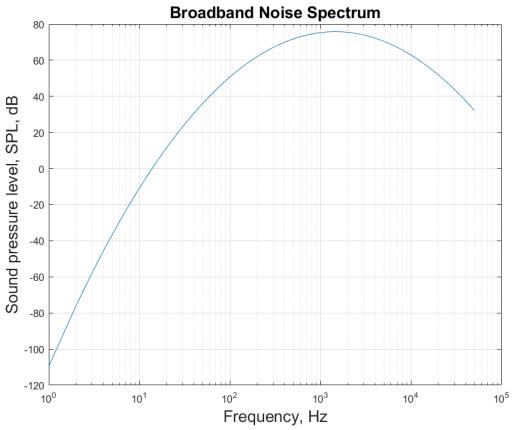

Figure 19.2: Broadband Noise Spectrum

Discrete Tone Noise

The second part of the noise estimation is concerned with discrete tone noise. This is estimated using Equation 19.9 and Equation 19.10. Equation 19.9 is the same equation as Equation 19.1, however, the empirical relations that are given by F_1 through F_5 are different for the discrete noise estimate. However, because the necessary values for these relations have already been determined in the previous subsection, the value for L_c can be simply determined by plugging in these values into the relations that are given for the discrete tone noise [6].

In order to calculate the sound pressure level spectrum of the discrete tone noise,Equation 19.10 is used. The relations F_4 and F_5 for the given engines is given by Equation 19.11 and Equation 19.12 respectively, where k is the value of the harmonic frequency and is determined by $k = \frac{f}{f_b}$, with f being the frequency of the noise and f_b the blade passing frequency. Plugging in the different values for f the SPL for each frequency can be determined using Equation 19.10 and then be plotted. The plot for the sound pressure level spectrum of the discrete tone noise can be seen in Figure 19.3a:

$$L_c = 20\log_{10}(\Delta T) + 10\log_{10}(\dot{m}) + F_1(M_{TR}) + F_2(RSS) + F_3(\theta) \quad (19.9)$$

$$\mathrm{SPL(f)} = \mathrm{L_c} + 10\log_{10}\left[10^{0.1\mathrm{F_4(f/f_b)}} + 10^{0.1\mathrm{F_5(f/f_b)}}\right] \quad (19.10)$$

$$L = 3 - 3k \quad (19.11)$$

$$L = 10 - 10k \quad (19.12)$$

After having determined the broadband noise spectrum and the discrete noise spectrum, both of these can be combined in order to give a complete total noise spectrum. To combine the two plots, the decibel values have to first be converted into pressure values to be added and then converted back into decibel values. The plot of this combined spectrum can be seen in Figure 19.3b

As mentioned previously, this noise estimation only determines the sound pressure level within a one-meter radius around the engine, however, most regulations are concerned with the experienced noise by people that live nearby the track and thus a web-based tool developed by the consultancy company MAS Environmental [88] was used in order to calculate the noise experienced at a meter distance from the track. This tool was originally built to determine the noise next to a highway or a train track, and also determines the effect a sound barrier would have on the experienced noise next to the track. This is especially useful as it also takes into account the sidewalls that the AeroCity track will have and thus a more accurate noise model is created. This model can be seen in Figure 19.4 and it was found that the noise one meter away from the track would be 76.3 dB, which is roughly 4 dB less than a train. This difference on the decibel scale means that the AeroCity vehicle creates less than half the noise that a train would create [84].

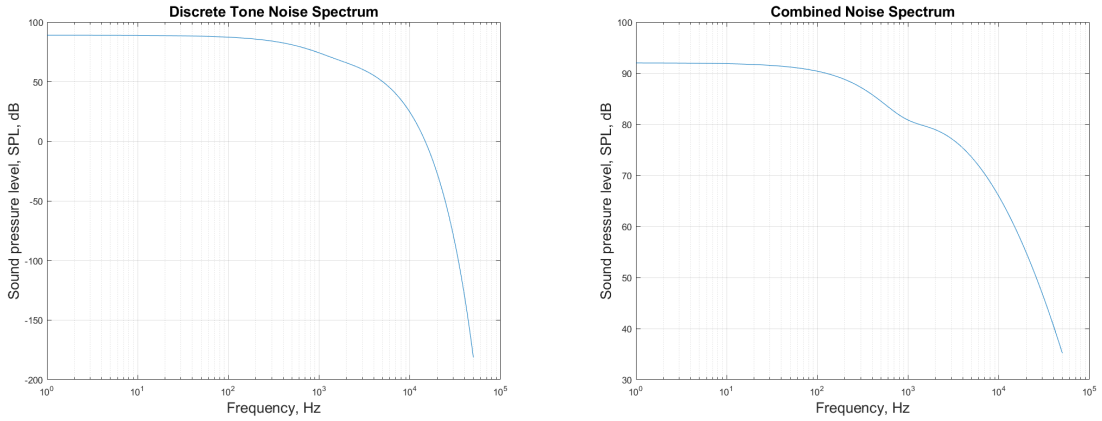

(a) Discrete Tone Noise Spectrum

(b) Combined Noise Spectrum

Figure 19.3: A comparison between the discrete and combined tone noise spectra.

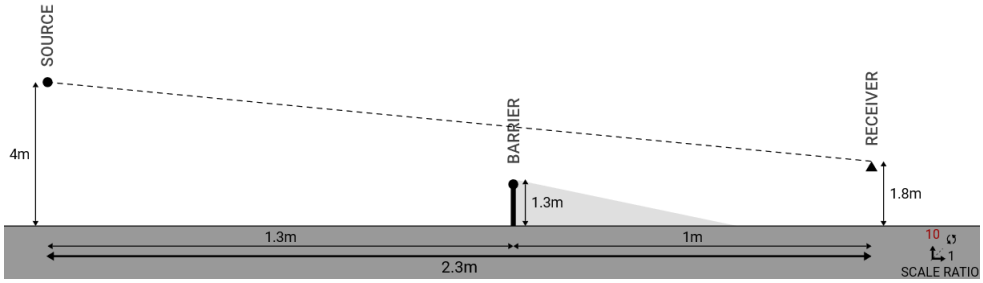

Figure 19.4: Noise estimation web tool [88]

19.4. Emissions and Efficiency

In this section, the Emissions and Efficiency of AeroCity compared to other transportation modes is considered. Even though the plan for AeroCity is to be powered entirely by renewable energy sources, the possible indirect emissions were still investigated in order to draw a comparison to more carbon-intensive transportation modes. Additionally, it is not entirely clear yet whether or not it will be possible due to availability or cost to completely use renewable energy sources and thus it is worth looking into possible emissions. After this, the energy efficiency per passenger is investigated and compared to existing transportation methods.

19.4.1. Emissions

The emissions were calculated using a weighted average between the average CO_2 per kWh in the Netherlands and Germany. This value came to be 477 CO_2/kWh and was then multiplied with the amount of kWh required per trip. This amounted to a total CO_2 production per trip of 1717 kg. It was found that when the vehicle is fully occupied and the total emissions are divided by the kilometres travelled and the number of passengers, the emissions per passenger kilometre are 22.7 g of CO_2. Using a load factor of 80 %, which is comparable to that of an aircraft, this number increases to 28.4 $gCO_2/pax/km$. When comparing it to existing transportation modes, it puts AeroCity above trains, which are the best mode of transport for carbon emissions, and below small cars that carry four people. A summary that compares the different transportation modes can be found in Table 19.1 [89]:

Table 19.1: Carbon Emissions per Passenger Kilometre

Transportation Mode	**Passengers**	**Emissions** $[gCO_2/pax/km]$
Train	156	14
AeroCity	116	23
small car	4	42
large car	4	55
Bus	12.7	68
Moped	1.2	72
small car	1.5	104
large car	1.5	158
Aircraft	88	285

This comparison shows that AeroCity, even without using renewable energy, would be a more sustainable transportation mode than most other options. With the added benefit of being fast and convenient to travel with and

also having lower emissions than more carbon-intensive transportation modes, such as air travel and cars, it could reduce the overall emissions substantially.

Another added benefit of AeroCity is that its emissions will be lower for a lower amount of passengers as the vehicle will not have to produce as much lift and thus can fly at a lower angle of attack. This will create less drag and overall reduce the amount of energy consumed during the trip. In chapter 7 it was found that if the vehicle was to carry only half the number of passengers, it would reduce the total energy consumption by 35%. For trains, the number of passengers does not influence energy consumption and thus they will roughly use the same amount of emissions independent of how many people are making use of it.

19.4.2. Efficiency

Because AeroCity is planning to use renewable energy sources for its electricity, another very important comparison has to be made with respect to energy efficiency. All of the trains in the Netherlands are already being powered by renewable energy sources thus a comparison with trains should involve the energy consumption efficiency.

This comparison is based on the energy consumption per equivalent seat number per kilometre ($kWh/Es/km$) of various transportation modes that were found by Pérez et al. [90]. An equivalent seat number was calculated in order to account for the difference in the number of seats within the same transportation mode. Since more seats would make a specific transport mode more efficient, this difference is accounted for with the equivalent seat number. Because there is only one AeroCity vehicle and there is no variance in the number of seats between AeroCity vehicles, no equivalent seat number has to be calculated. The energy consumption for one AeroCity trip has been calculated in chapter 16 and this number was simply divided by the distance the vehicle has to travel and the number of seats per vehicle. It resulted in a total specific energy consumption per equivalent seat kilometre of 0.047 $kWh/Es/km$, which is a lower value than any other transportation mode presented in Pérez et al. [90]. A summary of the comparison with other transportation modes can be found in Table 19.2:

Table 19.2: Energy consumption per different modes of transport [90]

Transportation Mode	**Energy Consumption** $[kWh/Es/km]$
Middle Class Car	0.23
4x4 Car	0.27
Microbus	0.10
Standard bus	0.09
Intercity train	0.11
High-speed train	0.10
AeroCity	0.05

In the case of the direct comparison to ICE, it was found that the energy consumption per kilometre for ICE varies between different routes. Taking an average value of 30 kWh/km from a report conducted for the European Commission [91], and dividing it by the number of the maximum amount of passengers, which is 444 [92]. This yielded a specific energy consumption per passenger kilometre for a full ICE3 train of 0.068 $kWh/pax/km$. For a fully occupied AeroCity this value was shown to be 0.047 $kWh/pax/km$. This shows that the AeroCity will consume roughly 30 % less per passenger kilometre than ICE3.

19.5. Material Choice for the Track

The design of the track has been described in chapter 6 and will make use of concrete. The problem with concrete is that the manufacturing process for concrete, unfortunately, creates a large amount of carbon dioxide that is released into the atmosphere. This is so severe that when considering all of the concrete that is produced every year, it makes up around 5.6 % of global annual carbon dioxide emissions [87]. An alternative method of producing concrete in a carbon-neutral way has already been developed and is currently being offered by the company carbon cure [7].

During the manufacturing process of the limestone for this concrete mixture, the carbon is captured and is ultimately stored within the concrete. Thus, in order to reduce carbon emissions during the construction of the track and the stations for AeroCity, this concrete will be used. This concrete has additional strength benefits and is comparative in price [7].

20 Verification & Validation

The verification and validation procedures are an essential component of the design process of complex products. This chapter presents the general verification and validation approach and the results obtained by its application to the AeroCity system.

From the very firsts phases of design process onward, the numerical models have been verified and validated, both to ensure convergence between the numerical solution and the reference model, and to ascertain that the modelled problem accurately describes the real-life scenario. The verification and validation procedures are presented respectively in section 20.1 and section 20.2. Subsection 20.3 closes the section with the design verification.

20.1. Model Verification

The model verification consists of checking the consistency between the numerical model and the analytical model from which the first was developed. Two types of model verification have been performed: code verification and calculation verification. Code verification is a process where the correctness of a software implementation of a numerical algorithm is evaluated, typically by comparison with an exact solution. Calculation verification is a process by which the discretisation error is estimated in simulations of problems of interest. Calculation verification employs techniques of both error estimation and uncertainty quantification [93]. Moreover, several unit tests are performed on the program and on the methods used for verification.

20.1.1. Noise Estimation

For the noise estimation, the method described by Heidmann [6] was used. This model has been validated and has been cited it numerous scientific articles and thus it is assumed that the model that is described in the paper does not have to be validated.

Parts of the calculations needed for the method were put into a MATLAB script and the remaining values were determined from graphs that originate from empirical relations. The parts of the method that were calculated in a MATLAB script were integrated in a for-loop in order to calculate the noise for a number of different frequencies. The correctness of the code was then verified by calculating noise estimates for a number of frequencies by hand.

20.1.2. Loading Diagrams

The loading diagrams for the vehicle are created using the simple principle of force and moment equilibrium. As the vehicle is modelled as a simple beam, this problem reduces to a beam loading problem as previously covered by the course 'Mechanics of Materials'. The verification of the code used to construct these diagrams is done by visual inspection of the produced graphs and comparison to analytical calculations of similar beam loading cases.

20.1.3. Landing Gear

For the landing gear, mainly hand calculations were performed and estimates based on several books were made. Calculations for the wheel placement and disc brakes were performed based on equations from books. Moreover, a thorough calculation check was performed and the correctness of the used equations and implemented values was verified. The method used for the sizing of the absorbers was verified by the method described by Torenbeek [54].

20.1.4. Performance Calculations

The performance calculation are calculation in detail under the given assumptions in chapter 16, with inputs as stated throughout the full report. The program uses simple one step calculations without iterations. The program has been checked by doing hand calculations. It has been checked that the output is as reliable as the input.

20.1.5. Propulsion

The calculations performed for the design of the propulsion system are relatively simple calculation that have been place in an iterative loop in order to provide results for different design points and to provide graphs. These calculations themselves have been verified by hand and the resulting graphs have been analysed by visual inspection.

20.1.6. Structures

For determining the structure of AeroCity vehicle, all possible failure modes have been analysed with the use of programming. In order to verify the calculations done on the structures a lot of unit tests are performed. By using examples from books on the subject and old exercises from courses on the subject, unit tests were done and the Python codes were verified. The code for the deflection was verified using methods discussed by Hibbeler [52]. The code was adjusted until the input and output matched with the examples showed in the books. Furthermore, the conclusion of each structural analysis have been check with compliance with reference aircraft and have been sketched in order to do a final sanity check.

20.2. Model Validation

The model validation consists of developing objective evidence that the models through which the system was analysed reflects the real-life scenario with the required accuracy. Evidence can be acquired throughout experience (with application of similar models in similar circumstances), by analysis (showing that the elements of the model are necessarily correct and are correctly integrated) or by comparison with test cases in the form of independent models of proven validity or actual test data [93]. The system presented in this work is an original concept; therefore, analysis was the preferred means of validation for the complete system. The effort was focused on showing that the elements of the model are of necessity correct and are correctly integrated.

Nevertheless, as some of the system's components are existing commercial products, validation by means of experience and comparison can be performed at the subsystem level.

20.2.1. Aerodynamics

During the conceptual design of the AeroCity vehicle, the aerodynamic model from the Nouwens's Master thesis [17] have been used as the primary reference. Lift, drag and moment coefficients reported in his thesis, along with preliminary vehicle weight estimations from the AeroCity Team S17 [94] and the mission requirements [81] have been used to estimate several of the AeroCity's operational parameters. The influence that the above-mentioned aerodynamic coefficients have on the performance of the vehicle and on several subsystems design, raised the necessity of a thorough validation of these values and of the process through which they have been obtained.

In his study, Nouwens [17] employed ENSOLV, a CFD code that has been developed by the NLR to accurately simulate 3D flow around civil and military aircraft and spacecraft. The code is considered to deliver remarkably accurate results, as it solves the full Reynolds Averaged Navier Stokes (RANS) equations. Moreover, it has been used regularly for a wide range of applications and it has been extensively compared and validated with experimental data. Nevertheless, CFD programs are complex tools. The reliability of the results greatly depends on the quality of pre-processing and post-processing. It is not uncommon that the software user generates an inappropriate grid, defines boundary conditions non-representative of the problem or chooses an unsuitable turbulence model. Moreover, the uncertainties and the errors are not always correctly reported in the results. In a nutshell, the CFD analysis performed by Nouwens provided valuable insight into some of the aerodynamic phenomena, but the lack of any experimental data limits the validity of its results.

The steady aerodynamics characteristics of AeroCity were subsequently investigated by Nasrollahi [95]. However, neither Nasrollahi provided validation for its results. Moreover, in its work, Nasrollahi used a fixed ground wind-tunnel set-up, that makes the results inherently non-representative of the actual AeroCity operating case [27].

Just two years ago, Martijn Van Sluis [27] performed an investigation on the suitability of computational fluid dynamics (CFD) for investigating the WIG effect, specifically related to the Aerocity's aerodynamic characteristics. In order to provide a solid basis for his numerical results, he simulated several test-cases with CFD and compared them with experimental and reference data. He successfully validated his model with the test-cases, but he found limitations for the analysis of the Aerocity model specifically.

The literature study revealed the difficulties and the limitations encountered when attempting to replicate and validate the aerodynamics of this extreme ground effect vehicle. Small variations in the airfoil shape, in the angle of attack, or in the sideskirts shape and distance from ground led to diverging results for at least some of the aerodynamic parameters.

In the work here presented, constraints on time and cost prevented the employment of CFD software and wind tunnel tests. Simpler programs were considered not adequate to analyse the extreme ground effect of the vehicle, because of the crucial role played by the viscosity. Therefore, at least for the aerodynamic design of the main body, a conservative approach was followed to obtain somewhat reliable data. Nevertheless, the limited angles of attack range on which Nouwens performed his analysis, was not sufficient to cover the AeroCity's flight envelope. Therefore interpolations and (limited) extrapolations were considered necessary. The extrapolations to lower angles of attack are especially considered inaccurate, as for those values the flat bottom of the wing transitions from creating a duct that is convergent to creating one that is divergent.

Besides, multiple control surfaces were deemed necessary, and their aerodynamics, as well as their interference with each other and with the main wing body, requires validation. The main control surface, the canard, is the most important addition. In order to obtain reliable aerodynamic data for the canard, the same airfoil and the same sideskirts ground clearance used for the main vehicle body were chosen. Nonetheless, a different chord distance from the ground and a different geometric aspect ratio were considered necessary for efficiency, safety and structural

reasons. The inability to replicate the exact wing shape of the main wing body required the assistance of the JavaFoil software for analysing the canard's aerodynamics. Unluckily, JavaFoil implements a classical panel method and does not model laminar separation bubbles and flow separation. Moreover, to model finite wings, JavaFoil uses classical wing theory formulas, that allow only for an approximation of the 3D wing effects. It is unknown if these formulas hold significance when the wing is analysed in extreme ground effect. Nevertheless, the ability of JavaFoil to model the ground effect with a moving ground boundary condition, the simplicity of use and rapidity and flexibility by which analysis can be conducted, were considered valuable characteristics for preliminary estimation of the canard control surface.

In any case, what above all needs validation, is the wing-canard aerodynamic interference. In the present work, the downwash of the canard experienced by the wing was considered negligible, and the upwash of the wing experienced by the canard was only roughly estimated. Moreover, the effect of the turbulent flow generated by the canard was deemed to have an insignificant effect on the wing aerodynamics. Lastly, the forward extension of the sideskirts necessary to connect the canard to the wing structure was considered only for the drag calculation, while it probably has a sensible effect on both the canard and the wing aerodynamic characteristics.

The rudders and the ailerons had been sized in advanced stages of the design process with limited time resources. Because of the lack of dynamic analysis, their sizing was somewhat arbitrary. The rationale consisted in placing them in the last sections of the engine ducts, to exploit the engines' exit velocity and the wingtip vortices containment, consequently augmenting the lift generation and the vehicle control capabilities. The JavaFoil software was used again, mostly to select the leading edge radius providing the maximum lift coefficient for the control surface. The drag contribution from these control surfaces was estimated by assuming the reference velocity to be the exit velocity of the engine. The limited knowledge on the flow behaviour in an engine duct and on the effect of placing control surfaces in these locations shows the amount of validation that is still required.

The exact magnitude of the spoiler contribution to the vehicle drag requires validation by test. Nonetheless, by experience and comparison [28] the estimated drag coefficient has been validated.

Regarding the vehicle-track interaction, two track types have been employed, and both of them have a yet unknown effect on the vehicle aerodynamics. When the track is on the ground, the bottom is reasonably flat and mostly covered by an anti-root fabric. The irregularities in the subgrade earth material, of which most of the central part of the track is covered, could have a detrimental effect on the vehicle aerodynamics. As for the anti-root fabric, its permeability, necessary to allow water drainage, could lead to a reduction of the high pressure generated under the vehicle and a consequent reduction in the aerodynamic efficiency. The second track type is the one employed on viaducts. This track presents a concave shape along with small piping to allow drainage. The effect of these features on the aerodynamic efficiency is expected to be negligible; nevertheless, in future development phases, these effects should be analysed.

One last track aspect which was not yet researched in the present work is the effect of the sidewalls on the wingtip vortices. Van Sluis [27] investigated the effect of a simple track geometry on the vehicle aerodynamics characteristics and discovered it had a substantial impact. The lift coefficient was slightly increased, but the drag coefficient was significantly increased, leading to a lift-to-drag ratio reduction of about 6%. Moreover, the pitching moment was slightly reduced.

Regarding the wing-propulsion system, it was assumed that it would have no contribution to the lift while the drag was estimated as explained in subsection 7.3.4.

20.2.2. Stability & control

The stability and controllability analysis was performed independently for the vehicle six degrees of freedom. Only static stability was addressed, and the controllability was limited to a quantitative analysis of the trimmed situations and a qualitative description of the dynamic behaviour.

By performing the analysis per degree of freedom, it was assumed that the stability and control for each degree of freedom were decoupled. This model does not represent precisely the real life-scenario but it is the standard procedure employed in aircraft design and is therefore somewhat validated by experience.

Regarding the pitch stability and controllability, it was assumed that the thrust and the drag vectors did not contribute to the moment equilibrium around the pitch axis, and therefore their derivatives with respect to the angle of attack were neglected too. Free stream velocity condition has been assumed for both the canard and the wing. The derivative of the downwash was considered to be null (because the downwash was considered negligible) and the derivative of the upwash was assumed to be constant and was roughly estimated by means of 2D flow fields

superposition. These assumptions allowed for the creation of a relatively simple model, quite practical in the first phases of the design. This model has been partially validated by observing, in the results, the deteriorating effect that a canard has on the neutral point location of a flying vehicle.

Regarding the height stability, the same assumptions used for the pitch stability analysis were employed. Moreover, the derivative of the upwash with respect to the sideskirts ground clearance has been neglected due to some difficulties encountered when attempting its calculation. Nevertheless, this stability derivative was found to be negative in the entire flight envelope, and this result is in accordance with what expected from a ground effect vehicle [96].

Validation of the roll stability is intrinsically connected to the validation of the height stability as the mechanism of the first is a direct consequence of the mechanism of the second. Validation of the roll controllability follows, instead, from the validation of the aerodynamic characteristics of the ailerons. Finally, the ballast system has been validated by experience, as it is a concept commonly used in the aeronautical industry.

Stability in yaw is provided artificially. The control mechanism, which employs rudders and differential thrust, is again a commonly used concept. Validation of the rudders' effectiveness follows from the validation of the rudders' aerodynamic characteristics. Validation of the differential thrust capabilities follows from the validation of the engines' characteristics.

Stability and control (guidance) in lateral direction is provided by the track by means of the bobsled cross-sectional shape and the banking angle at which the track is placed at the turns' location. This principle has been validated by analysing; nevertheless, the actual functioning needs to be tested with prototypes.

Lastly, the stability and control in the longitudinal direction have been addressed. This form of stability, which involves the balance between thrust and drag, has been easily validated through analysis, experience and comparison.

20.2.3. Structures

In the future, further verification can be done with the use of programs based on Finite Element Methods. This can help with verifying the overall structure instead of only the sub components and sub calculations separately.To validate the structure a test until failure can be performed on a prototype of the structure.

20.2.4. Landing Gear

The validation of the landing gear was mainly focused on validation through commonly used parts/systems in common aircraft. For the design of the tires, a choice was made based on aircraft tires which are widely used in aircraft nowadays. Furthermore, for the disc brakes, carbon as the disc material is a common material used for aircraft disc brakes. Also, for the wheel motor, requirements were set up and a motor example of what could be used in AeroCity was given and validated that the design is indeed a realistic option.

20.2.5. Performance Calculations

The performance of the full vehicle can only be validated by demonstration of the full vehicle on the designed track. During each stage in the design, the total vehicle performance should be checked by analysis if it meets the requirements. This can be done by adding validated data from subsystem prototypes in the analysis calculations.

20.2.6. Propulsion

The validation of the propulsion subsystem can be divided in three main parts: the effect of the duct on propulsive efficiency, the fan design and the motor sizing.

Firstly, the effect of the duct on propulsive efficiency. The knowledge that a duct could provide a higher propulsive efficiency by reducing tip losses and interference between several propellers mainly comes from literature such as Raymer and Roskam [30, 49] and from the bachelor program taught at the faculty of Aerospace Engineering of the Delft University of Technology. Furthermore, several design parameters such as the inlet and exhaust velocity of a duct were taken into account during the fan performance calculation in the last iteration of the fan sizing. This method has also been validated as it is lecture material from the AE2230-II Power & Propulsion course [97]

Secondly, the propeller design of the first two iterations have been validated in a similar fashion by using known and already validated data from Hamilton [3] and a calculation method presented in a Masters course of the FPP masters track [41]. The fan design of the third iteration however, is based on a method taught during the power and propulsion course [97].

Lastly, the motor sizing has to be considered. The base of the motor sizing and selection comes from the fan design as this introduces a shaft power and RPM requirement. The sizing is done such that the motors would be able to

provide sufficient power and this is based around the specifications listed on the manufacturers websites [4, 42]. Therefore this data is considered to be validated. As for now, there is still a discrepancy as the listed RPM of these motors does not correspond with the required RPM. It is however stated that during the further development of this concept this will be validated by optimising an electric motor for these requirements.

20.3. Product Verification

The product obtained at the end of the design process has to fulfil the requirements. To check if the designed product is on track to comply with these requirements, four possible methods can be employed:

- **Inspection:** inspection of the design documentation of the product to show compliance with the requirement.
- **Analysis:** mathematical models and numerical simulations are established to investigate whether the system performance is sufficient to fulfil the specified requirements.
- **Demonstration:** a prototype is built and put in real life condition, where its ability to meet some specific requirement can be observed and evaluated.
- **Test:** By means of specialized equipment and in controlled conditions, a representative model of the product (or part of it) is tested for compliance with requirements

Table 20.1: Verification of the system's requirements by means of inspection, analysis, demonstration, and testing.

Inspection	Analysis	Demonstration	Test
FR-IS-01	FR-PWR-02	FR-PWR-01	FR-SaC-02
FR-IS-03	NFR-S-07	FR-SPE-01	FR-NO-01
FR-IS-04	NFR-S-08	FR-SPE-02	
FR-IS-05	NFR-C-02	FR-SPE-03	
FR-OWC-01		FR-SaC-03	
NFR-S-01		FR-IS-02	
NFR-S-04		FR-JT-01	
NFR-S-05		FR-JT-02	
NFR-S-06		FR-MT-01	
NFR-C-01		FR-MT-02	
NFR-C-03		FR-SFT-01	
NFR-C-04			
NFR-R-01			
NFR-SaR-01			
NFR-SaR-02			
NFR-SaR-03			
NFR-SaR-04			

Each system requirement has been categorised in Table 20.1 according to its method of verification. It can be noticed that most of the requirements will be verified by inspection and demonstration. Nevertheless, these types of verification procedures can only be performed in the advanced stages of the development, as system prototypes are required. Therefore, as product verification is deemed to be a valuable tool for keeping the design process focused on the requirements, verification by means of analysis has been performed on all the requirements at the actual stage of the design.

A compliance matrix will be constructed and displayed in chapter chapter 24 to confirm that the design meets all system requirements mentioned in chapter 5.

21 Risk Management

This chapter discusses the project risks and the environmental risks involved in the AeroCity project. Initially, the risks are identified and their consequence and probabilities are determined. Subsequently, one risk map is created for each of the two risk categories. Finally some strategies to mitigate the risks are illustrated. The focus is placed on the risks that are relevant for the AeroCity system. This chapter is an update of the risk analysis that had been performed in the Midterm report [8].

21.1. Identified Risks

The kinds of risks that are encountered during the system development and operations can be divided into two main branches:

- Project risks: technical risks and performance uncertainties associated with any development or production process. These risks can interfere with the system's performance, cost and schedule objectives.
- Environmental risks: environmental, health and safety risks associated with the production, operation and disposal of systems. These risks have adverse impacts and compromise the sustainability of the system.

21.1.1. Project risks

Project risks are:

1. **High infrastructure cost** - The large width of the double track poses unknowns on the land acquisition cost.
2. **Lack of government support** - The high infrastructure cost makes governmental financial support necessary.
3. **Lack of public support** - The significant environmental footprint of the large infrastructure can result a in lack of public support.
4. **Construction delays** - Construction delays can result in serious loss of competitiveness as alternative systems could seize the market.
5. **Unexpected vehicle dynamic behaviour** - Because of the originality of the concept, the vehicle dynamics is not yet known.
6. **Optimistic lift and drag estimations** - Incorrect estimations of the vehicle aerodynamic characteristics would have a large impact on the design of several subsystems.
7. **Incorrect weight estimation** - Incorrect estimations of the weight of the subsystems could have a significant impact on the vehicle centre of gravity position and consequently on the vehicle stability and controllability.
8. **Underestimation of the energy requirements** - Underestimating the energy required by the vehicle's subsystems would require the redesign of the battery pack, with serious consequences on the vehicle performance.
9. **Incorrect loads estimation** - Failure to estimate the correct external loads (landing, centripetal or longitudinal accelerations) or internal loads could lead to the necessity of redesigning the airframe and/or landing gear.

21.1.2. Environmental risks

10. **Track obstruction** - The presence of a medium sized object (4-15cm) on the track would require the interruption of the system operations.
11. **Power failure** - A power failure would require the vehicle to decrease its cruise speed or even stop. This could lead to track obstruction and consequently to traffic congestion.
12. **Autonomous control failure** - A control system failure would result in the incapability to travel airborne. This would result in a possible hard landing and in traffic congestion.
13. **Impact with an external body** - In the case of an impact with an external body the vehicle could suffer serious damage and the passengers could suffer injuries depending on the nature of the collision.
14. **Telemetry failure** - Telemetry should be present in order to ensure that the vehicle can be remotely controlled in case of autonomous control failure. In case both telemetry and autonomous control are not operational, the vehicle comes to a stop with obvious consequences on the passengers and the traffic.
15. **Ice/snow on the track** - In case that ice and snow accumulate on the track, the take-off and especially the landing phases become dangerous.
16. **Strong winds** - In strong wind conditions the stability and the controllability characteristics of the vehicle could be substantially reduced.
17. **Deflation of tyres** In the case the tyres of the landing gear wheels fail while the vehicle is airborne, the sideskirts could come in contact with the ground and the landing procedure would become uncomfortable and unsafe.

21.2. Risk Map

Table 21.1: Project risk map.

Severity	Consequences				Increasing likelihood				
	System performance	Market value	Production delays	Production cost	Extremely improbable	Improbable	Remote	Occasional	Probable
0	No reduction	No reduction	No delays	within budget					
1	Slight reduction	Slight reduction	Slight increase	Slight increase					
2	Minor reduction	Minor reduction	Minor increase	Minor increase				6, 7 9	8
3	Major reduction	Moderate reduction	Moderate increase	Moderate increase				4	
4	Questionable system efficiency	Major reduction	Major increase	Major increase		3	5		
	Questionable concept validity	Bankruptcy	Halt of production	Massive debts		2		1	

Table 21.2: Environmental risk map.

Severity	Consequences				Increasing likelihood				
	People	Assets	Environment	Reputation	Never happened before	Once per 35 years	Once per year	Once per month	Once per week
0	No injury or healt effect	No damage	No effect	No impact					
1	Slight injury or health effect	Slight damage	Slight effect	Slight impact				11	
2	Minor injury or healt effect	Minor damage	Minor effect	Minor impact			14	17 16	10
3	Major injury or healt impact	Moderate damage	Moderate effect	Moderate impact			15		
4	Up to 3 fatalities	Major damage	Major effect	Major impact				13	
	>3 fatalities	Massive damage	Massive effect	Massive impact			12		

The risk is the product of the likelihood of the event and the consequence of the event.

The likelihood of the environmental risk events have been estimated by researching the frequency at which these events occur in railway and aircraft operation (depending on the subsystem). The consequence of the environmental risk events have been estimated considering the vehicle layout, the track shape and the nature of the vehicle operation. A risk map for the environmental risks can be seen in Table 21.1. The probability scale is divided into five steps from "Never happened before" to "Once per week" and the consequence scale is divided into five steps.

The likelihood and the consequences of the project risk events have been estimated by researching the frequency that these events occur in railway, aircraft and automotive industry (depending on the subsystem). A risk map for the project risks can be seen in Table 21.2. The probability scale is divided into five steps from "Extremely improbable" to "Probable" and the consequence scale is divided into five steps.

In the risk maps it is shown that a risk event can have consequences on different aspects. The severity of a risk event is not necessarily the same for every aspect: for example one event could have a large impact on the time schedule but no impact on the system performance. The overall severity of the risk event was determined to be the highest one.

Two risk events can have the same severity by having different consequences on different aspects.

21.3. Risk Mitigation

In this section all of the aforementioned risks will be reanalysed and a mitigation strategy will be developed to help reduce the probability and the severity of the risk events. The main philosophy consist of allocating scarce resources to the critical risk areas. These will then be placed in the mitigated risk maps (Table 21.3 and Table 21.4.

1. **High infrastructure cost** - Expensive track sections, involving tunnels and bridges or crossing densely populated areas, can be designed to be made by a single track serving both travel directions.
2. **Lack of government support** - The governmental support should be obtained by promoting the creation of an external committee tasked with the evaluation of the benefit of the AeroCity system for the public good.
3. **Lack of public support** - A research group should be created to investigate possible solutions to reduce the environmental footprint of the system's infrastructure.
4. **Construction delays** - Construction delays should be limited by increasing the total amount of working hours (more labour staff), or by employing more advanced construction techniques.
5. **Unexpected vehicle dynamic behaviour** - Dynamic tests should be given more importance than if the vehicle would be a conventional aircraft .
6. **Optimistic lift and drag estimations** - Extensive wind tunnel tests should be conducted to validate the optimistic aerodynamic characteristics obtained via CFD simulations.
7. **Incorrect weight estimation** - Reliable and accurate values for the subsystems weight should be computed. Proper contingency allowance values can aid in taking possible weight increases into account.
8. **Underestimation of the energy requirements** - Reliable and accurate values for the propulsion system parameters should be computed. Proper contingency allowance values can aid in taking possible decreases in performance of the energy provision and power and propulsion systems.

9. **Incorrect loads estimations** - Advance structural and flight dynamics analysis should be performed on the vehicle and prototypes should be tested as soon as possible in the entire flight envelope.
10. **Track obstruction** - The presence of medium sized objects (4-15cm) on the track must be avoided at all costs by placing nets or fences on the sides of the track.
11. **Power failure** - A complete power system failure can be partly mitigated by redundancy of the electrical connections. It can also be prevented by increasing the reliability by using parts that have been proven to be reliable.
12. **Autonomous control failure** - The autonomy of the vehicle can be compromised in case of flaws in the software, in the sensors or in the actuators. Software can be thoroughly tested in order to reduce the degree of uncertainty. The sensors and the actuators will be subject to routine maintenance and several levels of redundancy can efficiently mitigate this risk.
13. **Impact with external body** - This risk can be mitigated by continuous monitoring of the track (both from on-track and on-vehicle detection systems) and by implementing access restriction to the track area.
14. **Telemetry failure** - This item can easily be mitigated by adding a secondary communication system. This can translate with an addition of a backup antenna; this would re-enable any lost communication with the ground segment.
15. **Ice/snow on the track** - The sections of the track nearby the stations should have the possibility to be heated to prevent ice formation and snow accumulation.
16. **Strong winds** - The safest options for the passengers would consist in suspending the operations. For vehicles that are already travelling the safest option would be to stop the vehicle and to firmly place it on the ground as to prevent any associated damage with the severe weather. Depending on the gravity of the situation the vehicle could continue to travel on wheels at a properly reduced speed.
17. **Landing gear failure** The tyre should be made of an hardened rubber material with above average thickness. This measure will reduce the likelihood of tyre puncture and consequent deflation.

Table 21.3: Project risk map after mitigation.

Severity	Consequences				Increasing likelihood				
	System performance	Market value	Production delays	Production cost	Extremely improbable	Improbable	Remote	Occasional	Probable
0	No reduction	No reduction	No delays	within budget					
1	Slight reduction	Slight reduction	Slight increase	Slight increase					
2	Minor reduction	Minor reduction	Minor increase	Minor increase		8	6, 7 9		
3	Major reduction	Moderate reduction	Moderate increase	Moderate increase		4			
4	Questionable system efficiency	Major reduction	Major increase	Major increase	3	5	1		
5	Questionable concept validity	Bankruptcy	Halt of production	Massive debts		2			

Table 21.4: Environmental risk map after mitigation.

Severity	Consequences				Increasing likelihood				
	People	Assets	Environment	Reputation	Never happened before	Once per 35 years	Once per year	Once per month	Once per week
0	No injury or healt effect	No damage	No effect	No impact					
1	Slight injury or health effect	Slight damage	Slight effect	Slight impact		17			
2	Minor injury or healt effect	Minor damage	Minor effect	Minor impact		14 15	16 10		
3	Major injury or healt impact	Moderate damage	Moderate effect	Moderate impact					
4	Up to 3 fatalities	Major damage	Major effect	Major impact			13		
	>3 fatalities	Massive damage	Massive effect	Massive impact		12			

21.4. Technology Readiness Level

The technology readiness level (TRL) of the AeroCity system is on average high for what concerns the operations, medium for what concerns the infrastructure and low for what concerns the vehicle.

Regarding the operation, a high level of similarity with the train was ascertained. The largest difference is in the passengers limitation to freely choose their seating place and the limitations in the passengers' deambulation during the flight phases.

Regarding the infrastructure, a simple track structure is required. Nevertheless this structure is innovative and extensive tests and experimentation are required.

Regarding the vehicle, some similarities can be found with other WIG vehicles, but the use of sideskirts at a small distance from ground and the substitution of a conventional tail with a canard, makes the AeroCity vehicle concept far from a proven concept. The propulsion system is a full commercial application, while the power system is under development. The control system employs existing sensor and existing actuators. Nevertheless the wing rotation mechanism and the rudders and ailerons' effectiveness require validation. The landing gear system was designed by integrating existing components, by the integration itself is at a conceptual level. The remaining subsystems are all commercial systems with slight adaptation to ease the integration with the vehicle structure.

Te TRL level is expected to improve once the first complete prototypes are tested. To save on costs and time the test could also be conducted concurrently on the different unconventional subsystems.

For the evaluation of the TRL, 9 levels can be distinguished Figure 21.1 [98]:

Figure 21.1: Description of Technical Readiness Levels [99]

22 Sensitivity Analysis

In this chapter, the sensitivity of the design to a change in the driving parameters is discussed. In order to do so, first, the driving parameters of the design are identified and then the effect of changing them is described.

22.1. Driving design parameters

The driving parameters are identified in this section. The most important parameters that were considered during the design are:

- Cruise Speed
- Weight
- Aerodynamic Efficiency
- Vehicle Efficiency

22.2. Design Sensitivity

These various design parameters were very closely related and changing just one of these parameters would consequently affect the design of the vehicle. The following section will describe how changing these parameters will affect the performance of the AeroCity vehicle if the rest of the design would remain the same.

22.2.1. Cruise Speed

Depending on whether the cruise speed is increased or decreased, the vehicle will be affected in different ways. Increasing the speed will generate more lift if the shape and size of the vehicle remain the same. This can be adjusted by flying at a lower angle of attack. Considering that only the cruise speed changes and that the other design parameters stay the same, the way that the vehicle performance would be affected if the cruise speed was to be increase or decrease by 5% is summarised in Table 22.1.

As can be seen in Table 22.1, the increase in speed will increase the aerodynamic drag, which will increase the thrust and power requirement of the vehicle for cruise speed. This is also seen in the increase in overall energy consumption. Additionally, the lift over drag ratio goes down as the vehicle will fly at a less efficient speed. An added benefit to this would be that the journey time goes down.

Table 22.1: Effect of cruise speed deviation

Cruise Speed $[m/s]$	**Deviation** [%]	**Power Required** $[MW]$	**Energy Consumption** $[kWh]$	**Angle of Attack** $[deg]$	**L/D Ratio**	**Propulsive Efficiency** [%]	**Journey Time**
84.8	0	1.176	3680	2.75	25.5	80.0	2:11:16
89.0	+5	1.354	4077	2.58	24.0	81.5	2:05:32
80.6	-5	1.013	3366	2.88	26.9	78.5	2:17:40

As can be seen in Table 22.1, decreasing the speed would result in the vehicle not meeting the time requirement for the given route. Furthermore, it would have to fly at a steeper angle of attack in order to generate the same amount of lift. The lift over drag is increased since the drag decreases more than the added induced drag due to the higher angle of attack. Overall, except for the time requirement, which is only exceeded by two minutes if the speed decreases by 5%, the vehicle will still be able to perform its task and be able to transport passengers from Utrecht to Berlin. The only difference would be that the batteries would be closer to being fully drained, however, there would still remain some safety margin since the total battery capacity is 4.8 MWh and the total trip energy needed for the higher cruise speed would be 4.1 MWh. Increasing the battery size for a redesign could be considered, however, there is only limited space available and it would likely come at the cost of reducing the number of passengers slightly.

22.2.2. Weight

The weight of the vehicle is another important parameter and also has an effect on the acceleration, lift required, L/D ratio and energy consumption. With all other design parameters being constant, the way that the vehicle performance will be affected if the weight was to increase or decrease by 10% is summarised in Table 22.2.

For the case where the weight is increased by 10%, the vehicle will have to generate more lift and thus the lift coefficient will have to increase. This can be done by increasing the angle of attack. However, due to the added weight, the acceleration time is also increased. The added weight and higher lift produced as a consequence also increase the lift over drag ratio since the drag is not significantly increased by flying at a higher angle of attack. Thus

the vehicle would be flying at a more ideal lift over drag ratio. One drawback to this would be that the increase in weight also increases energy consumption, however, this is not increased significantly.

For the case where the weight is decreased, the acceleration time intuitively goes down. However, in order to still comply with the requirement to only accelerate at a rate of $0.1g$ the acceleration could be limited to stay below that value. Furthermore, less lift is required so the vehicle can fly at a lower angle of attack which also then decreases the value for the drag coefficient due to the lower induced drag. The total lift over drag ratio decreases and the energy consumption also decreases.

Table 22.2: Effect of weight deviation

Weight $[kg]$	**Deviation** [%]	**Acceleration Time** $[s]$	**Lift Coefficient** $[-]$	**L/D Ratio**	**Drag Coefficient** $[-]$	**Energy Consumption** $[kWh]$
36000	0	125	0.4986	25.5	0.0196	3680
39600	+10	133	0.5484	26.9	0.0203	3804
32400	-10	117	0.4487	23.5	0.191	3590

22.2.3. Aerodynamic Efficiency

The aerodynamic efficiency will be represented by the value for the lift over drag ratio. This value was varied by 10% and the results on the energy consumption and the required thrust can be seen in Table 22.3. An increase in aerodynamic efficiency will lead to less thrust required and lower energy consumption and the inverse is true for the case where the lift over drag ratio is decreased by 10%. This is very logical since a worse aerodynamic performance would mean that the vehicle would produce more drag at the same speed and thus a more powerful propulsion system would be needed in order to overcome the added drag. This would, of course, increase energy consumption.

In terms of battery capacity, the system would again not have a problem with coping with the increased power consumption. The design of the battery pack includes a margin for unexpected increased power consumption during the design and building of the vehicle and thus the power consumption of 4.0 MWh is not a problem for the designed battery, which has a capacity of 4.8 MWh.

Table 22.3: Effect of aerodynamic efficiency deviation

L/D Ratio	**Deviation** [%]	**Required Thrust** $[kN]$	**Energy** $[kWh]$
25.53	0	13.83	3680
28.08	+10	12.56	3307
22.97	-10	15.38	4048

The shaft power that can be delivered by the motors, is able to create 10.5 kN of thrust per engine for the current design of the propulsion system, which can be found in chapter 8. This means that with two engines, the vehicle will still be able to deliver the 15.4 kN of thrust that would be required for a 10 % decrease in aerodynamic efficiency.

22.2.4. Changing Vehicle Efficiency

The vehicle efficiency is defined as the efficiency from the electric energy in the batteries to the thrust delivered by the engines. This means it includes the propeller and duct efficiency, the efficiency of the motors, the battery and cable efficiency and the efficiency of the controller and DC converters.

A change in any of these efficiencies would have an effect on energy consumption and the required cooling. The total vehicle efficiency was varied by 5% and the result on the energy consumption and the cooling can be seen in Table 22.4. Of course, the decrease in efficiency results in higher energy consumption and a larger requirement for the cooling of the vehicle. Inversely, an increase in efficiency results in less energy consumed and less cooling required. The increase in power consumption is not as high as in the previous cases and thus battery capacity will again not be an issue. As for the cooling capacity, this can be simply increased by providing more power to the cooling system. This cooling system is described in chapter 9.

Table 22.4: Effect of vehicle efficiency deviation

Vehicle Efficiency [%]	**Deviation** [%]	**Energy Consumption** $[kWh]$	**Cooling Required** $[kW]$
69.3	0	3680	522
72.77	+5	3510	441
65.83	-5	3868	611

23 Production plan

In this chapter, the production plan (manufacturing, assembly, integration plan) is described. For this, a diagram is shown in Figure 23.1, to give a clear overview of the production plan for AeroCity. The core exists of a flow diagram, of which each individual block is broken down into more detail.

For this production plan, it was assumed that the production of the infrastructure of AeroCity is funded and made by the government.

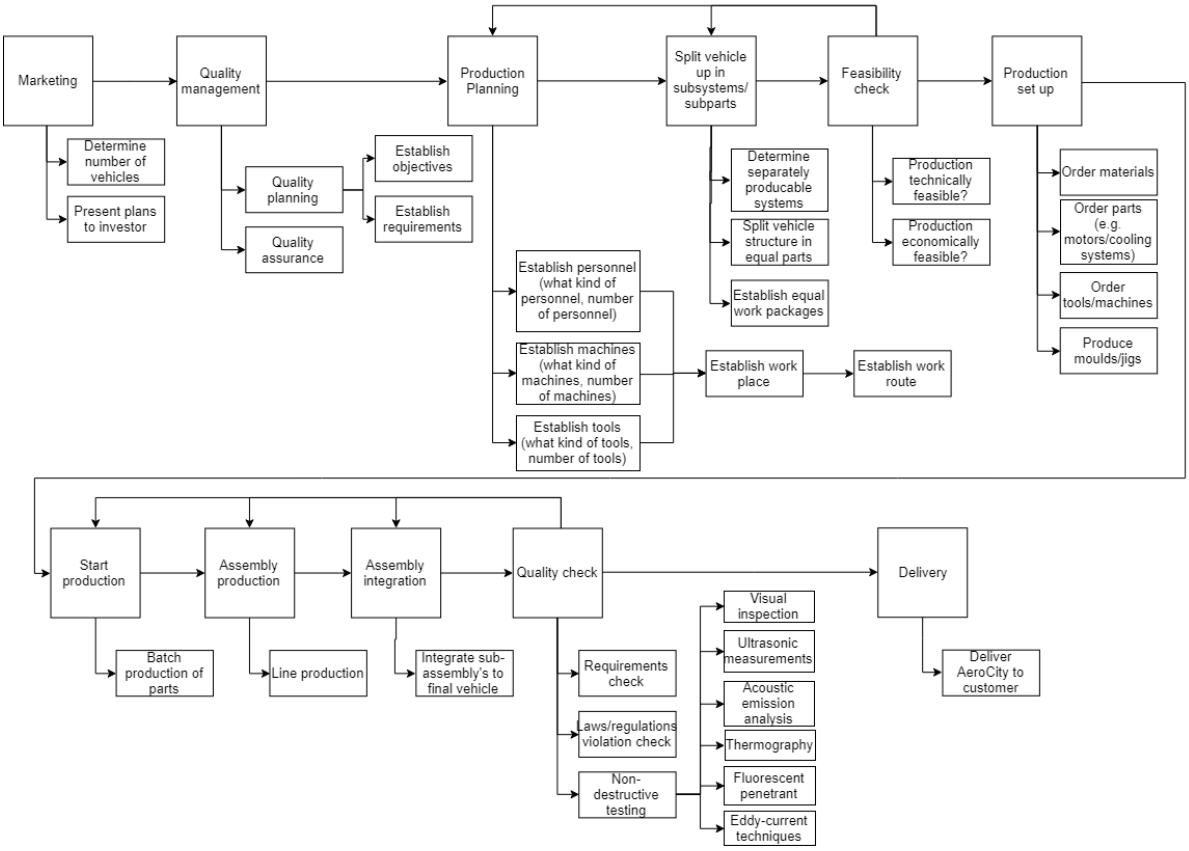

Figure 23.1: Production plan

Furthermore, in line with sustainability, lean manufacturing is implemented during the whole production process to reduce waste and emission to a minimum. This means that during the production process, all people who are involved continuously eliminate waste, with the goal of creating value. In this context, waste means anything that uses resources, but does not add any value to the final product.

24 Requirements compliance matrix

In this chapter, the requirements compliance matrix is given, in which the design values are compared with the actual values of the requirements. Moreover, the rationale on why some of the requirements were not met is given in a feasibility analysis.

24.1. Requirements compliance matrix

A requirements compliance matrix is a matrix in which the requirements that were set at the beginning of the design are analysed. The requirements that are met are indicated with a tick mark. Furthermore, the design value and the actual value of the specific requirement are given, if applicable. The requirements compliance matrix of the design of AeroCity is given in Table 24.1. The numbering of the requirements corresponds to the numbering used in chapter 5, in which all the requirements are stated.

24.2. Feasibility analysis

As shown in Table 24.1, some of the requirements were not met at the end of the design. The first requirement that was not met was FR-PWR-02: The CO_2 emissions shall be less than 25 % of TGV/ICE. The design value for this requirement was set to be 2.4 grams per kilometre per passenger, whereas the actual value for AeroCity was 28 grams per kilometre per passenger. However, it should be noted that for electricity that is used nowadays, still quite a lot of CO_2 is produced, which leads to the relatively high number for the AeroCity design. However, in 10 years, when AeroCity is expected to make its first ride, there is a big chance that AeroCity can make use of renewable sources of energy, thereby reducing the CO_2 to 0. Hence, when incorporating the technology that will be available in 10 years, the requirement is met.

The next requirement to be discussed is NFR-C-02: The break even time for the infrastructure shall not exceed 30 years. The infrastructure of the AeroCity will be subsidised by the government. AeroCity will have to pay a set amount of money to make use of the track, but this is not comparable to the cost of the infrastructure that the government will have to pay. Therefore, the infrastructure cost for AeroCity, from AeroCity's point of view, will most likely not reach the break even point, as the cumulative amount that AeroCity will pay will more than likely not reach the total cost. Meaning that the total amount paid will not reach the amount that was spent to design and construct the track. However, it will still be cheaper overall than constructing new high-speed train lines.

Table 24.1: Compliance matrix

Requirement	Met	Design value	Actual value	Can be found in chapter:
FR-PWR-01: The vehicle shall be electrically driven.	x			chapter 8
FR-PWR-02: The CO_2 emissions shall be less than 25% of TGV/ICE.		25% less than TGV/ICE (2.4)	28 for normal electricity, 0 for renewable	chapter 19
FR-SPE-01: The vehicle shall have a cruise speed of 305 km/h.	x	305 km/h	305 km/h	chapter 16
FR-SPE-02: The vehicle shall have a take-off speed of 200 km/h.	x	200 km/h	200 km/h	chapter 16
FR-SPE-03: The maximum taxiing speeds in the station shall be less than 35 km/h.	x	35 km/h	18 km/h	chapter 16
FR-SaC-01: THe vehicle shall be able to operate in extreme crosswind conditions up to 75 km/h.	x	75 km/h	75 km/h	chapter 12
FR-SaC-02: The vehicle shall be able to operate with nominal crosswind conditions of up to 65 km/h.	x	65 km/h	65 km/h	chapter 12
FR-SaC-03: The stability of the vehicle shall be done autonomsly.	x			chapter 12
FR-IS-01: The infrastructure shall be able to withstand snow.	x			chapter 6
FR-IS-02: The infrastructure will be able to drain up to 25 cm of rain per hour.	x			chapter 6
FR-IS-03: There will be a maximum altitude gradient of up to 4 %.	x			chapter 6
FR-IS-04: The station shall be accessible by other methods of public transportation.	x			chapter 6
FR-IS-05: The track surrounding the station (± 2km) shall be free of ice.	x			chapter 6
FR-JT-01: The journey time shall be less than 2 hours.		2 hours 15 min	2 hours 15 min	chapter 16
FR-JT-02: Boarding time will be on average less than 5 minutes.	x	5 minutes	5 minutes	chapter 17
FR-MT-01: There shall be one maintenance session per week that will last up to four hours.	x	One maintenance session per week for four hours	One maintenance session per week for four hours	chapter 17
FR-MT-02: There shall be one overhaul maintenance session every five years.	x	One session every five years	One session every five years	chapter 17
FR-NO-01: Noise levels during normal operations shall not exceed 120 dB.	x	120 dB	76.4 dB	chapter 19
FR-OWC-01: During normal operations, rainfall shall not exceed 25 cm per hour.	x			chapter 17
FR-SFT-01: Deceleration shall not exceed 0.981 m/s^2.	x	0.981 m/s^2	0.981 m/s^2	chapter 17
NFR-S-08: The net energy consumption per passenger per km shall be 25 % less than TGV/ICE.	x	0.051 (75% of 0.068)	0.046	chapter 19
NFR-C-01: The cost of the infrastructure and the ' vehicle combined shall be less than 50 % of TGV/ICE.	x	19 mld	22 mln vehicle, 9 mld for track.	chapter 18
NFR-C-02: The break even time for the infrastructure shall not exceed 30 years.	-	-	-	-
NFR-C-03: The designed track cost shall be less than 50 % of TGV/ICE.	x	Less than 24.2 million euro/km	13.85 million euro/km	chapter 6
NFR-C-04: The ticket prices are 50% of first class ICE tickets.	x	€ 89 (half of € 178)\	€ 44	chapter 18
NFR-R-01: The structural design shall comply with the airworthiness regulations, CS25.	x			chapter 10
NFR-SaR-01: The vehicle shall be designed with emergencies in mind.	x			chapter 17
NFR-SaR-02: The track shall have emergency escape paths.	x			chapter 17

25 Project design and development logic

The project design and development logic describes the activities that can be performed after the DSE is finished. For the design of AeroCity, a diagram was established to give a concise overview of the post-DSE activities. This diagram was also converted to a project Gantt chart, in which the activities were set to a time constraint. The diagram is shown in Figure 25.1:

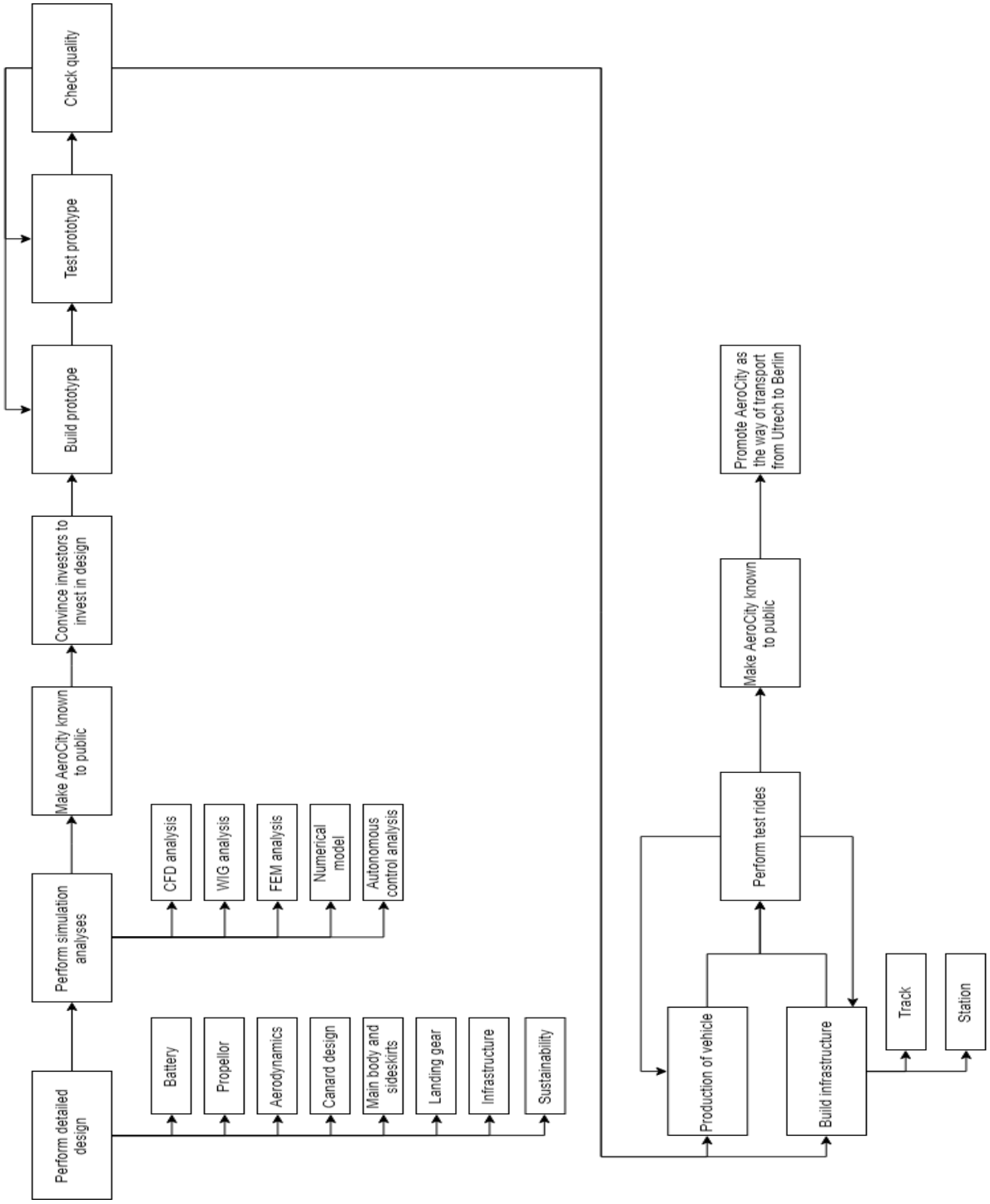

Figure 25.1: Post DSE project design and development logic

26 Project Gantt chart

The project gantt chart consists of the planning of the project design development and logic. For the post-DSE planning, the contingency time is implemented for each task. A 20% run out time was determined to cover any additional time spend on a task. This also means that the next task might start earlier than planned, since more time than needed is allocated to each task. This planning is shown in Figure 26.1:

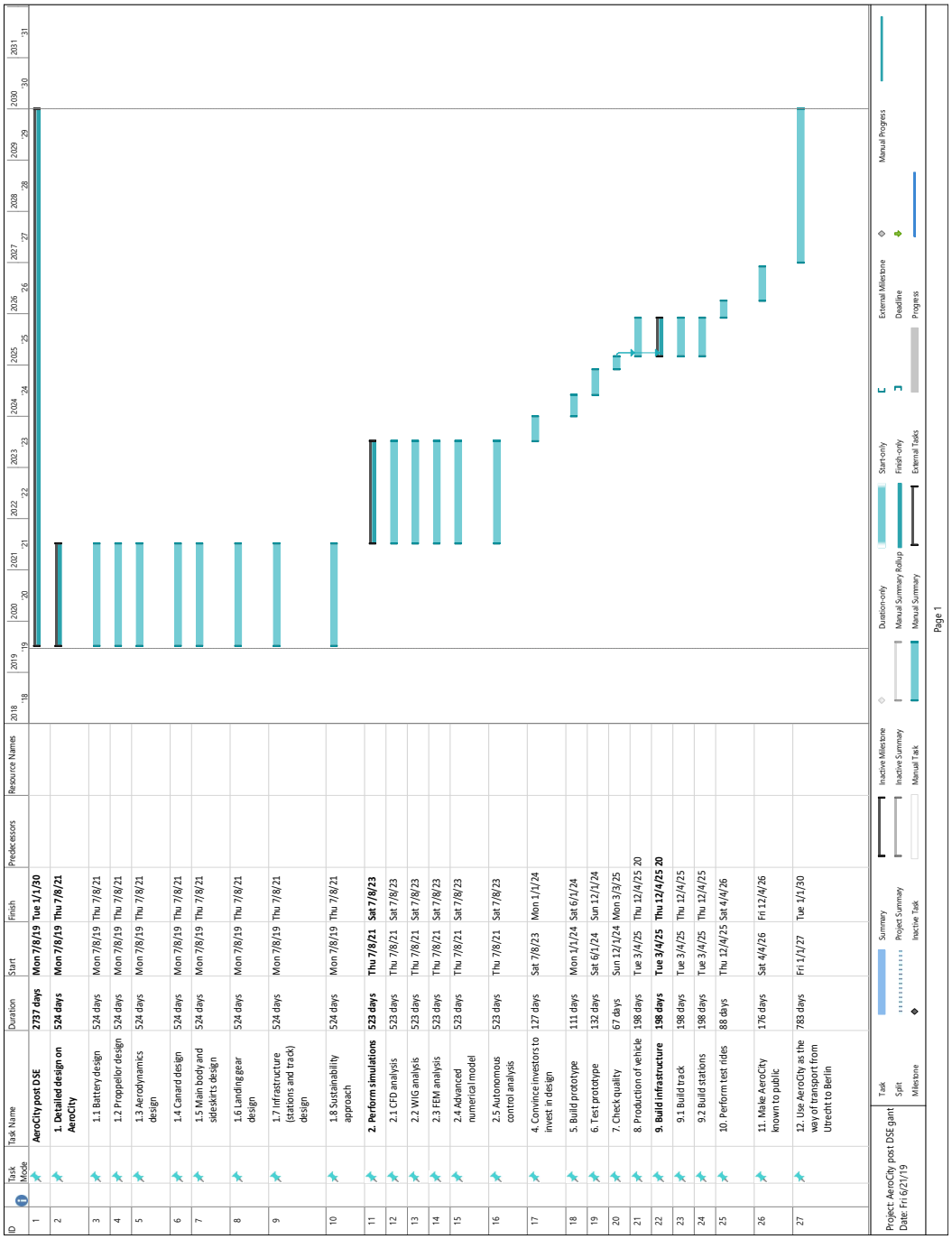

Figure 26.1: Project Gantt chart

V

Conclusion and Recommendations

Now that the project was introduced, the market gap was identified, the detailed design presented and a performance analysis on the final design was conducted, a conclusion is drawn in this part and some recommendations for future work on this project are given. This is to make sure that this report will help others to build on the work that was presented and to give some final remarks on the project.

27 Conclusion

For this report, the goal was to take a conceptual design and bring it to a final detailed design with a full market and cost analysis. The winning design from the previously done trade-off table was a podded fan vehicle, with swappable batteries, and a canard. Following this concept and knowing the requirements that were set at the start of the project, the design can be elaborated on and can be realised by performing various calculations and iterations. In this report, each aspect of AeroCity has been analysed, from the infrastructure of this new system to each subsystem of the vehicle as well as looking into the market potential for such a new concept.

The first part of this report discusses items that have been previously done in the Midterm, Baseline, and Project Plan report. Here the project objectives, market opportunity, and the final design concept are rediscussed, reminding the reader what has been previously done and what direction the project has been going into.

The second part of this report looks into the system requirements for AeroCity. More specifically this part of the report looks into a more detailed market analysis where it is seen that for a route between Utrecht and Berlin slight deviations can be made to both Duisburg and Hannover to significantly increase the market capacity. Additionally, the load cases during a normal operational phase are both discussed and shown. Lastly, a list of all of the system requirements is given. The user requirements are firstly listed, followed by functional requirements, and finished off with the non-functional requirements.

In the third part of the report, the majority of the design is discussed. Firstly the infrastructure of the track is discussed. Here a cross section of the track is given with additional discussion over what should happen when the track needs to cross over any obstacles or needs to be placed underground. Additionally, the placement of the stations is discussed, showing that the station in Utrecht will be placed in Utrecht-Lunetten, the station for the Rhine-Ruhr-Gebiet area will be placed underground in Duisburg, the station for Hannover will be placed underground close to the central station, and that the station in Berlin will be placed at Berlin-Westkreuz. Following this chapter, the aerodynamics of the vehicle is analysed. Here it can be seen how the main wing and the canard should be placed to achieve optimal performance. Following this section, the propulsion of the vehicle is discussed. It can be seen that, following iterations, only two engines will be needed and they will have a diameter of 1.4 m. This is sufficient to provide all the power that is needed for the operation of AeroCity. After the propulsion has been discussed, the power is looked into. Looking into the power it can be seen exactly which subsystems need power and how much power they will need in order to properly operate. This has been determined to be 83 kW, this is excluding the power required by the engines.
In the following section, the structure of the vehicle is analysed, here the required structural shape is determined and the different beams, thicknesses and their lengths are determined. Additionally here it is determined that aluminium will be used for the structure. Furthermore, the next section looked into the ground operations. More specifically how the vehicle will move around while it is on the ground. Following this is the stability and control section. Within this section, it is determined how to achieve stability within the six different degrees of freedom. After discussing the different technical subsystems, the traffic monitoring and control system is analysed and created. Here it is determined how the central computer will control the traffic and control the operations. After this, a small section discussing how the passengers will be laid out is done. It is here that it is determined that 116 passengers are able to fit in AeroCity in a comfortable manner. Additionally, the passenger experience is done, explaining all of the various amenities that an AeroCity passenger can expect. Lastly, in this part of the report, the system interaction is determined as well as the division of weight.

In the fourth part of this report, the performance is analysed. Firstly a performance analysis is done, looking into how will AeroCity accelerate and decelerate as well as how long each portion of the ride will take and just how much energy will be consumed during each portion. Here it is determined that the route can be completed in just under 2 hours and 10 minutes. After this, the operations of AeroCity is evaluated. Here it is seen that approximately 48 rides will be done in a day. Additionally, maintenance and safety are discussed here. Following this section, a detailed cost analysis is done for the vehicle and the infrastructure. It is determined that an AeroCity vehicle will cost 22 million euros, and the infrastructure will cost 9.4 million euros per km, this is 50% the cost of current HSR infrastructure cost. Additionally, it is determined that the cost of a ticket for AeroCity will be priced at €44, inclusive of tax. With those numbers, it was determined that AeroCity can have a yearly profit of 10 million euros. Furthermore, the next section describes the sustainability approach of the project. The noise estimations are calculated here and it is determined that AeroCity is quieter than a train by 4 dB. Additionally, the emissions are calculated and it is seen that AeroCity is more efficient than most forms of transportation including buses, small cars, and aircraft.

Following this, the procedure for the verification and validation for each subsystem that requires it is explained. This is important as to verify that all the work for each subsystem has been done is correct and there are no errors in the methods used to determine values. Next, a risk analysis is done. This looks into all of the potential risks that can occur for AeroCity and ranks them based on likelihood and consequence. Once the risks have been listed a way to mitigate the risks is listed and an updated risk map is given. Furthermore, a sensitivity analysis is done. This section looks into the sensitivity of the design and shows what happens if systems deviate from their expected nominal state. It was determined that if systems do deviate from the nominal state, there will be no major consequences and AeroCity can still operate normally. Following this, a production plan is created. This shows a potential plan for how AeroCity can be produced at a full-scale production line. Furthermore, the requirements from the start of the project are reanalysed and are shown to be complied with, or if not complied with, it is shown how much deviation there is from the original requirement. It is seen that the majority of the requirements have been met and some have exceeded the set requirement. Lastly, the project design and development logic are done showing what the post-DSE activities are to continue this project successfully.

In the final part of this report, a small section is given that lists future recommendations. This shows that there are some issues in the design that can be fixed or further looked into, as well as some items that are different from the current design that has the potential to be even better but must be looked into more.

In the end, a lot of time, work, and effort has been done in this project. The final product has taken countless hours put in by each individual and it is believed, that given the time that was invested, the best result has been achieved. A visually stunning vehicle was created, one that offers a smooth ride, offers the best in terms of passenger experience, and is fully sustainable, running fully on electric power. This is a vehicle that met all of its design goals and more. This vehicle has a cruise speed of 305 km/h, a range of over 650 km, and can carry 116 passengers. This vehicle has met all of its driving requirements, namely being electrically driven, a travel time of under 2 hours and 15 minutes, being quieter than a train, being more efficient than a train, and having cheaper infrastructure than that of high-speed rail. With all of these requirements having been met it is believed that the best possible design will be presented to the jury at the 2019 DSE symposium and that this option will be more than successful come 2027.

28 Future Recommendations

.

28.1. Market Analysis

The market for AeroCity has been sized for the direct Utrecht - Berlin route. As some AeroCity vehicles will also stop in Duisburg and Hannover it is likely that in the end the amount of potential customers will be higher. However, only the direct AeroCity is satisfying the 2h15m time requirement and therefore it is the most important. As a result it is chosen to size the market according to the direct AeroCity route.

Additionally, the introduction of this new travel mode will normally yield an additional increase in the current total market size. For example, people who are currently not travelling along this route will do so due to a faster commute. It is possible that the option to travel with AeroCity will enable people to work in Berlin but to live in Utrecht. This phenomenon is known as market stimulation. However, in the case of AeroCity, it is rather difficult to come up with an exact number as it is driven by numerous factors. The market stimulation factor is inversely proportional to the original market size and can range from low to multiple times the current market size. [2]

Hereby, a recommendation is given to perform further research into market simulation for AeroCity as well as including the stop in Duisburg and Hannover.

28.2. Infrastructure

For this project, a substantial amount of work has been put into infrastructure. As this is a new concept, there is not much previous work into how such a track should work or look like. However, work has been done and the track has been designed and should be more than sufficient to handle the AeroCity vehicle during normal operations. However, there are still additional things that could be done to improve the infrastructure and to make it more viable for future production.

One of the first recommendations is to perform further research into concrete. For example, analyse the life cycle, see how it degrades over time and what the main factors contributing to degradation are, as well as looking into how concrete can misalign itself over time. These items are important as the track is made from concrete and it is thus of integral importance to see how concrete behaves over time and how to further ensure that one can control concrete to not deviate from its original plan. Further research into the route and how the route will be, would also be recommended. Only a preliminary assessment of the route was within the scope of this report. However, to get a better idea of distances, curves, the amount of viaducts needed, etc, a more detailed analysis should be done. This would preferably be done with the help of both the Dutch and German government as they would have the most insight. Therefor, they can provide the best information. Moreover, they have the most control over the land that would be used for this project. Another item that should be looked at is how to better create a tunnelled station. As AeroCity has two tunnelled stations, in both Duisburg and Hannover, it is quite important to see how the layout should be for such a station and how these underground stations can interact with the existing above ground rail stations. Additionally, it should be looked into how much time and difficulty there is with making these underground stations while at the same time minimising impacting the above ground rail station. Lastly, a detailed research plan should be produced by a team of civil engineers to see what a production plan could look like and how ground works should be done to ensure that there will never be any issues with the track.

28.3. Aerodynamics

From a purely aerodynamic point of view, the AeroCity vehicle designed in the present work is not optimised for the cruise condition. Table 7.1 highlights how the L/D ratio is substantially higher at take-off, rather than in cruise condition. It is at high lift coefficient values that the wing finds its maximum aerodynamic efficiency. Unfortunately, by constraining the wing surface area to the payload capacity, these high lift coefficient values, and corresponding high L/D ratios, are obtained at relatively low cruise speeds. One option to increase the aerodynamic efficiency would be to develop an airfoil capable of providing a high L/D ratio at low lift coefficient values. Nevertheless, the effectiveness of this approach is dubious, as the extreme ground effect mechanism, on which this concept is based, is conceived to be most effective at high lift coefficients. Another possibility would be to increase the wing loading, by decoupling the wing size from the payload capacity. This would allow cruising at higher velocities with a high lift coefficient, and consequently, at a high L/D ratio. The challenge would then be to obtain even higher lift coefficients for take-off and landing, or, equivalently, increasing the take-off and landing speed.

With respect to the aerodynamic model, the recommendations given by Martijn van Sluis in his thesis [27] are shared. In particular the effect of the track side walls should be investigated.

28.4. Stability & Control

The most relevant addition to the stability and control of the AeroCity vehicle concept is without doubt the canard. The necessity of a system able to control and counteract the large shifts in the wing's longitudinal centre of pressure position with angle of attack was undeniable. Although the addition of a canard was the preferred choice, three other options are possible viable solutions; a tail, a ballast and elevons. The advantages and challenges that these alternatives entail are described in the Midterm Report [8].

The sideskirts' small ground clearance limits the allowable disturbances on the pitch angle substantially. A solution would be to employ movable sideskirts which can be rotated, extended, or retracted as to avoid contact with the ground and, at the same time, remaining close to it.

The height stability for the main wing body has already been studied by Nouwens in his thesis [17]. Nevertheless, the addition of the canard introduced uncertainties in the vehicle aerodynamics and consequently complicated the entire vehicle height stability analysis. It is therefore strongly suggested to perform, when possible, a CFD analysis.

Yaw and roll control are currently obtained by means of rudders and ailerons. Obviously these surfaces have an undesired contribution to the zero-lift drag. A more efficient alternative could be provided by rotating the engine ducts (thrust vectoring); this solution would satisfy the control requirements without any drag penalty.

Finally, significant effort should be channelled into the lateral stability and control, to ascertain if the passive guidance, provided by the track cross-sectional shape, does indeed behave as expected.

28.5. Structure

For further research, it is recommended to look further into the optimisation of the components. First of all, the ratios of the I beams could be optimised in terms of weight. Moreover, more elaborate calculations on the influence of the crosswinds on the structure should be done. Also, the materials could be investigated in more detail. In this report, it is chosen to use aluminium due to the high manufacturing cost and the lower weight benefits for quasi-isotropic composites. However, a lot of research is conducted on the production methods and properties of composites. Therefore, it is expected that in the future composites will be used more in structural elements and therefore this material could be useful in the weight optimisation process.

The stiffness of the structure could be increased by making a rigid connection between the main wing and the sideskirts. To still allow a change in angle of attack, the lower part of the structure must have retracting and extending aerodynamic surfaces to keep the ground clearance constant. This would also require the landing gear to be retractable and low friction first points of impact to be added.

Additionally, to increase the vehicle's pitch angle allowance, the same recommendation can be made. The movable aerodynamic surfaces could be actively controlled to keep the ground clearance constant.

28.6. Landing gear

For the optimisation of the landing gear placement, the static load case was assumed to be the highest. However, the load case in landing might be higher for either forward or aft wheels, so this has to be looked into. Also, additional loads on the wheels due to side wind have been neglected, which can be a topic for further research.

The wear of the tires has not been taken into account in the design of the AeroCity. AeroCity has a higher frequency of landing, but is expected to land a lot smoother than conventional aircraft. Therefore, it is nearly impossible to estimate the wear of the tires. This certainly has to be looked into for further research, since the implications of this are uncertain.

For the shock absorbers, an impact speed of 1.82 m/s (6 ft/s) was assumed. However, it is not even physically possible to reach such a high vertical velocity (unless a force from above pushes the vehicle down). If the vehicle would undergo a free fall of 3 cm (the distance between the wheels and the ground) the maximum vertical speed would be approximately 3 times as small as 1.82 m/s. Therefore, a more detailed analysis is needed to precisely determine the required shock damping.

The pre-spinning of the wheels is something that is not actually used in conventional aircraft. It works in theory, however, since it is not used (yet) in aircraft, a detailed analysis should be performed on pre-spinning, and sufficient testing should be done.

28.7. Cost

When considering costs, a lot of time and effort was put into calculating the infrastructure and the vehicle costs. However, the main way that costs was calculated was by comparing it with either high-speed rail or with aircraft. This is a great way to have a basis, however, for the future, it is recommended to hire an expert from within the field. This can create a better and more accurate estimate which will help better estimate the costs. Additionally, it is recommended to see if there are any areas in which costs can be saved. This can either be by producing the track in a different way, or by seeing if tunnelling or viaducts can be eliminated.

28.8. Sustainability

The sustainability considerations for the future can be improved upon in a number of different ways. One place of improvement would be the noise model, which currently still relies on an interim fan noise prediction method. For a more detailed noise analysis, advanced noise modelling software could be used and as a final test, a real world model of the fans should be put in a test set up and the noise should be measured. Additionally, considerations regarding the material choices could be improved, especially with respect to the materials chosen for the structure of the vehicle.

28.9. Propulsion

For the propulsion subsystem the recommendations can be split into five parts: The duct design, the fan design, the motor design, the aerodynamic interference and the operating points.

For the duct design, a more in depth analysis could be done on the inlet and nozzle design. As for now, an inlet and nozzle efficiency of 95 % have been assumed but more work could be done on how the inlet and nozzle shape influence their efficiencies at the operating conditions of the AeroCity vehicle.

Secondly, the fan design could be looked at in more detail as well. For this initial design a fan efficiency of 90 % has been assumed. This, combined with the inlet and nozzle efficiencies, resulted in a fan pressure ratio of 1.062 for the required operating case but did not yet result in a more detailed physical design of the fan blades. A suggestion would be to use a open-source program like Xrotor to develop a slightly more detailed fan design, which was not performed in the current design due to time constraints.

Furthermore, the motor design can be looked at in more detail as well. As for now the design is based around existing, of the shelf, state-of-the-art electric motors for aviation. These could already provide the required shaft power but are not optimised for this design in terms of rotational rate and size. As both Yasa and Magnix state on their website that they also provide custom solutions, a more optimised electric motor could be designed for the AeroCity vehicle.

As for the aerodynamic interference, more work could be done on the effect of the accelerated air in front and after the motors with respect to the main wing. Also the inlet conditions now assume a free flow velocity of 84.8 m/s that is perfectly in line with the motors. This is something which is not necessarily correct as the main wing is relatively large and will deflect the flow to a certain extent.

Lastly, the propulsion system is now optimised for the cruise condition, with a redundancy for acceleration, and has initially only been analysed at the cruise and at the take-off condition. At the very end of this project however, a small analysis has also been performed at every acceleration point in which the required thrust and velocity were taken into account. From this is was clear that with the current design the vehicle would not be able to accelerate as desired. Possible solutions would be to increase the fan diameter, optimise the fan design for a higher efficiency or to accelerate at a lower rate than 0.1 g. Therefore a further iteration is required, which could not be performed anymore within the timefram e of the DSE project.

28.10. Cooling

As for the cooling, more work could potentially be done on the sizing of the coolant lines, the radiator and the air inlet. This sizing mainly depends on the temperature difference between the coolant and the heat source, something of which the analysis was outside of the scope of this project.

Bibliography

[1] Algemene Rekenkamer. Hogesnelheidheidslijn-zuid: een rapportage in beeld, June 2014.

[2] SEO Amsterdam. *Market stimulation of new airline routes.* , 2017.

[3] Windsor LocksHamilton Standard. Generalized method of propeller performance estimation 1961-1963. https://hdl.handle.net/2144/10454, 1961. Last accessed on 13/06/2019.

[4] Products of today | empowering the future of flight. https://www.magnix.aero/products/, .

[5] Sinamics dcm dc converters. https://w3.siemens.com/drives/global/en/converter/dc-drives/sinamics-dcm/sinamics-dcm-dc-converter/Pages/sinamics-dcm-dc-converters.aspx, .

[6] Marcus F Heidmann. *Interim prediction method for fan and compressor source noise.* , 1975.

[7] Carboncure technologies. https://www.carboncure.com/, . Last Accessed on 23/06/2019.

[8] Group S02. Aerocity: Next generation high speed transportation, 2019.

[9] High-speed lines in europe, 2017. https://en.wikipedia.org/wiki/High-speed_rail_in_Europe#/media/File:High_Speed_Railroad_Map_of_Europe.svg, . Last Accessed on 30/4/2019.

[10] JRC Eurostat. Geostat, population grid 2011, .

[11] Utrecht centraal to berlijn hbf. https://www.nsinternational.nl/nl/treintickets#/NLUTC/DEBHF/ob/20190703?pax=A, . Last accessed on 28/06/2019.

[12] Ice international. https://www.nsinternational.nl/en/trains/ice-international, 2019. Last Accessed on 29/04/2019.

[13] Aerocity dse baseline report (ae3200), 2011.

[14] watkosteenauto.nl. Wat kost een auto per km? https://watkosteenauto.nl/wat-kost-een-auto-per-km/, 2019. Last Accessed on 24/06/2019.

[15] Gevolgen van winters weer. https://www.ns.nl/over-ns/seizoenen/winter/wat-zijn-de-gevolgen-van-winters-weer.html, . Last accessed on 28/06/2019.

[16] R. Dollevoet L. Houben A. Scarpas, S. Erkens. Weg- en railbouwkunde, 2015. Last accessed on 17/06/2019.

[17] Nouwens A.T. Aerodynamic performance and stability analysis of aerocity. Delft University of Technology, 2011.

[18] D. Nilsson F. Lundstrom, J. Ahlfont. The effect of raised walkway design on evacuation behaviour in rail tunnels. https://bit.ly/31paRIH, 2014. Last accessed on 07/06/2019.

[19] B. Yun J. Hong Wang. Concrete tunnel - an overview. https://www.sciencedirect.com/topics/engineering/concrete-tunnel, 2018. Last Accessed on 23/06/2019.

[20] Guideline for design of road tunnel. https://www.wsscwater.com/files/live/sites/wssc/files/pipeline20design/C-26-2015.pdf, 2017. Last accessed on 05/06/2019.

[21] B. Singh and R.K. Goel. *Engineering Rock Mass Classification.* Elsevier, 1 edition, 2011. ISBN 9780123858788.

[22] How are we reducing the cost of tunneling? https://www.boringcompany.com/faq, 2019. Last accessed on 05/06/2019.

[23] SBahn Berlin. Suburban and underground trains, regional train. https://bit.ly/30ScMVT, 2018.

[24] A. Jeannot. Les technologies des trains a grands vitesse. http://sciences-en-ligne.net/news/item/173, 2019. Last accessed on 07/06/2019.

[25] Demographia. Demographia world urban areas. http://www.demographia.com/db-worldua.pdf, . Last accessed on 14/05/2019.

[26] G. Harris. Technical memorandum: Alignment design standards for high-speed train operation. https://bit.ly/2F6jwq4, 2009. Last accessed on 13/06/2019.

[27] M. van Sluis. A numerical investigation into the aerodynamic characteristics of aerocity, Mar 2017. Last accessed on 20/05/2019.

[28] Hoerner S. F. Fluid-dynamic drag, 1965.

[29] Dr. Jan Roskam. *Part IV: Layout Design of Landing Gear and Systems.* Darcorporation, 1989.

[30] Dr. Jan Roskam and Dr. Chuan-Tau Edward Lan. *Airplane Aerodynamics and Performance.* DARcoroporation, 2 edition, 1997.

[31] Daniel P Raymer. *Aircraft Design: A Conceptual Approach.* AIAA, 3 edition, 1999.

[32] Frederick w. lanchester, contra-props. https://bit.ly/2MWh4ZI, . Last accessed on 13/06/2019.

[33] Antonov an-70 transport / cargo aircraft. https://www.airforce-technology.com/projects/antonovan70freighter/, . Last accessed on 13/06/2019.

[34] Tu-95 bear (tupolev). https://www.globalsecurity.org/wmd/world/russia/tu-95.html, . Last accessed on 13/06/2019.

[35] Deng S. and Ren Z. Experimental study of a ducted contra-rotating lift fan for vertical/short takeoff and landing unmanned aerial vehicle application. *Journal of Aerospace Engineering*, 232(16):3108–31175, 2018. doi: 10.1177/0954410017731441.

[36] Mieloszyk J., Galinski C., and Piechna J. Contra-rotating propeller for fixed wing mav: part 1. *Aircraft Engineering and Aerospace Technology: An International Journal*, 85(4):304–315, 2013. doi: 10.1108/AEAT-Jan-2012-0008].

[37] Mieloszyk J., Galinski C., and Piechna J. Contra-rotating propeller for fixed wing mav: part 2. *Aircraft Engineering and Aerospace Technology: An International Journal*, 85(4):316–324, 2013. doi: 10.1108/AEAT-Jan-2012-0009].

[38] Group 09. Design of a hydrogen-powered unmanned ultra large cargo aircraft, 2019.

[39] Kingan M., J. and Parry A., B. Acoustic theory of the many-bladed contra-rotating propeller: analysis of the effects of blade sweep on wake interaction noise, 2018.

[40] Vanderover J., S. and Visser K., D. Analysis of a contra-rotating propeller driven transport aircraft, 2000.

[41] Rao A., G. Ae3-020 aircraft design 020 aircraft design propulsion part propulsion part-2 - lecture slides, 2010. TUDelft Internal publication.

[42] Yasa electric motor solutions. https://www.yasa.com/, .

[43] Dual motor drive - técnico solar boat. http://tecnicosolarboat.tecnico.ulisboa.pt/opensource.php, .

[44] Licerion, sion power. https://sionpower.com/products/, .

[45] Leyden-jar battery technologies. https://leyden-jar.com/technology/, .

[46] Baes K., Kolk M, Carlot F., Merhabe A., and Ito Y. Future of batteries: Winner takes all? Arthur D Little: https://www.adlittle.com/sites/default/files/viewpoints/adl_future_of_batteries-min.pdf, May 2018. Last Accessed on 08/05/2019.

[47] Metabolic heat gain from persons. https://bit.ly/2XU42wN, .

[48] Cruden A. Sesm 6032 sustainable energy systems, resources and usage, lecture notes. University of Southampton, Internal Publication, 2014. Last Accessed on 20/05/2019.

[49] Daniel P. Raymer. *Aircraft Design: A Conceptual Approach*. American Institute of Aeronautics and Astronautics, 1999. ISBN 1-56347-281-0.

[50] T. H. G. Megson. *Aircraft Structures for Engineering Students*. Elsevier Science & Technology, 5 edition, 2012. ISBN 9780080969053.

[51] ASM. Metals handbook desk edition, 1990.

[52] C. Hibbeler, R. *Mechanics of Materials*. Pearson Education South Asia Pte Ltd, 9 edition, 2013. ISBN 9789810694364.

[53] C. Rans. Buckling, ae2135-i structural analysis and design, 2019. TUDelft Internal publication.

[54] Egbert Torenbeek. *Synthesis of subsonic airplane design*. Kluwer Academic Publishers, 1 edition, 1982. ISBN 9024727243.

[55] Michelin Aircraft Tire. Aircraft tire engineering data. https://bit.ly/2q2019K, 2015. Last accessed on 13/06/2019.

[56] S.F.N. Jenkins. Landing gear design and development. *Proceedings of the Institution of Mechanical Engineers*, 203, 1989.

[57] Norman S. Currey. *Aircraft Landing Gear design: Principles and Practices*. American Institute of Aeronautics and Astronautics, Inc., 1988.

[58] D.S. Chuang Y. Yang. Optimal design and control of a wheel motor for electric passenger cars. https://ieeexplore.ieee.org/stamp/stamp.jsp?tp=&arnumber=4033132&tag=1, 2019. Last accessed on 18/06/2019.

[59] Heerens N.C. Landing gear design in an automated design environment. Delft University of Technology, 2014F.

[60] A.f. Rumsey. Developments in train control worldwide. *11th IET Professional Development Course on Railway Signalling and Control Systems*, 2006. doi: 10.1049/ic.2006.0689.

[61] R. van Nes P.B.L. Wiggenraad I.A. Hansen, R.M.P. Goverde. Design and control of public transport systems, November 2008.

[62] European Aviation Safety Agency. Certification specifications for large aeroplanes cs-25. https://bit.ly/2L1d5Zg, 2007.

[63] Command and data handling system. http://starshipengineer.blogspot.com/2013/07/command-and-data-handling-system.html, 2013.

[64] Jacob Markish. Valuation techniques for commercial aircraft program design. , 2002. Last accessed on 17/06/2019.

[65] Campos J. and de Rus G. Some stylized facts about high-speed rail: A review of hsr experiences around the world. https://www.sciencedirect.com/science/article/pii/S0967070X09000109, 2009. Last accessed on 05/06/2019.

[66] West Gate Tunnel Project. Tunnel strata acquisition and compensation. https://bit.ly/2MEZHfx, 2017. Last accessed on 05/06/2019.

[67] M. Attina et all. Assessment of unit costs (standard prices) of rail projects (capital expenditure). https://bit.ly/2KHWERc, 2018. Last accessed on 07/06/2019.

[68] T. Vleeshouwer. The underground potential of the hyperloop system. https://hyperloopconnected.org/2018/04/the-underground-potential-of-the-hyperloop-system/, 2019. Last accessed on 05/06/2019.

[69] Scottish Executive Environment and Rural Affairs Department. Standard costs. https://www2.gov.scot/resource/doc/158202/0042819.pdf, 2001. Last accessed on 07/06/2019.

[70] black 90gsm weed stop cloth. https://bit.ly/2WD2o65, . Last accessed on 12/06/2019.

[71] J. H. Lever. Technical assessment of maglev system concepts. , October 1998.

[72] Ollivier G., Sondhi J., and Zhou N. High-speed railways in china: A look at construction costs. https://bit.ly/2XF9G5E, 2014. Last accessed on 12/06/2019.

[73] Infrastructure cost review: Technical report. https://assets.publishing.service.gov.uk/government/uploads/system/uploads/attachment_data/file/192589/cost_study_technicalnote211210.pdf, . Last accessed on 14/05/2019.

[74] Infrastructure cost review: Technical report. https://www.gov.uk/government/publications/infrastructure-cost-review, 2018. Last accessed on 04/06/2019.

[75] B. van Wee B. Flyvbjerg, N. Bruzelius. Comparison of capital costs per route-kilometre in urban rail. https://arxiv.org/pdf/1303.6569.pdf, 2008. Last accessed on 13/06/2019.

[76] M. Duursma. Vijf nieuwe stations, en dat mag wat kosten. https://www.nrc.nl/nieuws/2016/01/30/vijf-nieuwe-stations-en-dat-mag-wat-kosten-a1405207, 2016. Last accessed on 17/06/2019.

[77] R. Lenthall. Antwerp central: A project comparison for stuttgart 21. https://sightofthenavigator.wordpress.com/2010/08/25/antwerp-central-a-comparison-for-stuttgart-21/, 2010. Last accessed on 17/06/2019.

[78] Delft Hyperloop. The future of hyperloop. https://hyperloopconnected.org/2019/06/report-the-future-of-hyperloop/, 2019.

[79] Rail Delivery Group. Rail fares explained. https://bit.ly/2MUXYmI, 2018. Last accessed on 17/06/2019.

[80] Amadeus & Accenture. Trends in airline ancillaries. https://amadeus.com/documents/en/airlines/research-report/merchandising-17-trends-in-airline-ancillaries.pdf?crt=DownloadRequest, 2017. Last accessed on 18/06/2019.

[81] Group 02. Aerocity: Baseline report. Delft University of Technology, Internal Publication, 2018.

[82] ProRail B.V. Prorail jaarverslaag 2018. https://bit.ly/2RlaURk, 2018. Last accessed on 19/06/2019.

[83] Bahnstrompreisregelung ab 01.01.2019 für die rückfallversorgung. https://bit.ly/2WPZ8zB, Oct 2018. Last accessed on 21/05/2019.

[84] Paulo Henrique Trombetta Zannin and Fernando Bunn. Noise annoyance through railway traffic - a case study. https://www.ncbi.nlm.nih.gov/pmc/articles/PMC3896847/, Jan 2014. Last Accessed on 23/06/2019.

[85] Reducing railway noise pollution. http://www.europarl.europa.eu/RegData/etudes/etudes/join/2012/474533/IPOL-TRAN_ET(2012)474533_EN.pdf, 2012.

[86] Urban europe - statistics on cities, towns and suburbs - patterns of urban and city developments. https://ec.europa.eu/eurostat/statistics-explained/index.php?title=Urban_Europe_\T1\textemdash_statistics_on_cities,_towns_and_suburbs_\T1\textemdash_patterns_of_urban_and_city_developments&oldid=301961#The_growth.2Fdecline_of_urban_populations_and_their_economic_activity, Apr 2016. Last Accessed on 23/06/2019.

[87] Jeffrey Rissman. Concrete change: Making cement carbon-negative. https://www.greenbiz.com/article/concrete-change-making-cement-carbon-negative, Dec 2018. Last Accessed on 23/06/2019.

[88] sound propagation level calculator noise tools by mas environmental. http://noisetools.net/noisecalculator2?source=[4]&receiver=[1.8,2.3]&barrier=[1,0.8,1.3], .

[89] Co2 emissions from passenger transport. https://www.eea.europa.eu/media/infographics/co2-emissions-from-passenger-transport/view, Nov 2016. Last Accessed on 23/06/2019.

[90] Martinez P., J. P., and Sorba I., A. Energy consumption of passenger land transport modes. *Energy and Environment*, 21(6):577–600, 2010. doi: 10.1260/0958-305x.21.6.577.

[91] A comparative study of the environmental effects of rail and short-haul air travel. https://web.archive.org/web/20070426112620/http://www.cfit.gov.uk/docs/2001/racomp/racomp/a1.htm, Apr 2007. Last Accessed on 23/06/2019.

[92] Ice 3 (ms) br407 daten und fakten. https://www.bahn.de/p/view/mdb/bahnintern/services/im_zug/zuege_und_strecken/mdb_265167_ice3_br407.pdf, 2017. Last Accessed on 23/06/2019.

[93] William J. Rider, James R. Kamm, and V. Gregory Weirs. Procedures for calculation verification. https://cfwebprod.sandia.gov/cfdocs/CompResearch/docs/ProceduresCalculatioVerification Final.pdf, Jan 2011. Last accessed on 20/05/2019.

[94] Team S17. Aerocity: Design of the next generation high-speed transportation system, June 2011.

[95] S. Nasrollahi. Numerical and experimental aerodynamic performance analysis of aerocity. master's thesis, Jan 2014.

[96] Kim H. J., Chun H., and Jung K. H. Aeronumeric optimal design of a wing in ground effect craft., 2009. Journal of Marine Science and Technology, Vol. 14 , pp. 39 – 50.

[97] Melkert J. Ae2230-ii propulsion and power, lecture notes. Delft University of Technology, Internal Publication, 2018.

[98] Nasa|technology readiness level. https://www.nasa.gov/directorates/heo/scan/engineering/technology/tx-accordion1.html, .

[99] A brief refresher on technology readiness levels (trl). https://www.cloudwatchhub.eu/exploitation/brief-refresher-technology-readiness-levels-trl, .

[100] Ns dienstregeling 2019. https://nieuws.ns.nl/download/611967/spoorkaart2019-231351.pdf, 2019. Last accessed on 03/06/2019.

[101] Official multimodal map of the utrecht public transport network. http://www.inat.fr/map/utrecht/, 2016. Last accessed on 03/06/2019.

[102] Rail network map of nrw. http://www.fahr-mit.de/fahr-mit-en/fahrplan-und-liniennetz/liniennetzplaene/liniennetzplan-nrw.php, 2016. Last accessed on 03/06/2019.

[103] S-Bahn Hannover. Liniennetz der s-bahn hannover. https://bit.ly/2WuC2y9, 2017.

A Infrastructure Rail Networks

Figure A.1: Railway Network in The Netherlands, 2019 [100]

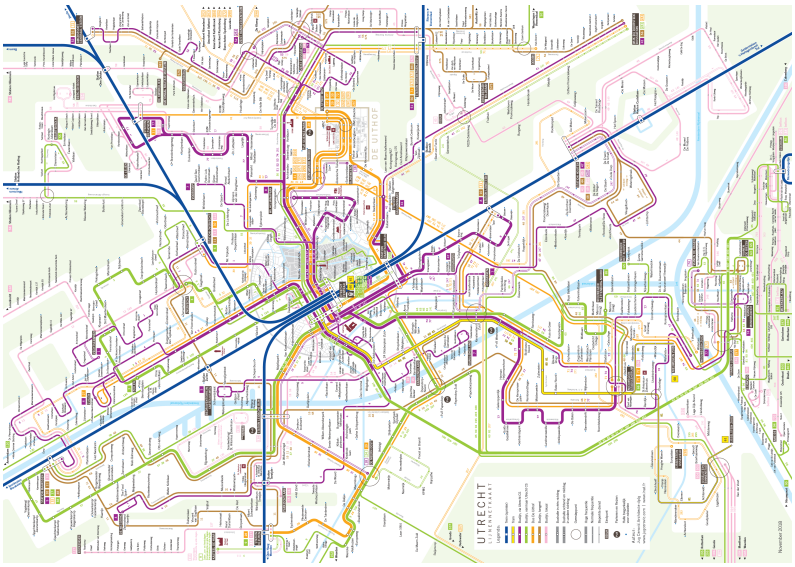

Figure A.2: Bus, Tram, Train Map Utrecht, 2016 [101]

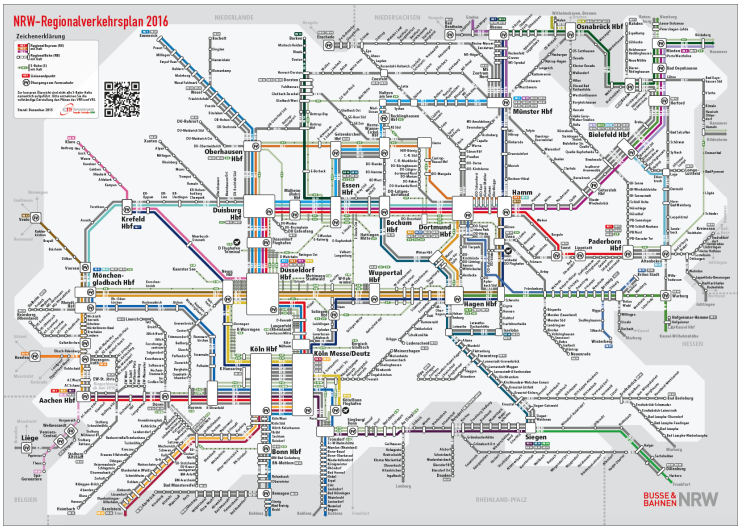

Figure A.3: Railway Network in the Rhein Ruhr Gebiet, 2016 [102]

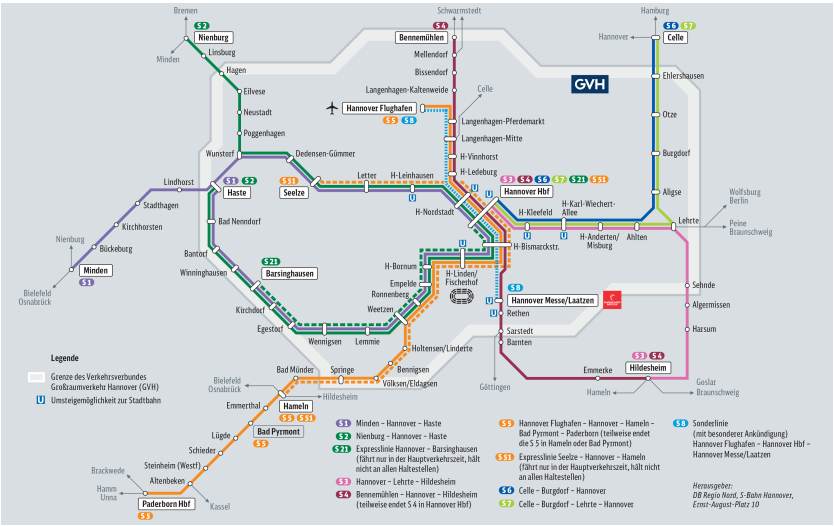

Figure A.4: Railway Network in Hannover, 2017 [103]

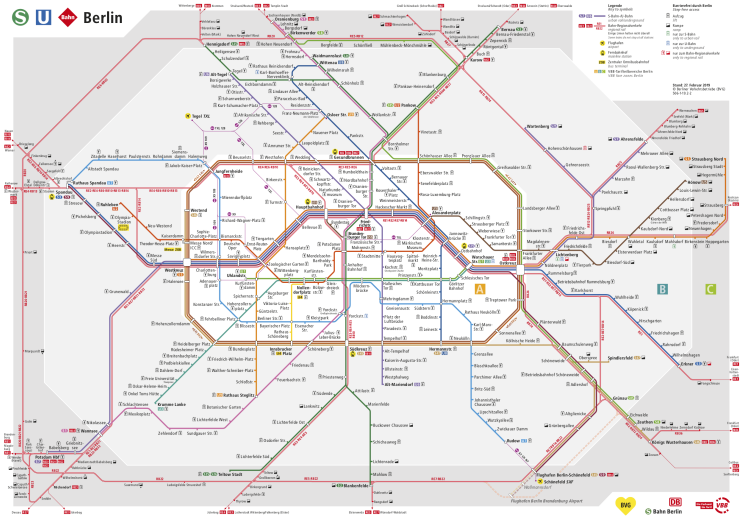

Figure A.5: Railway Network in Berlin, 2018 [23]

B Infrastructure Cost Breakdown

Cost Estimation Infrastructure 2019

On-ground Track Cost	[€/km]	M. €
Groundworks	1,000,000	1.00
Foundation Piles	100,000	0.10
Concrete Track	685,357	0.69
Steel Reinforcements	882,740	0.88
Manhours	2,000,000	2.00
Antiroot	3,762	0.00
Additional Cost (lighting, cables)	10,000	0.01
Total	**9,363,717**	**9.36**

Crossection Rail	2.74	m^2
Volume Rail	2741.43	m^3
Concrete Cost	250.00	€/m^3

Volume Reinforced Steel	54.83	m^3
Density Steel	8050.00	kg/m^3
Mass Reinforced Steel	441369.76	kg
Steel Cost	2.00	€/kg

Extra Cost for Viaduct	[€/km]		
	71,000,000	71.00	CNY 2010
	88,750,000	88.75	CNY 2019
Extra Cost Viaducts	**11,315,625**	**11.32**	€ 2019
Extra Cost for Tunnelling	[€/km]		
	42,000,000	42.00	GBP 2010
	51,240,000	51.24	GBP 2019
Extra tunnelling Cost	**57,542,520**	**57.54**	€ 2019

Station		Cost	
Station Utrecht Lunetten		€ 80	M. €
Station Dortmund		€ 320	M. €
Station Hannover		€ 320	M. €
Station Berlin Westkreuz		€ 80	M. €
Total		**€ 800**	M. €

Direct Costs	Length	Cost			
On Ground track	576	€ 5,393,500,741	€		
Track on Viaduct	30	€ 620,380,247	€		
Track in Tunnel	45	€ 3,010,780,645	€		
Total Direct Costs	**651**	**€ 9,024,661,663**	€	**€ 13,862,767**	Euro/km

Indirect Costs	Percentage	Cost	
Property charges (10%)	10%	€ 902,466,163	€
Engineering Charges (15%)	15%	€ 1,353,699,245	€
Cables and Ducts (3%)	3%	€ 270,739,849	€
Contractor Price (3%)	3%	€ 270,739,849	€
Total Indirect Costs		**€ 2,797,645,106**	€

Total Basic Estimate (incl. Stations)		**€ 12,622,306,739**	€
Unpredicted costs (10%)	10%	€ 1,262,230,674	€
Expected deviation (5%)	5%	€ 631,115,337	€

Total Investment costs excl. taxes		**€ 14,515,652,750**	€	**€ 22,297,470**	Euro/km
Taxes (21%)	21%	€ 3,048,287,077	€		

Total Investment costs incl. taxes	**€ 17,563,939,827**	€	**€ 26,979,938**	Euro/km

C Functional Breakdown Structure & Functional Flow Diagram

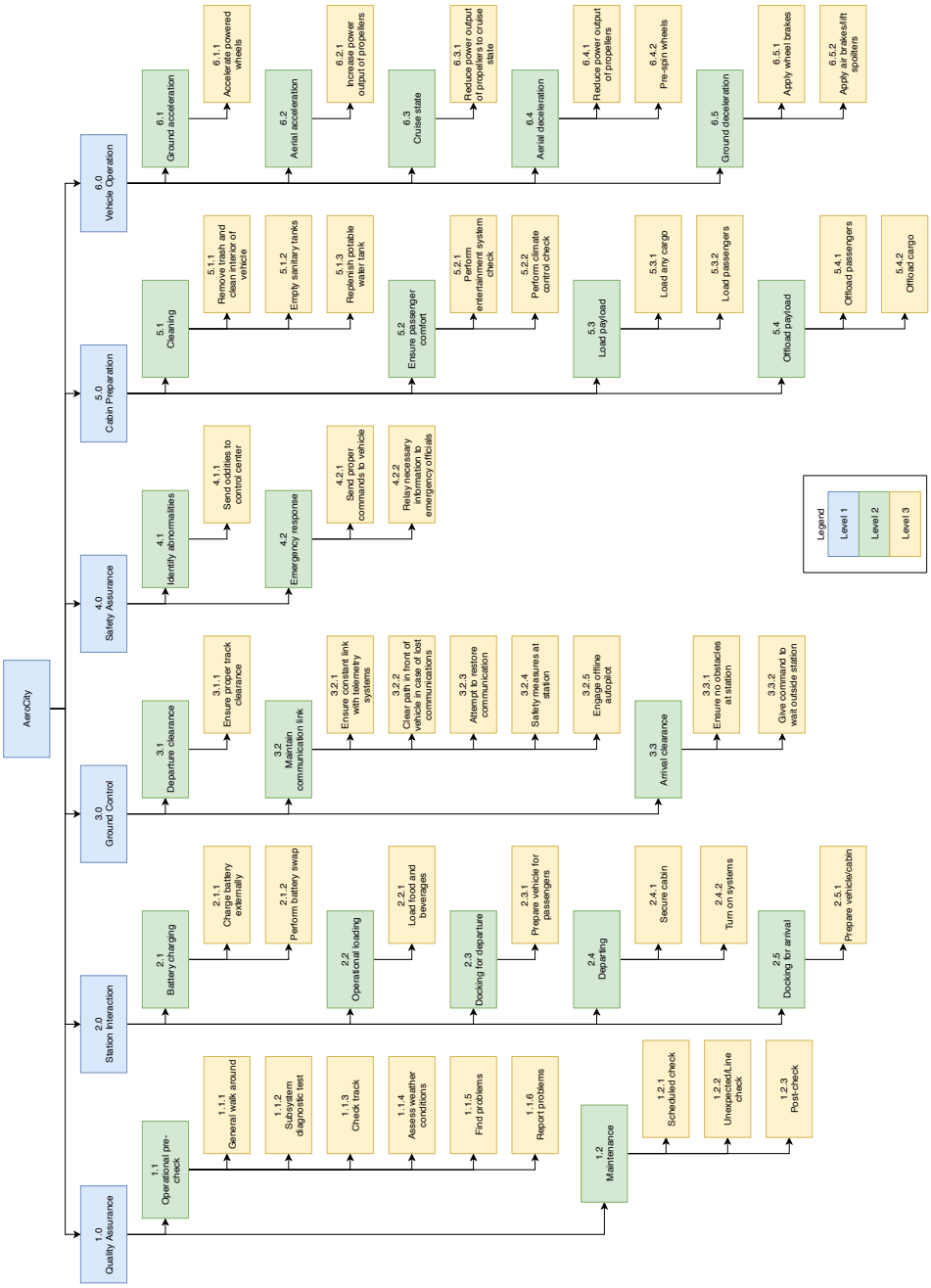

Figure C.1: Functional Breakdown Structure

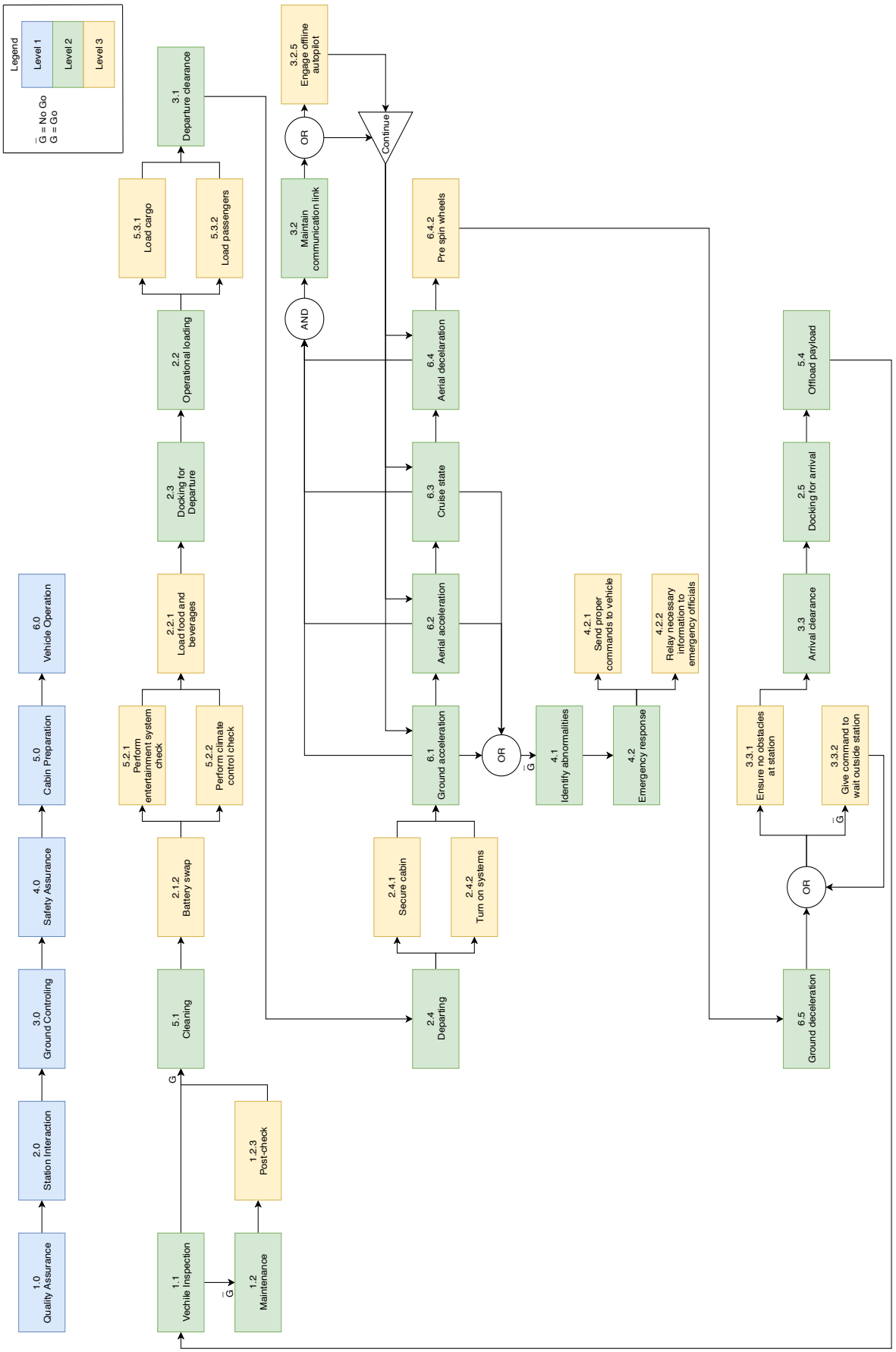

Figure C.2: Functional Flow Diagram